UNIVERSITY OF CALIFORNIA, SAN DIEGO

Composition and Sources of Biogenic Secondary Organic Aerosols in the Southeastern U.S. and Antarctica

A dissertation submitted in partial satisfaction of the
requirements for the degree
Doctor of Philosophy

in

Earth Sciences

by

Jun Liu

Committee in charge:

Lynn M. Russell, Chair
Ian Eisenman
Jan Kleissl
Dan Lubin
Joel R. Norris

2018

The Dissertation of Jun Liu as it is listed on UC San Diego Academic Records is approved, and it is acceptable in quality and form for publication on microfilm and electronically:

_____

_____

_____

_____

_____

Chair

University of California San Diego

2018

TABLE OF CONTENTS

LIST OF FIGURES

LIST OF TABLES

ACKNOWLEDGEMENTS

I would like to acknowledge Professor Lynn Russell for her support as the chair of my committee. Through multiple drafts and many long nights, her guidance has proved to be invaluable. I would also like to acknowledge my colleague Kevin Sanchez for his generous help in both work and in my life. It is their support that helped me in an immeasurable way.

Chapter 1, in full, is a reprint of the material as it appears in the *Geophysical Research Letters*, 2017 with slight modifications. Liu, J., Russell, L. M., Lee, A. K. Y., McKinney, K. A., Surratt, J. D., and Ziemann, P. J. "Observational evidence for pollution-influenced selective uptake contributing to biogenic secondary organic aerosols in the southeastern US", Geophysical Research Letters, 44, 8056-8064, 10.1002/2017gl074665, 2017. The dissertation author was the primary investigator and author of this paper.

Chapter 2, in full, has been submitted to *Journal of Geophysical Reserach* in 2018 with slight modifications. Liu, J., Russell, L.M., Ruggeri, G., Takahama, S., Claflin, M.S., Ziemann, P.J., Pye, H.O.T., Murphy, B.N., Xu, L., Ng, N.L., McKinney, K.A., Budisulistiorini, S.H., Bertram, T.H., Athanasios, N. and Surratt, J.D, "Regional Similarities and NO_x-related Increases in Biogenic Secondary Organic Aerosol in Summertime Southeastern U.S." The dissertation author was the primary investigator and author of this paper. The dissertation author was the primary investigator and author of this paper.

Chapter 3, in full, has been submitted to *Atmospheric Chemistry and Physics*. Liu, J., Dedrick, J., Russell, L.M., Senum, G.I., Uin, J., Kuang, C., Springston, S.R., Leaitch W. R.,

Aiken A.C. and Lubin, D, “High Summertime Aerosol Organic Functional Group Concentrations from Marine and Seabird Sources at Ross Island, Antarctica, during AWARE” The dissertation author was the primary investigator and author of this paper.

VITA

2013 B. E. in Environment Engineering, Tsinghua, University, Beijing

2016 M. S. in Earth Sciences, University of California, San Diego

2016 Graduate Teaching Assistant, University of California, San Diego

2017 Graduate Teaching Assistant, University of California, San Diego

2018 Ph. D. in Earth Sciences, University of California, San Diego

PUBLICATIONS

Liu, J., J. Dedrick, L.M. Russell, G.I. Senum, J. Uin, C. Kuang, S.R. Springston, W.R. Leaitch, A.C. Aiken and D. Lubin. (in review) High Summertime Aerosol Organic Functional Group Concentrations from Marine and Seabird Sources at Ross Island, Antarctica, during AWARE. *Atmos. Chem. Phys.*

Liu, J., Russell, L.M., Ruggeri G., Takahama, S., Claflin, M.S., Ziemann P.J., Pye, H.O. 4, Murphy, B.N., Xu L., Ng N,L, McKinney, K.A., Bertram, T.H., Athanasios, N. and Surratt, J.D. (in review) Regional Similarities and NOx-related Increases in Biogenic Secondary Organic Aerosol in Summertime Southeastern U.S. *J. Geophys. Res*.

Leaitch, W.R., L.M. Russell, **J. Liu**, F. Kolonjari, D. Toom, L. Huang, S. Sharma, A. Chivulescu, D. Veber and W. Zhang. (Accepted) Organic Functional Groups in the Submicron Aerosol at 82.5◦N from 2012 to 2014. *Atmos. Chem. Phys.*

Sanchez, K.J., C. Chen, L.M. Russell, R. Betha, **J. Liu**, D.J. Price, P. Massoli, L.D. Ziemba, E.C. Crosbie, R.H. Moore, M. Müller, S.A. Schiller, A. Wisthaler, A.K.Y. Lee, P.K. Quinn, T.S. Bates, J. Porter, T.G. Bell, E.S. Saltzman, R.D. Vaillancourt, M.J. Behrenfeld. (Accepted), Quantifying Contributions to Marine Aerosol Particles from Sea Spray and the Free Troposphere. *Sci. Rep.*

Liu, J., L.M. Russell, A.K.Y. Lee, K.A. McKinney, J.D. Surratt and P.J. Ziemann. (2017) Observational evidence for pollution-influenced selective uptake contributing to biogenic secondary organic aerosols in the southeastern US. *Geophys. Res. Lett.* Vol. 44, Iss. 15.

Betha R., L.M. Russell, C. Chen, **J. Liu**, D.J. Price, K.J. Sanchez, S. Chen, A.K.Y. Lee, S.C. Collier, Q. Zhang, X. Zhang, and C.D. Cappa. (2017) Larger submicron particles for emissions with residential burning in wintertime San Joaquin Valley (Fresno) than for vehicle combustion in summertime South Coast Air Basin (Fontana). *J. Geophys. Res.*

Chen C., S. Chen, L.M. Russell, **J. Liu**, D.J. Price, R. Betha, K.J. Sanchez, A.K.Y. Lee, S.C. Collier, Q.Zhang, A. Kumar, M. Kleeman, X. Zhang, and C.D. Cappa. (in review) Organic aerosol particle chemical properties associated with residential burning and fog in wintertime San Joaquin Valley (Fresno) and with vehicle and firework emissions in summertime South Coast Air Basin (Fontana). *J. Geophys. Res*.

Price, D.J., C. Chen, L.M. Russell, M.A. Lamjiri, R. Betha, K.J. Sanchez, **J. Liu**, A.K.Y. Lee, and D.R. Cocker. (2017) More unsaturated, cooking-type hydrocarbon-like organic aerosol particle emissions from renewable diesel compared to ultra low sulfur diesel in at-sea operations of a research vessel. *Aerosol Science And Technology.* Vol. 51 , Iss. 2.

Betha, R., L.M. Russell, K.J. Sanchez, **J. Liu**, D.J. Price, M.A. Lamjiri, C. Chen, X.M. Kuang, G.O. da Rocha, S.E. Paulson, J.W. Miller, and D.R. Cocker. (2017) Lower NOx but higher particle and black carbon emissions from renewable diesel compared to ultra low sulfur diesel in at-sea operations of a research vessel. *Aerosol Science And Technology*. Vol. 51 , Iss. 2.

ABSTRACT OF THE DISSERTATION

Composition and Sources of Biogenic Secondary Organic Aerosols in the Southeastern U.S. and Antarctica

by

Jun Liu

Doctor of Philosophy in Earth Sciences

University of California, San Diego, 2018

Professor Lynn M. Russell, Chair

Biogenic Secondary Organic Aerosols (bSOA) account for a large fraction of the global aerosols budget, and thus have a significant impact on climate and public health. Observations of bSOA in the southeastern U.S. included Fourier Transform Infrared Spectroscopy (FTIR) and Aerosol Mass Spectrometer (AMS) measurements of submicron mass at Look Rock (LRK), Tennessee, and Centreville (CTR), Alabama. At LRK, Organic mass (OM) sources were apportioned to three factors, including "sulfate-related bSOA" that correlated to sulfate (r=0.72). Single-particle mass spectra also showed three composition types that corresponded to the mass-

based factors with spectra cosine similarity of 0.93 and time series correlations of r>0.4. The similarity of the m/z spectra (cosine similarity=0.97) and the time series correlation (r=0.80) of the "sulfate-related bSOA" to the sulfate-containing single-particle type provide evidence for particle composition contributing to selective uptake of isoprene oxidation products onto sulfate particles. NO_x had nighttime-to-early-morning peaks 3~10 times higher at CTR than at LRK, but OM sources identified by FTIR had three very similar factors at both sites including Biogenic Organic Aerosols (BOA). The BOA spectrum from FTIR is similar (cosine similarity > 0.6) to that of lab-generated particle mass from isoprene and monoterpene with NO_x. NO_x was correlated with FTIR-BOA and AMS related biogenic factors for NO_x concentrations higher than 1 ppb at both sites, producing 0.5 to 1 μg m^{-3} additional biogenic OM for each 1 ppb increase of NO_x. Submicron organic mass (OM), particle number, and cloud condensation nuclei concentrations were measured at a costal Antarctica site and were found to be highest in summer. Natural sources that included marine sea spray and seabird emissions contributed 56 % of OM in austral summer but only 3 % in austral winter. Fourier transform infrared spectra showed the natural sources of organic aerosol were characterized by amide group absorption, which may be from seabird populations. Carboxylic acid group contributions from natural sources were correlated to incoming solar radiation, indicating both seasonal sources and likely secondary reactions.

Introduction

Aerosols are an important component of the atmosphere because of their significant impact on climate [*Charlson et al*., 1992; *Ramanathan et al*., 2001], visibility [*Watson*, 2002], and public health [*Ostro and Chestnut*, 1998; *Pope et al*., 2009]. Organic compounds contribute the largest fraction of fine aerosols, and secondary organic aerosols (SOA) make up as much as 70% of the organic carbon (OC) mass in aerosol particles [*Hallquist et al*., 2009]. SOA formation starts with emissions of volatile organic compounds (VOCs). VOCs are oxidized with chemical reactions in the atmosphere, and their volatility decreases [*Ziemann and Atkinson*, 2012]. The lower volatility of the oxidized VOCs causes them to partition preferentially to the particle phase by condensation on preexisting aerosol particles or by forming new particles [*Odum et al*., 1996].

At the global scale, plant foliage contributes more than two-thirds of total VOC emissions to the atmosphere [*Guenther et al*., 1995; *Guenther et al*., 2006]. The high emission rate of isoprene (600 Tg yr^{-1}) makes it the most abundant non-methane VOC [*Guenther et al*., 2006]. The southeastern United States is one of the highest biogenic VOC (BVOC) emission regions in the world. The emission rates of both isoprene and monoterpenes rival the rates measured in tropical rainforests [*Goldstein et al*., 2009]. Although BVOCs are abundant in the region, SOA components correlate with emissions that are largely from anthropogenic combustion sources, such as carbon monoxide (CO) [*Weber et al*., 2007]. The current understanding of this apparent contradiction is that SOA is most likely from BVOCs but that anthropogenic emissions can contribute to the formation process. Consequently, for many years biogenic SOA (BSOA) was not considered to be controllable by policy or regulations because they are produced by natural

vegetation [*Kleeman et al*., 2007; *Park et al*., 2003]. However, modeling studies now show it is possible to affect the amount of BSOA formation by regulating the anthropogenic emissions that contribute to the SOA-forming reactions [*Carlton et al*., 2010].

In polar regions, the sources of biogenic aerosols are completely different due to the absence of terrestrial vegetation [*Guenther et al.*, 1995; *Guenther et al.*, 2006] but the presence of coastal species. VOCs emitted from the ocean are small compared to terrestrial vegetation [*Stocker et al.*, 2013], but biogenic aerosols are still important in polar regions. For example, natural aerosols can explain seasonal and spatial patterns of Southern Ocean cloud albedo [*McCoy et al.*, 2015]. Ammonia from seabird-colony guano may be a key factor contributing to bursts of newly formed particles in the Arctic [*Croft et al.*, 2016]. There are few places on Earth where measurements of ambient aerosol and CCN (Cloud condensation nuclei) are as scarce as in Antarctica. Yet since West Antarctica is one of the most rapidly warming regions on Earth [*Bromwich et al.*, 2013; *Lambeck et al.*, 2002; *Steig et al.*, 2009], these measurements may be crucial to understanding the changing climate – especially given the close connection between the Antarctic ice sheets and potential global sea level rise.

Identification of the contributions of different natural and man-made emission sources to SOA measured in the atmosphere is essential for better understanding and quantifying BSOA. However, measurements of aerosol organic composition are extremely difficult due to its low concentration and high complexity. Before 2000, there was very little instrumentation for measuring the composition of organic aerosol species [*McMurry*, 2000], and other chemical analyses were limited by sampling constraints and resolution. Source apportionment of SOA was largely dependent on tracers for specific sources, such as vehicle emission and wood burning [*Cass*, 1998; *Rogge et al*., 1993a; b; *Rogge et al*., 1991]. This method was found to be useful for

direct or "primary" emissions of so-called primary organic aerosols (POA, i.e. aerosols that are emitted rather than formed by reactions in the atmosphere), but it is not an appropriate approach for SOA since the components of SOA change with oxidation reactions making it difficult to identify a conservative tracer [*Russell*, 2014].

With the introduction of the Aerosol Mass Spectrometer (AMS) in 2000, quantification of non-refractory ion fragments from size-resolved aerosol particles with high time resolution was made possible [*Jayne et al.*, 2000]. The AMS provides measurements of the mass distribution of fragments that have different ratios of mass to charge (m/z), providing the m/z spectra that characterize the chemical composition every 5 min. Further, FTIR spectroscopy, which quantifies organic aerosol composition on filter substrates by quantifying the absorption spectrum as a function of wavelength, has greatly improved quantification of the major organic functional groups (OFGs) in aerosol particles [*Maria et al.*, 2002; *Russell et al.*, 2009a; *Takahama et al.*, 2013]. AMS and FTIR have provided two independent methods for characterizing the chemical composition in sufficient detail to allow SOA apportionment, i.e. separation of an observed mixture into its uncorrelated components, allowing us to improve our understanding of SOA formation processes. One common statistical method that has been used to assist in solving this type of partially-constrained inversion problems for the complex chemical measurements provided by AMS and FTIR is Positive Matrix Factorization (PMF). PMF incorporates weighting of the residuals from factorization by measurement errors [*Paatero and Tapper*, 1994], and has been widely used for atmospheric source apportionment [*Reff et al.*, 2007; *Weber et al.*, 2007]. Factors have been identified by PMF for measurements from around the world, and these factors have been used to apportion organic aerosol components to specific emission sources [*Jimenez et al.*, 2009; *Lanz et al.*, 2007; *Ulbrich et al.*, 2009]. PMF has also

been applied to FTIR spectra to effectively separate contributions from different organic particle sources in multiple studies [*Russell et al*., 2011].

This dissertation focuses on two key aspects of bSOA: first, the interaction of bSOA with anthropogenic emissions, such as sulfate and NO_x in the southeastern U.S., and, second, the apportionment of particle organic mass to seabird emission sources at McMurdo Station, Antarctica. The first two chapters are based on the Southern Oxidant and Aerosol Study (SOAS in 2013. Website: http://soas2013.rutgers.edu), a comprehensive study aimed at studying bSOA in the southeastern U.S. The measurements in the third chapter were collected during the ARM West Antarctica Radiation Experiment (AWARE in 2016; Website: https://www.arm.gov/research/campaigns/amf2015aware).

Chapter 1 describes measurements collected at an elevated (800m ASL) forested site as part of the SOAS campaign, at Look Rock, Tennessee. The main objective of this study was to understand the mixing state of anthropogenic sulfate-containing particles and the isoprene-derived bSOA. In this chapter, PMF factors from ensemble mass and k-means [*Hartigan and Wong*, 1979] clusters from single particles, both from AMS, were compared. The sources of aerosols were apportioned by the two statistical approaches and direct evidence of heterogeneous reactions of bSOA were evaluated.

Chapter 2 compares measurements from two SOAS sites: Look Rock, Tennessee, and Centreville, Alabama. While both sites are rural, the Centreville site had higher NO_x concentration. The objective of this study was to compare the measurements from the two sites and gain information about the role of NO_x on bSOA formation. AMS, FTIR, and their PMF factors from both sites were evaluated to compare the two sites in this chapter. The bSOA formed at the two sites are very similar except for the NO_x related bSOA. Comparison of the

ambient measurements to FTIR from lab-generated bSOA provides additional insights on the formation pathways of the SOA. The measurements were also compared to simulated bSOA from CMAQ model [*B N Murphy et al.*, 2017; *Pye et al.*, 2010; *Pye et al.*, 2015; *Pye et al.*, 2017; *Pye et al.*, 2013] to assess the implications for the region.

Chapter 3 reviews an entire year of FTIR measurements of organic aerosol composition at McMurdo Station, which is on Ross Island, Antarctica, as a part of the AWARE campaign. Two methods were used to separate contributions to particle number and composition from activities at McMurdo Station from those from natural biogenic sources. The first method used spike removal from the concentration time series to identify short contamination events. The second method was PMF, which used the organic chemical composition and seasonal variation to separate anthropogenic sources from natural sources. The natural aerosols are likely from the nearby seabird colonies on Ross Island based on the seasonal variation and the unique amide signal in the FTIR spectra. Evidence of photochemical bSOA in Antarctica is also described in this chapter.

Together, this dissertation investigates the identification of bSOA in the southeastern U.S. and coastal Antarctica, and the extent to which bSOA in the southeastern U.S. is influenced by anthropogenic emissions. The sources and composition of the OM at rural sites in the summertime southeastern U.S. were identified. The dependence of bSOA formation on anthropogenic emission, particularly sulfate and NO_x was investigated. Evidence of heterogeneous reactions in bSOA formation was shown. The composition of lab-generated bSOA was compared to the composition of ambient aerosol particles from field studies. OM sources at coastal Antarctica and seasonal variation were also studied.

References

Bromwich, D. H., Nicolas, J. P., Monaghan, A. J., Lazzara, M. A., Keller, L. M., Weidner, G. A., and Wilson, A. B.: Central West Antarctica among the most rapidly warming regions on Earth, Nature Geoscience, 6, 139-145, 10.1038/ngeo1671, 2013.

Carlton, A. G., Pinder, R. W., Bhave, P. V., and Pouliot, G. A.: To What Extent Can Biogenic SOA be Controlled?, Environmental Science & Technology, 44, 3376-3380, 10.1021/es903506b, 2010.

Cass, G. R.: Organic molecular tracers for particulate air pollution sources, Trac-Trends in Analytical Chemistry, 17, 356-366, 10.1016/s0165-9936(98)00040-5, 1998.

Charlson, R. J., Schwartz, S. E., Hales, J. M., Cess, R. D., Coakley, J. A., Hansen, J. E., and Hofmann, D. J.: CLIMATE FORCING BY ANTHROPOGENIC AEROSOLS, Science, 255, 423-430, 10.1126/science.255.5043.423, 1992.

Croft, B., Wentworth, G. R., Martin, R. V., Leaitch, W. R., Murphy, J. G., Murphy, B. N., Kodros, J. K., Abbatt, J. P. D., and Pierce, J. R.: Contribution of Arctic seabird-colony ammonia to atmospheric particles and cloud-albedo radiative effect, Nature Communications, 7, 10.1038/ncomms13444, 2016.

Goldstein, A. H., Koven, C. D., Heald, C. L., and Fung, I. Y.: Biogenic carbon and anthropogenic pollutants combine to form a cooling haze over the southeastern United States, Proceedings of the National Academy of Sciences of the United States of America, 106, 8835-8840, 10.1073/pnas.0904128106, 2009.

Guenther, A., Hewitt, C. N., Erickson, D., Fall, R., Geron, C., Graedel, T., Harley, P., Klinger, L., Lerdau, M., McKay, W. A., Pierce, T., Scholes, B., Steinbrecher, R., Tallamraju, R., Taylor, J., and Zimmerman, P.: A GLOBAL-MODEL OF NATURAL VOLATILE ORGANIC-COMPOUND EMISSIONS, Journal of Geophysical Research-Atmospheres, 100, 8873-8892, 10.1029/94jd02950, 1995.

Guenther, A., Karl, T., Harley, P., Wiedinmyer, C., Palmer, P. I., and Geron, C.: Estimates of global terrestrial isoprene emissions using MEGAN (Model of Emissions of Gases and Aerosols from Nature), Atmospheric Chemistry and Physics, 6, 3181-3210, 2006.

Hallquist, M., Wenger, J. C., Baltensperger, U., Rudich, Y., Simpson, D., Claeys, M., Dommen, J., Donahue, N. M., George, C., Goldstein, A. H., Hamilton, J. F., Herrmann, H., Hoffmann, T., Iinuma, Y., Jang, M., Jenkin, M. E., Jimenez, J. L., Kiendler-Scharr, A., Maenhaut, W., McFiggans, G., Mentel, T. F., Monod, A., Prevot, A. S. H., Seinfeld, J. H., Surratt, J. D., Szmigielski, R., and Wildt, J.: The formation, properties and impact of secondary organic aerosol: current and emerging issues, Atmospheric Chemistry and Physics, 9, 5155-5236, 2009.

Hartigan, J. A., and Wong, M. A.: Algorithm AS 136: A k-means clustering algorithm., Journal of the Royal Statistical Society. Series C (Applied Statistics), 28, 100-108, 1979.

Jayne, J. T., Leard, D. C., Zhang, X. F., Davidovits, P., Smith, K. A., Kolb, C. E., and Worsnop, D. R.: Development of an aerosol mass spectrometer for size and composition analysis of submicron particles, Aerosol Science and Technology, 33, 49-70, 10.1080/027868200410840, 2000.

Jimenez, J. L., Canagaratna, M. R., Donahue, N. M., Prevot, A. S. H., Zhang, Q., Kroll, J. H., DeCarlo, P. F., Allan, J. D., Coe, H., Ng, N. L., Aiken, A. C., Docherty, K. S., Ulbrich, I. M., Grieshop, A. P., Robinson, A. L., Duplissy, J., Smith, J. D., Wilson, K. R., Lanz, V. A., Hueglin, C., Sun, Y. L., Tian, J., Laaksonen, A., Raatikainen, T., Rautiainen, J., Vaattovaara, P., Ehn, M., Kulmala, M., Tomlinson, J. M., Collins, D. R., Cubison, M. J., Dunlea, E. J., Huffman, J. A., Onasch, T. B., Alfarra, M. R., Williams, P. I., Bower, K., Kondo, Y., Schneider, J., Drewnick, F., Borrmann, S., Weimer, S., Demerjian, K., Salcedo, D., Cottrell, L., Griffin, R., Takami, A., Miyoshi, T., Hatakeyama, S., Shimono, A., Sun, J. Y., Zhang, Y. M., Dzepina, K., Kimmel, J. R., Sueper, D., Jayne, J. T., Herndon, S. C., Trimborn, A. M., Williams, L. R., Wood, E. C., Middlebrook, A. M., Kolb, C. E., Baltensperger, U., and Worsnop, D. R.: Evolution of Organic Aerosols in the Atmosphere, Science, 326, 1525-1529, 10.1126/science.1180353, 2009.

Kleeman, M. J., Ying, Q., Lu, J., Mysliwiec, M. J., Griffin, R. J., Chen, J., and Clegg, S.: Source apportionment of secondary organic aerosol during a severe photochemical smog episode, Atmospheric Environment, 41, 576-591, 10.1016/j.atmosenv.2006.08.042, 2007.

Lambeck, K., Esat, T. M., and Potter, E. K.: Links between climate and sea levels for the past three million years, Nature, 419, 199-206, 10.1038/nature01089, 2002.

Lanz, V. A., Alfarra, M. R., Baltensperger, U., Buchmann, B., Hueglin, C., and Prevot, A. S. H.: Source apportionment of submicron organic aerosols at an urban site by factor analytical modelling of aerosol mass spectra, Atmospheric Chemistry and Physics, 7, 1503-1522, 2007.

Maria, S. F., Russell, L. M., Turpin, B. J., and Porcja, R. J.: FTIR measurements of functional groups and organic mass in aerosol samples over the Caribbean, Atmospheric Environment, 36, 5185-5196, 10.1016/s1352-2310(02)00654-4, 2002.

McCoy, D. T., Burrows, S. M., Wood, R., Grosvenor, D. P., Elliott, S. M., Ma, P.-L., Rasch, P. J., and Hartmann, D. L.: Natural aerosols explain seasonal and spatial patterns of Southern Ocean cloud albedo, Science advances, 1, e1500157-e1500157, 10.1126/sciadv.1500157, 2015.

McMurry, P. H.: A review of atmospheric aerosol measurements, Atmospheric Environment, 34, 1959-1999, 10.1016/s1352-2310(99)00455-0, 2000.

Murphy, B. N., Woody, M. C., Jimenez, J. L., Carlton, A. M. G., Hayes, P. L., Liu,, S., N., N. L., Russell,, L. M., S., A., X., L., Young,, J., Z., R. A., Z., Q.,, and Pye, H. O. T.: Semivolatile POA and parameterized total combustion SOA in CMAQv5.2: impacts on source strength and partitioning, Atmos. Chem. Phys. Discuss , in review, https://doi.org/10.5194/acp-2017-193, 2017.

Odum, J. R., Hoffmann, T., Bowman, F., Collins, D., Flagan, R. C., and Seinfeld, J. H.: Gas/particle partitioning and secondary organic aerosol yields, Environmental Science & Technology, 30, 2580-2585, 10.1021/es950943+, 1996.

Ostro, B., and Chestnut, L.: Assessing the health benefits of reducing particulate matter air pollution in the United States, Environmental Research, 76, 94-106, 10.1006/enrs.1997.3799, 1998.

Paatero, P., and Tapper, U.: Positive Matrix Factorization: A Non-Negative Factor Model with Optimal Utilization of Error Estimates of Data Values, Environmetrics, 5, 111-126, 10.1002/env.3170050203, 1994.

Park, R. J., Jacob, D. J., Chin, M., and Martin, R. V.: Sources of carbonaceous aerosols over the United States and implications for natural visibility, Journal of Geophysical Research-Atmospheres, 108, 10.1029/2002jd003190, 2003.

Pope, C. A., III, Ezzati, M., and Dockery, D. W.: Fine-Particulate Air Pollution and Life Expectancy in the United States, New England Journal of Medicine, 360, 376-386, 10.1056/NEJMsa0805646, 2009.

Pye, H. O. T., Chan, A. W. H., Barkley, M. P., and Seinfeld, J. H.: Global modeling of organic aerosol: the importance of reactive nitrogen (NOx and NO3), Atmospheric Chemistry and Physics, 10, 11261-11276, 10.5194/acp-10-11261-2010, 2010.

Pye, H. O. T., Pinder, R. W., Piletic, I. R., Xie, Y., Capps, S. L., Lin, Y. H., Surratt, J. D., Zhang, Z. F., Gold, A., Luecken, D. J., Hutzell, W. T., Jaoui, M., Offenberg, J. H., Kleindienst, T. E., Lewandowski, M., and Edney, E. O.: Epoxide pathways improve model predictions of isoprene markers and reveal key role of acidity in aerosol formation, Environmental Science & Technology, 47, 11056-11064, 10.1021/es402106h, 2013.

Pye, H. O. T., Luecken, D. J., Xu, L., Boyd, C. M., Ng, N. L., Baker, K. R., Ayres, B. R., Bash, J. O., Baumann, K., Carter, W. P. L., Edgerton, E., Fry, J. L., Hutzell, W. T., Schwede, D. B., and Shepson, P. B.: Modeling the Current and Future Roles of Particulate Organic Nitrates in the Southeastern United States, Environmental Science & Technology, 49, 14195-14203, 10.1021/acs.est.5b03738, 2015.

Pye, H. O. T., Murphy, B. N., Xu, L., Ng, N. L., Carlton, A. G., Guo, H. Y., Weber, R., Vasilakos, P., Appel, K. W., Budisulistiorini, S. H., Surratt, J. D., Nenes, A., Hu, W. W., Jimenez, J. L., Isaacman-VanWertz, G., Misztal, P. K., and Goldstein, A. H.: On the implications of aerosol liquid water and phase separation for organic aerosol mass, Atmospheric Chemistry and Physics, 17, 343-369, 10.5194/acp-17-343-2017, 2017.

Ramanathan, V., Crutzen, P. J., Kiehl, J. T., and Rosenfeld, D.: Atmosphere - Aerosols, climate, and the hydrological cycle, Science, 294, 2119-2124, 10.1126/science.1064034, 2001.

Reff, A., Eberly, S. I., and Bhave, P. V.: Receptor modeling of ambient particulate matter data using positive matrix factorization: Review of existing methods, Journal of the Air & Waste Management Association, 57, 146-154, 2007.

Rogge, W. F., Hildemann, L. M., Mazurek, M. A., Cass, G. R., and Simonelt, B. R. T.: Sources of fine organic aerosol. 1. charboilers and meat cooking operations, Environmental Science & Technology, 25, 1112-1125, 10.1021/es00018a015, 1991.

Rogge, W. F., Hildemann, L. M., Mazurek, M. A., Cass, G. R., and Simoneit, B. R. T.: SOURCES OF FINE ORGANIC AEROSOL .3. ROAD DUST, TIRE DEBRIS, AND ORGANOMETALLIC BRAKE LINING DUST - ROADS AS SOURCES AND SINKS, Environmental Science & Technology, 27, 1892-1904, 10.1021/es00046a019, 1993a.

Rogge, W. F., Hildemann, L. M., Mazurek, M. A., Cass, G. R., and Simoneit, B. R. T.: SOURCES OF FINE ORGANIC AEROSOL .2. NONCATALYST AND CATALYST-EQUIPPED AUTOMOBILES AND HEAVY-DUTY DIESEL TRUCKS, Environmental Science & Technology, 27, 636-651, 10.1021/es00041a007, 1993b.

Russell, L. M., Bahadur, R., Hawkins, L. N., Allan, J., Baumgardner, D., Quinn, P. K., and Bates, T. S.: Organic aerosol characterization by complementary measurements of chemical bonds and molecular fragments, Atmospheric Environment, 43, 6100-6105, 10.1016/j.atmosenv.2009.09.036, 2009.

Russell, L. M., Bahadur, R., and Ziemann, P. J.: Identifying organic aerosol sources by comparing functional group composition in chamber and atmospheric particles, Proceedings of the National Academy of Sciences of the United States of America, 108, 3516-3521, 10.1073/pnas.1006461108, 2011.

Russell, L. M.: Carbonaceous particles: Source-based characterization of their formation, composition, and structures, in: Turekian KK, editor. Treatise on Geochemistry (Second Edition), Oxford: Elsevier, p. 291-316., 2014.

Steig, E. J., Schneider, D. P., Rutherford, S. D., Mann, M. E., Comiso, J. C., and Shindell, D. T.: Warming of the Antarctic ice-sheet surface since the 1957 International Geophysical Year, Nature, 457, 459-462, 10.1038/nature07669, 2009.

Stocker, T. F., D. Qin, G. K. Plattner, M. Tignor, S. K. Allen, J. Boschung, A. Nauels, Y. Xia, V. Bex, and Midgley, P. M.: IPCC, 2013: summary for policymakers in climate change 2013: the physical science basis, contribution of working group I to the fifth assessment report of the intergovernmental panel on climate change, in, 2013.

Takahama, S., Johnson, A., and Russell, L. M.: Quantification of Carboxylic and Carbonyl Functional Groups in Organic Aerosol Infrared Absorbance Spectra, Aerosol Science and Technology, 47, 310-325, 10.1080/02786826.2012.752065, 2013.

Ulbrich, I. M., Canagaratna, M. R., Zhang, Q., Worsnop, D. R., and Jimenez, J. L.: Interpretation of organic components from Positive Matrix Factorization of aerosol mass spectrometric data, Atmospheric Chemistry and Physics, 9, 2891-2918, 2009.

Watson, J. G.: Visibility: Science and regulation, Journal of the Air & Waste Management Association, 52, 628-713, 2002.

Weber, R. J., Sullivan, A. P., Peltier, R. E., Russell, A., Yan, B., Zheng, M., de Gouw, J., Warneke, C., Brock, C., Holloway, J. S., Atlas, E. L., and Edgerton, E.: A study of secondary organic aerosol formation in the anthropogenic-influenced southeastern United States, Journal of Geophysical Research-Atmospheres, 112, 10.1029/2007jd008408, 2007.

Ziemann, P. J., and Atkinson, R.: Kinetics, products, and mechanisms of secondary organic aerosol formation, Chemical Society Reviews, 41, 6582-6605, 10.1039/c2cs35122f, 2012.

Chapter 1

Observational Evidence for Pollution-influenced Selective Uptake Contributing to Biogenic Secondary Organic Aerosols in the Southeastern US

During the 2013 Southern Oxidant and Aerosol Study, aerosol mass spectrometer measurements of submicron mass and single-particles were taken at Look Rock, Tennessee. Their concentrations increased during multi-day stagnation events characterized by low wind, little rain, and increased daytime isoprene emissions. Organic mass (OM) sources were apportioned as 42% "vehicle-related" and 54% biogenic secondary organic aerosol (bSOA), with the latter including “sulfate-related bSOA” that correlated to sulfate (r=0.72) and “nitrate-related bSOA” that correlated to nitrate (r=0.65). Single-particle mass spectra showed three composition types that corresponded to the mass-based factors with spectra cosine similarity of 0.93 and time series correlations of r>0.4. The vehicle-related OM with m/z 44 was correlated to black carbon, “sulfate-related bSOA” was on particles with high sulfate, and “nitrate-related bSOA” was on all particles. The similarity of the m/z spectra (cosine similarity=0.97) and the time series

correlation (r=0.80) of the “sulfate-related bSOA” to the sulfate-containing single-particle type provide evidence for particle composition contributing to selective uptake of isoprene oxidation products onto particles that contain sulfate from power plants.

1.1 Introduction

Organic compounds contribute the largest fraction of submicron aerosol mass in many regions worldwide, and secondary organic aerosols (SOA) contribute as much as 70% of the organic carbon mass (OM) in aerosol particles [Hallquist et al., 2009]. Emission rates of both isoprene and monoterpenes in the southeastern United States [Goldstein et al., 2009] compete with the rates measured in tropical rain forests [Rinne et al., 2002]. One reason that mean annual temperatures in the southeastern United States decreased in the 20th century despite overall global-mean warming may be the direct radiative effect of the SOA formed from biogenic volatile organic compounds, known as bSOA [Goldstein et al., 2009; Portmann et al., 2009]. This recent cooling trend may also have contributions from internal variability [Banerjee et al., 2017], aerosol sources aloft [Ford and Heald, 2013], cloud forcing [Yu et al., 2014], particle phase water [Nguyen et al., 2016], and other changes in particle composition [Kim et al., 2015]. The high global flux of biogenic volatile organic compounds of 1000 Tg yr-1 [Guenther et al., 2012] provides ample precursors that may form bSOA in many regions of the world.

Identifying the contributions of different natural and man-made emission sources to SOA quantifies the factors that control bSOA. Data inversion methods have been applied to aerosol mass spectrometry (AMS) measurements to separate and quantify different types or "factors" of bSOA in aerosol OM with both reasonable accuracy and consistency [Budisulistiorini et al., 2013; Budisulistiorini et al., 2015; Chen et al., 2015; Corrigan et al., 2013; Robinson et al., 2011; Slowik et al., 2011; Xu et al., 2015b]. Two biogenic factors in particular have been identified at multiple locations and shown to have similar chemical compositions (spectra of

mass fragments) and correlations [Devore and Berk, 2012] to tracers: one factor with high m/z 82 (which we refer to as Factor82, also referred to as 82fac, IEPOX OA, or Isoprene OA, as noted in Table 1.1) [Budisulistiorini et al., 2013; Budisulistiorini et al., 2015; Chen et al., 2015; Robinson et al., 2011; Slowik et al., 2011; Xu et al., 2015b]) showed moderate to strong (r=0.7 to 0.88) correlations to sulfate [Budisulistiorini et al., 2013; Budisulistiorini et al., 2015; Xu et al., 2015b] and another factor with a characteristic fragment ion at m/z 91 (which we refer to as Factor91, also referred to as 91fac, OOA3, BSOA1, BSOA2, or Isoprene OA as noted in Table 1.1) [Budisulistiorini et al., 2015; Chen et al., 2015; Lee et al., 2016b; Robinson et al., 2011]). The consistent identification of these two factors in studies across North and South America as well as Europe indicates both the prevalence of bSOA worldwide and the general similarity of their composition (Table 1.1).

Table 1.1: AMS Biogenic Secondary Organic Aerosol PMF Factors Reported Previously.

Factor Name	Reference	*m/z* Markers	Factor-related Information
Factor82	This study	44>43 53,82	Selective uptake of isoprene related aerosol onto preexisting sulfate particles
82fac	[*Robinson et al.*, 2011]	44>43 53,82	Product of Isoprene oxidation similar to methylfuran AMS *m/z* 82 and *m/z* 53 correlated to methylvinylketone and methacrolein in both airborne and ground-based measurements
UNKN(Unknown)	[*Slowik et al.*, 2011]	43>>44 31,82	Reactive uptake of isoprene onto preexisting sulfate aerosol and/or condensation of early-generation isoprene reaction products; Highest concentration during sulfate plume
IEPOX OA	[*Budisulistiorini et al.*, 2013]	44<43 53,82 44>>43, 91	IEPOX as oxidation products. IEPOX-OA factor correlates well (R^2 = 0.59) with the summed mass concentrations of the measured IEPOX-derived SOA tracer

Table 1.1 AMS Biogenic Secondary Organic Aerosol PMF Factors Reported Previously. (Continued)

OOA-2	[*Chen et al.*, 2015]	44<43 53,82	Produced by the reactive uptake of isoprene photo-oxidation, including possible aqueous-phase oxidation in haze, fog, and cloud droplets. Factor loading correlated with isoprene concentration (R^2 =0.65)
Isoprene-OA	[*Xu et al.*, 2015]	44>43 53,82	Isoprene-SOA formed via reactive uptake of IEPOX and correlated with methyl tetrols (R=0.68) as well as sulfate (R=0.77)
IEPOX OA	[*Budisulistiorini et al.*, 2015]	44>43 53,82	IEPOX as oxidation products. Factor strongly correlated (R^2 >0.7) with 2- methyltetrols, C5-alkene triols, IEPOX-derived organosulfates, and dimers of organosulfates. Factor strongly correlated with sulfate (R^2 = 0.58)
Factor91	This Study	44<<43 91	Biogenic SOA correlated to nitrate
91fac	[*Robinson et al.*, 2011]	44<<43 91	Biomass burning aerosols, except for absence of *m/z* 60 and 73 expected from levoglucosan

Table 1.1 AMS Biogenic Secondary Organic Aerosol PMF Factors Reported Previously. (Continued)

OOA3	[*Chen et al.*, 2015]	44<<43 91	Freshly produced Biogenic SOA. A linear combination of the three chamber spectra (50% isoprene- derived Secondary Organic Material (SOM), 30% α-pinene-derived SOM, and 20% β- caryophyllene-derived SOM) largely reproduced the OOA-3 factor
91fac	[*Budisulistiorini et al.*, 2015]	44>43	An aged aerosol that may be associated with nitrate radical chemistry or as yet unidentified pathways Both from gas-phase oxidation of monoterpenes and perhaps sesquiterpenes
BSOA1 BSOA2	[*Lee et al.*, 2016]	44<43, 91	BSOA1: gas-phase ozonolysis and nitrate radical chemistry at night BSOA2: gas-phase oxidation by OH radical and ozone during daytime

These similarities in bSOA chemical composition suggest commonalities in their atmospheric formation processes, for which chamber studies provide a proxy. Recent studies have provided a link between chamber-generated and atmospheric isoprene-related bSOA by identifying the characteristic fragment ion at m/z 82 found in AMS datasets to be associated to isomeric isoprene epoxydiols (IEPOX)-derived SOA [Budisulistiorini et al., 2013; Lin et al., 2012]. To understand what factors contribute to forming this IEPOX-derived bSOA, chamber studies have investigated a variety of different atmospheric conditions: particle acidity [Gaston et al., 2014b; Surratt et al., 2010] and particle-phase water [Nguyen et al., 2011; Nguyen et al., 2015; H Zhang et al., 2011] were both found to increase IEPOX-related bSOA. The source of

the other bSOA (Factor91) is less clear but is likely associated (in part) with gas-phase isoprene oxidation pathways that do not involve particle-phase reactions such as low-volatility multifunctional hydroperoxides produced from oxidation of isoprene hydroxyhydroperoxides [Budisulistiorini et al., 2016; Krechmer et al., 2015; Liu et al., 2016; Riva et al., 2016]. A high m/z 91 signal was measured in chamber studies of reactions of β-pinene and NO3 radical [Boyd et al., 2015] and of ozonolysis of β-caryophyllene [Chen et al., 2015], suggesting that m/z 91 could be an indicator for bSOA formed from monoterpene or sesquiterpene oxidation in ambient aerosol mass spectra [Boyd et al., 2015].

Atmospheric bSOA measurements have not found a correlation between IEPOX-related bSOA and either calculated particle-phase water or acidity [Budisulistiorini et al., 2015; Rattanavaraha et al., 2016; Worton et al., 2013; Xu et al., 2015b], but other atmospheric factors could have hidden such relationships because of larger variability in other field conditions. Xu et al. [2016] showed that, in sulfate-rich plumes, sulfate enhances the heterogeneous reaction rates of IEPOX due to both enhanced particle surface area and particle acidity. Hu et al. [2016] used the similarity in the mass size distribution peak of the characteristic m/z 82 fragment ion and sulfate in particles from both the southeastern U.S. and the Amazon to suggest sulfate control of the IEPOX uptake formation pathway. Both studies provide indirect evidence of contributions to bSOA from heterogeneous reactions of IEPOX with sulfate based on correlations of tracers and submicron mass composition.

To provide more direct evidence of the processes controlling bSOA formation, we compared characteristic fragment ions associated with bSOA identified in submicron particle mass and in single particles measured during the 2013 Southern Oxidant and Aerosol Study (SOAS) at Look Rock, Tennessee. The prevalence of biogenic emissions and the meteorological

conditions resulted in large contributions of bSOA to OM. Single-particle AMS measurements with light scattering (LS) provided direct information on differences in particle composition. As a result, this work provides biogenic-specific single-particle spectra to evaluate the role of particle-composition dependent processes in SOA formation.

1.2 Methods

As part of the SOAS campaign from 1 June to 17 July 2013 in a forested area at Look Rock, Tennessee, we measured size-resolved non-refractory chemical composition of submicron particles with a high-resolution time-of-flight aerosol mass spectrometer (AMS, Aerodyne Research, Inc.). The LS module attached to the AMS triggered collection of single-particle non-refractory mass fragment ion spectra for particles in the vacuum aerodynamic diameter range of 350 to 700 nm (*i.e.* mobility diameter of 230 to 500 nm, using 5% sampling efficiency as the cutoff diameters, see Appendix) [*Cross et al.*, 2007; *Cross et al.*, 2009; *Kostenidou et al.*, 2007]. The same aerosol inlet [*Bates et al.*, 2012] was used for filter collection for Fourier Transform Infrared (FTIR) spectroscopy [*Russell et al.*, 2009; *Takahama et al.*, 2013] and particle size distributions by Scanning Electrical Mobility Spectrometer (SEMS, Model 2000C, Brechtel Manufacturing Incorporated). Specific details of instrument operation, performance and calibration, including evaluation of the AMS collection efficiency (CE), are provided in the Appendix.

Two statistical methods were used to identify characteristic compositions in the AMS mass fragment spectra. Positive Matrix Factorization (PMF) incorporates weighting of residuals from factorization by measurement errors [*Paatero*, 1997; *Paatero and Tapper*, 1994; *Paatero and Hopke*, 2003; *Paatero et al.*, 2002] and has been widely used for atmospheric source

apportionment [*Reff et al.*, 2007; *Weber et al.*, 2007]. AMS PMF factors associate mixtures of organic aerosol components to specific emission sources [*Jimenez et al.*, 2009; *Lanz et al.*, 2007; *Ulbrich et al.*, 2009]. K-means clustering aims to partition observations into clusters in which each observation belongs to the cluster with the nearest mean [*Hartley*, 1955]. K-means clustering has been applied to AMS light scattering single particle spectra to identify atmospheric particle types [*Lee et al.*, 2015; *Lee et al.*, 2016a; *Liu et al.*, 2013; *Willis et al.*, 2016]. The criteria used for identifying the most accurate and robust solutions for both PMF and K-means clustering are provided in the Appendix.

Three factors were identified by PMF of the AMS high-resolution measurements: Factor44 ("vehicle-related SOA") with a high fraction of oxygenated organic mass fragment ions (including *m/z* 44), Factor82 ("sulfate-related bSOA") with high *m/z* 82 ion signals (IEPOX-OA), and Factor91 ("nitrate-related bSOA") with high *m/z* 91 ion signals. K-means clustering of LS mode single-particle measurements also identified three types of particles: Cluster44 with a high fraction of oxidized organic fragment ions at *m/z* 43 and 44, Cluster82 with a high sulfate fraction and *m/z* 82 fragment ion signals, and Cluster91 with a high fraction of less oxidized organic mass fragment ions (including *m/z* 91). Interestingly, although the clusters were based on single-particle measurements while factors were from mass-based measurements, they resulted in very similar mass spectra, as indicated by the near-unity values of the cosine similarity between the *m/z* spectra and moderate to strong correlations of the time series (shown in Table 1.2). The correlation of the time series of the concentrations of Factor82 mass and Cluster82 number was r=0.80, which was higher than that of Factor44 and Cluster44 (r=0.66) and of Factor91 and Cluster91 (r=0.48).

Table 1.2: Cosine Similarities of m/z Spectra and Correlations of Time Series of HR AMS Factors, LS AMS Clusters and m/z 44, 82 and 91 Signals.

Spectral Cosine Similarity/ Time Series Correlation Coefficient (R)	Factor44	Factor82	Factor91
Cluster44	0.93/0.66	0.91/0.48	0.66/0.50
Cluster82	0.66/0.55	0.97/0.80	0.74/0.45
Cluster91	0.56/0.55	0.88/0.66	0.93/0.48
m/z 44	NA/0.91	NA/0.69	NA/0.86
m/z 82	NA/0.82	NA/0.92	NA/0.77
m/z 91	NA/0.91	NA/0.69	NA/0.94

1.3 Results

1.3.1 Enhancement of Particle Concentrations by Stagnation

One interesting feature of the AMS submicron particle mass concentration time series is that multiple-day events of nearly-continuously increasing concentrations are much more evident than diurnal cycles. Each event consists of 3-6 days of concentrations higher than 2 μg m^{-3}, typically ended by a rain event that scavenged most of the aerosol mass. Dividing the campaign according to these criteria shows there are seven multi-day periods of aerosol accumulation that are separated by low AMS organic concentration during the 7-week campaign (Figure 1.1).

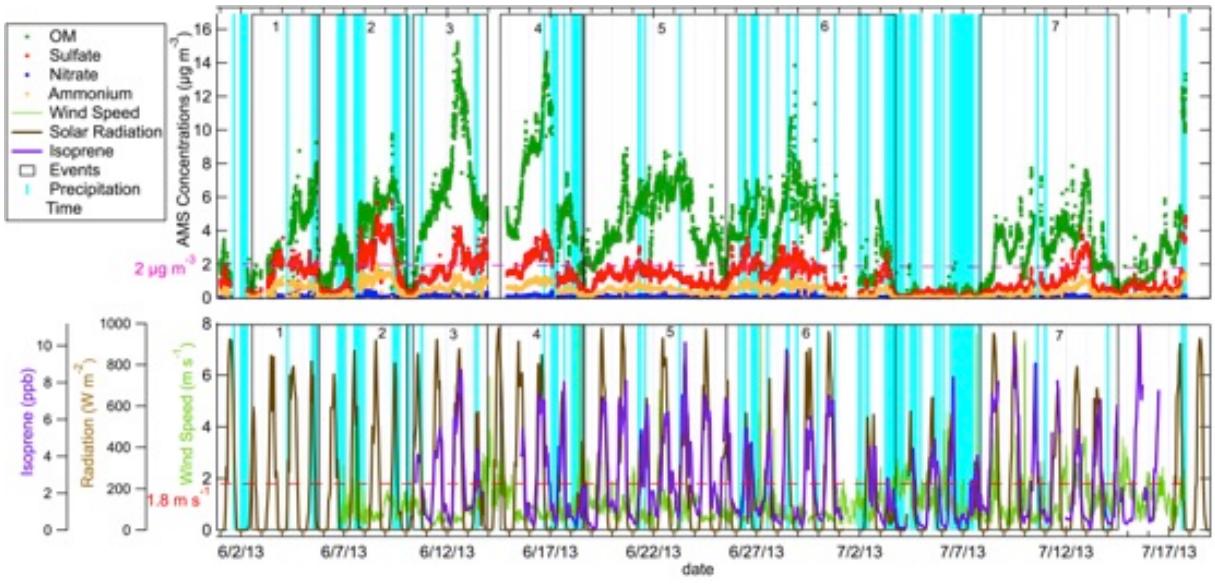

Figure 1.1: Top: Time series of AMS non-refractory submicron mass concentrations of OM, sulfate, nitrate and ammonium (2 g m-3 OM is marked on the plot to indicate the criterion for separation between the seven events identified). Bottom: Time series of isoprene concentration, solar radiation, precipitation and wind speed (1.8 m s-1 is marked on the plot as a cutoff for low wind speed associated with stagnation conditions).

Most of these events are characterized by 3-4 days of continually increasing concentration that obscure the mid-day peaks expected for daytime production of photochemical SOA. To illustrate the photochemical contribution to SOA, we calculated the loading in the boundary layer column, assuming a well-mixed boundary layer source and negligible concentrations above the layer ([*Wagner et al.*, 2015], details in the Appendix) with regional soundings and reanalyses for mixed layer height (Figure 1.2) [*Draxier and Hess*, 1998; *Wang and Wang*, 2014]. Figure 1.3 shows the daytime loading in the boundary layer column (defined as from 0900 to 2100) accounted for 92% of the daily loading in the boundary layer column for non-refractory organic components for the 48-day campaign. The diurnal cycles of the three PMF factors are similar to that of the combined non-refractory organic components. Higher isoprene concentrations were moderately correlated (r=0.68) to higher daily maximum radiation,

which likely contributed to part of the multi-day event pattern by contributing more SOA on days with fewer clouds.

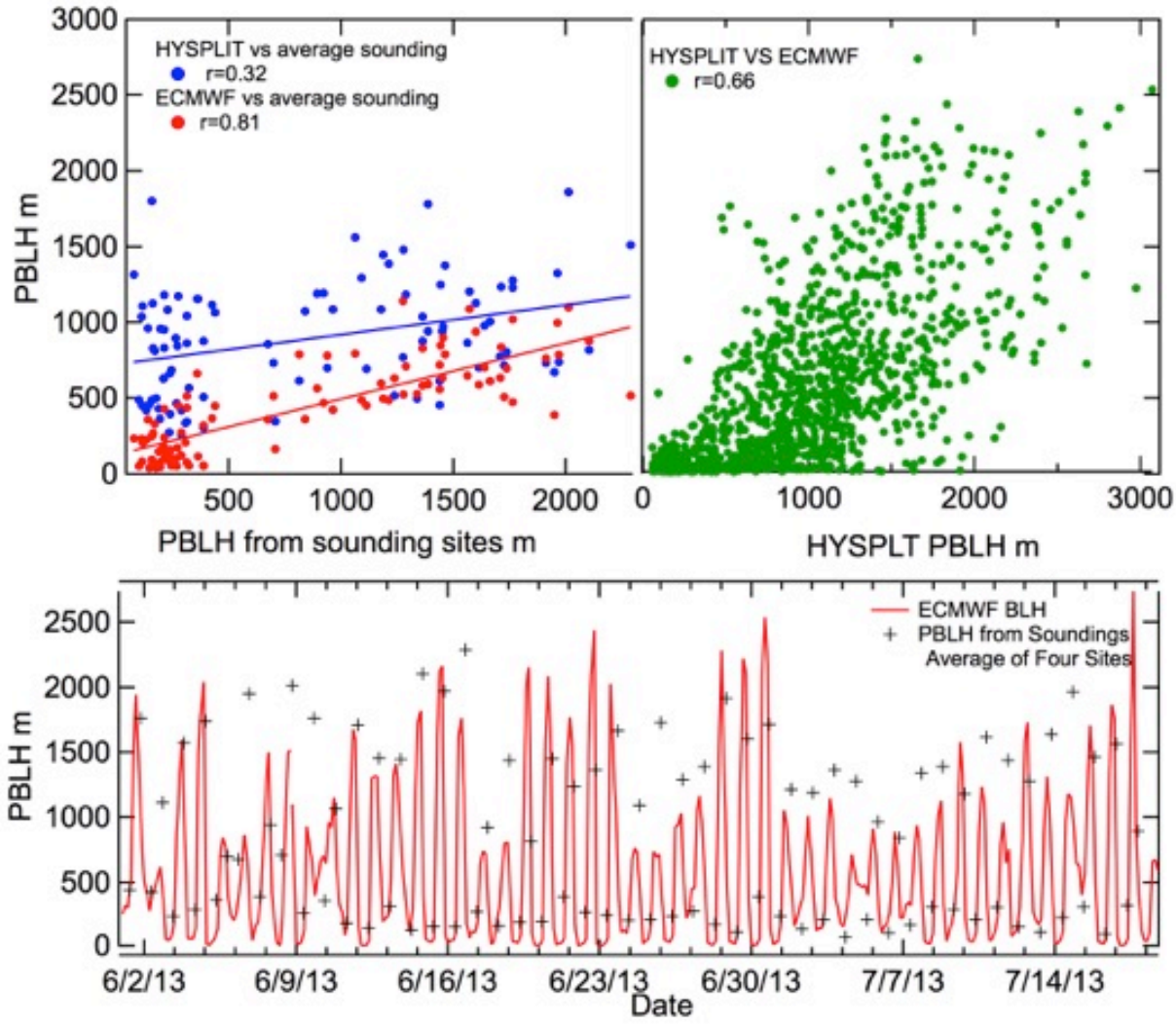

Figure 1.2: Bottom: Boundary layer height (BLH) retrieved from ECMWF reanalysis and measured average of boundary layer height at four surrounding sounding locations (Nashville, Peachtree City, Blacksburg and Greensboro). Top left: ECMWF and HYSPLIT reanalysis vs Sounding; Top right: ECMWF reanalysis vs HYSPLIT reanalysis. All heights are above ground level.

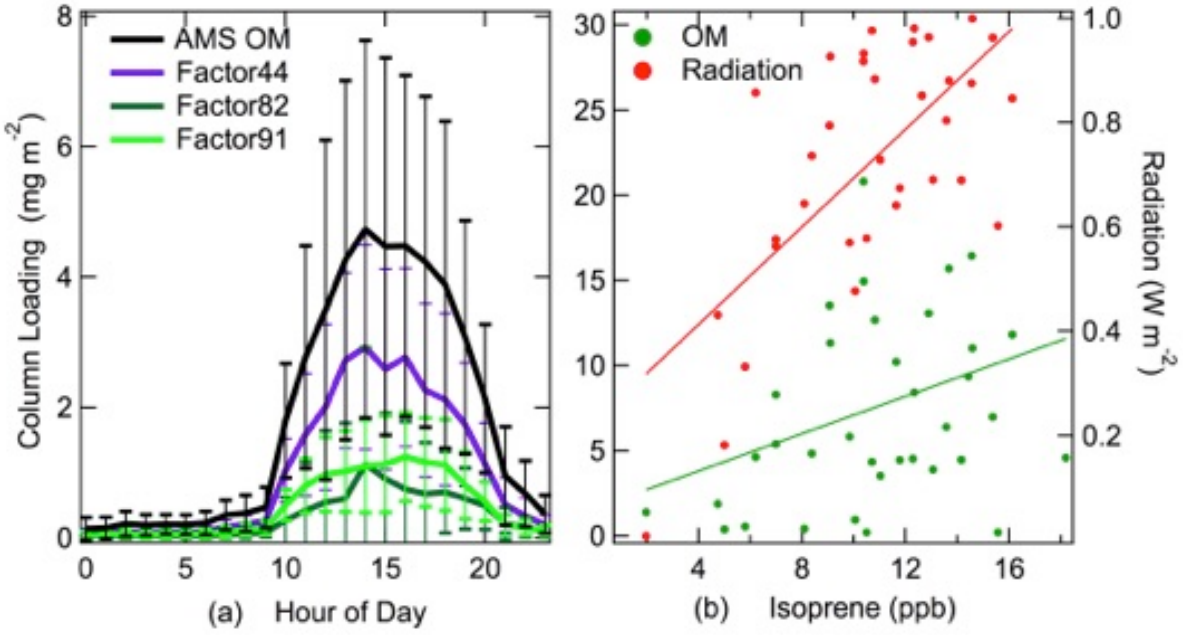

Figure 1.3: (a) Diurnal pattern of loading in the boundary layer column of the three PMF factors. Errors bars give the standard deviation to indicate variability. (b) Comparison of organic loading in the boundary layer column and maximum daily solar radiation (400 to 1100 nm wavelength) with isoprene (R=0.32 and 0.68, respectively).

1.3.2 Comparison of mass-based AMS Factor and number-based LS Cluster Sources

By comparing the AMS PMF factor mass spectra to factors reported in the literature and by evaluating the correlations of time series of factor concentrations to tracers, the probable source of each factor was identified. Factor44 and Cluster44 had moderate correlations with several anthropogenic emission tracers ($r>0.5$ for Black Carbon (BC), CO, NO_y and O_3) and had clear diurnal cycles that peaked for about 3 hours after local noon each day, similar to the results of Zhang et al. [2011]. The moderate correlation ($r=0.73$ and 0.58, respectively) of both Factor44 and Cluster44 time series to BC concentration time series (shown in Figure 1.4) suggests that the factor is influenced by aged anthropogenic combustion emissions from regional vehicle traffic emissions. Factor44 also showed moderate correlations to sulfate ($r=0.76$) and nitrate ($r=0.63$),

consistent with transported and aged OM typically from anthropogenic emissions [*Jimenez et al.*, 2009]. The afternoon maximum indicated that photochemical reactions likely caused the aerosol formation. Factor44 was similar to AMS spectra of gasoline and diesel SOA in a region with high *m/z* 44 fraction (~0.1) and low *m/z* 43 fraction (~0.05) [Presto et al., 2014] and to their ambient LV-OOA factor, which was attributed to vehicle sources (see also in Appendix [*Elsasser et al.*, 2012; *Fine et al.*, 2001; *Mano and Andreae*, 1994]).

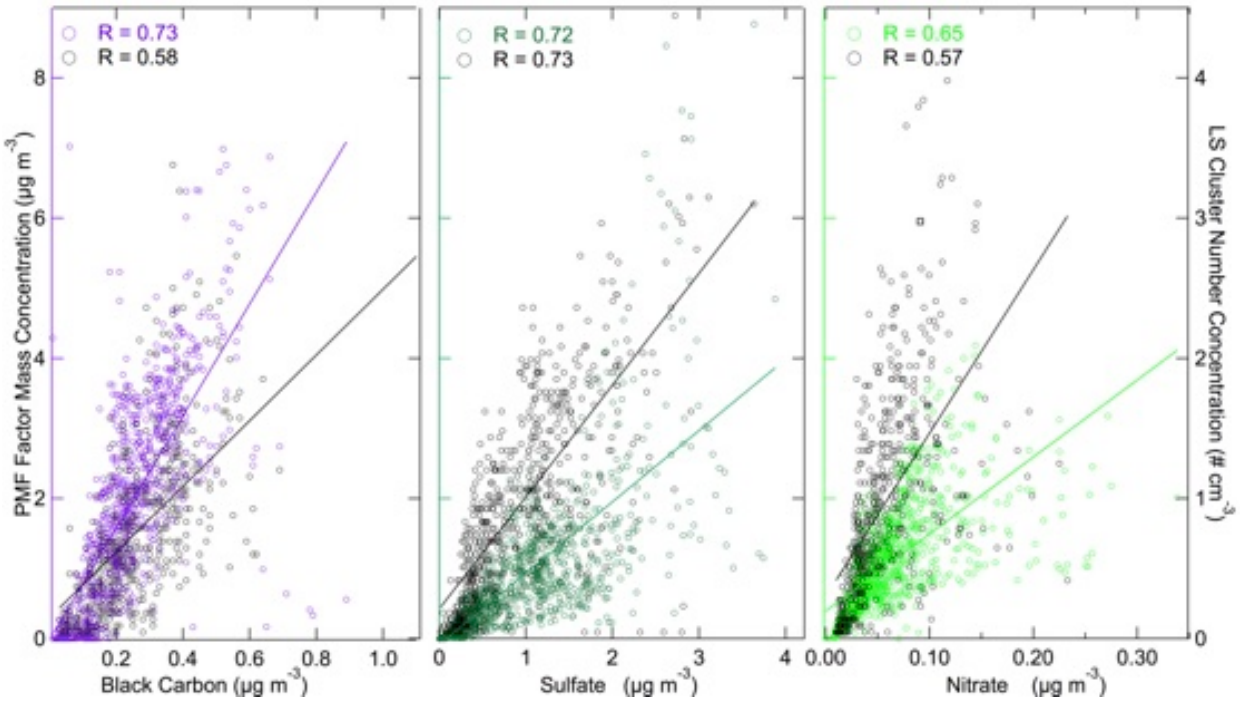

Figure 1.4: Hourly averaged scatter plots of AMS HR PMF factors and LS-AMS clusters with tracers for anthropogenic emissions: Left shows Factor44 and Cluster44 vs Black Carbon (BC), r=0.73 and 0.58, respectively; Middle: Factor82 and Cluster82 vs sulfate, r=0.72 and 0.73, respectively; Right: Factor91 and Cluster91 vs nitrate, r=0.65 and 0.57, respectively; Normalized hourly-averaged concentration are shown in the plots; Lines are the linear regression of factors and clusters. Only hours for which the LS-detectable range (230 < mobility diameter < 500 nm, measured by SEMS) represented more than 50% of submicron mass were included in this correlation, which was approximately 87% of the 33-day study.

Factor82 and Cluster82 were moderately correlated (r=0.72 and 0.73, respectively) with sulfate concentration time series, as given in Figure 1.4. This correlation suggests Factor82 and Cluster82 are likely from acid-catalyzed reactive uptake of IEPOX that occurred in the presence

of acidic sulfate, consistent with previous studies [*Lin et al.*, 2012; *Surratt et al.*, 2010]. Factor91 and Cluster91 time series were moderately correlated (r=0.65 and 0.57, respectively) with nitrate concentration, which can indicate several types of combustion and oxidants [*Song et al.*, 2001] as well as N_2O_5 reactive uptake [*Finlayson-Pitts et al.*, 1989]. Isoprene concentration (~2 ppb) is higher than monoterpene (<1 ppb) during the SOAS study [Budisulistiorini et al., 2015]. Factor91 had a maximum concentration at 1300 (Figure 1.5). Both of these features are more consistent with isoprene as a source of Factor91 since isoprene concentration had a strong correlation (r=0.83) to the measured radiation at the surface. Therefore, Factor91 is likely to also be formed from isoprene through a non-IEPOX route based on the similarity to published mass spectra from smog chamber products of isoprene oxidized under relatively low-sulfate and NO_x conditions [*Budisulistiorini et al.*, 2016; *Chen et al.*, 2015; *Liu et al.*, 2016; *Riva et al.*, 2016]. Factor91 could also be from a number of other sources, given the many associations of this marker fragment reported previously (Table 1.1). Factor91 is similar to a previously reported OOA3 PMF factor in Chen et al. [2015] with cosine similarity of 0.87, which was adequately reconstructed by a linear combination of multiple lab generated bSOA (30% α-pinene-derived OM, 20% β-caryophyllene-derived OM, and 50% isoprene-derived OM). Organic nitrate has also been calculated in this study with the NO^+/NO_2^+ ratio method [Xu et al., 2015a], as described in Appendix. The estimated fraction of molecules containing organonitrate groups (3.2 - 16.4% of OM) is comparable with Xu et al. [2015a] (5 - 12%) and could indicate a potential connection between organic nitrate and Factor91. However, there were no nighttime increases of Factor91, NO_x, or nitrate (Figure 1.5), which rules out a contribution to Factor91 from nighttime monoterpene-NO_x reactions. In addition, the weak correlation (r=0.48) of the time series of Factor91 and Cluster91 and the similar fractions of nitrate on all three particle types (26%, 37%,

39% of nitrate were on Cluster44, Cluster82, and Cluster91, respectively) indicate that Factor91 was not forming selectively on Cluster91 particles.

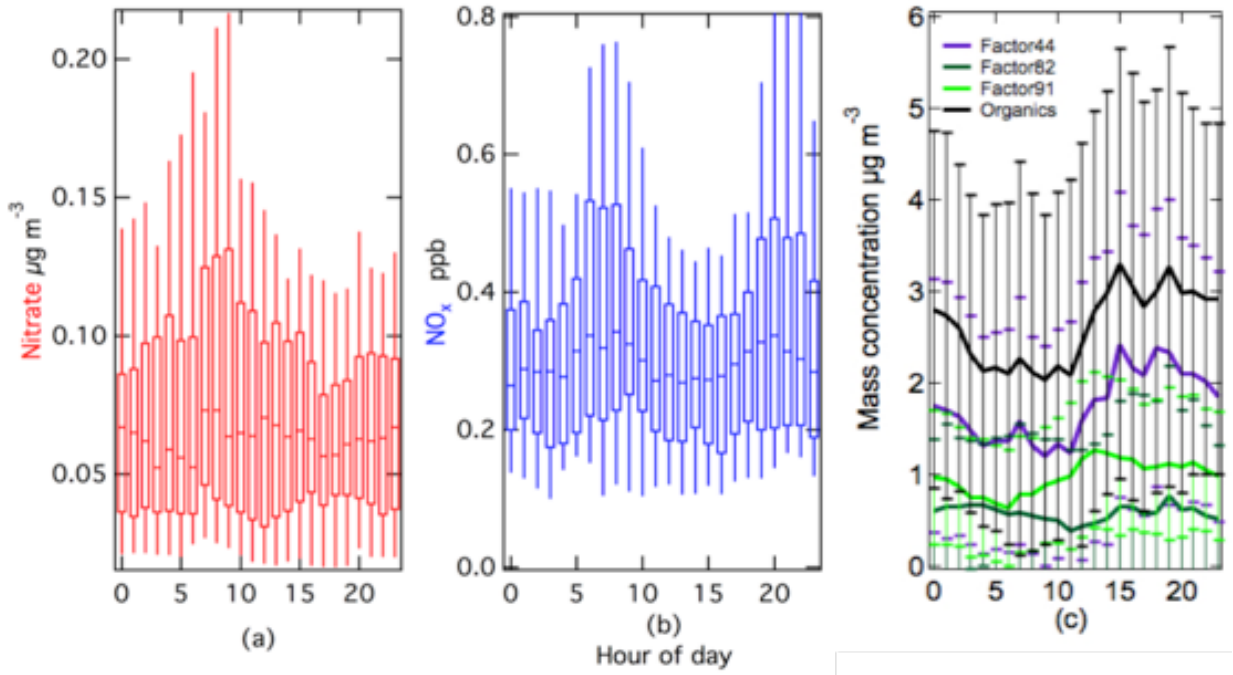

Figure 1.5: Diurnal patterns of (a) Nitrate; (b) NOx; (c) AMS OM and PMF factors. The boxes show the 25th and 75th percentile values; the Whiskers show the 5th and 95th percentile values, and errors bars give the standard deviation to indicate variability.

1.3.3 Evidence for Selective Formation of *m/z* 82 Factor and Sulfate-Containing Particles

To investigate the dependence of the clustering of the organic mass fragment ions on the inorganic components, K-means clustering was carried out with only organic mass fragment ions and with all non-refractory mass fragment ions. The two clustering approaches produced nearly identical groups of particles, and this high degree of consistency shows the method was robust in producing similar particle types with or without inorganic components. In addition, spectra

within each cluster were very similar to the spectrum of the centroid for that cluster. The distributions of cosine similarities of the individual particles and the cluster centroid spectra in Figure 1.6(a) shows that all of the spectra in each cluster were both well separated from other clusters and very similar to the centroid spectrum.

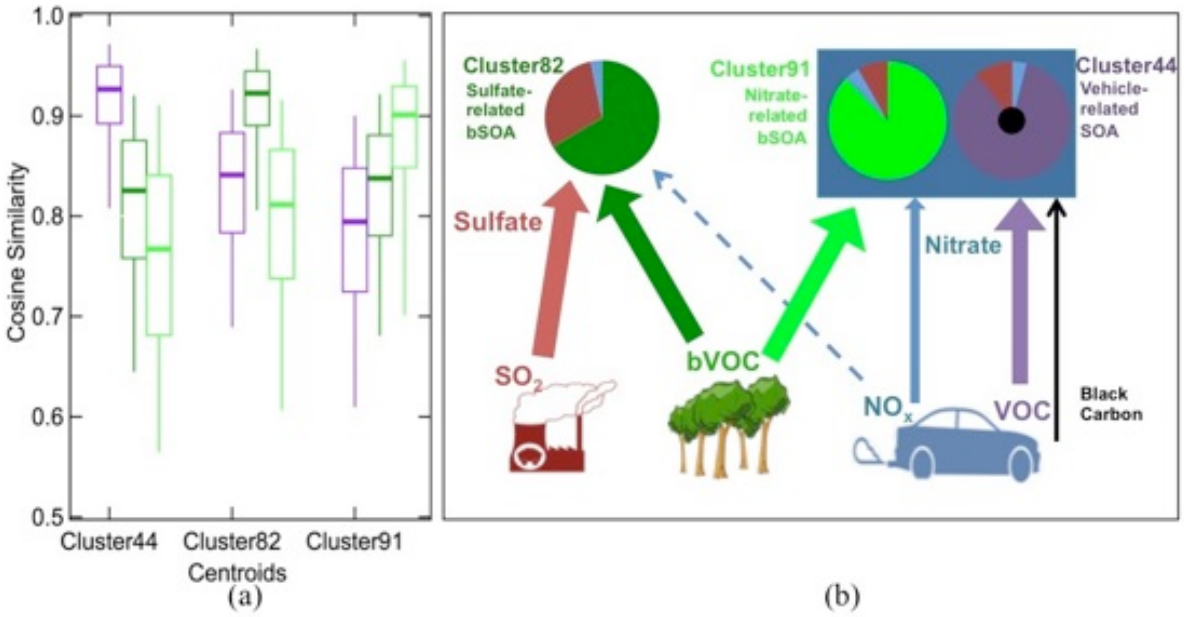

Figure 1.6: (a) Cosine similarity of individual single particle LS-AMS mass spectra to the centroids of the three clusters. Purple: cluster44, 9808 particles; Dark green: cluster82; 12022 particles; Light green: cluster 91, 12598 particles. The boxes show the 25th and 75th percentile values; the Whiskers show the 5th and 95th percentile values. (b) Schematic diagram of sources, processes and final mixing state of aerosols in Look Rook, Tennessee, for summer 2013. The particle pie graphs are proportional to the non-refractory signal fractions of the three Clusters (ammonium is excluded because of baseline noise in LS spectra [*Lee et al.*, 2015], and chloride is excluded because it is negligible). The processes shown are based on both direct measurements and correlations.

Other causes of the high-OM events likely include the low wind conditions associated with all seven events, suggesting that stagnation might be contributing to the high aerosol concentration events (Figure 1.7). The frequencies of occurrence of the highest concentrations of OM and all three factors are higher at lower wind speeds, in particular at less than 1.8 m s^{-1}. The seven high-OM events are not associated with back trajectories from a particular region,

indicating that a single location of emission sources (power plant or forest) does not explain the pattern of events, as shown in Figure 1.8.

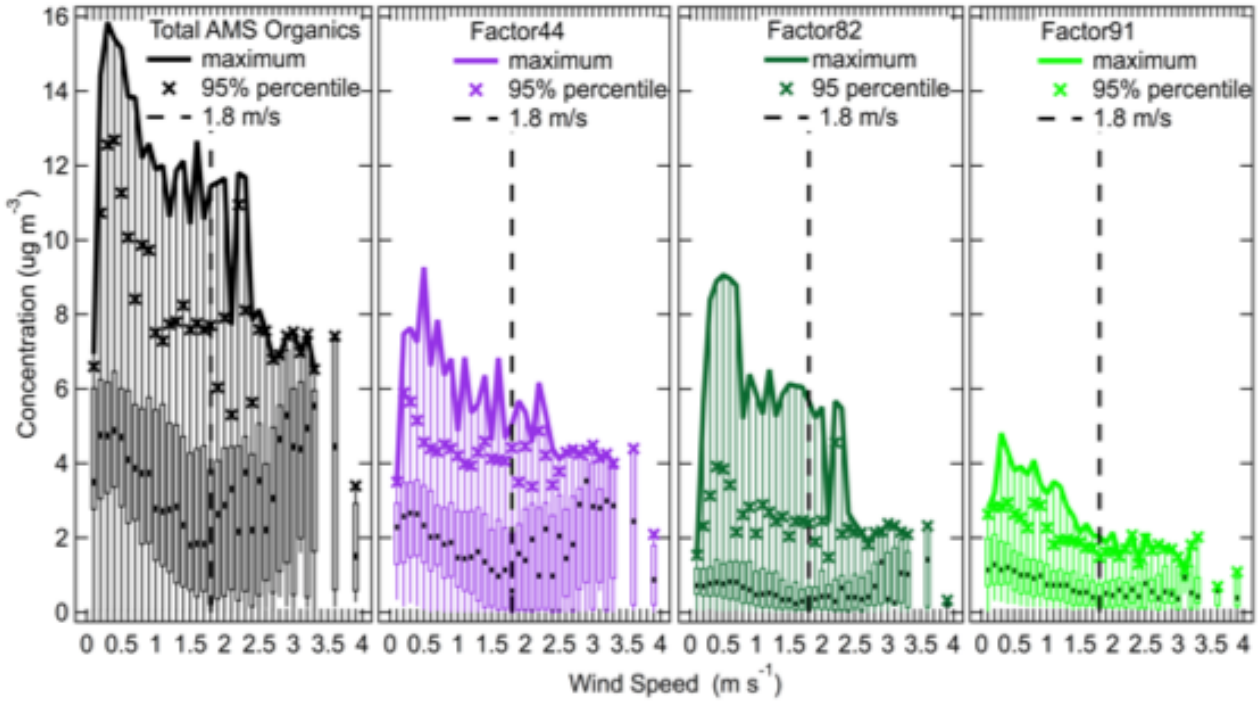

Figure 1.7: Distribution of 5-minute averaged HR AMS organic concentration and PMF factor concentrations as a function of measured local wind speed: solid line shows maximum valus; bars give median values; boxes are 25th and 75th percentile values; whiskers show the 0 and 100 percentile values; markers are 5th and 95th percentile values; dashed lines indicate wind speed of 1.8 m s^{-1}.

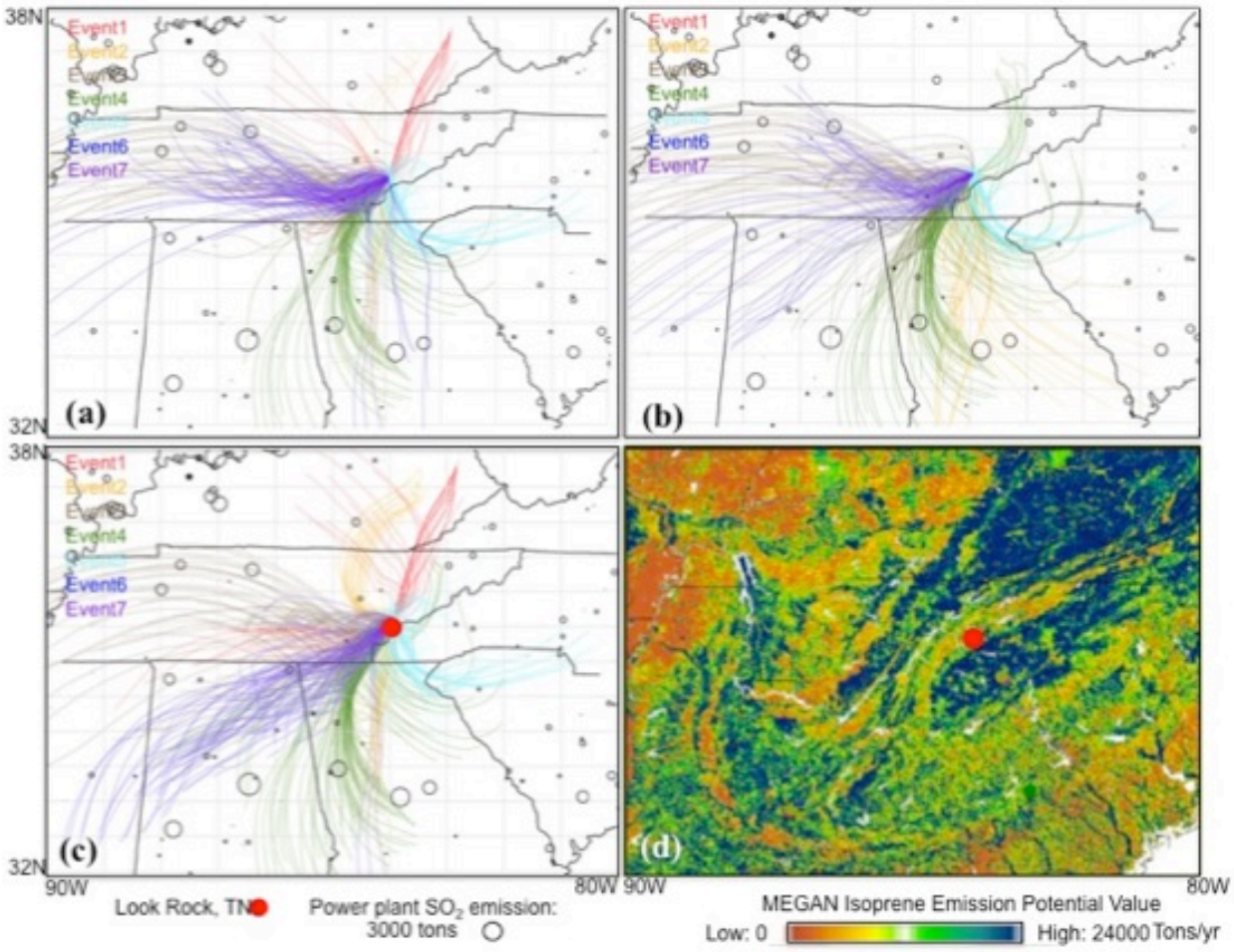

Figure 1.8: Mass size 24-hour HYSPLIT back trajectories for times with the highest 25% of concentrations of (a) Factor44, (b) Factor91 and (c) Factor82. The 7 events separated by low organic mass concentration (<1 μg m-3) identified in Figure 1 are shown in different colors. SO2 emission in 2012 from coal power plants is marked on the map, with the area of the circles proportional to emission (EPA Egrid2012). (d) Model estimated isoprene emission potential from the MEGAN model [Guenther et al., 2012].

The robustness and separation of the clusters show that the particles are externally mixed, namely that the three distinct types of particles have different compositions. The strong association of Factor82 with bSOA on Cluster82 particles that contain sulfate from power plants (time series correlation of r=0.80 and cosine similarity of mass spectra of 0.97) indicates that partitioning of IEPOX to particles was likely chemically selective. More than 76% of the sulfate ion signal is in Cluster82, and the sulfate signal fraction is 0.17 for Cluster82 but less than 0.08

for the other two clusters. This difference is shown in Figure 1.9. This preference for Factor82 condensing onto particular particles could be driven by reactive uptake caused by sulfate, acidity, or other components [*Gaston et al.*, 2014a; *Lin et al.*, 2012; *Riedel et al.*, 2015; *Surratt et al.*, 2010; *Surratt et al.*, 2006] but the correlation to sulfate indicates that sulfate is likely a controlling reactant. In addition, potential organosulfate group concentrations measured by FTIR correlated moderately with Factor82 (r=0.69), providing a direct role for sulfate in the particle-phase reactions. The organosulfate is likely related to the IEPOX-derived organosulfates that were previously reported at Look Rock to be the most abundant organosulfates [*Budisulistiorini et al.*, 2015], further showing that particle-phase reactions of IEPOX with sulfate may have been the reactions that effectively pulled the gas-to-particle equilibrium toward the particle phase. In contrast, the inorganic components from Cluster44 and Cluster91 are very similar to each other, and Factor91 is not as strongly correlated to Cluster91 (Table 1.2), meaning that production pathways of the "vehicle-related SOA" and the "nitrate-related bSOA" are, in contrast, independent of inorganic particle composition and hence likely limited by gas-phase reactions. Figure 1.6(b) shows a schematic diagram of the sources, processes, and resulting mixture of aerosol particle types that are consistent with these observations.

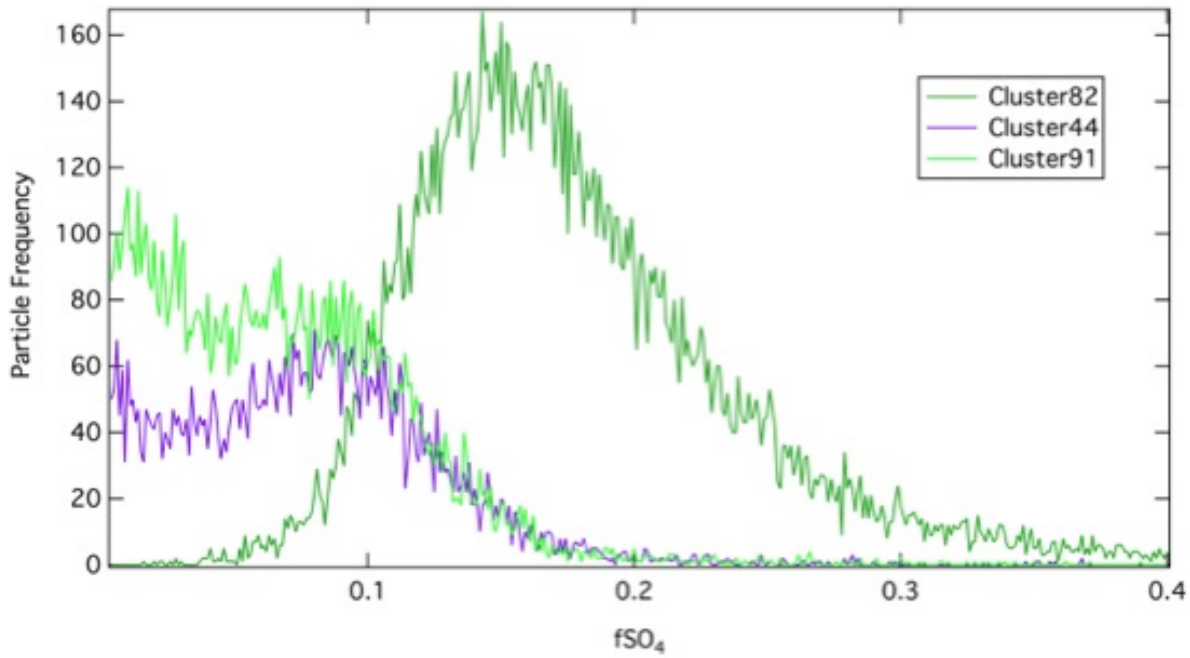

Figure 1.9: Frequency histogram of sulfate mixing ratio in three LS clusters.

The timing of emissions from collocated sources could also have contributed to the separation of the factors onto different particles and may explain the association of Factor44 with Cluster44 (r=0.66) and BC (r=0.73) since vehicles emit both BC and Factor44 precursors. However, the correlation of Factor82 (isoprene-related) bSOA with (anthropogenic) sulfate (r=0.72) and organosulfate (r=0.69) cannot be explained by collocation.

1.4 Conclusions

Stagnation events with lower wind speed were an important factor controlling day-to-day changes in aerosol concentration at Look Rock during SOAS, masking the typical diurnal pattern expected for secondary photochemical aerosol. However, aerosol loading in the boundary layer column from scaling concentrations by reanalysis estimates of boundary layer height showed a peak in the afternoon for all factors and clusters that correlated to solar radiation and isoprene concentration, consistent with sunlight-driven reactions. Daytime loading in the boundary layer

column of organic aerosols is estimated to account for 92% of the daily column loading during the campaign, consistent with the expectation that photochemical reaction is the likely mechanism for most of the secondary aerosol formation at the site.

The similarity of the three types of single particles and the three mass-based factors as well as the significant differences between the particle types suggest that the aerosol particles were largely separated into three distinct types of organic particles. The most oxidized organic aerosol type and factor (Factor44 and Cluster44) were from (at least in part) vehicle-related sources and accounted for 42% of particle mass and 28% of particle number. The "sulfate-related" bSOA Factor82 and Cluster82 were similar to factors identified previously as produced from isoprene oxidation under low-NO pathways in the presence of acidic sulfate aerosol [*Budisulistiorini et al.*, 2013; *Budisulistiorini et al.*, 2015; *Xu et al.*, 2015b] and accounted for 20% of the mass and 35% of the number of the measured aerosol. The "nitrate-related" bSOA (Factor91 and Cluster91) had similar time series correlation to nitrate concentration as Factor44 and similar nitrate fraction as Cluster 44 and accounted for 34% of mass and 37% of number of the measured aerosol.

The strong time series correlation (r=0.80) of the mass-based Factor82 and the number-based Cluster82 as well as the distinct differences between the three particle types provides the most direct single-particle composition evidence to date of the selective uptake of biogenic volatile organic compound oxidation products onto particles containing (anthropogenic) sulfate. Since the Cluster82 particle type has 76% of the sulfate on all clusters of the detected single particle size range, this correlation and composition provide a strong indication that particle-phase reactions of isoprene-derived oxidation products with sulfate were responsible for

Factor82. This pathway is also consistent with the moderate correlation (r=0.69) between Factor82 and organosulfate groups and fragments as well as with laboratory identification of organosulfate formation pathways [*Budisulistiorini et al.*, 2015; *Surratt et al.*, 2010]. In contrast, the moderate correlation (r=0.65) of nitrate with "nitrate-related" bSOA (Factor91) and the weak correlation of Factor91 with Cluster91 (r=0.48), as well as the lower nitrate signal (39%) on Cluster91 than sulfate signal (76%) on Cluster82, mean that composition-dependent particle-phase reactions likely did not contribute to Factor91 bSOA.

The similarity and correlation of the mass and single particle chemical compositions provide the first direct evidence of selective uptake of isoprene-related bSOA onto sulfate-containing particles. These results show the significance of heterogeneous reactions on sulfate particles from anthropogenic emissions for bSOA and specifically link the near doubling of bSOA to sulfate from power plants in the region. Recent studies have shown that hygroscopicity [Cerully et al., 2015] and optical properties [Washenfelder et al., 2015] are related to different PMF factors of organic aerosols in the southeastern U.S. Combining these findings with the identification of the three distinct particle types in this study implies that the optical and drop-nucleating properties of each particle type may be different from those of other types. For this reason, future work linking the chemical characterization of particle types to their different properties explicitly would improve constraints on the direct and indirect radiative forcing of particles in the southeastern U.S.

1.5 Acknowledgements

We thank Ashley Corrigan, Janin Guzman-Morales, Katie Kolesar, Xiaolu Zhang, Chris Cappa, Timothy H. Bertram for assistance at the field site. The authors thank Annmarie Carlton, Joost deGouw, Jose Jimenez, and Allen Goldstein for organizing the SOAS campaign and Sherri Hunt for supporting this project. This work was supported by U.S. Environmental Protection Agency grant RD-83540801. This work has not been formally reviewed by the EPA. The views expressed in this document are solely those of the authors, and the EPA does not endorse any products or commercial services mentioned in this publication. The measurements used in this study are curated at http://doi.org/10.6075/J0P26W1T and are available at the project archive http://esrl.noaa.gov/csd/groups/csd7/measurements/2013senex/Ground/DataDownload

Chapter 1, in full, is a reprint of the material as it appears in the *Geophysical Research Letters*, 2017 with slight modifications. Liu, J., Russell, L. M., Lee, A. K. Y., McKinney, K. A., Surratt, J. D., and Ziemann, P. J. "Observational evidence for pollution-influenced selective uptake contributing to biogenic secondary organic aerosols in the southeastern US", Geophysical Research Letters, 44, 8056-8064, 10.1002/2017gl074665, 2017. The dissertation author was the primary investigator and author of this paper.

1.6 Appendix

1.6.1 Instrument Deployment and Field Campaign Specifications

At the Look Rock field site, the aerosol instruments used for this study were housed in a 20’x20’x8’ container with air conditioning set to 21 °C. The nozzle of the inlet for air sampling

was ~5 m AGL and the site was at an elevation of 802 m. Concentration data are reported at ambient pressure. Ambient air was pulled isokinetically through the inlet at about 900 L min^{-1} using a blower to provide sufficient bypass air to keep flow conditions constant [*Bates et al.*, 2012]. Sampled air lines were dried by diffusion driers in the van before distribution to instruments. Teflon filters (Teflo, Gelman Sciences, Ann Arbor, MI) were collected twice per day after a 2.5 μm cyclone (SCC, Rupprecht & Patashnick, East Greenbush, NY) from 0800 to 1900 and from 2000 to 0700 and four per day behind a 1 μm cyclone from 0800~1200, 1200~1600,1600~1900 and 2000~0700. Flow rates were controlled by mass flow controllers at constant volume (MCR-100SLPM, Alicat, Tucson, AZ) and recorded. Collected filters were analyzed by Fourier Transform Infrared spectroscopy (FTIR) to quantify organic functional groups [*Russell et al.*, 2009; *Takahama et al.*, 2013] and 42 filters were selected for X-ray fluorescence (XRF) of major elements above 23 amu (Chester Labnet, Tigard, OR). Dust mass was calculated from XRF assuming elements were present as the following oxides: Na_2O, $MgCO_3$, Al_2O_3, SiO_2, K_2O, $CaCO_3$, TiO_2, Fe_2O_3, MnO, and BaO [*Usher et al.*, 2003].

Isoprene was measured using a proton-transfer-reaction time-of-flight mass spectrometer (PTR-TOF-MS 8000, Ionicon Analytik GmbH, Austria) equipped with switchable reagent ion capability as described in Budisulistiorini et al. [*Budisulistiorini et al.*, 2015] Ambient air was sampled from an inlet mounted on a tower 2 m above the rooftop of a permanent building at the Look Rock site located approximately 20 m from the van in which the aerosol measurements were made.

The light scattering (LS) module of the high-resolution time-of-flight aerodynamic mass spectrometer (AMS, Aerodyne Research, Inc.) uses a 405 nm source that emits a laser beam

through the air beam of the AMS. The length of the AMS chamber is divided by the difference between the time that the laser light is scattered and the time the chopper allows a particle to enter the chamber to give the particle velocity, which is used to determine the time to record the *m/z* spectra of that single particle. The AMS was operated with a 6 min duty cycle. Each cycle consisted of V-mode mass spectra (MS) mode and particle time-of-fight (ptof) mode (2 min), W mode MS (2 min) and a light scattering mode (90 s). The remaining 30 sec in the cycle allowed time for voltage switching between modes.

The particle size distribution from 10 nm to 20 μm was measured by a Scanning Electrical Mobility System (SEMS, Model 2000C, Brechtel Manufacturing Incorporated), an Optical Particle Sizer (OPS, Model 3330,TSI), and an Aerodynamic Particle Sizer (APS, Model 3321, TSI). Meteorological conditions including temperature, relative humidity, precipitation, and wind direction and speed were monitored by a meteorological sensor (HMP45C RH/T, Vaisala Vantaa, Finland). Black carbon (BC), organic carbon (OC) as well as gas-phase sulfur dioxide (SO_2), nitric oxide (NO), and sum of reactive and reservoir nitrogen oxides (NO_y) were also measured in the permanent structure that houses the IMPROVE Great Smoky Mountains National Park site 20 m away, for which details are provided in the supplement file of Budisulistiorini et al. [*Budisulistiorini et al.*, 2015]. IMPROVE sampling during the study Included OC/EC, PM_{10}, $PM_{2.5}$, standard metals and common inorganic components in fine particles every three days.

Density of submicron particles was estimated to be 1.5 g cm^{-3} by comparing the size of the AMS mass-based and SEMS number-based particle modes; AMS Collection efficiency (CE)

was found to be 0.8 by comparing non-refractory mass concentration of AMS and SEMS mass concentration excluding BC and dust [*Kostenidou et al.*, 2007] (Figure 1.10).

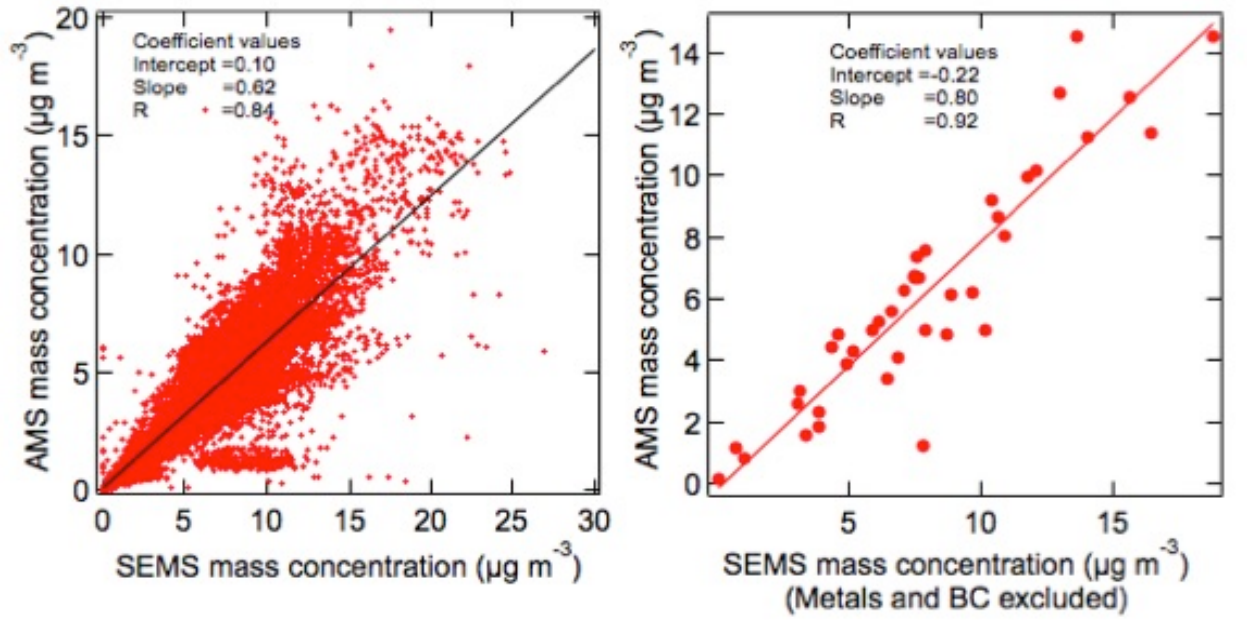

Figure 1.10: Left: Comparison between 6-min averaged V-mode AMS non-refractory mass concentration and EMS mass concentration; Right: Comparison between AMS non-refractory mass concentration and SEMS mass concentration (BC and dust subtracted) for the 42 XRF-analyzed filter sample periods.

1.6.2 PMF Analysis and Factor Selection of AMS Ensemble MS Mode

PMF analysis of the AMS ensemble MS mode measurements was carried out after pretreatment of the PMF input matrix. The data matrix and error matrix were generated from HR organic fragments from the whole campaign using the PIKA module (Tof-AMS HR Analysis 1.15D). The PMF Evaluation Toolkit (PET V2.06) [*Ulbrich et al.*, 2009] was used for PMF analysis. PET served as a front-end for the PMF2 V4.2 executable [*Paatero*, 1997]. No spike removal or data smoothing was applied to the matrices. Signal to noise ratios (SNR) were calculated for each *m/z* value. Values of *m/z* with SNR values smaller than 0.2 were removed

from the PMF analysis. For SNR between 0.2 and 2, the *m/z* was down-weighted by a factor of 2 [*Paatero and Hopke*, 2003]. Since the information from *m/z* 44 is repeated in several related ions (*m/z* 16, 17, 18, 28, 44), we down-weighted those ions so that *m/z* 44 will only contribute to the signal once. The details of this approach are provided by the Appendix of [*Ulbrich et al.*, 2009].

PMF solutions with 1 to 7 factors were explored at 11 different Fpeak values (±1, ±0.8, ±0.6, ±0.4, ±0.2,0). The decrease of minimum Q/Qexpected was used as a mathematical diagnostic [*Paatero et al.*, 2002] and was significant from the 1-factor to 2-factor solution and from the 2-factor to 3-factor solution. The decrease was negligible for more than 3 factors, indicating that the improvement of the solution for 4 or more factors was limited. The different rotations resulted in nearly identical factors and the minimum Q/Qexpected was always at zero rotation, leading us to choose Fpeak = 0 to represent the results. The sum of the factors reconstructed 90% of the OM even with only the 2-factor solution. The 2-factor solution consisted of one oxygenated factor and one HOA-like factor and was not useful because the time series of the two factors were nearly identical. The results from solutions with 4, 5, 6, and 7 factors also had at least one pair of factors that had almost identical *m/z* profiles. That is likely due to splitting of some sources into multiple factors. For example, two factors in the 4 factor-solution have similar time series (r=0.87) and spectra profiles (r=0.93) (Figure 1.11).

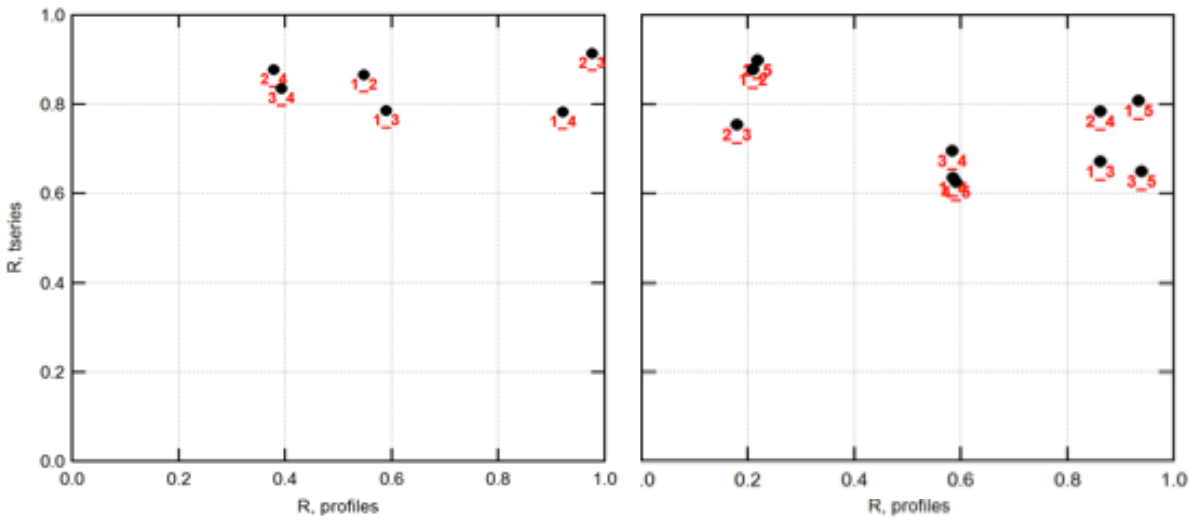

Figure 1.11: The uncentered correlation coefficients plot for (a) 4-factor solution (fpeak=0) and (b) 5-factor solution (fpeak=0).

To describe correlation strength, we use the definition that the correlation is weak if $0 < |r| < 0.5$, strong if $0.80 < |r| < 1$, and moderate if $0.5 < |r| < 0.80$ [Devore and Berk, 2012]. The time series correlations reported here are for instantaneous rather than time-lagged measurements. Since SOA involves multiple precursors and products, some of which are anti-correlated to each other, the correlations are not expected to be very strong, consistent with the fact that none are above 0.9. The correlations of all factors with tracers are in Table 1.3.

Table 1.3: Tracer Correlations with AMS PMF Factors.

Correlation Coefficient (R)	Factor44	Factor82	Factor91
SO_2	0.16	0.16	0.03
NO_x	0.10	-0.01	0.06
CO	0.61	0.50	0.47
NO	0.05	-0.03	-0.11
NO_Y	0.55	0.29	0.46
BC	0.73	0.52	0.53
SO_4 AMS	0.75	0.72	0.56
NO_3 AMS	0.63	0.35	0.65
NH_4 AMS	0.74	0.66	0.57
O_3	0.68	0.37	0.47
Radiation	0.18	0.01	0.20
Isoprene	0.26	0.11	0.26
MVK and	0.66	0.56	0.67
Benzene	0.49	0.29	0.51
Potential	0.43	0.69	0.31
Organonitrate	0.18	0.12	0.17
Factor44	-	0.59	0.72
Factor82	0.59	-	0.49
Factor91	0.72	0.49	-

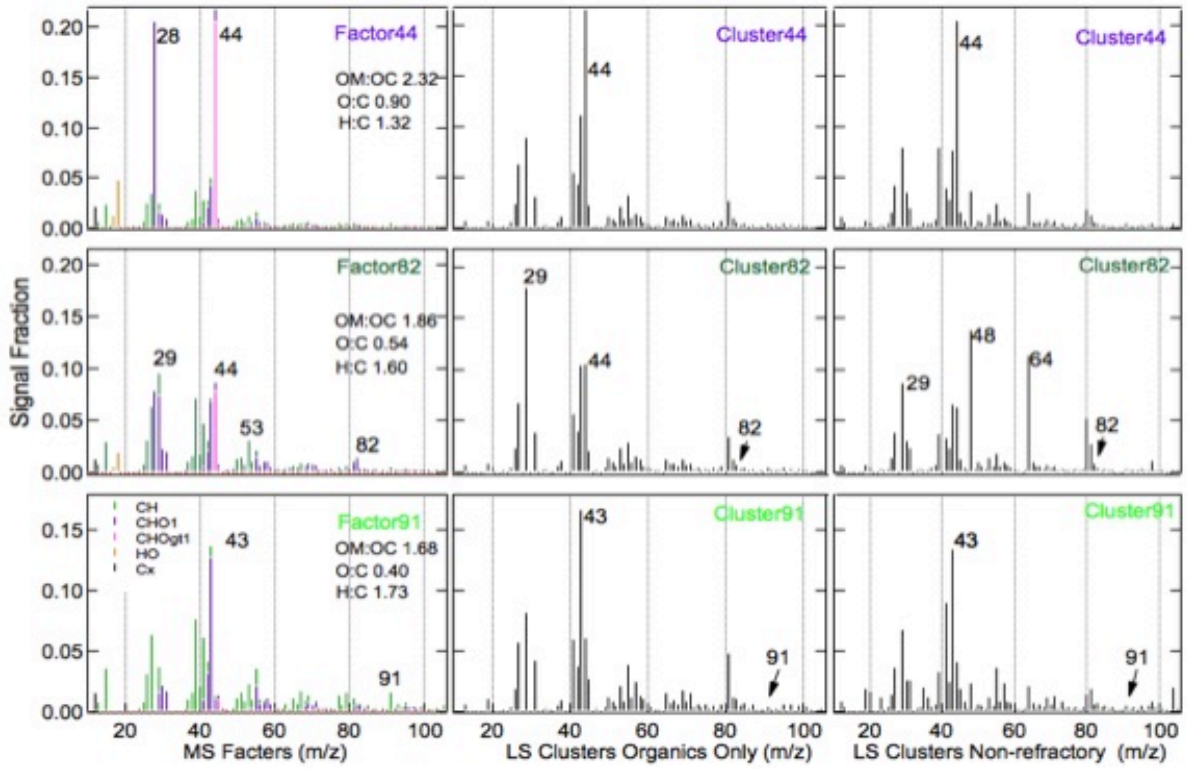

Figure 1.12: AMS m/z spectra for MS V mode factors and LS mode clusters. For clusters, both solutions including non-refractory and organic only are shown.

The 3-factor solution (Figure 1.12) with Fpeak=0 was selected because it minimized Q/Qexpected and contained distinct spectra and independent factors (no correlation between any two factors has uncentered R larger than 0.8, as shown in Table 1.4). Factors were named by characteristic *m/z* values. The three factors are similar to three PMF factors from Aerosol Chemical Speciation Monitor (ACSM) in the same campaign [Budisulistiorini et al., 2015] with cosine similarities higher than 0.66 and time series correlations of greater than 0.87.

Table 1.4: AMS PMF Factor Number Evaluation.

Criteria \ Factor Number	1	2	3	4	5	6	7
Q/Q_{exp}	3.10	2.66	2.20	1.99	1.79	1.70	1.60
Absolute residual	13.1%	9.0%	8.2%	7.8%	6.6%	5.9%	5.6%
Temporal correlation factor strength (r>0.8)	N/A	1 pair	None	1 pair	1 pari	1 pair	1 pair
Similarity of factor spectra (r>0.8)	N/A	None	None	1 pair	4 pairs	6 pairs	8 pairs
Factors with less than 10% OM	None	None	None	None	None	1 pair	2 pairs

Factor44 is not likely to be associated with biomass burning because there was no evidence of biomass burning tracers, such as *m/z* 60 associated with levoglucosan [Elsasser et al., 2012]). In addition, elemental biomass burning markers potassium [Fine et al., 2001] and bromine [Mano and Andreae, 1994] measured by XRF were consistently low (0.0018± 0.0014 μg m^{-3} and 0.0012± 0.0008 μg m^{-3}, respectively) during the campaign and their correlation with BC was weak (r=0.44 and 0.41, respectively). HYSPLIT back-trajectories associated with high Factor44 were not associated with power plant locations (Appendix Figure 1.8). The association of Factor44 with BC and not with biomass burning or power plants makes vehicle combustion the most likely source of VOC precursors of this factor, but an additional contribution from bVOCs [Budisulistiorini et al., 2015; Xu et al., 2015b] has not been ruled out.

1.6.3 AMS LS Mode Operation, K-means Analysis and Cluster Selection

AMS LS-mode measurements were collected for 33 days during the campaign (11-13 June and 20 June to 17 July). 184012 particle events were triggered, 43921 (25%) of them were considered to be "prompt" (the mass spectrum of the particle is recorded at a time consistent with the particle size and velocity) [*Cross et al.*, 2009]. The threshold of "null" particles was set in the

CIPP panel [*Lee et al.*, 2015], and the light scattering measurements were processed by SPARROW 1.04F (http://cires1.colorado.edu/jimenez-group/ToFAMSResources/ToFSoftware/).

The number of particles measured was scaled by the duty cycle of the LS mode (90 s in 360 s) in order to represent the ensemble aerosol components. 4 background-related fragments *m/z* 18 (H_2O^+), 28 (N_2^+), 32 (O_2^+), and 39 (K^+) were removed from the analysis. 16 *m/z* signals containing both organic and inorganic fragments (*m/z* 15, 30, 35, 36, 41, 43, 46, 48, 55, 57, 64, 71, 73, 80, 81, 98) were chosen based on MS mode measurements to estimate signal abundance of single particles.

The distribution of LS "prompt" particles was compared to the SEMS distribution to calibrate the size range of single particles collected in this study. The density of 1.5 g cm^{-3} was applied to convert from aerodynamic to mobility diameter based on the comparison of pToF and SEMS peaks described above. Figure 1.8 shows that LS particles were detected in the dry vacuum aerodynamic diameter range of 350 to 700 nm, which corresponds to 230 to 460 nm mobility diameters at 1.5 g cm^{-3}. LS only detected about 16% of the particles at 450 nm vacuum aerodynamic diameter (Dva), similar to the results of Liu et. al. [2013]. The likely explanation for the lower detection efficiency relative to the theoretical value is that the laser beam was not aligned to completely coincide with the air beam of the AMS. Comparing the SEMS and LS particle size distributions shows that LS captured the majority of particle mass and number since they were below 400 nm Dva (270 mobility diameter), reducing the extent to which the low collection efficiency could bias the analysis.

K-means clustering was applied to the LS measurements using the cluster analysis panel (CAP) after ammonium signals were removed [*Lee et al.*, 2015]. The clustering was applied to

the mass fragment spectra both including and excluding inorganic fragments. Solutions with 1 to 10 clusters were explored, and the 3-cluster solution (Figure 1.12) was chosen because the total distance from the 1- and 2-factor solutions are still large while similar clusters from splitting showed up in 4 and more cluster solutions (Table 1.5). The 3-cluster solutions with and without inorganic components were nearly identical in both concentration and *m/z* spectra. The clusters without inorganic components are more suitable for comparison to PMF factors. Cluster44 accounts for 28% of the particle number while Cluster82 and Cluster91 have 35% and 37%, respectively.

Table 1.5: AMS LS K-Means Cluster Number Evaluation.

Cluster Number / Criteria	1	2	3	4	5	6	7	8	9	10
Total distance	1071	916	830	784	753	739	715	698	684	671
Temporal correlation Cluster strength (r>0.8)	N/A	None	None	2 pairs	2 pairs	1 pair	3 pairs	4 pairs	5 pairs	6 pairs
Similarity of Cluster spectra (r>0.8)	N/A	None	None	1 pair	6 pairs	5 pairs	7 pairs	11 pairs	11 pairs	15 pairs
Cluster with less than 10% of particle number	None	None	None	None	None	None	None	2 pairs	2 pairs	4 pairs

All particle clusters that were identified contained a substantial fraction of organic components. The fragments *m/z* 82 and *m/z* 91 have lower signal fractions in Cluster82 and

Cluster91 than in the factors, but the cosine similarity is high between Cluster82 and Factor82 (0.97) and between Cluster91 and Factor91 (0.93). Comparing the cluster compositions shows that *m/z* 91 in Cluster91 has the highest signal fraction of all three clusters as does m/z 82 in Cluster82. Since the correlations of *m/z* 44 and Factor44, *m/z* 82 and Factor82, and *m/z* 91 and Factor91 are strong (r=0.91,0.92 and 0.94, respectively, as given in Table 1.2), the size distributions of *m/z* 44, 82 and 91 provide proxies for the size distributions of the three factors. The size distribution of m/z 44 and OM show a size mode with peak near 400 nm, and *m/z* 82 and sulfate mass had modes centered near 500 nm, similar to Hu [2016]. The difference between the mass fraction of Factor44 and the number fraction of Cluster44 results in part from the lower limit of detection of LS compared to MS modes of the HR-AMS, since the mass mode of *m/z* 44 (which is correlated in time with Factor44) is smaller than that of *m/z* 82 or *m/z* 91 (which are associated with Factor82 and Factor91, respectively), as shown in Fig. S4. Specifically the fraction of *m/z* 44 mass that is smaller than 350 nm Dva is 40% compared to only 25% of *m/z* 82 (Figure 1.13), meaning that more Cluster44 particles are missed by LS than Cluster82 particles.

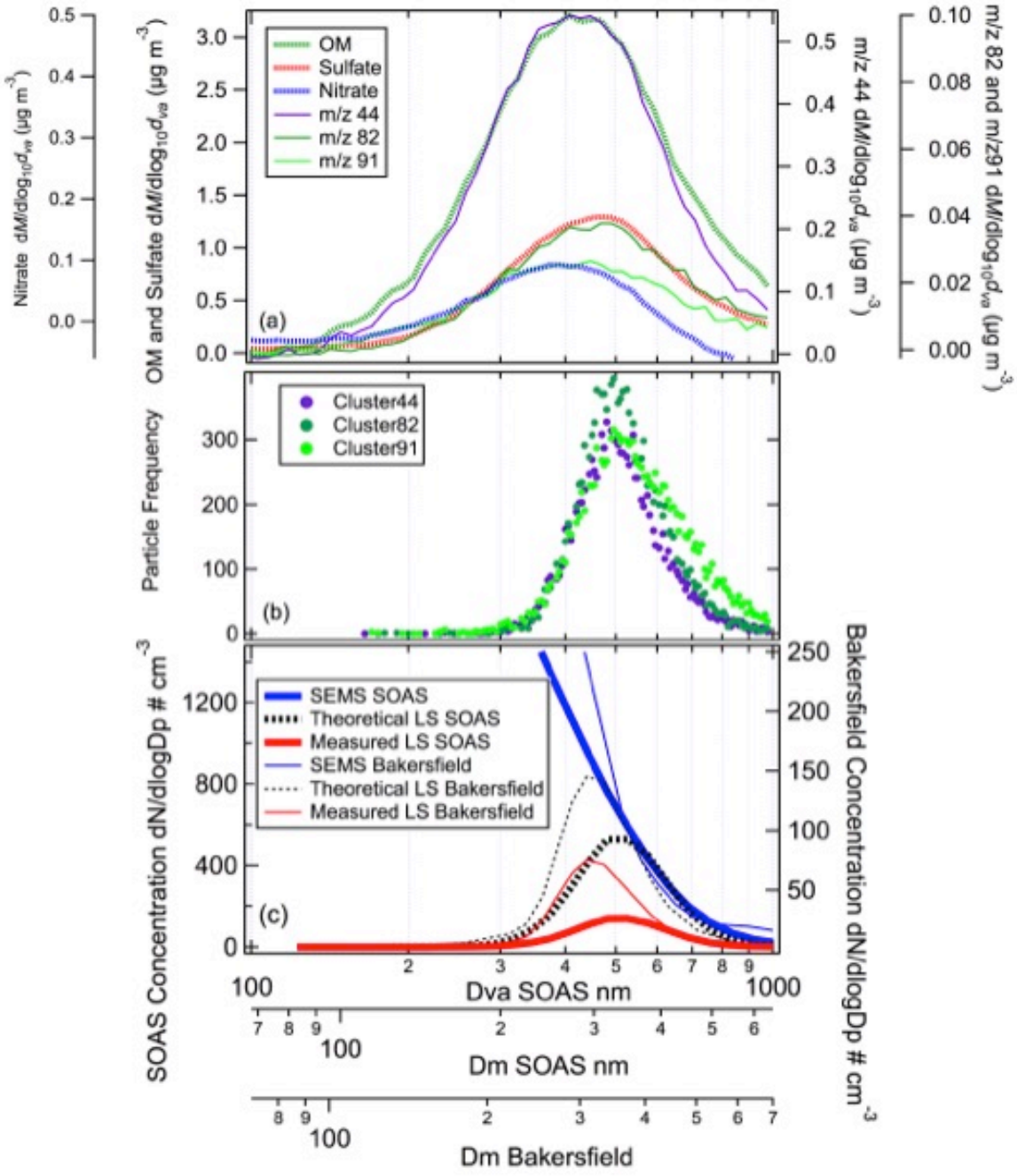

Figure 1.13: (a) Size distributions of OM, sulfate, nitrate, m/z 44, m/z 82 and m/z 91. (b) Size distributions of Cluster44, Cluster82 and Cluster91. (c) Light Scattering collection efficiency compared to SEMS from SOAS (this study) and Bakersfield [Liu et al., 2013]. Both Dva (Vacuum Aerodynamic Diameter) and Dm (Mobility Diameter) are shown.

1.6.4 Back Trajectories and Boundary Layer Heights from Reanalysis Models

The Hybrid Single Particle Lagrangian Integrated Trajectory (HYSPLIT) model was used to compute back trajectories of air parcels ending at the Look Rock site [*Draxier and Hess*, 1998]. The starting points of back trajectories were at 50 m, 100 m and 200 m above the site, and the default option of constraining the vertical velocity to the meteorological data field was used. To evaluate the performance of the HYSPLIT model for this location and time period, the modeled transport speed of the air parcel arriving at the site was found to compare reasonably well to the wind speed measured at the site (Figure 1.14).

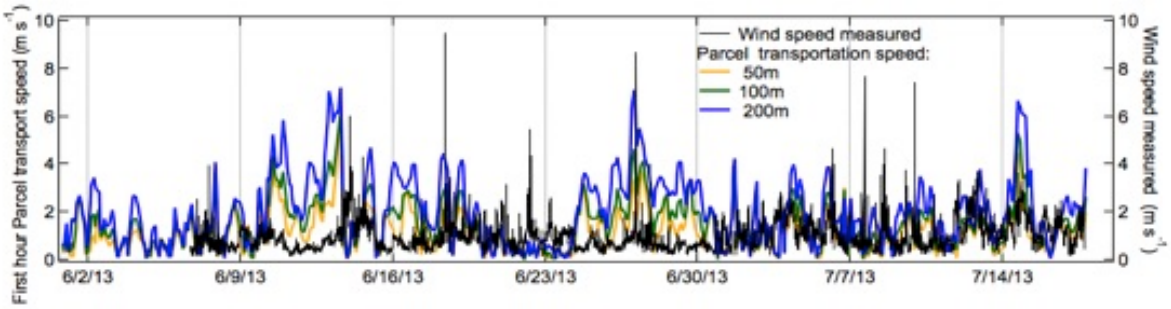

Figure 1.14: Measured CDNC and LWC correlate for the SJL01A (left) and SJL13A (right) cases.

Two reanalysis models and four regional atmospheric sounding locations were compared to estimate the boundary layer height (BLH) at the Look Rock site. Hourly BLH data was retrieved from 12 km NAM (North American Mesoscale Model) hybrid sigma pressure coordinate data though HYPSLIT. The Monitoring Atmospheric Composition and Climate (MACC) model from the European Centre for Medium-Range Weather Forecasts (ECMWF) was also used for BLH hourly with a 0.125-degree grid box. The four atmospheric sounding locations used are Nashville, Greensboro, Blacksburg and Peachtree City. BLH was retrieved

and interpreted as the mixed layer height according to the method of Wang and Wang [2014]. BLH from the soundings and reanalysis models generally agreed well (Figure 1.2). Since there was no evident daily pattern of upslope and downslope winds or any indication of free troposphere intrusions in the concentrations at the site, BLH was assumed to be terrain-following such that the grid-cell BLH from ECMWF was interpreted to be the same height above the site as simulated for the height above the grid-cell average altitude.

The assumption of a well-mixed boundary layer is used in the calculation of OM loadings in the boundary layer column. The aircraft profiles from non-mountainous parts of the southeastern US consistently show an approximately 1.2 km well-mixed boundary layer topped by a transition layer that extends to a height of 2.2 km above ground on average [Wagner et al., 2015]. If these results are representative of the Look Rock region and constant throughout the day, then the magnitude of the loading should be adjusted to include the transition layer but the daily pattern and the relative fraction of OM from daytime photochemistry that is reported here (92%) would not be changed. In the absence of aircraft profiles for Look Rock during this study to characterize a transition layer, we have used the simple approach of the single well-mixed layer retrieved from the HYSPLIT and ECMWF model simulations.

1.6.5 Organic Nitrate Calculation using NO^+ and NO_2^+ Method

The AMS organic nitrate calculation followed the method in Xu et. al. [2015a]. The organic nitrate is calculated with the following equation:

$$NO^+_{2,org} = \frac{NO^+_{2,obs} \times (R_{obs} - R_{AN})}{(R_{ON} - R_{AN})}, \quad NO^+_{org} = R_{ON} \times NO^+_{2,org}$$

Where

R_{AN} = ratio of $NO^+_{AN}/NO^+_{2,AN}$ from ammonium nitrate from Ionization Efficiency (IE) calibrations;

R_{ON} = ratio of $NO^+_{ON}/NO^+_{2,ON}$ from organonitrate standard;

R_{obs}= ratio of $NO^+_{obs}/ NO^+_{2,obs}$ from AMS ambient measurements.

Since R_{AN} is instrument dependent, R_{AN}=3 was used, consistent with SOAS calibration measurements. Given upper and lower bound values of $\chi = R_{ON}/R_{AN}$ of 1.9 and 4.3 [Xu et al. [2015a] assuming the conditions of that study are sufficiently similar to this study, the resulting values were 0.053 μg m^{-3} for NO^+_{obs} and 0.008 μg m^{-3} for NO^+_{obs}. Organic nitrate accounted for 29% to 100% of nitrate mass depending on the value used for χ, accounting for 0.49% to 1.6% of OM. If we assume the molecular weight of the molecule that contains organic nitrate is between 200 g mol^{-1} and 300 g mol^{-1}, then organic nitrate can account for 3.2% to 16.4% of the OM. This range is comparable to 5-12% found by [*Xu et al.*, 2015a] at multiple southeastern U.S. sites during summertime.

References

Allan, J. D., Topping, D. O., Good, N., Irwin, M., Flynn, M., Williams, P. I., Coe, H., Baker, A. R., Martino, M., Niedermeier, N., Wiedensohler, A., Lehmann, S., Mueller, K., Herrmann, H., and McFiggans, G.: Composition and properties of atmospheric particles in the eastern Atlantic and impacts on gas phase uptake rates, Atmospheric Chemistry and Physics, 9, 9299-9314, 2009.

Bahadur, R., Russell, L. M., Jacobson, M. Z., Prather, K., Nenes, A., Adams, P., and Seinfeld, J. H.: Importance of composition and hygroscopicity of BC particles to the effect of BC mitigation on cloud properties: Application to California conditions, Journal of Geophysical Research-Atmospheres, 117, 10.1029/2011jd017265, 2012.

Barahona, D., West, R. E. L., Stier, P., Romakkaniemi, S., Kokkola, H., and Nenes, A.: Comprehensively accounting for the effect of giant CCN in cloud activation parameterizations, Atmospheric Chemistry and Physics, 10, 2467-2473, 2010.

Betancourt, R. M., Lee, D., Oreopoulos, L., Sud, Y. C., Barahona, D., and Nenes, A.: Sensitivity of cirrus and mixed-phase clouds to the ice nuclei spectra in McRAS-AC: single column model simulations, Atmospheric Chemistry and Physics, 12, 10679-10692, 10.5194/acp-12-10679-2012, 2012.

Betancourt, R. M., and Nenes, A.: Droplet activation parameterization: the population-splitting concept revisited, Geoscientific Model Development, 7, 2345-2357, 10.5194/gmd-7-2345-2014, 2014.

Bohren, C. F., and Battan, L. J.: RADAR BACKSCATTERING BY INHOMOGENEOUS PRECIPITATION PARTICLES, Journal of the Atmospheric Sciences, 37, 1821-1827, 10.1175/1520-0469(1980)037<1821:rbbipp>2.0.co;2, 1980.

Charlson, R. J., Lovelock, J. E., Andreae, M. O., and Warren, S. G.: OCEANIC PHYTOPLANKTON, ATMOSPHERIC SULFUR, CLOUD ALBEDO AND CLIMATE, Nature, 326, 655-661, 10.1038/326655a0, 1987.

Chuang, P. Y.: Sensitivity of cloud condensation nuclei activation processes to kinetic parameters, Journal of Geophysical Research-Atmospheres, 111, 10.1029/2005jd006529, 2006.

Coggon, M. M., Sorooshian, A., Wang, Z., Metcalf, A. R., Frossard, A. A., Lin, J. J., Craven, J. S., Nenes, A., Jonsson, H. H., Russell, L. M., Flagan, R. C., and Seinfeld, J. H.: Ship impacts on the marine atmosphere: insights into the contribution of shipping emissions to the properties of marine aerosol and clouds, Atmospheric Chemistry and Physics, 12, 8439-8458, 10.5194/acp-12-8439-2012, 2012.

Collins, D. B., Ault, A. P., Moffet, R. C., Ruppel, M. J., Cuadra-Rodriguez, L. A., Guasco, T. L., Corrigan, C. E., Pedler, B. E., Azam, F., Aluwihare, L. I., Bertram, T. H., Roberts, G. C., Grassian, V. H., and Prather, K. A.: Impact of marine biogeochemistry on the chemical mixing state and cloud forming ability of nascent sea spray aerosol, Journal of Geophysical Research-Atmospheres, 118, 8553-8565, 10.1002/jgrd.50598, 2013.

Conant, W. C., VanReken, T. M., Rissman, T. A., Varutbangkul, V., Jonsson, H. H., Nenes, A., Jimenez, J. L., Delia, A. E., Bahreini, R., Roberts, G. C., Flagan, R. C., and Seinfeld, J. H.: Aerosol-cloud drop concentration closure in warm cumulus, Journal of Geophysical Research-Atmospheres, 109, 10.1029/2003jd004324, 2004.

Craven, J. P., Jewell, R. E., and Brooks, H. E.: Comparison between observed convective cloud-base heights and lifting condensation level for two different lifted parcels, Weather and Forecasting, 17, 885-890, 10.1175/1520-0434(2002)017<0885:cboccb>2.0.co;2, 2002.

Cruz, C. N., and Pandis, S. N.: A study of the ability of pure secondary organic aerosol to act as cloud condensation nuclei, Atmospheric Environment, 31, 2205-2214, 10.1016/s1352-2310(97)00054-x, 1997.

Cruz, C. N., and Pandis, S. N.: Deliquescence and hygroscopic growth of mixed inorganic-organic atmospheric aerosol, Environmental Science & Technology, 34, 4313-4319, 10.1021/es9907109, 2000.

DeCarlo, P. F., Kimmel, J. R., Trimborn, A., Northway, M. J., Jayne, J. T., Aiken, A. C., Gonin, M., Fuhrer, K., Horvath, T., Docherty, K. S., Worsnop, D. R., and Jimenez, J. L.: Field-deployable, high-resolution, time-of-flight aerosol mass spectrometer, Analytical Chemistry, 78, 8281-8289, 10.1021/ac061249n, 2006.

Dusek, U., Frank, G. P., Hildebrandt, L., Curtius, J., Schneider, J., Walter, S., Chand, D., Drewnick, F., Hings, S., Jung, D., Borrmann, S., and Andreae, M. O.: Size matters more than chemistry for cloud-nucleating ability of aerosol particles, Science, 312, 1375-1378, 10.1126/science.1125261, 2006.

Erlick, C., Khain, A., Pinsky, M., and Segal, Y.: The effect of wind velocity fluctuations on drop spectrum broadening in stratocumulus clouds, Atmospheric Research, 75, 15-45, 10.1016/j.atmosres.2004.10.007, 2005.

Ervens, B., Cubison, M. J., Andrews, E., Feingold, G., Ogren, J. A., Jimenez, J. L., Quinn, P. K., Bates, T. S., Wang, J., Zhang, Q., Coe, H., Flynn, M., and Allan, J. D.: CCN predictions using simplified assumptions of organic aerosol composition and mixing state: a synthesis from six different locations, Atmospheric Chemistry and Physics, 10, 4795-4807, 10.5194/acp-10-4795-2010, 2010.

Facchini, M. C., Rinaldi, M., Decesari, S., Carbone, C., Finessi, E., Mircea, M., Fuzzi, S., Ceburnis, D., Flanagan, R., Nilsson, E. D., de Leeuw, G., Martino, M., Woeltjen, J., and O'Dowd, C. D.: Primary submicron marine aerosol dominated by insoluble organic colloids and aggregates, Geophysical Research Letters, 35, 10.1029/2008gl034210, 2008.

Feingold, G., Eberhard, W. L., Veron, D. E., and Previdi, M.: First measurements of the Twomey indirect effect using ground-based remote sensors, Geophysical Research Letters, 30, 10.1029/2002gl016633, 2003.

Feingold, G., McComiskey, A., Rosenfeld, D., and Sorooshian, A.: On the relationship between cloud contact time and precipitation susceptibility to aerosol, Journal of Geophysical Research-Atmospheres, 118, 10544-10554, 10.1002/jgrd.50819, 2013.

Fountoukis, C., and Nenes, A.: Continued development of a cloud droplet formation parameterization for global climate models, Journal of Geophysical Research-Atmospheres, 110, 10.1029/2004jd005591, 2005.

Frossard, A. A.: Investigation of the sources and composition of submicron organic aerosol particles in marine environments through artificial generation and atmospheric measurements, Doctor of Philosophy in Oceanography, Scripps Institution of Oceanography, University of California, San Diego, La Jolla, CA, 243 pp., 2014.

Geresdi, I., Meszaros, E., and Molnar, A.: The effect of chemical composition and size distribution of aerosol particles on droplet formation and albedo of stratocumulus clouds, Atmospheric Environment, 40, 1845-1855, 10.1016/j.atmosenv.2005.11.012, 2006.

Ghate, V. P., Albrecht, B. A., and Kollias, P.: Vertical velocity structure of nonprecipitating continental boundary layer stratocumulus clouds, Journal of Geophysical Research-Atmospheres, 115, 10.1029/2009jd013091, 2010.

Gysel, M., Crosier, J., Topping, D. O., Whitehead, J. D., Bower, K. N., Cubison, M. J., Williams, P. I., Flynn, M. J., McFiggans, G. B., and Coe, H.: Closure study between chemical composition and hygroscopic growth of aerosol particles during TORCH2, Atmospheric Chemistry and Physics, 7, 6131-6144, 2007.

Hawkins, L. N., Russell, L. M., Covert, D. S., Quinn, P. K., and Bates, T. S.: Carboxylic acids, sulfates, and organosulfates in processed continental organic aerosol over the southeast Pacific Ocean during VOCALS-REx 2008, Journal of Geophysical Research-Atmospheres, 115, 10.1029/2009jd013276, 2010.

Hayden, K. L., Macdonald, A. M., Gong, W., Toom-Sauntry, D., Anlauf, K. G., Leithead, A., Li, S. M., Leaitch, W. R., and Noone, K.: Cloud processing of nitrate, Journal of Geophysical Research-Atmospheres, 113, 10.1029/2007jd009732, 2008.

Healy, R. M., Evans, G. J., Murphy, M., Juranyi, Z., Tritscher, T., Laborde, M., Weingartner, E., Gysel, M., Poulain, L., Kamilli, K. A., Wiedensohler, A., O'Connor, I. P., McGillicuddy, E., Sodeau, J. R., and Wenger, J. C.: Predicting hygroscopic growth using single particle chemical composition estimates, Journal of Geophysical Research-Atmospheres, 119, 9567-9577, 10.1002/2014jd021888, 2014.

Hegg, D. A., Covert, D. S., Jonsson, H. H., and Woods, R. K.: The contribution of anthropogenic aerosols to aerosol light-scattering and CCN activity in the California coastal zone, Atmospheric Chemistry and Physics, 10, 7341-7351, 10.5194/acp-10-7341-2010, 2010.

Hersey, S. P., Sorooshian, A., Murphy, S. M., Flagan, R. C., and Seinfeld, J. H.: Aerosol hygroscopicity in the marine atmosphere: a closure study using high-time-resolution, multiple-RH DASH-SP and size-resolved C-ToF-AMS data, Atmospheric Chemistry and Physics, 9, 2543-2554, 2009.

Hsieh, W. C., Nenes, A., Flagan, R. C., Seinfeld, J. H., Buzorius, G., and Jonsson, H.: Parameterization of cloud droplet size distributions: Comparison with parcel models and observations, Journal of Geophysical Research-Atmospheres, 114, 10.1029/2008jd011387, 2009.

Hudson, J. G., and Noble, S.: CCN and Vertical Velocity Influences on Droplet Concentrations and Supersaturations in Clean and Polluted Stratus Clouds, Journal of the Atmospheric Sciences, 71, 312-331, 10.1175/jas-d-13-086.1, 2014.

Jacobson, M. Z., Turco, R. P., Jensen, E. J., and Toon, O. B.: MODELING COAGULATION AMONG PARTICLES OF DIFFERENT COMPOSITION AND SIZE, Atmospheric Environment, 28, 1327-1338, 10.1016/1352-2310(94)90280-1, 1994.

Lance, S., Brock, C. A., Rogers, D., and Gordon, J. A.: Water droplet calibration of the Cloud Droplet Probe (CDP) and in-flight performance in liquid, ice and mixed-phase clouds during ARCPAC, Atmospheric Measurement Techniques, 3, 1683-1706, 10.5194/amt-3-1683-2010, 2010.

Leaitch, W. R., Banic, C. M., Isaac, G. A., Couture, M. D., Liu, P. S. K., Gultepe, I., Li, S. M., Kleinman, L., Daum, P. H., and MacPherson, J. I.: Physical and chemical observations in marine stratus during the 1993 North Atlantic Regional Experiment: Factors controlling cloud droplet number concentrations, Journal of Geophysical Research-Atmospheres, 101, 29123-29135, 10.1029/96jd01228, 1996.

Leaitch, W. R., Lohmann, U., Russell, L. M., Garrett, T., Shantz, N. C., Toom-Sauntry, D., Strapp, J. W., Hayden, K. L., Marshall, J., Wolde, M., Worsnop, D. R., and Jayne, J. T.: Cloud albedo increase from carbonaceous aerosol, Atmospheric Chemistry and Physics, 10, 7669-7684, 10.5194/acp-10-7669-2010, 2010.

Leck, C., and Bigg, E. K.: Source and evolution of the marine aerosol - A new perspective, Geophysical Research Letters, 32, 10.1029/2005gl023651, 2005.

Lenschow, D. H., and Stephens, P. L.: THE ROLE OF THERMALS IN THE CONVECTIVE BOUNDARY-LAYER, Boundary-Layer Meteorology, 19, 509-532, 10.1007/bf00122351, 1980.

Li, X., Wang, L., Chen, D., Yang, K., Xue, B., and Sun, L.: Near-surface air temperature lapse rates in the mainland China during 1962-2011, Journal of Geophysical Research-Atmospheres, 118, 7505-7515, 10.1002/jgrd.50553, 2013.

Massling, A., Stock, M., Wehner, B., Wu, Z. J., Hu, M., Brueggemann, E., Gnauk, T., Herrmann, H., and Wiedensohler, A.: Size segregated water uptake of the urban submicrometer aerosol in Beijing, Atmospheric Environment, 43, 1578-1589, 10.1016/j.atmosenv.2008.06.003, 2009.

McFiggans, G., Artaxo, P., Baltensperger, U., Coe, H., Facchini, M. C., Feingold, G., Fuzzi, S., Gysel, M., Laaksonen, A., Lohmann, U., Mentel, T. F., Murphy, D. M., O'Dowd, C. D., Snider, J. R., and Weingartner, E.: The effect of physical and chemical aerosol properties on warm cloud droplet activation, Atmospheric Chemistry and Physics, 6, 2593-2649, 2006.

Ming, Y., and Russell, L. M.: Organic aerosol effects on fog droplet spectra, Journal of Geophysical Research-Atmospheres, 109, 10.1029/2003jd004427, 2004.

Mochida, M., Nishita-Hara, C., Furutani, H., Miyazaki, Y., Jung, J., Kawamura, K., and Uematsu, M.: Hygroscopicity and cloud condensation nucleus activity of marine aerosol particles over the western North Pacific, Journal of Geophysical Research-Atmospheres, 116, 10.1029/2010jd014759, 2011.

Modini, R. L., Frossard, A. A., Ahlm, L., Russell, L. M., Corrigan, C. E., Roberts, G. C., Hawkins, L. N., Schroder, J. C., Bertram, A. K., Zhao, R., Lee, A. K. Y., Abbatt, J. P. D., Lin, J., Nenes, A., Wang, Z., Wonaschuetz, A., Sorooshian, A., Noone, K. J., Jonsson, H., Seinfeld, J. H., Toom-Sauntry, D., Macdonald, A. M., and Leaitch, W. R.: Primary marine aerosol-cloud

interactions off the coast of California, Journal of Geophysical Research-Atmospheres, 120, 4282-4303, 10.1002/2014jd022963, 2015.

Moffet, R. C., Henn, T., Laskin, A., and Gilles, M. K.: Automated Chemical Analysis of Internally Mixed Aerosol Particles Using X-ray Spectromicroscopy at the Carbon K-Edge, Analytical Chemistry, 82, 7906-7914, 10.1021/ac1012909, 2010.

Moore, R. H., and Nenes, A.: Scanning Flow CCN Analysis-A Method for Fast Measurements of CCN Spectra, Aerosol Science and Technology, 43, 1192-1207, 10.1080/02786820903289780, 2009.

Nenes, A., Pandis, S. N., and Pilinis, C.: ISORROPIA: A new thermodynamic equilibrium model for multiphase multicomponent inorganic aerosols, Aquatic Geochemistry, 4, 123-152, 10.1023/a:1009604003981, 1998.

Nenes, A., Ghan, S., Abdul-Razzak, H., Chuang, P. Y., and Seinfeld, J. H.: Kinetic limitations on cloud droplet formation and impact on cloud albedo, Tellus Series B-Chemical and Physical Meteorology, 53, 133-149, 10.1034/j.1600-0889.2001.d01-12.x, 2001.

Nenes, A., and Seinfeld, J. H.: Parameterization of cloud droplet formation in global climate models, Journal of Geophysical Research-Atmospheres, 108, 10.1029/2002jd002911, 2003.

Nicholls, S., and Leighton, J.: AN OBSERVATIONAL STUDY OF THE STRUCTURE OF STRATIFORM CLOUD SHEETS .1. STRUCTURE, Quarterly Journal of the Royal Meteorological Society, 112, 431-460, 10.1002/qj.49711247209, 1986.

Nicholls, S.: THE STRUCTURE OF RADIATIVELY DRIVEN CONVECTION IN STRATOCUMULUS, Quarterly Journal of the Royal Meteorological Society, 115, 487-511, 10.1002/qj.49711548704, 1989.

Noone, K. J., Ogren, J. A., Heintzenberg, J., Charlson, R. J., and Covert, D. S.: DESIGN AND CALIBRATION OF A COUNTERFLOW VIRTUAL IMPACTOR FOR SAMPLING OF ATMOSPHERIC FOG AND CLOUD DROPLETS, Aerosol Science and Technology, 8, 235-244, 10.1080/02786828808959186, 1988.

Novakov, T., and Corrigan, C. E.: Cloud condensation nucleus activity of the organic component of biomass smoke particles, Geophysical Research Letters, 23, 2141-2144, 10.1029/96gl01971, 1996.

Peng, Y. R., Lohmann, U., and Leaitch, R.: Importance of vertical velocity variations in the cloud droplet nucleation process of marine stratus clouds, Journal of Geophysical Research-Atmospheres, 110, 10.1029/2004jd004922, 2005.

Petters, M. D., and Kreidenweis, S. M.: A single parameter representation of hygroscopic growth and cloud condensation nucleus activity, Atmospheric Chemistry and Physics, 7, 1961-1971, 2007.

Petters, M. D., Kreidenweis, S. M., and Ziemann, P. J.: Prediction of cloud condensation nuclei activity for organic compounds using functional group contribution methods, Geoscientific Model Development, 8, 7445-7475, 10.5194/gmdd-8-7445-2015, 2015, 2015.

Prabhakar, G., Ervens, B., Wang, Z., Maudlin, L. C., Coggon, M. M., Jonsson, H. H., Seinfeld, J. H., and Sorooshian, A.: Sources of nitrate in stratocumulus cloud water: Airborne measurements during the 2011 E-PEACE and 2013 NiCE studies, Atmospheric Environment, 97, 166-173, 10.1016/j.atmosenv.2014.08.019, 2014.

Quinn, P. K., Bates, T. S., Schulz, K. S., Coffman, D. J., Frossard, A. A., Russell, L. M., Keene, W. C., and Kieber, D. J.: Contribution of sea surface carbon pool to organic matter enrichment in sea spray aerosol, Nature Geoscience, 7, 228-232, 10.1038/ngeo2092, 2014.

Raatikainen, T., Nenes, A., Seinfeld, J. H., Morales, R., Moore, R. H., Lathem, T. L., Lance, S., Padro, L. T., Lin, J. J., Cerully, K. M., Bougiatioti, A., Cozic, J., Ruehl, C. R., Chuang, P. Y., Anderson, B. E., Flagan, R. C., Jonsson, H., Mihalopoulos, N., and Smith, J. N.: Worldwide data sets constrain the water vapor uptake coefficient in cloud formation, Proceedings of the National Academy of Sciences of the United States of America, 110, 3760-3764, 10.1073/pnas.1219591110, 2013.

Raymond, T. M., and Pandis, S. N.: Cloud activation of single-component organic aerosol particles, Journal of Geophysical Research-Atmospheres, 107, 10.1029/2002jd002159, 2002.

Reutter, P., Su, H., Trentmann, J., Simmel, M., Rose, D., Gunthe, S. S., Wernli, H., Andreae, M. O., and Poeschl, U.: Aerosol- and updraft-limited regimes of cloud droplet formation: influence of particle number, size and hygroscopicity on the activation of cloud condensation nuclei (CCN), Atmospheric Chemistry and Physics, 9, 7067-7080, 2009.

Rissman, T. A., Nenes, A., and Seinfeld, J. H.: Chemical amplification (or dampening) of the Twomey effect: Conditions derived from droplet activation theory, Journal of the Atmospheric Sciences, 61, 919-930, 10.1175/1520-0469(2004)061<0919:caodot>2.0.co;2, 2004.

Russell, L. M., and Seinfeld, J. H.: Size- and composition-resolved externally mixed aerosol model, Aerosol Science and Technology, 28, 403-416, 10.1080/02786829808965534, 1998.

Russell, L. M., Seinfeld, J. H., Flagan, R. C., Ferek, R. J., Hegg, D. A., Hobbs, P. V., Wobrock, W., Flossmann, A. I., O'Dowd, C. D., Nielsen, K. E., and Durkee, P. A.: Aerosol dynamics in ship tracks, Journal of Geophysical Research-Atmospheres, 104, 31077-31095, 10.1029/1999jd900985, 1999.

Russell, L. M., Sorooshian, A., Seinfeld, J. H., Albrecht, B. A., Nenes, A., Ahlm, L., Chen, Y.-C., Coggon, M., Craven, J. S., Flagan, R. C., Frossard, A. A., Jonsson, H., Jung, E., Lin, J. J., Metcalf, A. R., Modini, R., Muelmenstaedt, J., Roberts, G. C., Shingler, T., Song, S., Wang, Z., and Wonaschuetz, A.: EASTERN PACIFIC EMITTED AEROSOL CLOUD EXPERIMENT, Bulletin of the American Meteorological Society, 94, 709-+, 10.1175/bams-d-12-00015.1, 2013.

Schroder, J. C., Hanna, S. J., Modini, R. L., Corrigan, A. L., Macdonald, A. M., Noone, K. J., Russell, L. M., Leaitch, W. R., and Bertram, A. K.: Size-resolved observations of refractory

black carbon particles in cloud droplets at a marine boundary layer site, Atmospheric Chemistry and Physics Discussions, 14, 11447-11491, 10.5194/acpd-14-11447-2014, 2014.

Shingler, T., Dey, S., Sorooshian, A., Brechtel, F. J., Wang, Z., Metcalf, A., Coggon, M., Muelmenstaedt, J., Russell, L. M., Jonsson, H. H., and Seinfeld, J. H.: Characterisation and airborne deployment of a new counterflow virtual impactor inlet, Atmospheric Measurement Techniques, 5, 1259-1269, 10.5194/amt-5-1259-2012, 2012.

Shulman, M. L., Jacobson, M. C., Carlson, R. J., Synovec, R. E., and Young, T. E.: Dissolution behavior and surface tension effects of organic compounds in nucleating cloud droplets, Geophysical Research Letters, 23, 277-280, 10.1029/95gl03810, 1996.

Snider, J. R., and Brenguier, J. L.: Cloud condensation nuclei and cloud droplet measurements during ACE-2, Tellus Series B-Chemical and Physical Meteorology, 52, 828-842, 10.1034/j.1600-0889.2000.00044.x, 2000.

Snider, J. R., Guibert, S., Brenguier, J. L., and Putaud, J. P.: Aerosol activation in marine stratocumulus clouds: 2. Kohler and parcel theory closure studies, Journal of Geophysical Research-Atmospheres, 108, 10.1029/2002jd002692, 2003.

Sorooshian, A., Wang, Z., Coggon, M. M., Jonsson, H. H., and Ervens, B.: Observations of Sharp Oxalate Reductions in Stratocumulus Clouds at Variable Altitudes: Organic Acid and Metal Measurements During the 2011 E-PEACE Campaign, Environmental Science & Technology, 47, 7747-7756, 10.1021/es4012383, 2013.

Sorooshian, A., Crosbie, E., Maudlin, L. C., Youn, J.-S., Wang, Z., Shingler, T., Ortega, A. M., Hersey, S., and Woods, R. K.: Surface and airborne measurements of organosulfur and methanesulfonate over the western United States and coastal areas, Journal of Geophysical Research-Atmospheres, 120, 8535-8548, 10.1002/2015jd023822, 2015.

Stevens, B., Feingold, G., Cotton, W. R., and Walko, R. L.: Elements of the microphysical structure of numerically simulated nonprecipitating stratocumulus, Journal of the Atmospheric Sciences, 53, 980-1006, 10.1175/1520-0469(1996)053<0980:eotmso>2.0.co;2, 1996.

Tiitta, P., Miettinen, P., Vaattovaara, P., Joutsensaari, J., Petaja, T., Virtanen, A., Raatikainen, T., Aalto, P., Portin, H., Romakkaniemi, S., Kokkola, H., Lehtinen, K. E. J., Kulmala, M., and Laaksonen, A.: Roadside aerosol study using hygroscopic, organic and volatility TDMAs: Characterization and mixing state, Atmospheric Environment, 44, 976-986, 10.1016/j.atmosenv.2009.06.021, 2010.

Twohy, C. H., Anderson, J. R., Toohey, D. W., Andrejczuk, M., Adams, A., Lytle, M., George, R. C., Wood, R., Saide, P., Spak, S., Zuidema, P., and Leon, D.: Impacts of aerosol particles on the microphysical and radiative properties of stratocumulus clouds over the southeast Pacific Ocean, Atmospheric Chemistry and Physics, 13, 2541-2562, 10.5194/acp-13-2541-2013, 2013.

Twomey, S.: Atmospheric Aerosols (Developments in atmospheric science), Elsevier Science Ltd, 316 pp., 1977

Tzivion, S., Feingold, G., and Levin, Z.: An efficient numerical solution to the stochastic collection equation, Journal of the Atmospheric Sciences, 44, 3139-3149, 10.1175/1520-0469(1987)044<3139:aenstt>2.0.co;2, 1987.

VanReken, T. M., Rissman, T. A., Roberts, G. C., Varutbangkul, V., Jonsson, H. H., Flagan, R. C., and Seinfeld, J. H.: Toward aerosol/cloud condensation nuclei (CCN) closure during CRYSTAL-FACE, Journal of Geophysical Research-Atmospheres, 108, 10.1029/2003jd003582, 2003.

Wang, J., Cubison, M. J., Aiken, A. C., Jimenez, J. L., and Collins, D. R.: The importance of aerosol mixing state and size-resolved composition on CCN concentration and the variation of the importance with atmospheric aging of aerosols, Atmospheric Chemistry and Physics, 10, 7267-7283, 10.5194/acp-10-7267-2010, 2010.

West, R. E. L., Stier, P., Jones, A., Johnson, C. E., Mann, G. W., Bellouin, N., Partridge, D. G., and Kipling, Z.: The importance of vertical velocity variability for estimates of the indirect aerosol effects, Atmospheric Chemistry and Physics, 14, 6369-6393, 10.5194/acp-14-6369-2014, 2014.

Wonaschuetz, A., Coggon, M., Sorooshian, A., Modini, R., Frossard, A. A., Ahlm, L., Muelmenstaedt, J., Roberts, G. C., Russell, L. M., Dey, S., Brechtel, F. J., and Seinfeld, J. H.: Hygroscopic properties of smoke-generated organic aerosol particles emitted in the marine atmosphere, Atmospheric Chemistry and Physics, 13, 9819-9835, 10.5194/acp-13-9819-2013, 2013.

Youn, J. S., Crosbie, E., Maudlin, L. C., Wang, Z., and Sorooshian, A.: *Dimethylamine* as a major alkyl amine species in particles and cloud water: Observations in semi-arid and coastal regions, in, Atmospheric Environment, 250-258, 2015.

Zhu, P., Albrecht, B. A., Ghate, V. P., and Zhu, Z.: Multiple-scale simulations of stratocumulus clouds, Journal of Geophysical Research-Atmospheres, 115, 10.1029/2010jd014400, 2010.

Chapter 2

Regional Similarities and NO_x-related Increases in Biogenic Secondary Organic Aerosol in Summertime Southeastern U.S.

During the 2013 Southern Oxidant and Aerosol Study, Fourier Transform Infrared Spectroscopy (FTIR) and Aerosol Mass Spectrometer (AMS) measurements of submicron mass were collected at Look Rock (LRK), Tennessee, and Centreville (CTR), Alabama. Carbon monoxide and submicron sulfate and organic mass concentrations were 15-60% higher at CTR than at LRK but their time series had moderate correlations (r~0.5). However, NO_x had no correlation (r=0.08) between the two sites with nighttime-to-early-morning peaks 3~10 times higher at CTR than at LRK. Organic mass (OM) sources identified by FTIR Positive Matrix Factorization (PMF) had three very similar factors at both sites: Fossil Fuel Combustion (FFC) related organic aerosols, Mixed Organic Aerosols (MOA), and Biogenic Organic Aerosols (BOA). The BOA spectrum from FTIR is similar (cosine similarity > 0.6) to that of lab-generated particle mass from the photochemical oxidation of both isoprene and monoterpenes

under high NO_x conditions from chamber experiments. The BOA mass fraction was highest during the night at CTR but in the afternoon at LRK. AMS PMF resulted in two similar pairs of factors at both sites and a third nighttime NO_x-related factor (33% of OM) at CTR but a daytime nitrate-related factor (28% of OM) at LRK. NO_x was correlated with BOA, LO-OOA and Factor91 for NO_x concentrations higher than 1 ppb at both sites, producing 0.5 to 1 μg m^{-3} additional biogenic OM for each 1 ppb increase of NO_x.

2.1 Introduction

Biogenic secondary organic aerosols (SOA) are estimated to be increased by as much as 78% because of interactions involving anthropogenic emissions on the U.S. east coast [*Carlton et al.*, 2010] and in eastern Asia [*Matsui et al.*, 2014]. The resulting aerosol particle mass may account for as much as 70% of the global organic aerosol budget [*Spracklen et al.*, 2011]. More than 90% of sulfate (from SO_2) and nitrogen oxides (NO_x, or $NO+NO_2$) are anthropogenic and increase the yield of biogenic SOA [*Shilling et al.*, 2013; *Shrivastava et al.*, 2017; *Spracklen et al.*, 2011; *Xu et al.*, 2015a]. For example, some field studies have shown that a 1 μg m^{-3} decrease in sulfate can lead to a 0.2–0.42 μg m^{-3} decrease in isoprene SOA [*Blanchard et al.*, 2016; *Budisulistiorini et al.*, 2017; *Pye et al.*, 2013; *Shrivastava et al.*, 2017; *Xu et al.*, 2015a; *Xu et al.*, 2016]. Similarly, decreases in NO_x have been shown to decrease biogenic SOA formation but there are also studies that have shown increases of biogenic SOA in some regimes with decreased NO_x (Table 1) [*de Sa et al.*, 2017; *Edwards et al.*, 2017; *Kroll et al.*, 2006; *Lane et al.*, 2008; *Liu et al.*, 2016; *Matsui et al.*, 2014; *Ng et al.*, 2007; *Pye et al.*, 2010; *Pye et al.*, 2015; *Pye et al.*, 2013; *Rollins et al.*, 2012; *Wildt et al.*, 2014; *Xu et al.*, 2015a; *Xu et al.*, 2014; *Zhang et al.*, 2017; *Zheng et al.*, 2015]. Since these effects of NO_x have been shown by laboratory studies to affect biogenic SOA formation by changing oxidation pathways and ultimate products [*Atkinson et al., 2004; Hoyle et al., 2011; Kroll et al., 2006; Presto et al., 2005; Shrivastava et al., 2017; Surratt et al., 2006; Ziemann and Atkinson, 2012*], it is important to quantify them in atmospheric field studies.

Chemical transport models capture some aspects of the influence of NO_x on organic aerosols. Zheng et al. [2015] used an updated SOA scheme in the global NCAR (National Center for Atmospheric Research) Community Atmospheric Model version 4 with chemistry (CAM4-chem) with a 4-product volatility basis set scheme with NO_x-dependent SOA yields and aging parameterizations and predicted only 6–12% biogenic SOA decreases in the southeastern U.S. for 50% NOx reductions. Pye et al. [2015] updated the comprehensive coupled gas and aerosol processes in CMAQ5.1 with SAPRC07tic (State Air Pollution Research Center mechanism update, https://www.airqualitymodeling.org/index.php/CMAQ_v5.1_SAPRC07tic_AE6i) [*Hutzell et al.*, 2012; *Lin et al.*, 2013; *Xie et al.*, 2013]. NO_3–related reactions of monoterpenes (MTNO3) and isoprene as well as monoterpene peroxy radical reactions with NO resulted in semivolatile organic nitrates that contributed to organic aerosol [*Pye et al.*, 2015]. The model predicted a 25% reduction in NO_x emissions would cause a 9% reduction in organic aerosol for June 2013 in Centreville, Alabama.

Table 2.1: Summary of effects of NO_x on biogenic SOA formation from field studies and model simulations.

Simulated Effect	Effect of NO_x on bSOA	Model Version	Mechanism	Reference
25% of NO_x reduction will increase 5% bSOA from June to	**Negative**	CMAQ5.0	SOA formation based on semivolatile organic	[*Pye et al.*, 2013]
25% of NO_x reduction will reduce 9% bSOA for June 2013 SOAS	**Positive**	CMAQ5.1 with SAPRC07tic (Centreville, AL)	SOA formation based on semivolatile organic	[*Pye et al.*, 2015]
NO_x and preexisting OA and anthropogenic VOCs enhanced bSOA formation and accounted for 78% of	**Positive**	WRF-CHEM MOZART-MOSAIC (East Asia)	VBS fit to β-pinene + NO_3 experiment	[*Matsui et al.*, 2014]
By including aerosol from NO_x-depending nitrate radical oxidation, Terpene (monoterpene + sesquiterpene) aerosol approximately doubles and isoprene aerosol is enhanced by 30 to 40% in the southeastern U.S.	**Positive**	GEOS-CHEM with VBS fit (Southeastern U.S.)	VBS fit with isoprene+ NO_3 and terpene NO_3	[*Pye et al.*, 2010]
SOA concentrations increase in northern U.S. cities by around 3% but decrease in the rural southeastern U.S. by approximately 5% with 25% NO_x reduction; 50% reduction in NO_x will decease bSOA by ~0.5 μg m^{-3}	**Conditionally Positive**	PMCAMx (Eastern U.S.)	NO_3 SOA yields same as photooxidation (OH+ O_3) yields	[*Lane et al.*, 2008]
50% NOx reduction gives limited SOA reductions of 0.9–5.6, 6.4–12.0, and 0.9–2.8 % for global, southeastern U.S., and Amazon (respectively)	**Positive** but **limited**	CAM4 with VBS (Global)	NO_3 SOA yields same as photooxidation (OH + ozone) yields	[*Zheng et al.*, 2015]
Measured Effect	**Effect of NO_x on bSOA**	**Campaign**	**Measured Correlation**	**Reference**
NO_x positively correlated with nighttime oxidation of bVOCs when NO_x to bVOC ratio is lower than 0.5; they are independent when the ratio is higher than 0.5	**Conditionally Positive**	Night-time flights during SENEX	VOCs loss and NO_x	[*Edwards et al.*, 2017]
43% to 70% of bSOA are enhanced by NO_x and SO_2	**Positive**	SOAS at Centreville, AL	AMS factor LOOA and NO_x	[*Xu et al.*, 2015a]

Table 2.1 Summary of effects of NO_x on biogenic SOA formation from field studies and model simulations. (Continued)

NO_x related OM was negatively correlated with bVOCs; NO_x + bVOCs products are more volatile than NO_x + anthropogenic VOCs products	**Conditionally Negative**	CalNex at Bakersfield, CA	Particulate total alkyl and multifunctional nitrates and NO_x	[*Rollins et al.*, 2012]
NO_y suppress bSOA formation through IEPOX pathway	**Negative**	Amazon, Brazil	IEPOX SOA and NO_y	[*De Sa et al.*, 2017]
High concentrations of NO_x (average: 21 ppb) suppress bSOA formation through IEPOX pathway	**Negative**	Nanjing, Eastern China	IEPOX SOA and NO_x	[*Zhang et al.*, 2017]
Isoprene SOA yields increase and then decrease as NO_x concentration increases	**Positive** and **negative**	Lab studies	Isoprene SOA yield and NO_x	[*Kroll et al.*, 2006; *Ng et al.*, 2007; *Xu et al.*, 2014]
Addition of NO_x has minor effect on SOA yield up to a threshold and SOA yields decrease afterwards	**None** or **negative**	Lab study	Isoprene SOA yield and NO_x	[*Liu et al.*, 2016]
Nucleation of bSOA was suppressed by NO_x reactions with monoterpenes	**Negative**	Lab study	New particle formation rates and NO_x	[*Wildt et al.*, 2014]

These model schemes incorporate the results of laboratory experiments that show that NO_x affects biogenic SOA formation in at least three different, competing and counteracting ways. First, NO_x can reduce O_3 formation in the high-NO_x regime but under low-NO_x conditions increasing NO_x will result in increases in OH radicals and O_3 [*Seinfeld and Pandis*, 2016], both of which result in higher SOA yields [*Zheng et al.*, 2015]. Second, high concentrations of nighttime nitrate radical (NO_3) increased SOA formation from isoprene in chamber experiments [*Ng et al.*, 2008] by forming organonitrates [*Ng et al.*, 2017]. Third, reaction of NO with organo-peroxy radicals (RO_2) in the high NO_x regime can lower SOA yields due to more volatile products compared to reaction with hydroperoxy radicals (HO_2) [*Kroll et al.*, 2006; *Kroll and Seinfeld*, 2008; *Zheng et al.*, 2015; *Ziemann and Atkinson*, 2012]. However, the role of NO_x in systems that undergo autoxidation, particularly monoterpenes [*Ehn et al.*, 2014], has not been elucidated. These multi-faceted effects mean that the role of NO_x on biogenic SOA formation in the atmosphere depends on the specific atmospheric conditions and precursors that are present.

In order to use field measurements as constraints for models, we need sufficient aerosol chemical composition measurements to separate biogenic SOA from other organic aerosol components. The separation is difficult because biogenic SOA formation is influenced by the same oxidants that form other SOA, and there is often overlap between primary and secondary emission sources. Positive Matrix Factorization (PMF) of AMS measurements [Lanz et al., 2007; Ulbrich et al., 2009] use high time resolution to separate small differences in the timing of emissions and photochemical accumulation [*Corrigan et al.*, 2013; *Liu et al.*, 2012], but FTIR [*Hallquist et al.*, 2009; *Russell*, 2014; *Russell et al.*, 2009] provides specific chemical

fingerprints that associate co-emitted primary and secondary components [*Russell et al.*, 2011]. For example, PMF of FTIR has provided substantial evidence for non-acid carbonyl groups associated with biogenic SOA in forest conditions [*Corrigan et al.*, 2013; *Schwartz et al.*, 2010; *Takahama et al.*, 2011]. One challenge is that a common AMS PMF factor has highly oxidized organic fragments with high *m/z* 28 and *m/z* 44 and accounts for a substantial fraction of OM both from anthropogenic sources like vehicle emissions [*Presto et al.*, 2014] and from natural biogenic emissions [*Chen et al.*, 2015; *Xu et al.*, 2015a]. In addition, oxidized organic fragments can also result from vegetative detritus [*Corrigan et al.*, 2013; *Takahama et al.*, 2011], which often coincide with biogenic Volatile Organic Compounds (bVOC) emissions and contain high O/C from hydroxyl groups in primary plant materials [*Medeiros et al.*, 2006]. Biomass burning factors [*Corrigan et al.*, 2013; *Hawkins and Russell*, 2010; *Takahama et al.*, 2011] from FTIR PMF also have high non-acid carbonyl group content similar to biogenic factors, possibly from oxidation at higher temperatures in wildfires or lower temperatures in residential burning [*Corrigan et al.*, 2013].

FTIR biogenic SOA has been characterized by PMF and clustering in several field studies and shows 15 to 25% hydroxyl, 14 to 41% carbonyl, and 14 to 25% carboxylic acid groups in a variety of atmospheric conditions [*Corrigan et al.*, 2013; *Schwartz et al.*, 2010; *Takahama et al.*, 2011] and chamber studies [*Palen et al.*, 1992; *Russell et al.*, 2011; *Schwartz et al.*, 2010]. Organic functional groups of FTIR biogenic factors identified at Whistler, British Colombia, were similar to SOA reported from chamber oxidation of bVOCs [*Schwartz et al.*, 2010].

To understand the influence of NO_x and other pollutants on biogenic SOA, we compared measurements from the Southern Oxidant and Aerosol Study (SOAS) 2013 at Look Rock (LRK), Tennessee, and Centreville (CTR), Alabama. The differences and similarities between the aerosol sources and composition at these two sites were evaluated by comparing the AMS and FTIR PMF factor concentrations with anthropogenic source marker concentrations. Comparisons to FTIR results from lab-generated biogenic SOA properties provide the likely source of biogenic SOA. Model simulations were compared at the two sites and used to investigate the regional representativeness of these two sites. Both the measurements and the simulations illustrate how NO_x affects biogenic SOA composition and concentration in the southeastern U.S.

2.2 Methods

Aerosol measurements were made from 1 June 2013 to 18 July 2013 at LRK and CTR in the southeastern U.S. The LRK site (35.63314 N, 83.94185 W) is on the northern slope of the Great Smoky Mountains and has an elevation of 801 m above sea level, where a permanent structure with a long-term IMPROVE sampling program has measured O_3 and $PM_{2.5}$ components. The CTR site (32.90289 N, 87.24968 W) is part of the Southeastern Aerosol Research and Characterization (SEARCH) air quality sampling network within a high isoprene-emitting broad-leaf forest and is located on the west side of the Cahaba River at an elevation of 126 m. Both sites are forested and rural. Local times are used in all comparisons to better reflect diurnal patterns in the measurements. Note that in summer LRK uses Eastern Daylight Time zone and CTR uses Central Daylight Time, but time correlations are calculated based on local time at both sites. For example, 4pm EDT at LRK is compared with 4pm CDT at CTR.

Following Devore and Berk [2012], the sample Pearson correlation coefficient (r) is used to discriminate among relationships which exhibit weak ($|r| < 0.5$), moderate ($0.5 < |r| < 0.8$), and strong ($|r| > 0.8$) correlations. $|r| < 0.35$ is identified as "no correlation" [Taylor, 1990].

2.2.1 Aerosol Particle Measurements

At LRK, a climate-controlled van with an isokinetic inlet pulled air into the van for distribution to a high-resolution time-of-flight aerosol mass spectrometer (AMS), a scanning electrical mobility spectrometer (SEMS), and filters for FTIR and X-ray fluorescence (XRF). At CTR, submicron aerosol particles were collected in a van with air drawn from a window-mounted inlet and through a silica gel denuder with a sharp-cut cyclone for collection of dry PM_1 and $PM_{2.5}$ particles on filters.

Filter samples were collected on pre-scanned Teflon filters (Teflon, Pall Life Science Inc., 37mm diameter, 1.0 μm pore size) at CTR and LRK behind PM_1 and $PM_{2.5}$ sharp-cut cyclones (SCC2.229 PM_1 and SCC2.229 $PM_{2.5}$, BGI Inc). Four PM_1 (from 0800 to 1200, from 1200 to 1600, from 1600 to 1900, and from 2000 to 0700 local time) and two $PM_{2.5}$ (from 0800 to 1900 and from 2000 to 0700 local time) samples were collected each day at each site. Samples were frozen and transported to the Scripps laboratory for FTIR spectroscopy. A Bruker Tensor 27 FTIR spectrometer with a deuterated triglycine sulfate (DTGS) detector (Bruker, Waltham, MA) was used to scan the filters both before and after sampling. Filters were installed in the sampling van each morning and solenoid valves controlled the start and stop of collection; the filter holders were mounted in a 5 ft^3 refrigerator to keep the filter holders at 4 °C during and after collection each day and minimize losses due to vaporization of higher vapor pressure

components, as well as reactions that could change organic composition during storage. An automated algorithm was applied to quantify the mass of the organic functional groups [*Russell et al.*, 2009; *Takahama et al.*, 2013]. Five groups (alkane, amine, hydroxyl, carbonyl and carboxylic acid) were quantified by the area of absorption peaks, and the sum of the mass of the five functional groups is used as the quantified OM [*Maria et al.*, 2002]. Absorption peaks for other groups (organosulfate, organonitrate, aromatic and alkene group) were fit but more than 90% of the samples were below the limit of quantification and are excluded. Fifty-four filters at LRK and 2 at CTR were selected for X-ray fluorescence (XRF) (Chester Labnet, OR) quantification of major elements above 23 amu. The mass of dust was calculated from the metals on these filters by assuming the dust consists of Na_2O, $MgCO_3$, Al_2O_3, SiO_2, K_2O, $CaCO_3$, TiO_2, Fe_2O_3, MnO and BaO using the following equation:

$$C_{dust} = \frac{M_{Na_2O} \times C_{Na}}{2 \times M_{Na}} + \frac{M_{MgCO_3} \times C_{Mg}}{M_{Mg}} + \frac{M_{Al_2O_3} \times C_{Al}}{2 \times M_{Al}} + \frac{M_{SiO_2} \times C_{Si}}{M_{Si}} + \frac{M_{K_2O} \times C_K}{2 \times M_K} + \frac{M_{CaCO_3} \times C_{Ca}}{M_{Ca}} + \frac{M_{TiO_2} \times C_{Ti}}{M_{Ti}} + \frac{M_{Fe_2O_3} \times C_{Fe}}{2 \times M_{Fe}} + \frac{M_{MnO} \times C_{Mn}}{M_{Mn}} + \frac{M_{BaO} \times C_{Ba}}{2 \times M_{Ba}}$$

where C_{dust} is mass concentration of dust, M is the molar weight of the compound or metal, and C_{metal} is the mass concentration of the measured metal [*Usher et al.*, 2003].

The high-resolution time-of-flight AMS measured non-refractory particle mass ionized by electron impact after vaporizing at 600-650°C surface [*DeCarlo et al.*, 2006]. The AMS operation, calibration, and measurements at LRK and CTR are reported by Liu et al. [2017] and

Xu et al. [2015a]. Measurements at both sites were collected in two modes, V-mode with higher m/z resolving power and W-mode with higher mass sensitivity; single particle light scattering (LS) mode was also used at LRK [*Liu et al.*, 2017; *Xu et al.*, 2015a]. V-mode is reported here because of its high signal sensitivity at 5 min time resolution. Aerosol Chemical Speciation Monitor (ACSM) [*Ng et al.*, 2011] was also deployed at LRK and the ACSM scanning rate was set at 200 ms amu^{-1} and collected for 30 min intervals [*Budisulistiorini et al.*, 2015]. CE (Collection Efficient) was applied to mass concentration from AMS and ACSM. Budisulistiorini et al. [2015] used a CE value of 0.5 calculated based on Middlebrook et al. At LRK, the AMS CE of 0.80 was calculated by scaling to SEMS mass distribution (after removing refractory components) using density of 1.5 (calculated from matching the modal peak from AMS to that from SEMS). AMS CE-corrected sulfate was correlated to sulfate from XRF Sulfur with R=0.74 and slope of 1.14) [*Liu et al.*, 2017]; at CTR, a composition-dependent CE with a mean value of 0.59 was applied based on the sulfate and ammonium composition [*Middlebrook et al.*, 2012; *Xu et al.*, 2015a].

Cloud condensation nuclei (CCN) measurements were collected at LRK and CTR. At CTR, the CCN counter was operated in Scanning Flow CCN Analysis mode [*Moore and Nenes*, 2009], scanning flow rate sinusoidally from 0.2 to 0.9 L min^{-1} then back to 0.2 L min^{-1} over 2 min to give CCN spectrum between 0.15 and 0.54 % supersaturation [*Cerully et al.*, 2015]. At LRK size-resolved CCN measurements were conducted at 0.20%, 0.37% and 0.58% supersaturation.

2.2.2 CMAQ Model

CMAQ v5.1 simulations described by Pye et al. [2015; 2017] and Murphy et al. [2017] cover the southeastern United States domain for June 2013 at 12 km by 12 km horizontal resolution using meteorology from Advanced Research Weather Research and Forecasting (WRF) model (ARW) version 3.6.1 [*Pye et al.*, 2015; *Pye et al.*, 2017]. The model includes gas-phase chemistry based on SAPRC07tic [*Xie et al.*, 2013] with additional updates for the formation of isoprene-epoxydiol (IEPOX) SOA [*Pye et al.*, 2015; *Pye et al.*, 2017] and semivolatile organic nitrates, primarily from monoterpene reactions with nitrate radicals [*Pye et al.*, 2015] as well as other semivolatile SOA [Pye et al., 2017]. The semivolatile primary organic aerosol (POA) and potential secondary organic aerosol from combustion emissions (pcSOA) introduced by Murphy et al. [2017] were included to better represent anthropogenic OM.

2.2.3 FTIR Measurements of Chamber Experiments

Chamber biogenic SOA experiments were carried out at CU Boulder using isoprene and α-pinene (https://cfpub.epa.gov/ncer_abstracts/index.cfm/fuseaction/display.abstractDetail/abstract/9975/report/F). Three different types of oxidation (NO_3 radicals, O_3, and OH radicals + NO_x) were investigated in the experiments. Neutral ammonium sulfate particles were used as seed particles in some of the experiments. RH was 50% in all the experiments. NO_3 radicals were formed with N_2O_5 with mixing ratio from 0.33 to 1 ppm. For OH radicals + NO_x conditions, oxidants were 10 ppm CH_3ONO and 10 ppm NO with ultraviolet light. Two FTIR samples were collected on filters in each biogenic SOA formation experiment. The filters were scanned and spectral peaks

were integrated following the same procedure used for the ambient samples [*Russell et al.*, 2009; *Takahama et al.*, 2013].

2.3 Results

The LRK and CTR sites are influenced by the Bermuda-Azores High in summer, with warm humid air moving northward and northeastward from the Gulf of Mexico into the interior of the continent [*Davis et al.*, 1997]. The aerosol particle concentrations accumulated for periods of several days with low wind and little precipitation before being washed out [*Liu et al.*, 2017]. The precipitation events overlapped 70% of the time at the two sites during SOAS, synchronizing particle removal and thus contributing to the correlation of the time series of concentrations (Figure 2.1).

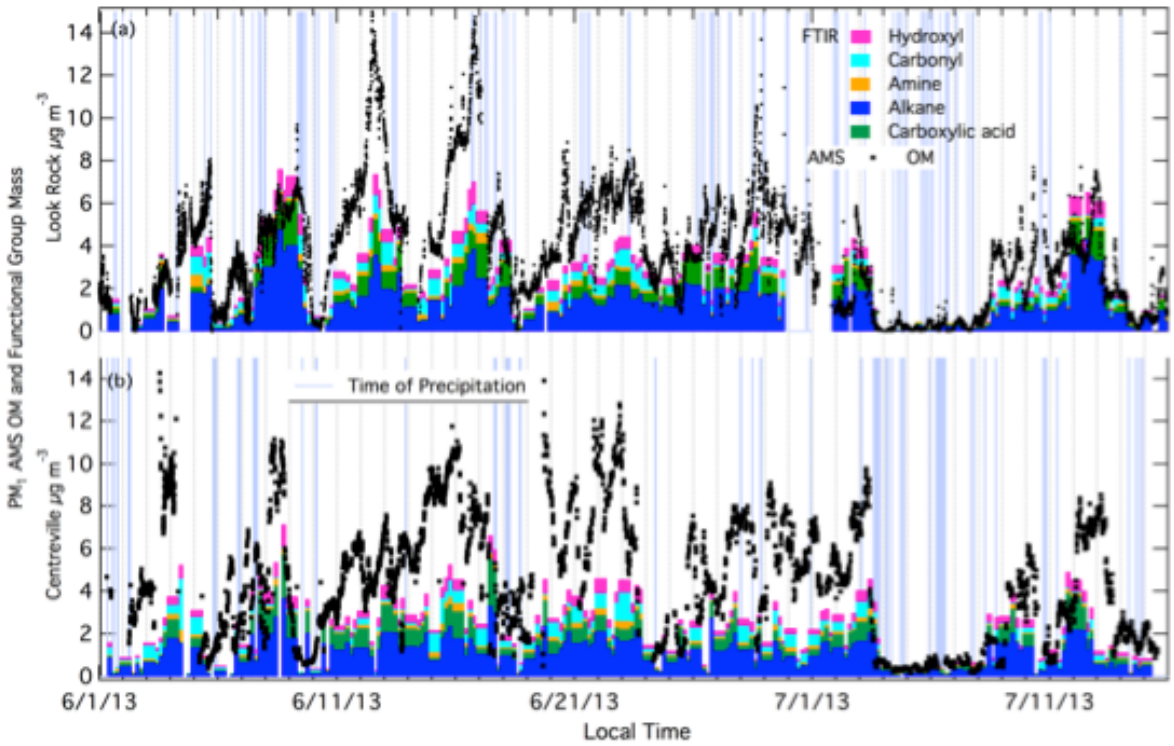

Figure 2.1: Time series of AMS OM and FTIR functional group concentrations at (a) LRK and (b) CTR. Time of percipitation is marked on the plot.

2.3.1 Fine and submicron chemical components of aerosols and level of pollutants

Figure 2.1 shows the project average AMS PM_1 non-refractory component and FTIR functional group mass concentrations. AMS non-refractory mass had average concentrations of 5.3 ± 3.7 μg m^{-3} at LRK and 7.5 ± 4.0 μg m^{-3} at CTR. The fractions of non-refractory components were similar with high OM fractions (67% and 67%, at LRK and CTR, respectively) followed by sulfate (23% and 26% at LRK and CTR, respectively), and ammonium (9% and 6% at LRK and CTR, respectively). Nitrate and chloride mass concentrations were below 2% of OM at both sites (Figure 2.2). For comparison, ACSM OM concentrations were 4.9 ± 3.0 μg m^{-3} at

LRK [*Budisulistiorini et al.*, 2015] and 5.2 ± 3.0 μg m^{-3} at CTR [*Saha et al.*, 2017]. FTIR OM varied from 0.1 to 12 μg m^{-3} at LRK and from 0.2 to 12 μg m^{-3} at CTR, with average concentrations of 2.7 ± 1.4 μg m^{-3} at LRK and 2.7 ± 1.8 μg m^{-3} at CTR. The functional group compositions were very similar at the two sites with 52% alkane group mass, followed by 17% carboxylic acid, 14% hydroxyl, 12% carbonyl, and 5% amine group mass at LRK. At CTR, the organic functional group mass fractions were less than 4% different from LRK. $PM_{2.5}$ OM was correlated to that of PM_1 (r=0.89 and 0.85) but about 15% higher and with similar concentration (2% higher) at LRK and CTR, respectively. $PM_{2.5}$ organic functional group concentrations were also very similar at the two sites.

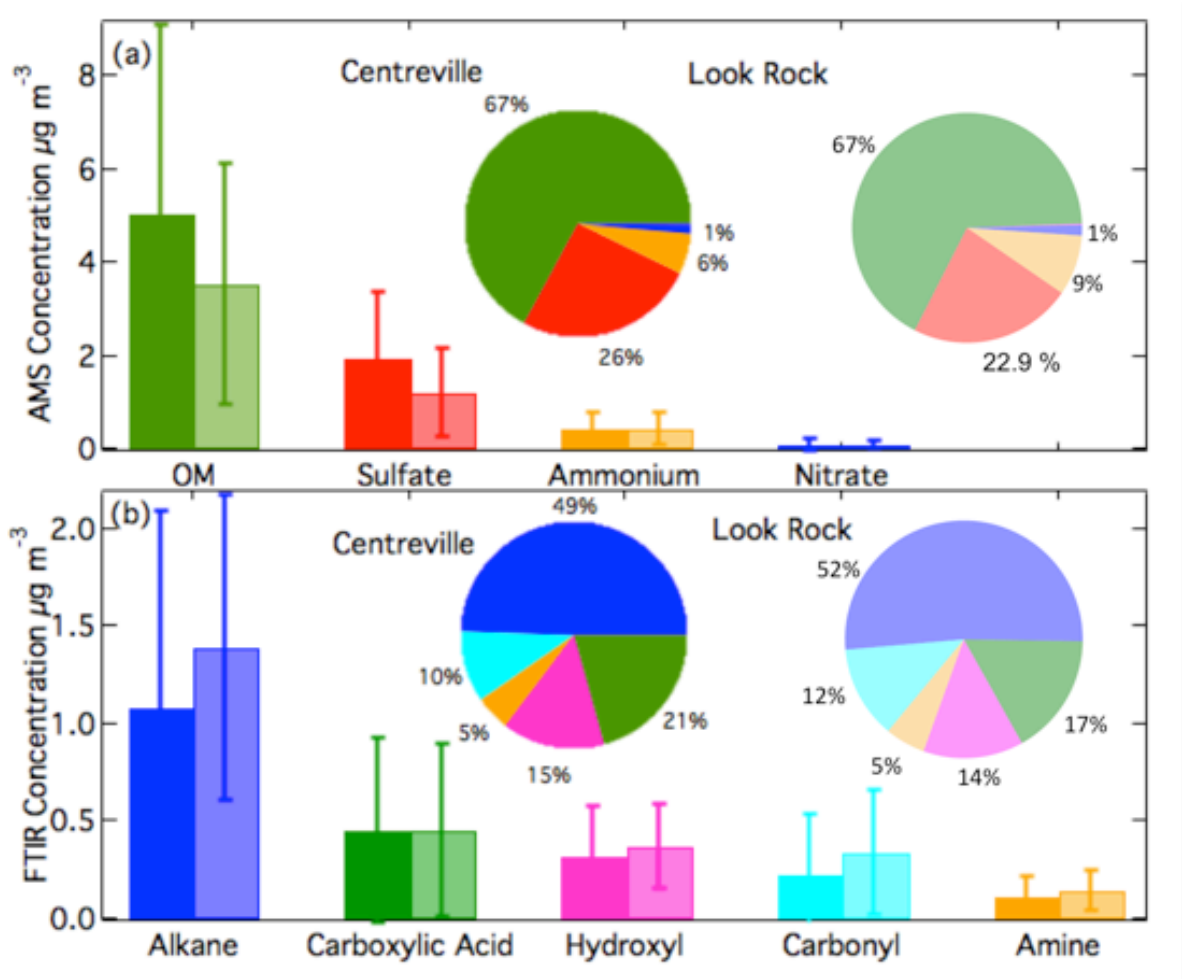

Figure 2.2: Average of (a) FTIR organic functional group concentrations and (b) AMS OM at LRK and CTR. AMS OM is correlated with FTIR OM (r=0.75 and 0.65, respectively). Pies are mass fractions of organic functional groups (FTIR) and non-refractory species (AMS).

AMS and FTIR OM concentration had moderate correlation coefficients between the two sites with r=0.80 at LRK and r=0.68 at CTR (Figure 2.3). FTIR OM concentrations were 20% to 40% lower than ACSM and AMS OM at both sites, consistent with the ±20% uncertainty of each measurement [*Allan et al.*, 2003a; *Allan et al.*, 2003b; *Bahreini et al.*, 2009; *Jimenez et al.*, 2016; *Russell et al.*, 2011; *Takahama et al.*, 2013]. Much of the AMS uncertainty is associated with correcting ambient measured concentrations by the AMS CE. Since semi-volatile

compounds may evaporate from filters contributing to lower concentrations, the difference in OM concentration between FTIR and AMS may suggest that there were more semi-volatile compounds at CTR, since FTIR has been found to be approximately 70% to 80% of AMS OM at urban sites where substantial HOA (Hydrocarbon-like Organic Aerosol) can be semivolatile [*Day et al.*, 2010; *Gilardoni et al.*, 2009; *Liu et al.*, 2012]. Losses of semivolatile components at CTR are also consistent with the CIMS measurements of volatilized OM from filters, which detected 50% of the CTR AMS OM [*Lopez-Hilfiker et al.*, 2016].

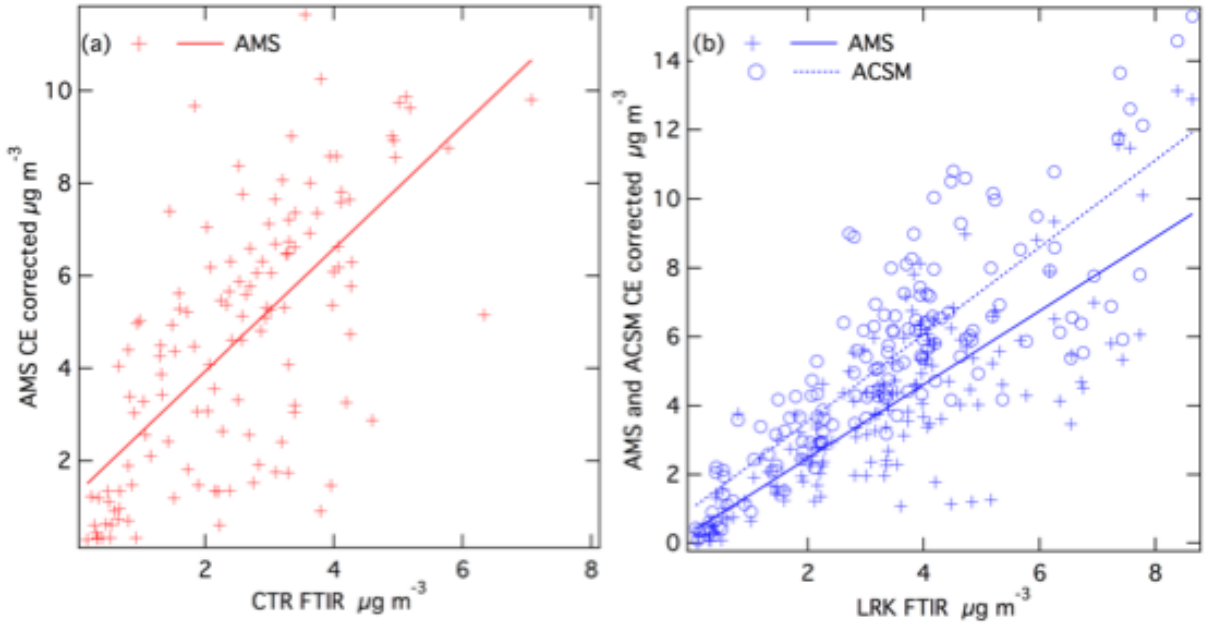

Figure 2.3: Scatter plots of (a) AMS OM with FTIR OM at CTR (R=0.68, slope=1.33) and (b) AMS OM (R=0.80, slope=1.07) and ACSM OM (R=0.80, slope=1.26) with FTIR OM at LRK

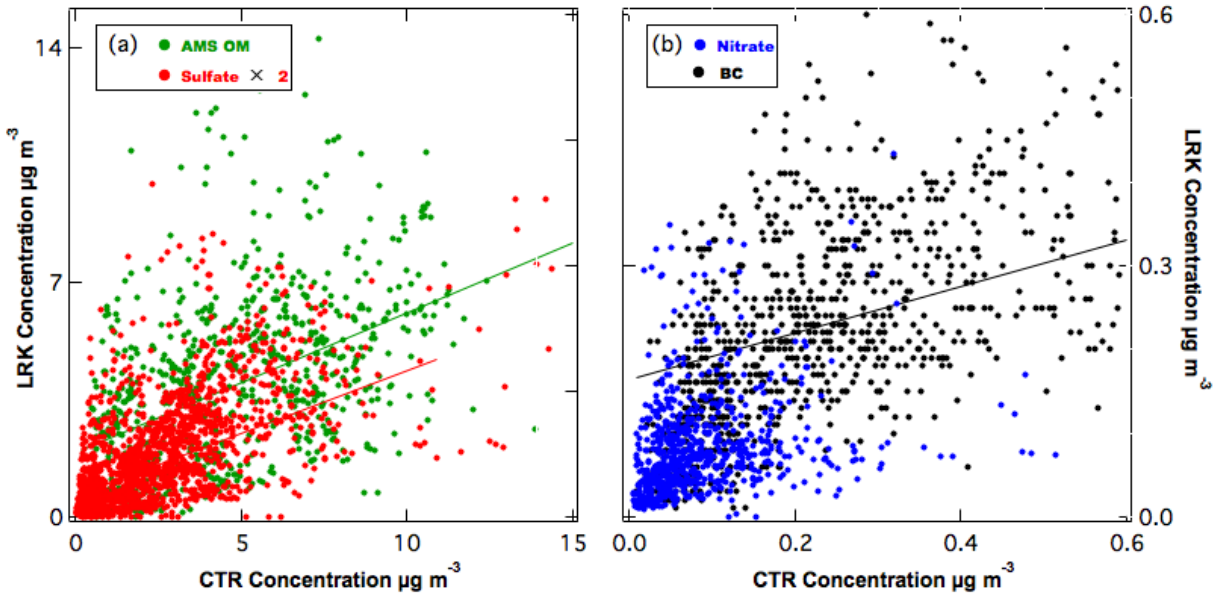

Figure 2.4: Scatter plots of (a) AMS OM μg m-3 , r=0.47 , slope=0.37, 3 outliers omitted; sulfate μg m-3, r=0.51, slope=0.39, 3 outliers omitted; (b) BC μg m-3, r=0.40, slope=0.27, 19 outliers omitted; nitrate μg m-3, r=0.30, slope=0.23 of LRK and CTR.

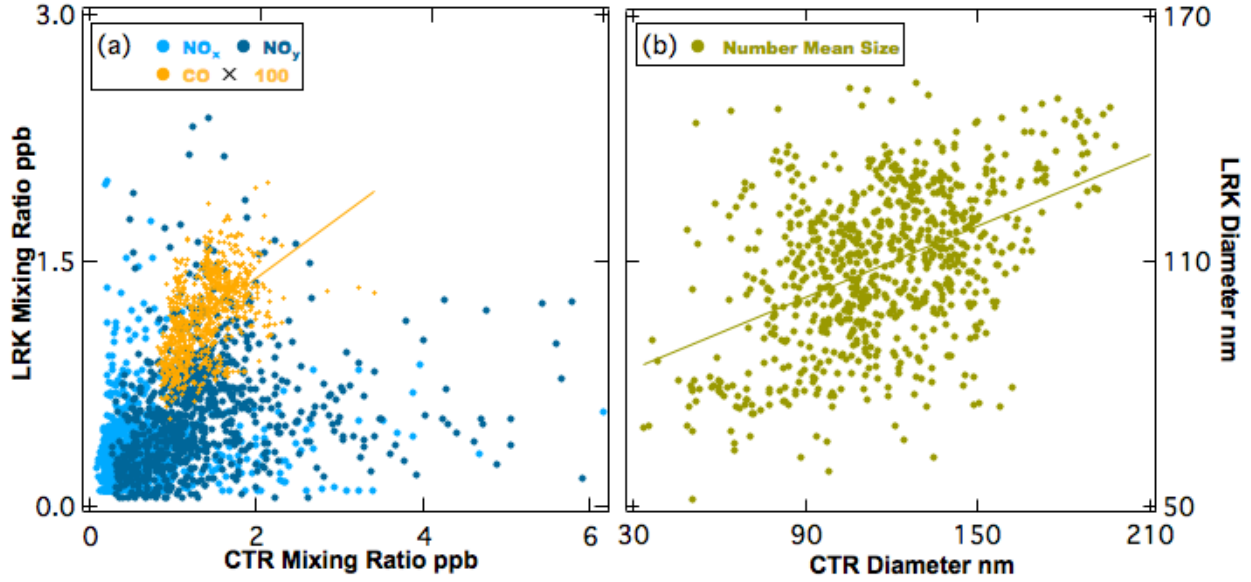

Figure 2.5: Scatter plots of (a) CO ppb, r=0.51, slope=0.38; NO_x ppb, r=0.08, slope=0.03, 1 outlier omitted, concentrations were multiplied by 100; NO_y ppb, r=0.22, slope=0.10, 3 outliers omitted; (b) SMPS and SEMS number mean size of LRK and CTR

OM, sulfate, BC, and CO concentrations as well as particle sizes had weak to moderate correlations (r= 0.47, 0.51, 0.40, 0.51 and 0.46 respectively) of the time series at the two sites, and the concentrations were all lower at LRK than CTR (Figure 2.4 and Figure 2.5). Average concentrations were 3.6 and 5.0 μg m^{-3} for OM, 1.2 and 1.9 μg m^{-3} for sulfate (both observed by AMS), 0.23 and 0.26 μg m^{-3} for BC, and 115 and 134 ppb for CO at LRK and CTR, respectively. NO_x and NO_y showed almost no correlation of the time series at the two sites, with different mixing ratios and diurnal cycles: NO_x mixing ratio at CTR was 3 to 10 times higher than at LRK during late night and early morning hours (0100~0900) but was roughly the same mixing ratio during the rest of the day (Figure 2.6). The higher mixing ratio at CTR suggest that CTR has more anthropogenic emissions than LRK during SOAS for two reasons: (1) substantial vehicle NO_x emissions surrounding CTR and (2) the higher altitude at LRK (801 m) resulted in less transport of short-lived local emissions. Dust was 3% of submicron mass.

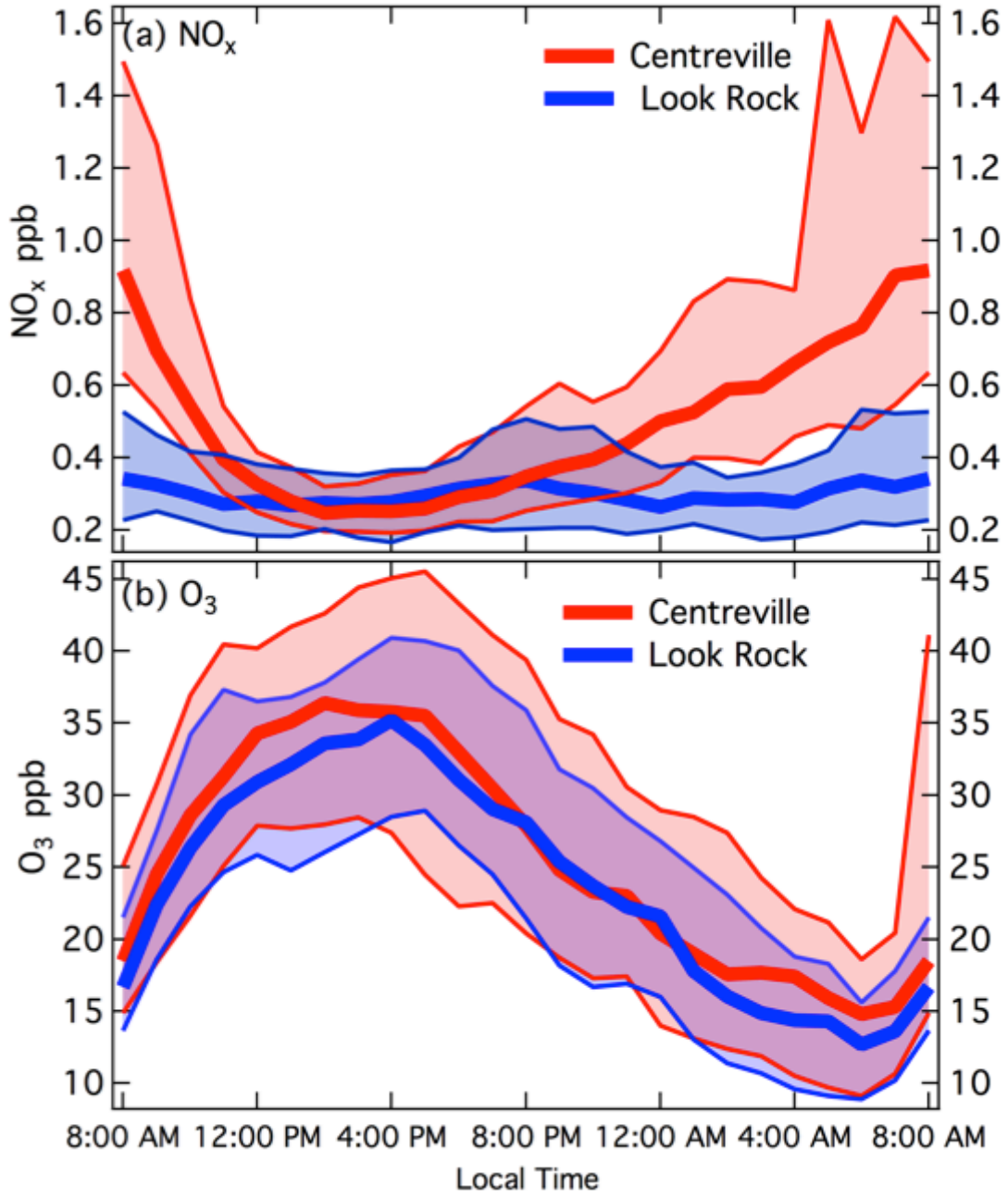

Figure 2.6: Diurnal plot of (a) NO_x and (b) O_3 at both sites. Medians, 25th percentiles and 75 percentiles are shown on the figure.

2.3.2 AMS PMF Organic Factors

The AMS PMF factors that were identified by Xu et al. [2015a] and Liu et al. [2017] at LRK and CTR during SOAS include two pairs of factors that showed almost identical *m/z* spectra with cosine similarities higher than 0.98: LRK-Factor44 and CTR-MO-OOA (with characteristic *m/z* 44 signal) and LRK-Factor82 and CTR-Isoprene-OA (with *m/z* 82 signal), (Table 2.2). The factor with high m/z 82 was also referred to as 82fac, IEPOX OA, IEPOX-SOA or Isoprene-OA measured in other studies [*Budisulistiorini et al.*, 2013; *Budisulistiorini et al.*, 2015; *Chen et al.*, 2015; *de Sa et al.*, 2017; *Hu et al.*, 2015; *Robinson et al.*, 2011; *Slowik et al.*, 2011; *Xu et al.*, 2015a] as noted in Liu et al. [2017], and showed moderate to strong (r=0.6 to 0.88) correlations to sulfate: similar to results reported previously [*Budisulistiorini et al.*, 2013; *Budisulistiorini et al.*, 2015; *Xu et al.*, 2015a]. The factor with high m/z 44 was also referred to as LV-OOA in other publications [*Presto et al.*, 2014; *Zhang et al.*, 2011]. Both LRK-Factor44 and CTR-MO-OOA have high contributions of oxygen-containing organic fragments and account for roughly the same fraction of OM (48% at LRK and 39% at CTR). LRK-Factor44 and CTR-MO-OOA have the highest correlation with atmospheric anthropogenic emission tracers (BC, CO, O_3, NO_y). For example, LRK-Factor44 was correlated to CO (R=0.61), with O_3 (R=0.68) and CTR-MO-OOA with CO (R=0.62), with O_3 (R=0.49) with 1 hour time resolution. The correlations are more reflective of day-to-day differences. The high m/z 44 level suggested that this factor likely includes substantial contributions from secondary sources. LRK-Factor82 and CTR-Isoprene-OA have been associated with isomeric isoprene epoxydiols (IEPOX) [*Liu et*

al., 2017; *Xu et al.*, 2015a]. This factor contributed 20% to OM at LRK and 18% to OM at CTR. CTR had a nighttime factor (CTR-LO-OOA) and a biomass burning factor (CTR-BBOA) but LRK did not. LRK also had a less oxidized daytime OM identified as LRK-Factor91 but no factor similar to CTR-LO-OOA. The LRK AMS PMF factors have cosine similarity greater than 0.6 and temporal correlation efficient great than 0.8 for the ACSM PMF factors identified at LRK, which were identified by Budisulistiorini et al. [2015] (Table 2.2). If the smaller, more common and variable peaks of CO^+, CO_2^+, H_2O^+, and CHO^+ are excluded, the cosine similarity is 0.99 for the m/z spectra of CTR-LO-OOA and LRK-Factor91. This indicates that the larger ions at m/z 55, 67,77, 91, which are more representative of the parent molecules, have consistent relative concentrations that indicate that both factors have contributions from similar bVOCs. Cosine similarity is a measure of angular separation between two non-zero vectors of an inner product space that measures the cosine of the angle between them.

Table 2.2: Cosine similarity of AMS PMF factors at CTR and LRK. Numbers in bold are the highest numbers in each column (if above 0.7).

Cosine Similarity	LRK-Factor82	LRK-Factor44	LRK-Factor91
CTR-Isoprene-OA	**0.99**	0.78	0.65
CTR-MO-OOA	0.81	**0.98**	0.35
CTR-LO-OOA	0.95	0.84	0.66
CTR-BBOA	0.95	0.87	0.55
ACSM LRK-IEPOXOA	**0.80**	0.82	0.36
ACSM LRK-LVOOA	0.67	**0.84**	0.49
ACSM LRK-91fac	0.82	0.80	0.66
Correlation of Time Series	LRK-Factor82	LRK-Factor44	LRK-Factor91
ACSM LRK-IEPOXOA	**0.93**	0.43	0.51
ACSM LRK-LVOOA	0.59	**0.87**	0.71
ACSM LRK-91fac	0.51	0.74	**0.87**

2.3.3 FTIR PMF Organic Factors

Three factors are identified by PMF from baselined FTIR spectra at both sites by the method of Takahama et al. [2013] as described in Appendix. More than 85% of the spectra could be reconstructed by the FTIR PMF factors at LRK and more than 87% at CTR. FTIR PMF spectra for PM_1 and $PM_{2.5}$ factors are shown in Figure 2.7. Spectra of PM_1 and $PM_{2.5}$ factors at both sites are almost identical (cosine similarity > 0.94). Cosine similarities between each of the three identified FTIR factors ranged from 0.40 to 0.75. The first factor contributed 36% and 41% of the FTIR OM at LRK and CTR, respectively, and had high cosine similarity (0.99 at Bakersfield and 0.98 at Hyytiälä) to FTIR spectra of fossil fuel combustion factors identified at Bakersfield and Hyytiälä [*Corrigan et al.*, 2013; *S Liu et al.*, 2012]. Alkane groups made up 70% of the OM of this first factor, followed by hydroxyl (17%) and carboxylic acid (10%) groups.

The O/C of the factor is 0.3, indicating a high fraction of hydrocarbon-like organic components. Consequently, the ratio of carboxylic and carbonyl groups to alkane groups is the lowest of the three factors, consistent with factors related to combustion emissions in other studies [*Russell et al.*, 2011]. The O/C of 0.3 is similar to values reported for AMS SV-OOA (O/C=0.37) and higher than those of HOA (O/C=0.06) AMS [*Zhang et al.*, 2011] likely suggesting the factor includes secondary organic products from combustion sources rather than primary emissions. The factor had weak to moderate correlations with CO (r=0.53), NO_y (r=0.40), and BC (r=0.51) at LRK but had lower correlations with CO (r=0.28), NO_y (r=0.23), and BC (r=0.23) at CTR (Table 2.3). The Fossil Fuel Combustion (FFC) factor time series was correlated more strongly to Ca, Mn and Fe concentrations (r = 0.3 to 0.6) than the other FTIR factors (r = -0.4 to 0.3) at both sites. These metals were found in combustion sources and can serve as combustion tracers in previous studies [*Agarwal et al.*, 2015; *Cheung et al.*, 2010; *Verma et al.*, 2010]. The FFC factors at the two sites peaked in the late afternoon (1600-1900, 40% higher than the rest of the day), indicating a photochemical contribution to the OM, for example, 8 June to 9 June at both sites (Figure 2.8). This factor has accounted for ~40% fraction of OM at these two rural sites, but it is likely not exclusively from fossil fuel combustion sources. A similar factor accounted for less than 10% of OM at a boreal forest site, consistent with the lower man-made emissions at Whistler [*Takahama et al.*, 2011]. This factor is named as FFC factor following the nomenclature of previous studies [*Corrigan et al.*, 2013; *Takahama et al.*, 2011]. Although the factor is affected by combustion source, the weak to intermediate correlations indicate that combustion is not the exclusive source of the factor.

Table 2.3: Time series correlation coefficients of FTIR PMF factors with tracers. Numbers in bold are the highest numbers in each column (if above 0.4).

	LRK			CTR		
Correlation Coefficient (R)	FFC	BOA	MOA	FFC	BOA	MOA
SO_2	0.15	0.12	-0.01	0.26	0.01	0.11
NOx	0.1	-0.02	0.07	0.1	**0.41**	0.12
NO_y	**0.4**	0.34	0.28	0.23	**0.54**	0.25
CO	**0.53**	0.45	0.46	0.28	**0.71**	0.38
O_3	0.32	**0.51**	0.36	0.27	0.22	0.19
BC	**0.51**	**0.55**	0.43	0.23	**0.62**	0.28
Ca	**0.64**	0.31	0.06	0.31	0.06	0.28
Fe	0.32	0	-0.25	0.32	0.01	0.28
Mn	0.37	0.09	-0.37	**0.41**	0.16	0.31
MVK/MACR	0.28	**0.66**	0.36	-	-	-
SO_4	**0.64**	0.45	**0.65**	0.31	0.28	0.38
NO_3	0.25	0.44	0.37	0.09	**0.51**	0.29
NH_4	**0.59**	0.44	**0.62**	0.35	0.34	0.43
CTR-Isoprene-OA/ LRK-Factor82	0.43	0.56	**0.58**	0.41	0.34	**0.47**
CTR-MO-OOA/LRK-Factor44	0.47	**0.76**	0.45	0.33	**0.51**	0.25
LRK-Factor91	0.25	**0.73**	0.28	-	-	-
/CTR-LO-OOA	-	-	-	0.04	**0.61**	0.16

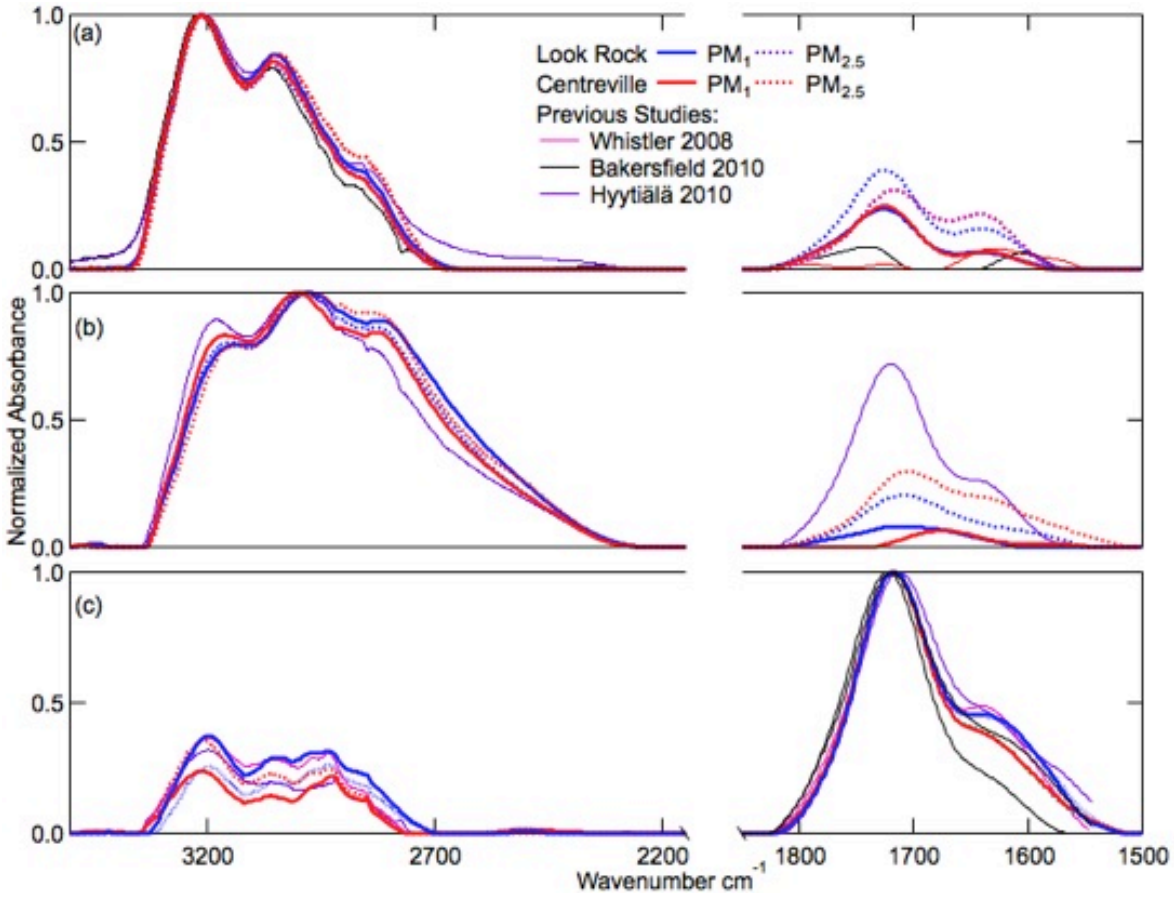

Figure 2.7: FTR PMF factors spectra in this study and pervious studies: Whistler 2008[Schwartz et al., 2010] Bakersfield 2010[Liu et al., 2012] and Hyytiälä 2010[Corrigan et al., 2013]: (a) Factors similar to FFC, cosine similarity is higher than 0.97; (b) Factors similar to MOA, cosine similarity is higher than 0.95; (c) Factors similar to BOA, cosine similarity is higher than 0.94.

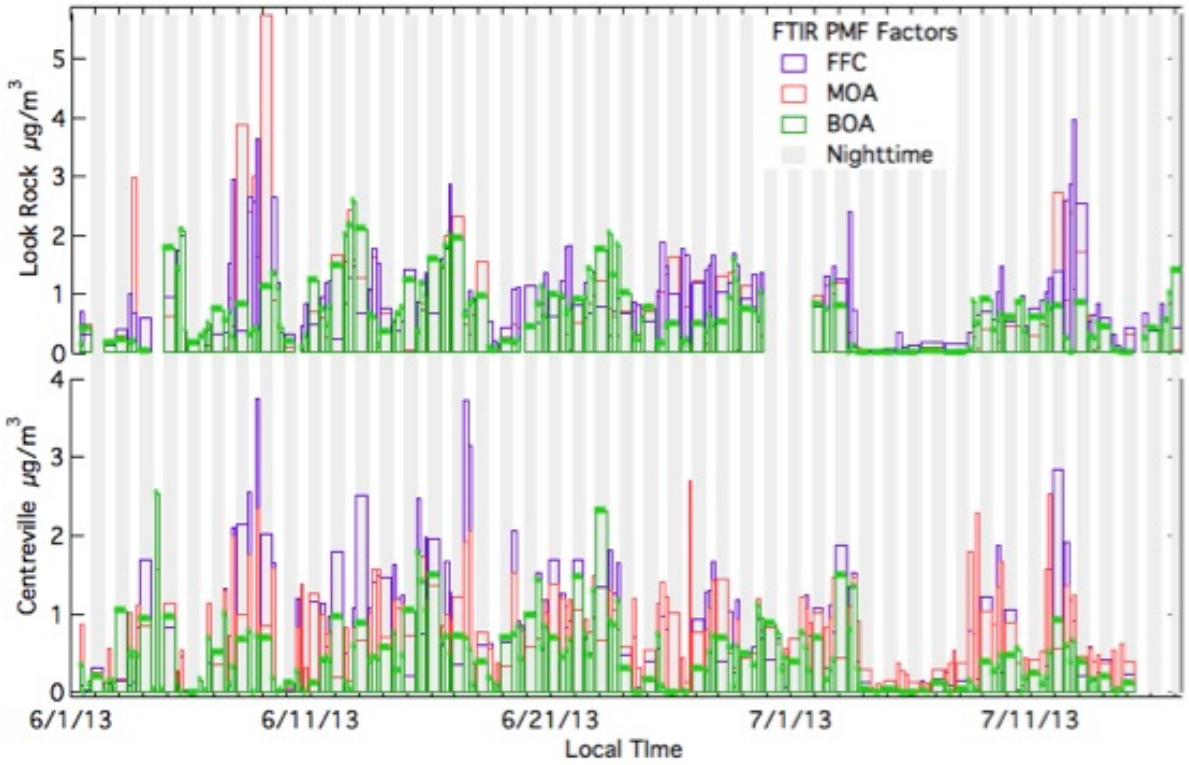

Figure 2.8: Time series of FTIR PMF factor OM at (a) LRK and (b) CTR.

The second factor has substantial alkane group (57%) and also an absorption region at 2600 cm^{-1} associated with carboxylic acid groups (23%), making it more oxidized than the FFC factor with an O/C of 0.5. This factor contributed 25% and 27% of FTIR OM at LRK and CTR, respectively. A similar factor was identified in boreal forests in Hyytiälä, Finland [*Corrigan et al.*, 2013], which had a similar spectrum (cosine similarity >0.94, shown in Figure 2.7) and the highest correlations to sulfate (r=0.64 and 0.38 for LRK and CTR, respectively), CTR-Isoprene-OA (r=0.75), and LRK-Factor82 (r=0.47). This factor had evidence of man-made primary or secondary organic components and is named Mixed Organic Aerosols (MOA) since it has both anthropogenic sulfate and biogenic isoprene-related organic contributions.

The third factor has high carbonyl group absorption at 1800 cm^{-1} and contributed 25% OM at LRK and 19% OM at CTR. The high non-acid carbonyl group concentration can indicate particles from both biomass burning and biogenic emissions reported previously [*Corrigan et al.*, 2013; *Hawkins and Russell*, 2010]. This factor is identified as biogenic organic aerosols (BOA) because it includes primary and secondary sources of particles from plant vapor emissions and decaying plant matter. The BOA factor is similar to factors identified at forested sites [*Corrigan et al.*, 2013; *Schwartz et al.*, 2010], as shown by the similarity of the FTIR spectra in Figure 2.7, even though monoterpenes account for more of the bVOC than isoprene at these pine forest sites. The coincidence of the emission timing and locations as well as the similarities in organic functional group biogenic SOA composition does not allow separation of isoprene and monoterpene sources. The largest organic functional group fraction is carbonyl groups (29%), which is consistent with the carbonyl group mass fraction reported for pine forest sites [*Corrigan et al.*, 2013; *Schwartz et al.*, 2010; *Takahama et al.*, 2011]. A biomass burning factor [*Corrigan et al.*, 2013; *Hawkins and Russell*, 2010; *Takahama et al.*, 2011] was not identified by the multi-hour FTIR samples at either CTR or LRK during SOAS, which is consistent with the small and short-duration biomass burning emissions identified by AMS [*Xu et al.*, 2015a]. The small methylene peaks in BOA at both CTR and LRK indicate a very small fraction of BOA could be vegetative detritus. Alkane and hydroxyl groups each contributed approximately 25% of BOA OM. Carboxylic acid and amine group contributions to the BOA factor are lower than 10% and the factor is highly oxidized with O/C of 0.45. The BOA factor time series correlated to Methyl Vinyl Ketone/Methacrolein (MVK/MACR) concentration time series with r=0.66 at LRK, consistent with these intermediate products serving as markers of isoprene [*Liu et al.*, 2013] and

pinene [*Zhang et al.*, 2009] biogenic SOA formation. The correlation of BOA with sulfate is weak with correlation coefficient of 0.45 at LRK and 0.28 at CTR (Table 2.3), perhaps because the BOA factor does not include the sulfate-enhanced biogenic oxidation products as these may be included in MOA instead.

In summary, FTIR PMF factors were consistent with AMS factors in apportioning OM to sources (Figure 2.9), despite the differences in apportioning oxidized SOA fragments and groups noted by previous work [*Corrigan et al.*, 2013]. Specifically, the lower time resolution and lack of fragmentation of FTIR tends to associate oxidation products with functional groups that are associated with products from specific classes of precursor molecules, so that primary and secondary components are in the same factor [*Russell et al.*, 2011]. The higher time resolution of AMS often separates POA hydrocarbon fragments that peak in the morning and evening from the SOA fragments produced during afternoon photochemistry. In addition, fragmentation of molecules in the AMS means that many secondary components (such as CO_2^+) occur in different peaks than the primary molecules that may have similar chemical composition that were emitted from the same source. These differences in resolution and fragmentation mean that primary and secondary components from the same source are separated into different factors in AMS measurements even though FTIR tends to retain products from the same source in a single factor. In addition, the higher time resolution AMS chemical signatures identified CTR-BBOA, which only had several 1- or 2- hour sharp concentration peaks during the campaign [Xu et al., 2015a].

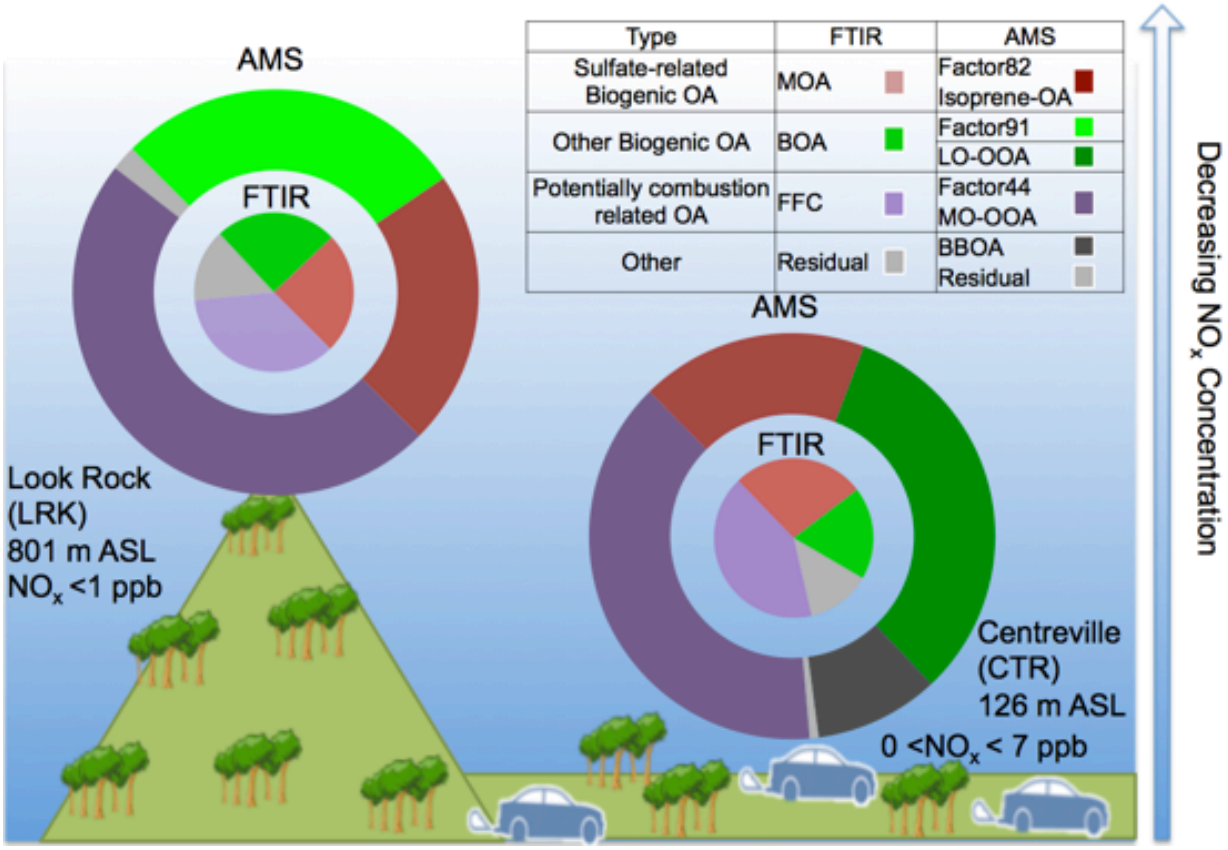

Figure 2.9: Schematic diagram of sources, processes and components of aerosol particles in Centreville, Alabama, and Look Rook, Tennessee, for SOAS 2013. Corresponding FTIR and AMS factors are plotted to illustrate the consistency of the source attribution of organic components. The processes shown are based on both direct measurements and correlations.

2.4 Discussions

The parallel deployment of both FTIR and AMS OM measurement techniques at CTR and LRK during SOAS provided an opportunity to evaluate the similarities and differences of biogenic SOA formation at the different NO_x conditions at the two sites. The chemical compositions of biogenic SOA are very similar at both sites and are similar to chamber experiments, but the minor differences show an important role for NO_x.

2.4.1 Regional Uniformity of Biogenic SOA in the Southeastern U.S.

Although the two SOAS sites in this study are approximately 500 km apart, OM, BC, CO, and sulfate concentrations as well as particle size showed weak to moderate correlations of the time series at the two sites (Figure 2.4 and Figure 2.5). Organic functional groups and submicron non-refractory mass components (nitrate, sulfate, organic, and ammonium) were similar fractions of submicron particle mass (Figure 2.2). OM was approximately 70% and sulfate was 20% of the non-refractory mass. Oxidized organic functional groups (non-acid carbonyl, hydroxyl and carboxylic acid) accounted for 50% of OM (Figure 2.2). Despite the similarity in chemical composition and in submicron particle size (Figure 2.4, Figure 2.5 and Figure 2.10), it is not surprising that the CCN/CN had weak positive correlation at both sites at three different supersaturation levels (r=0.22 to 0.37, Figure 2.11). The fact that the correlation is lower relative to the correlations to sulfate, size and number could suggest a role for local factors in organic composition and associated particle hygroscopicity, even though the concentrations are controlled to a substantial extent by scavenging of regional rain (Figure 3.2). These similarities indicate that the aerosol particle concentrations at these two rural locations in the southeastern U.S. are controlled both by scavenging of regional rain and by very similar mixtures of precursor emissions and photochemical reaction pathways.

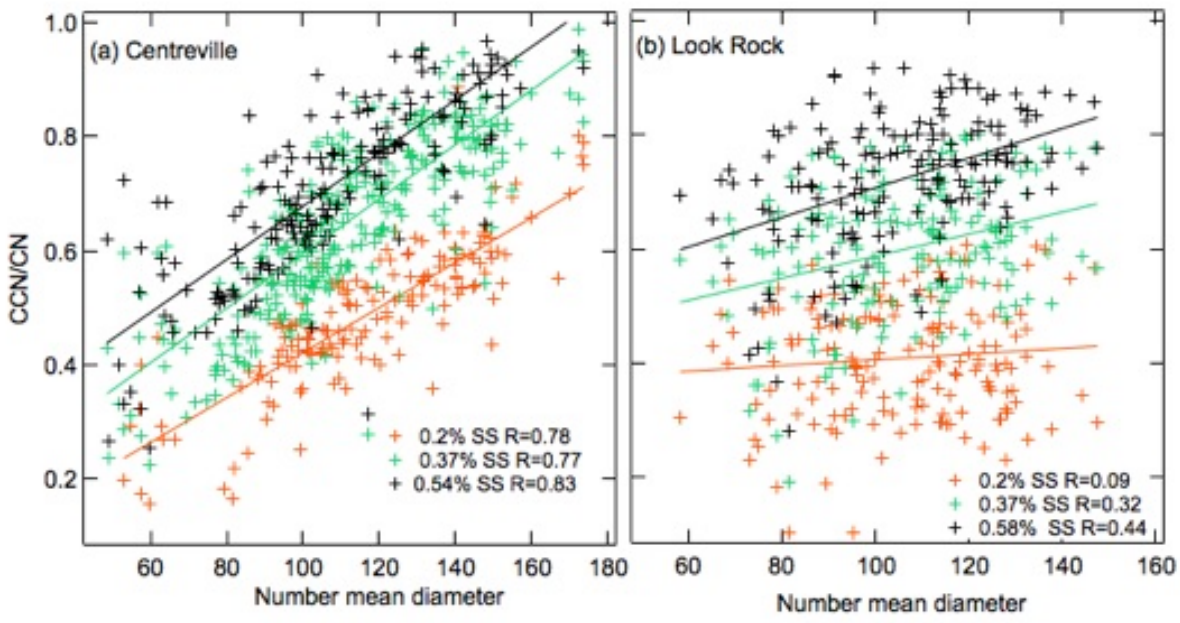

Figure 2.10: Scatter plot of CCN/CN and number mean diameters at both sites for supersaturation of 0.1%, 0.2%, and 0.5%.

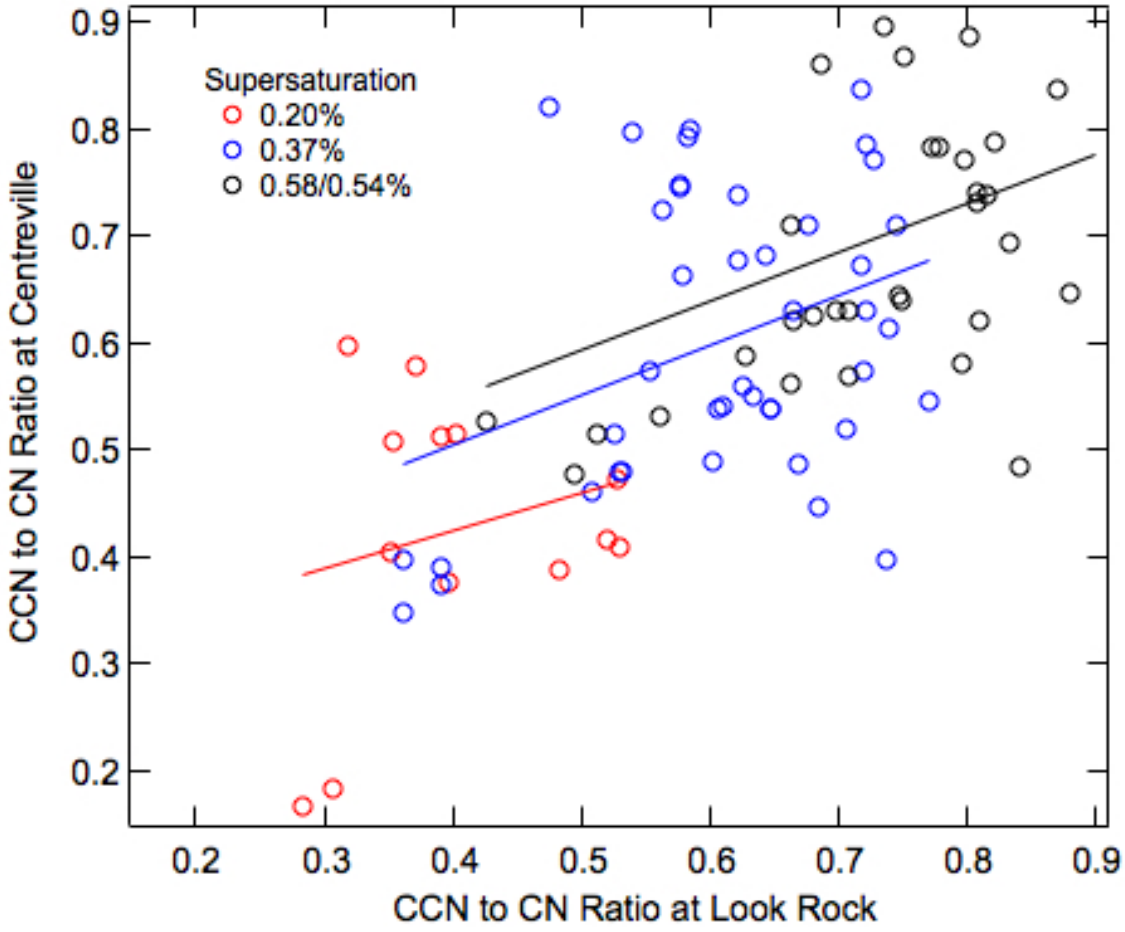

Figure 2.11: Scatter plot for CCN/CN ratio at both sites (R=0.22 and Slope=0.35 with 0.2% supersaturation. R=0.26 and Slope=0.47 with 0.37% supersaturation.R=0.37 Slope=0.45 with 0.58% in LRK and 0.54% in CTR) .

The three very similar FTIR factors and two nearly identical AMS factors measured at both sites were consistent with biogenic SOA formation from largely the same emissions and reactions. The two isoprene-related factors LRK-Factor82 and CTR-Isoprene-OA accounted for approximately 20% of OM and were correlated strongly to sulfate (r>0.75), suggesting heterogeneous sulfate reactions with IEPOX [*Liu et al.*, 2017] were important at both sites. Factors similar to LRK-Factor82 and

CTR-Isoprene-OA were also identified by other summertime studies in the Southeastern U.S. [*Budisulistiorini et al.*, 2016; *Budisulistiorini et al.*, 2017; *Xu et al.*, 2015b]. LRK-MOA and CTR-MOA from FTIR contributed approximately 25% of OM at each site and had a weak correlation of CTR-MOA to CTR-Isoprene-OA (r=0.47) and a moderate correlation of LRK-MOA to LRK-Factor91 (r=0.58), indicating that MOA may also have contributions from biogenic emissions [*Budisulistiorini et al.*, 2015; *Xu et al.*, 2015a].

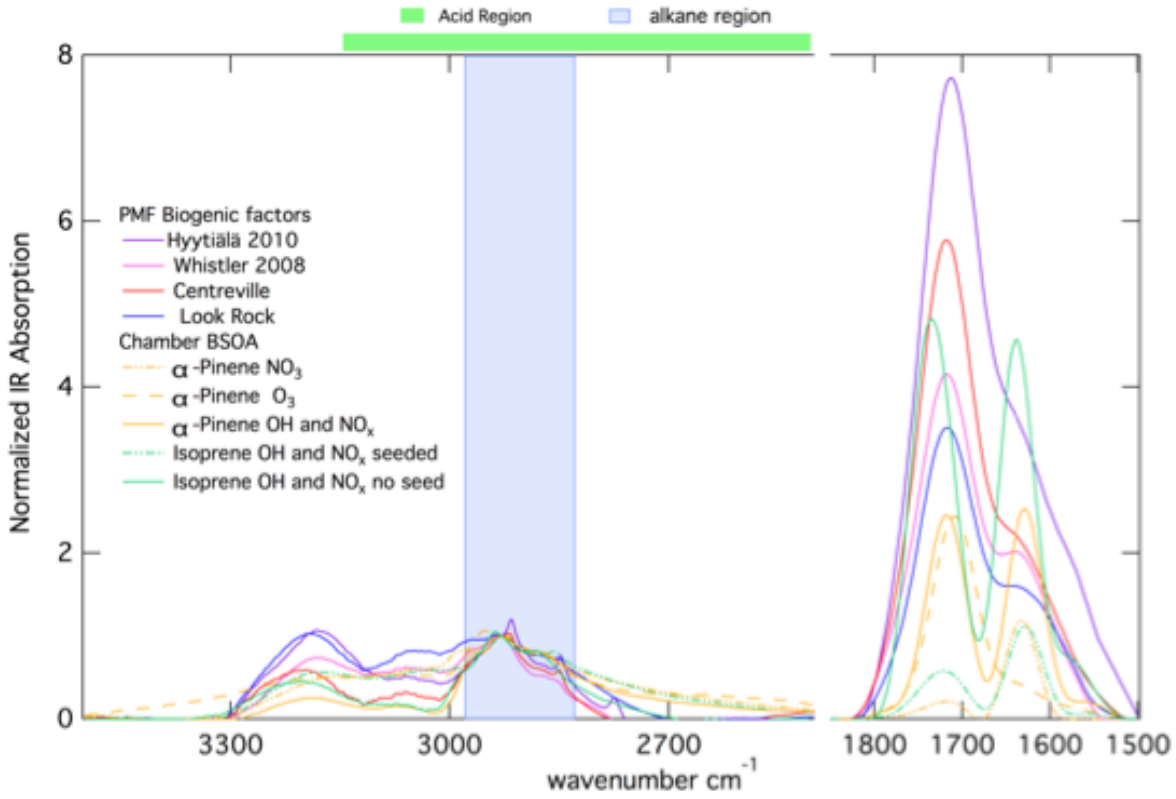

Figure 2.12: Comparison of laboratory-generated biogenic SOA from α-pinene and isoprene to BOA factors from the two SOAS sites, Whistler [Schwartz et al., 2010] and Hyytiälä [Corrigan et al., 2013]. Spectra are normalized at 2927 cm-1, a common methylene peak showed up in all spectra. Ammonium signals were fitted and removed.

With NO_x + OH and O_3 as oxidants, chamber biogenic SOA were very similar to BOA factors at multiple sites (cosine similarities = 0.84 to 0.90), as shown in Table 2.4. Most of these

chamber and factor spectra (Figure 2.12) have both acid and non-acid carbonyl groups and similar shapes of peaks, indicating similar mixtures of functional groups. The peak at 3200 cm^{-1} shows a high and broad hydroxyl functional group absorption consistent with previous biogenic factors at Whistler [*Schwartz et al.*, 2010]. The ammonium peak reflects seed particles in chamber samples and ambient ammonium in the field samples were removed from spectra. In contrast, low carbonyl and high organonitrate groups measured in the NO_3 oxidation products of α-pinene were not similar to BOA factors (cosine similarities = 0.38 to 0.61). The high degree of similarity of the chamber isoprene and monoterpene biogenic SOA spectra from NO_x + OH and O_3 may be one reason that the FTIR PMF BOA factors from Whistler, Hyytiala, and the southeastern U.S. are similar even though they have differing amounts of these two bVOCs (Figure 2.12). The samples from chamber experiments had lower carbonyl group mass concentration compared to the field studies in which biogenic SOA underwent a longer reaction time with lower oxidants compared to chamber. Chamber biogenic SOA had significantly higher organonitrate group fraction (10 to 20% OM) than the ambient BOA, likely because chamber experiments with OH were run in a high NO_x regime whereas field samples could have had contributions from low NO_x conditions as well. The high oxidant level also contributes to the differences between ambient and chamber biogenic SOA. The seeded chamber bSOA was less similar, possibly because the neutral ammonium sulfate did not represent ambient seeds well. The ammonium subtraction process might also contribution to the difference. CTR-BOA and LRK-BOA could have had contributions from both NO_x + OH and O_3 reactions. FFC and MOA are not similar to chamber biogenic SOA, with cosine similarities lower than 0.4. IEPOX biogenic SOA was not formed because the chamber experiments did not include conditions for

low-NO_x, acid-catalyzed chemistry of isoprene oxidation [*Lin et al.*, 2012; *Surratt et al.*, 2010; *Surratt et al.*, 2007].

Table 2.4: Cosine similarity of FTIR biogenic factors and chamber isoprene and α-pinene bSOA. Ammonium absorption was removed.

Cosine Similarity	Experiment Conditions	Ambient BOA Factors+				
		Hyytiala/ Whistler	CTR pm_1	CTR $pm_{2.5}$	LRK pm_1	LRK $pm_{2.5}$
α- Pinene + NO_3 seeded*	RH=50%; UV light off	0.38/0.48	0.38	0.44	0.61	0.57
α - Pinene + O_3 unseeded	RH=0; UV light off	**0.8/0.85**	**0.83**	**0.86**	**0.91**	**0.9**
α - Pinene + OH and NO_x unseeded	RH=50%; UV light: 30 min at 50%	**0.84/0.87**	**0.85**	**0.85**	**0.88**	**0.88**
Isoprene + OH and NO_x unseeded	RH=0; UVlight: 40 min at 100%	**0.88/0.9**	**0.89**	**0.89**	**0.87**	**0.88**
Isoprene + OH and NO_x seeded*	RH=50%; UV light: 30 min at 50%	0.52/0.61	0.53	0.58	0.74	0.70

The CMAQ model simulations (Appendix) also had similar concentrations at the two sites, except for the higher monoterpene-related biogenic SOA at CTR (Figure 2.13). The model components that tracked biogenic SOA from isoprene (Appendix) had similar and substantial concentrations at both sites (0.70 μg m^{-3} at LRK and 0.61 μg m^{-3} at CTR), consistent with the substantial contribution to OM from LRK-Factor82 and CTR-Isoprene-OA. The spatial distribution of simulated IEPOX products is more uniform than the NO_x in the southeastern U.S. (Figure 2.14). The sulfate simulated by CMAQ model was prevalent across the region during the month of June (Figure 2.14), and distribution of isoprene and monoterpene emissions shows spatially uniform across the region because of the high forest coverage over most of the region [Guenther et al., 2012; A Guenther et al., 2006; McRoberts et al., 2005]. Consistent with this study, simultaneous ACSM and AMS measurements from multiple field campaigns at multiple sites showed that OA is homogeneous in the great Atlanta area in summer [Xu et al., 2015b].

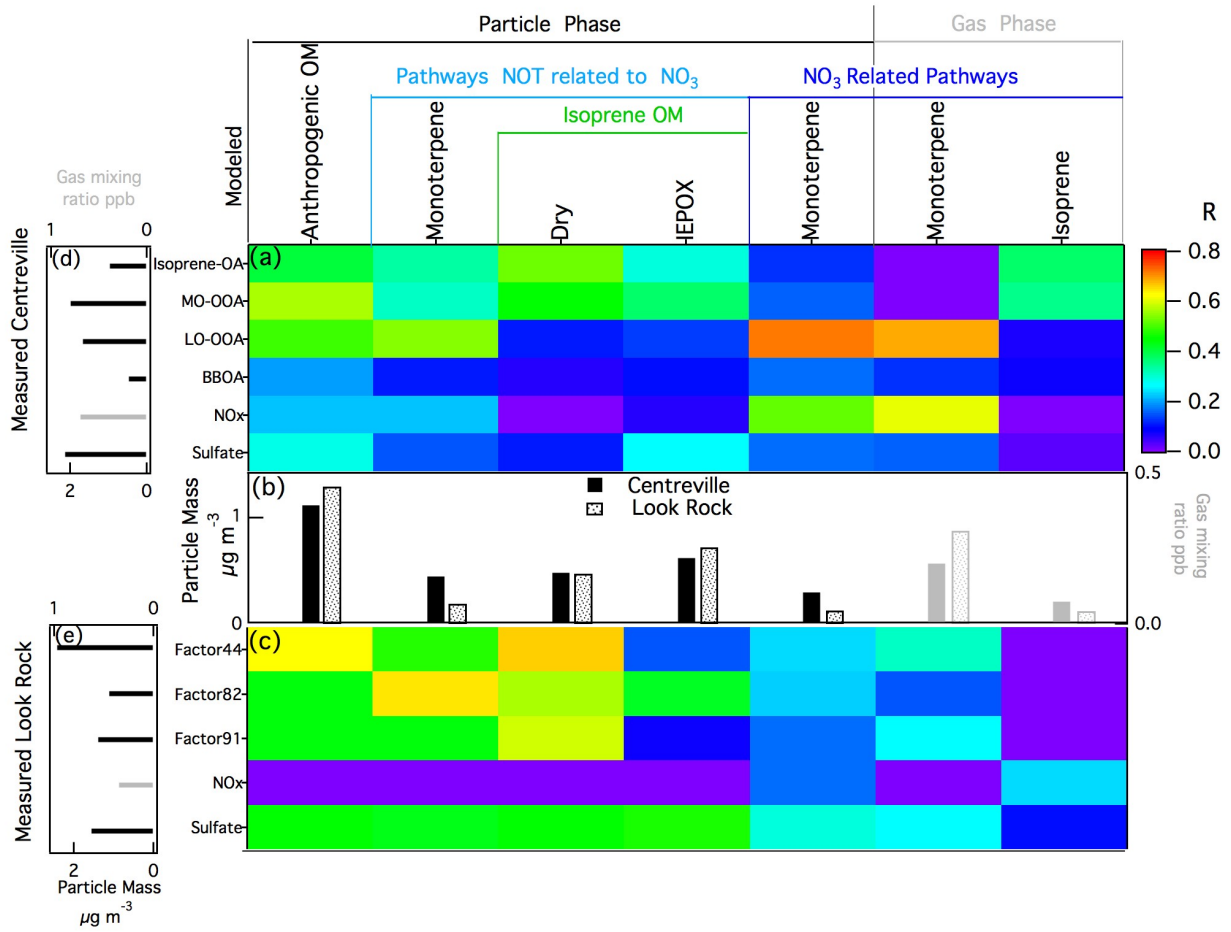

Figure 2.13: Average concentration of CMAQ modeled species and heat map of correlation coefficients of CMAQ model species to measurements in (a) CTR and (c) LRK. Low 24-hour significance level pairs (P>0.05) are shaded. (b) Concentrations of CMAQ modeled species. Concentrations of measured species at (d) CTR and (e) LRK. Details of the modeled species can be found in Appendix. Low concentration species (<0.05 μg m^{-3}) are excluded in this figure.

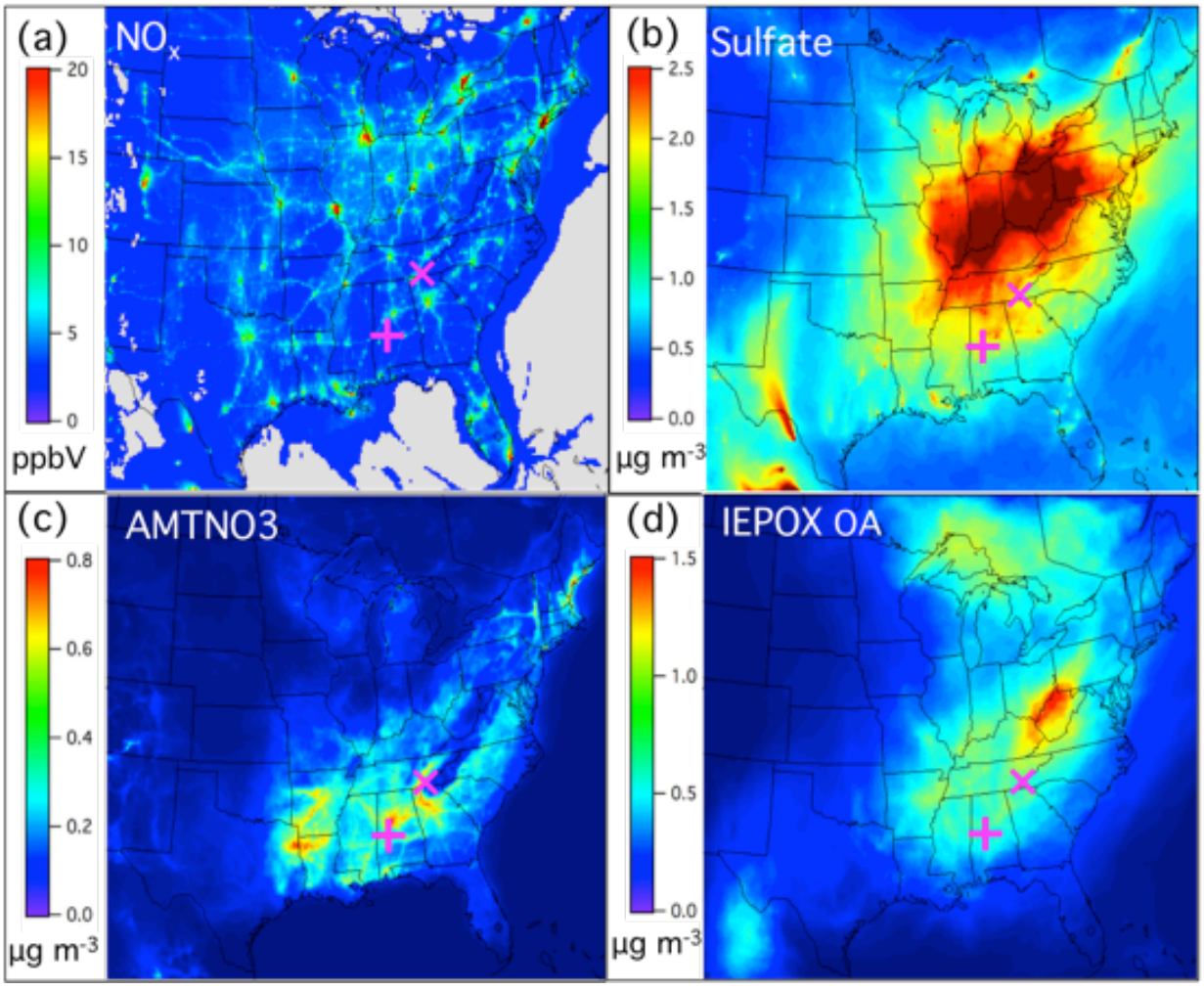

Figure 2.14: Spatial distribution of (a) NOx, (b) sulfate, (c) monoterpene organic nitrate biogenic SOA, and (d) IEPOX related biogenic SOA in Southeastern U.S. from CMAQ model. + sign marks Centreville and × sign marks Look Rock

2.4.2 Difference in NO_x Reactions with bVOC in the Southeastern U.S.

Despite the regional uniformity of particle composition discussed above, there were also important differences between the two sites. Although the two sites are both rural, LRK is more pristine because it is at 801 m altitude and more than 15 km away from cities and highways while CTR is at 126 m altitude and also less than 10 km from the Centreville city, resulting in the higher NO_x and NO_y concentrations at CTR than LRK (Figure 2.4). Aircraft measurements

during the campaign showed a consistent NO_x decrease with increasing altitude in the lowest 2 km of the atmosphere, with the NO_x concentration approaching zero at 2 km above ground level [*Travis et al.*, 2016]. NO_x concentration at CTR also had a clear peak from 0200 to 0900 (Figure 2.6). Similar nighttime NO_x increases have been observed at both urban [*Alghamdi et al.*, 2014] and forested sites [*Alghamdi et al.*, 2014; *Seok et al.*, 2013]. Limited ventilation of surface NO_x emissions in the low nighttime boundary layers may contribute to this the diurnal pattern. Since the high concentration of NO_x coincides with the northerly wind at CTR (Figure 2.15), the early morning NO_x peak at CTR is likely due to transport from vehicle sources from the I-20 morning commute, which is located 30 km north of the site. The resulting NO_x spatial distribution (Figure 2.14) is consistent with National Emissions Inventory at Bibb County (https://www.epa.gov/air-emissions-inventories/national-emissions-inventory-nei), where NO_x is largely from mobile sources (50%)).

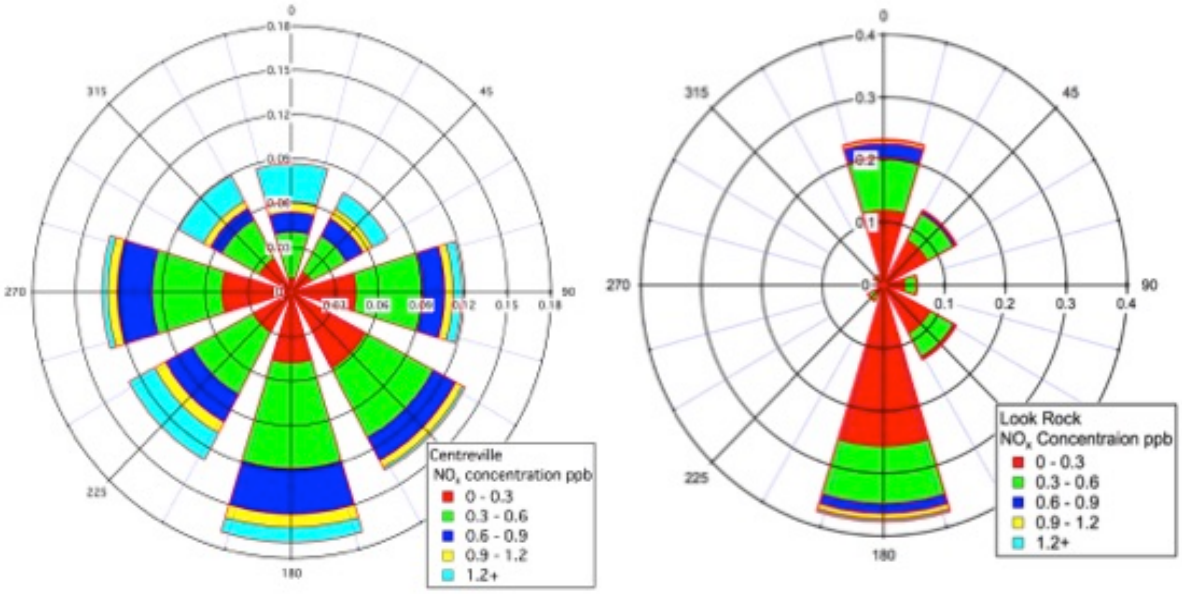

Figure 2.15: Wind rose plot of NO_x concentration at LRK and CTR.

Since the measured mixing ratio and diurnal cycle of isoprene (~3 ppb) and monoterpenes (<1 ppb) were similar at the two sites [*Budisulistiorini et al.*, 2015; *Xu et al.*, 2015a], the different NO_x loadings at LRK and CTR were likely the cause of the differences in the OM concentrations and diurnal patterns [*Liu et al.*, 2017; *Xu et al.*, 2015a]. While OM peaked in the early afternoon (1200-2000) at LRK consistently, it peaked both in late afternoon (1800) and at night (0200) at CTR. The nighttime CTR-BOA was 2.5 times higher than the rest of the time while the nighttime CTR-BOA had similar concentration (92%) with the rest of the time. For example, this diurnal trend is obvious from 11 June to 14 June (Figure 2.8). These different diurnal patterns of the two FTIR BOA factors from LRK and CTR suggests that they were driven by different oxidation pathways. In addition, the correlation of NO_y to O_3 is higher at CTR than LRK in afternoons (1200-1600) with r values of 0.55 and 0.17, respectively, suggesting that NO_x could have contributed to daytime ozone formation at CTR but not, or not directly, at LRK [*Milford et al.*, 1994]. For this reason, NO_x at CTR may have contributed both directly to biogenic SOA formation and indirectly by increasing O_3.

The direct role of NO_x in contributing to CTR-BOA is evident in its early morning peak similar to that of CTR-LO-OOA [*Xu et al.*, 2015a], which suggests a contribution of dark NO_3 oxidation as well as OH + NO_x oxidation (RNO_2 + NO) after sunrise [*Lee et al.*, 2016] that is not present at LRK. Further, the two BOA factors were correlated to NO_x (r=0.41) at CTR but to O_3 (r=0.51) at LRK. NO_x had little effect on biogenic SOA formation at LRK (Figure 2.16) and nighttime BOA factor (analogous to CTR-LO-OOA) was not observed. The daytime LRK-Factor91 accounted for 34% of OM and was correlated to nitrate (r=0.65) and radiation at the surface (r=0.83), consistent with NO_x contributing to oxidants in a photochemically-driven

reaction. Chamber measurements of m/z 91 in products of gas phase isoprene oxidation [*Budisulistiorini et al.*, 2016; *Krechmer et al.*, 2015; *Liu et al.*, 2016; *Riva et al.*, 2016] support this type of formation given the measured *m/z* 91 in LRK-Factor91. Although the factor peaked in daytime with isoprene, we cannot rule out a contribution of monoterpene to this biogenic SOA type [*Liu et al.*, 2017]. This factor was not evident at CTR, indicating its formation may rely on photochemical reactions favored by low NO_x conditions. CTR-LO-OOA and CTR-BOA had weak to moderate correlations to NO_x (r=0.36 and 0.69, respectively) for NO_x higher than 1 ppb (Figure 2.17). LRK-Factor91 and LRK-BOA had moderate correlations of the very limited number of measurements for NO_x >1 ppb (Table 2.5). There was no correlation (r<0.2) of NO_x with CTR-LOOA, LRK-Factor91, CTR-BOA or LRK-BOA for NO_x mixing ratio below 0.5 ppb (Table 2.5). The measurements of CTR-LO-OOA and CTR-BOA for NO_x lower than 1 ppb were excluded from the linear regression because the variability below 1 ppb made the correlation coefficients low and fitted slopes uncertain (Table 2.6). These results suggest that the enhancement of biogenic SOA by NO_x is only clear for NO_x concentrations greater than 1 ppb. NO_x-related enhancement of biogenic SOA formation resulted in 0.5 μg m^{-3} per 1 ppb NO_x for CTR-LO-OOA and 0.6 per 1 ppb NO_x for CTR-BOA, based on the slopes of the regression lines shown. The 1 ppb cutoff does not indicate a chemical threshold but rather results from the many other factors that affect OM concentration during the course of the SOAS campaign at the two sites. These other factors include meteorological events (rain, cloud, transport) during the 36 days of the SOAS study that cause day-to-day differences in OM. In addition, since NO_x can either enhance or suppress bSOA formation, these processes may cancel themselves out when NO_x is low. In the high NO_x regime (>1 ppb), the enhancement effect is sufficiently large that it

is evident despite other factors. The threshold is also consistent with a role for autoxidation as NO_x levels continue to decrease below1 ppb [*Praske et al.*, 2018].

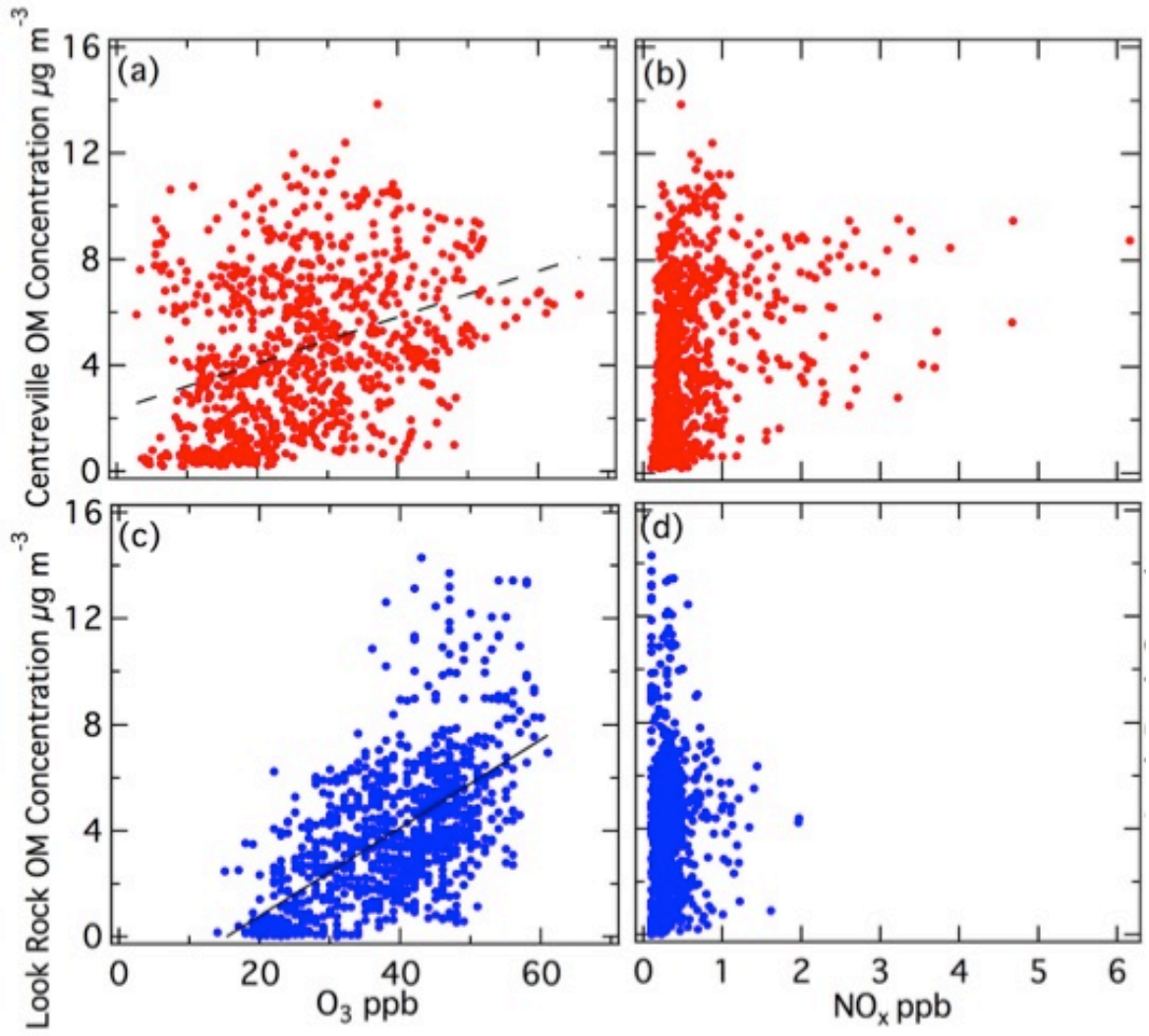

Figure 2.16: Scatter plots of AMS OM at CTR with (a) O3 with r=0.42 and (b) NOx with r=0.22, respectively. Scatter plots of AMS OM at LRK with (a) O3 with r=0.61 and (b) NOx with r=0.08.

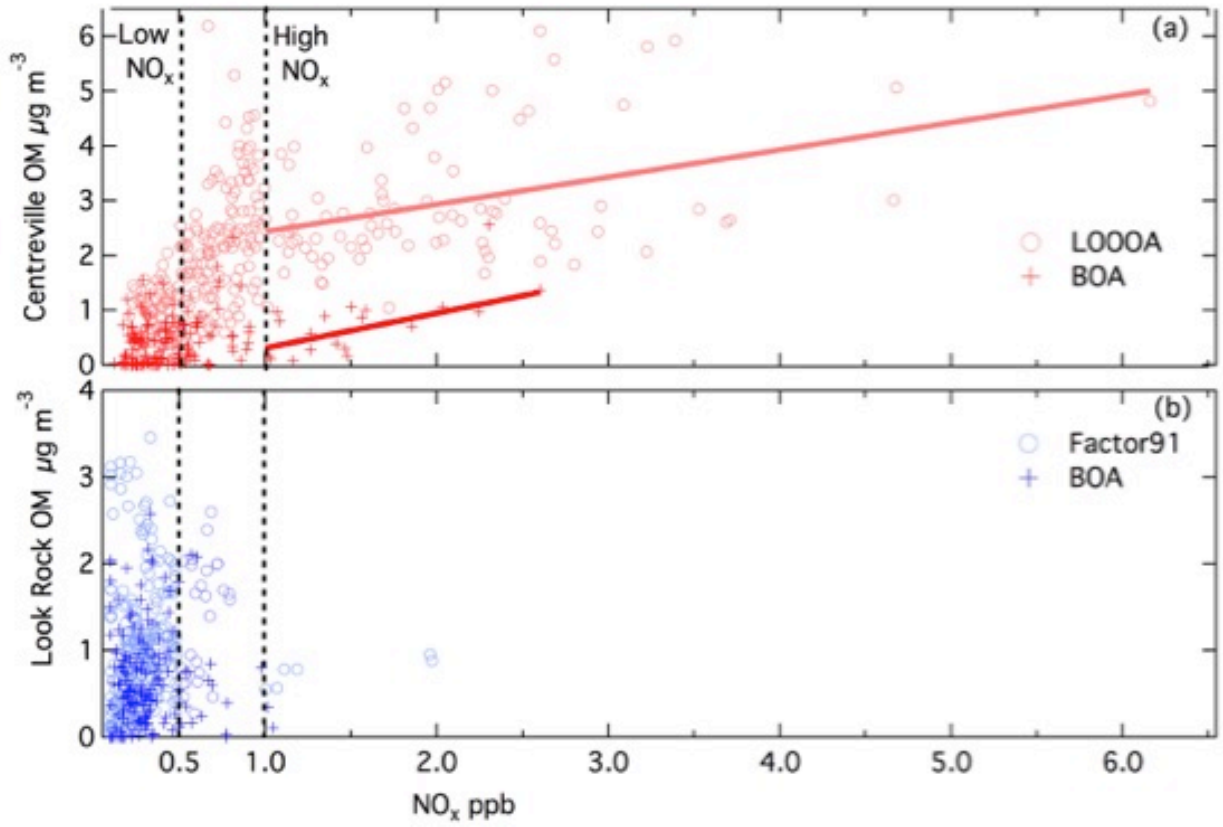

Figure 2.17: Scatter plot of (a) CTR-LO-OOA, CTR-BOA; (b) LRK-Factor91 and LRK-BOA, and NO_x.

Table 2.5: Correlation table of NO_x to AMS and FTIR OM and factors for low NO_x (<0.5 ppb) and high NO_x (>1 ppb) regimes.

Correlation Coefficient	Low NOx (<0.5 ppb)	High NOx (>1 ppb)
CTR-LO-OOA/CTR-BOA	-0.18/0.13	**0.36/0.69**
LRK-Factor91/LRK-BOA	0.16/0.15	0.83/NA*
CTR-MO-OOA/CTR-FFC	-0.22/0.00	-0.26/0.37
LRK-Factor44/LRK-FFC	0.23/0.01	0.45/NA*
CTR-Isoprene-OA/CTR-MOA	-0.11/0.04	0.25/0.23
LRK-Factor82/ LRK-MOA	0.10/0.09	0.12/NA*
CTR-AMS OM/CTR-FTIR OM	0.03/0.06	0.14/**0.58**
LRK-AMS OM/LRK-FTIR OM	0.00/0.08	-0.36/NA*

*NA indicates that there were too few measurements for a comparison, namely less than 6 AMS or 2 FTIR measurements.

Table 2.6: Sensitivity analysis for the slope, correlation coefficients and normalized standard deviation.

Threshold		0.7	0.8	0.9	1	1.1	1.2	1.3
AMS LOOOA	Normailized SD	0.51	0.48	0.48	0.49	0.49	0.49	0.49
	Slope	0.53	0.45	0.48	0.53	0.52	0.50	0.46
	R	0.36	0.32	0.35	0.36	0.36	0.33	0.30
FTIR BOA	Normailized SD	0.81	0.78	0.78	0.76	0.69	0.66	0.65
	Slope	0.37	0.42	0.88	0.98	1.06	1.01	1.03
	R	0.27	0.30	0.61	0.69	0.58	0.54	0.52

In the CMAQ simulation, NO_x and NO_x-related biogenic SOA was more spatially variable than sulfate-related biogenic SOA in the SOAS study region and was very low (<0.2 μg m^{-3}) in some areas, such as at LRK (Figure 2.14). The high spatial variation of NO_x-related biogenic SOA is consistent with the spatial distribution of NO_x emissions as well as significant contributions from nitrate radical reactions, which tend to occur at night when atmospheric conditions are more stable and reduce transport. Measured NO_x mixing ratio was moderately correlated to model components from NO_3 oxidation products of monoterpene, namely particule-phase monoterpene-derived organic nitrates (Appendix) at CTR (r=0.64 to 0.72) but not at LRK (r<0.25) (Figure 2.13). The mass concentration of NO_3 oxidation products of monoterpene was 2.3 times higher at CTR at 0.28 μg m^{-3} compared to 0.12 μg m^{-3} at LRK from the CMAQ model simulation.

2.5 Conclusions

Fourier Transform Infrared Spectroscopy and Aerosol Mass Spectrometer measurements of submicron mass at LRK, Tennessee, and CTR, Alabama, showed that CTR was more polluted by emissions from cities and highways while LRK was more pristine because of its higher elevation. OM composition and source apportionment were very similar at these two sites, although biomass burning and nighttime NO_x contributed to OM at CTR but not at LRK. The time series of CO, sulfate, BC and OM concentrations at LRK and CTR had weak and moderate correlations of r= 0.51, 0.51, 0.40 and 0.47, respectively. However, NO_x had a very low correlation (r=0.08) between the sites with nighttime-to-early-morning peaks 3 to 10 times higher at CTR than at LRK.

The organic functional group and submicron non-refractory component (sulfate, nitrate, ammonium, organic) compositions were very similar at both sites. Three almost identical FTIR PMF factors of both PM_1 and $PM_{2.5}$ had nearly identical contributions to OM with ~40% related to fossil fuel combustion (FFC), ~25% related to mixed organic aerosol (MOA), and ~20% associated with biogenic organic aerosol (BOA) sources. BOA was similar to chamber SOA generated from both isoprene and monoterpene precursors for NO_x + OH and O_3 oxidants with cosine similarity higher than 0.8. LRK Factor82 and CTR-Isoprene-OA factor was associated with sulfate and with isoprene oxidation products such as IEPOX. This isoprene related factor contributed 22% at LRK and 18% at CTR, consistent with summertime observations from several other sites in the southeastern U.S. [*Budisulistiorini et al.*, 2016; *Budisulistiorini et al.*, 2017; *Xu et al.*, 2015b] and despite the differences in NO_x concentrations.

The enhancement of biogenic SOA by NO_x was only evident for NO_x higher than 1 ppb, which only occurred at CTR during SOAS. NO_x enhanced biogenic SOA formation by 0.5 to 1 μg m^{-3} per ppb NO_x. The negligible contribution of NO_x-enhanced OM at lower than 1 ppb NO_x at LRK provided the most striking difference between the two sites. Organic mass (OM) had a maximum in the afternoon at both sites but increased again during nighttime only at CTR. The correlation of biogenic SOA species from the CMAQ model simulations also showed NO_x produced more OM at CTR during late-night-early-morning periods than at LRK, which may be associated with nitrate-radical oxidation pathways at high NO_x.

2.6 Acknowledgements

We thank Ashley Corrigan, Janin Guzman-Morales, and Katie Kolesar for assistance at the LRK field site and Annmarie Carlton, Joost deGouw, Jose Jimenez, and Allen Goldstein for organizing the SOAS campaign. We thank Eric Edgerton for gas concentration and meteorological measurements at Centreville and IMPROVE network for ozone concentration at Look Rock. We appreciate the support of Sherri Hunt for this project. This work was supported by U.S. Environmental Protection Agency (EPA) grant RD-83540801. Lu Xu and Nga L. Ng acknowledge National Science Foundation grant 1242258 and US Environmental Protection Agency STAR grant RD-83540301. The US EPA through its Office of Research and Development collaborated in the research described here. It has been subjected to Agency administrative review and approved for publication but may not necessarily reflect official Agency policy. The EPA does not endorse any products or commercial services mentioned in this publication. Timothy Bertram was supported by the Office of Science (Office of Biological

and Environmental Research), US Department of Energy (grant no. DE-SC0006431). LRK AMS and FTIR measurements used in this study are curated at http://doi.org/10.6075/J0P26W1T, and all measurements are also available at the project archive http://esrl.noaa.gov/csd/groups/csd7/measurements/2013senex/Ground/DataDownload. CMAQ model code is available via https://github.com/USEPA/CMAQ.

Chapter 2, in full, has been submitted to *Journal of Geophysical Reserach* in 2018 with slight modifications. Liu, J., Russell, L.M., Ruggeri, G., Takahama, S., Claflin, M.S., Ziemann, P.J., Pye, H.O.T., Murphy, B.N., Xu, L., Ng, N.L., McKinney, K.A., Budisulistiorini, S.H., Bertram, T.H., Athanasios, N. and Surratt, J.D, "Regional Similarities and NO_x-related Increases in Biogenic Secondary Organic Aerosol in Summertime Southeastern U.S." The dissertation author was the primary investigator and author of this paper. The dissertation author was the primary investigator and author of this paper.

2.7 Appendix

Figure 2.1 shows the time series of AMS OM and organic functional group concentrations. The correlations of AMS/ ACSM OM to FTIR OM are moderate to strong (r=0.68~0.80) at CTR and LRK (Figure 2.3). Emissions by county were available from Nation Emission Inventory (NEI). Both counties have vehicles as the most abundant source of NO_x.AMS and ACSM PMF factors at CTR and LRK are compared in Table 2.7. Time series correlations of FTIR PMF factors to tracers are shown in Table 2.3. The chamber generated bSOA FTIR spectra are compared with ambient biogenic factor spectra in Table 2.4. The

threshold effect of NO_x on bSOA formation is shown in Table S4 and sensitivity analysis is shown in Table 2.6.

Table 2.7: Properties of FTIR PMF factor solution evaluation at LRK and CTR.

Criteria \ Factor Number	2	3	4	5	6
Q/Q_{exp}	2.35/1.33	0.95/0.57	0.62/0.42	0.54/0.36	0.48/0.34
Absolute residual	20.6/18.3%	14.7/13.0%	13.9/11.7%	13.4/10.9%	12.9%/10.1%
Temporal correlation factor strength (r>0.8)	None/None	None/None	None/None	None/None	1 pair/None
Similarity of factor spectra (r>0.8)	None/None	None/None	2 /1 pair(s)	4/2 pairs	4/3 pairs
Factors with less than 6% OM	None/None	None/None	None/None	1/1	1/2

2.7.1 FTIR PMF operation and factor selection

Factorization was applied to the baselined IR spectra from FTIR for both PM1 and PM2.5 samples at LRK and at CTR. Six factor spaces (1~6) were analyzed. Fpeaks were explored from -2 to 2 at 0.5 increments. Seeds of 1, 10 and 100 were used for each Fpeak and factor to examine the robustness of each solution. Figure 2.18 and Figure 2.19 and Table 2.7 show that the properties of the solutions are generally robust. The change of solutions with rotation values is small in all solutions. Q/Qexpected decreases smoothly when factor number increases in solutions with more than 3 factors (Table 2.7). The Q/Qexpected of PM1 is lower

than PM2.5, which is consistent with their higher time resolution of the PM1 samples, making PM1 the stronger solution. The PM2.5 solution is similar to that of PM1, so only the PM1 PMF solutions at LRK are reported here.

Two factors that contain a large amount of ammonium were identified from the PMF in the 2-factor space, See Figure 2.18 and Figure 2.19. Those two factors are produced in almost all solutions with different factor numbers and rotations. However, with only these two factors, ~20% of the OM cannot be explained and is categorized as residual. A third factor with higher hydroxyl and carbonyl group is identified from the 3-factor solution and accounts for ~20% of the total OM. The 3-factor solution reduces the residual to <15%. The time series of the factors are independent with the highest correlation coefficient of 0.72 in the 3-factor solution. Degenerate spectra appear in solutions with 4 or more factors. Two pairs of factors at LRK and one pair at CTR have similar cosine similarity (>0.80) in the 4-factor solutions.

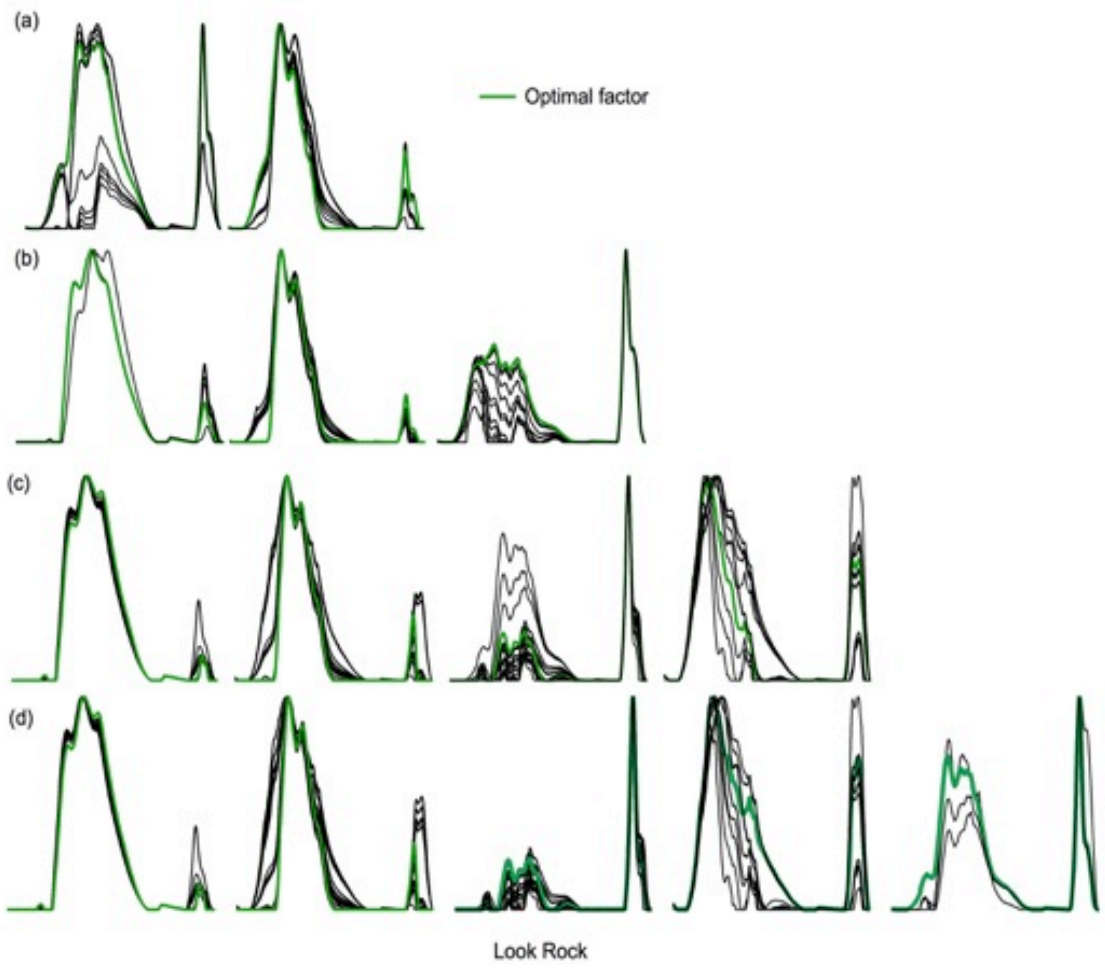

Figure 2.18: FTIR PMF factors for solutions with 2 to 5 factors and fpeak values of -2 to 2 at LRK.

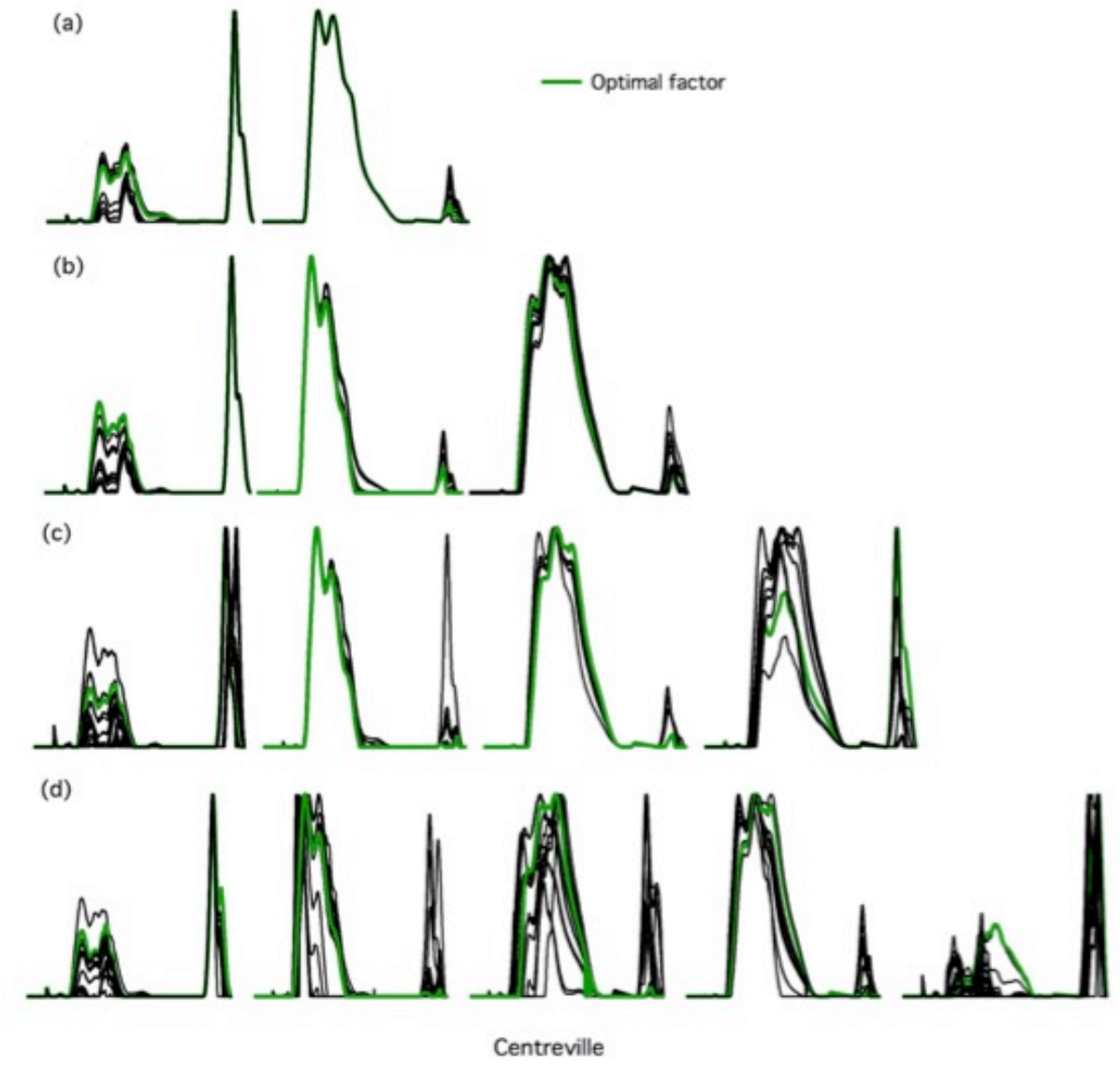

Figure 2.19: FTIR PMF factors for solutions with 2 to 5 factors and fpeak values of -2 to 2 at CTR.

2.7.2 Group of model species in CMAQ model

The CMAQ model simulations are used here to show the regional uniformity of bSOA [Murphy et al., 2017; Pye et al., 2015; Pye et al., 2017]. CMAQ predictions for summer 2013

have been evaluated regionally with measurements from the SEARCH network, IMPROVE network, CSN network, and CASTNET for species including OA, nitrate (nitric acid + aerosol nitrate), sulfate, ammonium, NOx, VOCs, oxidants, and other atmospheric constituents [Pye et al., 2015; Pye et al., 2017]. The names of CMAQ model species can be found in the supplement of two recent CMAQ model papers [*Pye et al.*, 2015; *Pye et al.*, 2017]. The nitrate radical related species are ISOPNN, MTNO3 (gas phase), AISOPNN and AMTNO3 (aerosol phase). The chemistry processes were introduced in the introduction of main text. ASQT (sesquiterpene species) is not included since it's small (0.05 μg m^{-3}). The species from CMAQ model were simplified in Figure 6, and the simplified groups are defined in Table 2.8.

Table 2.8: Nomenclature of the bSOA categories from the CMAQ model.

Category				Average Concentration (CTR/LRK) μg m^{-3}	CMAQ model species
bSOA	NOx related	Monoterpene		0.3/0.1	AMTNO3
		Isoprene		<0.1/<0.1	AISOPNN
	Not related to NOx	Isoprene	Dry	0.5/0.5	AISO1+AISO2+ AOLGB*(AISO1+AISO2)/(ATRP1+ATRP2+ASQT+AISO1J+AISO2)
			IEPOX	0.6/0.7	AIETET+AIEOS+AIDIM
			MAE, HMML	<0.1/<0.1	AIMGA+AIMOS
		Monoterpene		0.4/0.2	ATRP1+ATRP2+ AOLGB*(ATRP1+ATRP2)/(ATRP1+ATRP2+ASQT+AISO1J+AISO2)
Anthropogenic OA	Anthropogenic			1.1/1.3	Benzene OA+ toluene OA+ xylene OA + PCSOA+POA+OPOA.

References

Agarwal, A. K., Gupta, T., Shukla, P. C., and Dhar, A.: Particulate emissions from biodiesel fuelled CI engines, Energy Conversion and Management, 94, 311-330, 10.1016/j.enconman.2014.12.094, 2015.

Alghamdi, M. A., Khoder, M., Harrison, R. M., Hyvarinen, A. P., Hussein, T., Al-Jeelani, H., Abdelmaksoud, A. S., Goknil, M. H., Shabbaj, II, Almehmadi, F. M., Lihavainen, H., Kulmala, M., and Hameri, K.: Temporal variations of O-3 and NOx in the urban background atmosphere of the coastal city Jeddah, Saudi Arabia, Atmospheric Environment, 94, 205-214, 10.1016/j.atmosenv.2014.03.029, 2014.

Allan, J. D., Alfarra, M. R., Bower, K. N., Williams, P. I., Gallagher, M. W., Jimenez, J. L., McDonald, A. G., Nemitz, E., Canagaratna, M. R., Jayne, J. T., Coe, H., and Worsnop, D. R.: Quantitative sampling using an Aerodyne aerosol mass spectrometer: 2. Measurements of fine particulate chemical composition in two UK cities (vol 108, art no 4091, 2003), Journal of Geophysical Research-Atmospheres, 108, 10.1029/2003jd001608, 2003a.

Allan, J. D., Jimenez, J. L., Williams, P. I., Alfarra, M. R., Bower, K. N., Jayne, J. T., Coe, H., and Worsnop, D. R.: Quantitative sampling using an Aerodyne aerosol mass spectrometer: 1. Techniques of data interpretation and error analysis (vol 108, art no 4090, 2003), Journal of Geophysical Research-Atmospheres, 108, 10.1029/2003jd001607, 2003b.

Atkinson, R., Baulch, D. L., Cox, R. A., Crowley, J. N., Hampson, R. F., Hynes, R. G., Jenkin, M. E., Rossi, M. J., and Troe, J.: Evaluated kinetic and photochemical data for atmospheric chemistry: Volume I - gas phase reactions of O-x, HOx, NOx and SOx species, Atmospheric Chemistry and Physics, 4, 1461-1738, 2004.

Bahreini, R., Ervens, B., Middlebrook, A. M., Warneke, C., de Gouw, J. A., DeCarlo, P. F., Jimenez, J. L., Brock, C. A., Neuman, J. A., Ryerson, T. B., Stark, H., Atlas, E., Brioude, J., Fried, A., Holloway, J. S., Peischl, J., Richter, D., Walega, J., Weibring, P., Wollny, A. G., and Fehsenfeld, F. C.: Organic aerosol formation in urban and industrial plumes near Houston and Dallas, Texas, Journal of Geophysical Research-Atmospheres, 114, 10.1029/2008jd011493, 2009.

Blanchard, C. L., Hidy, G. M., Shaw, S., Baumann, K., and Edgerton, E. S.: Effects of emission reductions on organic aerosol in the southeastern United States, Atmospheric Chemistry and Physics, 16, 215-238, 10.5194/acp-16-215-2016, 2016.

Budisulistiorini, S. H., Canagaratna, M. R., Croteau, P. L., Marth, W. J., Baumann, K., Edgerton, E. S., Shaw, S. L., Knipping, E. M., Worsnop, D. R., Jayne, J. T., Gold, A., and Surratt, J. D.: Real-time continuous characterization of secondary organic aerosol derived from isoprene

epoxydiols in downtown Atalanta, Georgia, using the Aerodyne Aerosol Chemical Speciation Monitor, Environmental Science & Technology, 47, 5686-5694, 10.1021/es400023n, 2013.

Budisulistiorini, S. H., Li, X., Bairai, S. T., Renfro, J., Liu, Y., Liu, Y. J., McKinney, K. A., Martin, S. T., McNeill, V. F., Pye, H. O. T., Nenes, A., Neff, M. E., Stone, E. A., Mueller, S., Knote, C., Shaw, S. L., Zhang, Z., Gold, A., and Surratt, J. D.: Examining the effects of anthropogenic emissions on isoprene-derived secondary organic aerosol formation during the 2013 Southern Oxidant and Aerosol Study (SOAS) at the Look Rock, Tennessee ground site, Atmospheric Chemistry and Physics, 15, 8871-8888, 10.5194/acp-15-8871-2015, 2015.

Budisulistiorini, S. H., Baumann, K., Edgerton, E. S., Bairai, S. T., Mueller, S., Shaw, S. L., Knipping, E. M., Gold, A., and Surratt, J. D.: Seasonal characterization of submicron aerosol chemical composition and organic aerosol sources in the southeastern United States: Atlanta, Georgia,and Look Rock, Tennessee, Atmospheric Chemistry and Physics, 16, 5171-5189, 10.5194/acp-16-5171-2016, 2016.

Budisulistiorini, S. H., Nenes, A., Carlton, A. G., Surratt, J. D., McNeill, V. F., and Pye, H. O. T.: Simulating Aqueous-Phase Isoprene-Epoxydiol (IEPOX) Secondary Organic Aerosol Production During the 2013 Southern Oxidant and Aerosol Study (SOAS), Environmental Science & Technology, 51, 5026-5034, 10.1021/acs.est.6b05750, 2017.

Carlton, A. G., Pinder, R. W., Bhave, P. V., and Pouliot, G. A.: To what extent can biogenic SOA be controlled?, Environmental Science & Technology, 44, 3376-3380, 10.1021/es903506b, 2010.

Cerully, K. M., Bougiatioti, A., Hite, J. R., Guo, H., Xu, L., Ng, N. L., Weber, R., and Nenes, A.: On the link between hygroscopicity, volatility, and oxidation state of ambient and water-soluble aerosols in the southeastern United States, Atmospheric Chemistry and Physics, 15, 8679-8694, 10.5194/acp-15-8679-2015, 2015.

Chen , Q., Farmer, D. K., Rizzo, L. V., Pauliquevis, T., Kuwata, M., Karl, T. G., Guenther, A., Allan, J. D., Coe, H., Andreae, M. O., Poschl, U., Jimenez, J. L., Artaxo, P., and Martin, S. T.: Submicron particle mass concentrations and sources in the Amazonian wet season (AMAZE-08), Atmospheric Chemistry and Physics, 15, 3687-3701, 10.5194/acp-15-3687-2015, 2015.

Cheung, K. L., Ntziachristos, L., Tzamkiozis, T., Schauer, J. J., Samaras, Z., Moore, K. F., and Sioutas, C.: Emissions of Particulate Trace Elements, Metals and Organic Species from Gasoline, Diesel, and Biodiesel Passenger Vehicles and Their Relation to Oxidative Potential, Aerosol Science and Technology, 44, 500-513, 10.1080/02786821003758294, 2010.

Corrigan, A. L., Russell, L. M., Takahama, S., Aijala, M., Ehn, M., Junninen, H., Rinne, J., Petaja, T., Kulmala, M., Vogel, A. L., Hoffmann, T., Ebben, C. J., Geiger, F. M., Chhabra, P., Seinfeld, J. H., Worsnop, D. R., Song, W., Auld, J., and Williams, J.: Biogenic and biomass burning organic aerosol in a boreal forest at Hyytiala, Finland, during HUMPPA-COPEC 2010, Atmospheric Chemistry and Physics, 13, 12233-12256, 10.5194/acp-13-12233-2013, 2013.

Davis, R. E., Hayden, B. P., Gay, D. A., Phillips, W. L., and Jones, G. V.: The North Atlantic subtropical anticyclone, Journal of Climate, 10, 728-744, 10.1175/1520-0442(1997)010<0728:tnasa>2.0.co;2, 1997.

Day, D. A., Liu, S., Russell, L. M., and Ziemann, P. J.: Organonitrate group concentrations in submicron particles with high nitrate and organic fractions in coastal southern California, Atmospheric Environment, 44, 1970-1979, 10.1016/j.atmosenv.2010.02.045, 2010.

de Sa, S. S., Palm, B. B., Campuzano-Jost, P., Day, D. A., Newburn, M. K., Hu, W. W., Isaacman-VanWertz, G., Yee, L. D., Thalman, R., Brito, J., Carbone, S., Artaxo, P., Goldstein, A. H., Manzi, A. O., Souza, R. A. F., Mei, F., Shilling, J. E., Springston, S. R., Wang, J., Surratt, J. D., Alexander, M. L., Jimenez, J. L., and Martin, S. T.: Influence of urban pollution on the production of organic particulate matter from isoprene epoxydiols in central Amazonia, Atmospheric Chemistry and Physics, 17, 6611-6629, 10.5194/acp-17-6611-2017, 2017.

DeCarlo, P. F., Kimmel, J. R., Trimborn, A., Northway, M. J., Jayne, J. T., Aiken, A. C., Gonin, M., Fuhrer, K., Horvath, T., Docherty, K. S., Worsnop, D. R., and Jimenez, J. L.: Field-deployable, high-resolution, time-of-flight aerosol mass spectrometer, Analytical Chemistry, 78, 8281-8289, 10.1021/ac061249n, 2006.

Devore, J. L., and Berk, K. N.: Modern Mathematical Statistics with Application, Second ed., Springer Science+Business Media, LLC, Springer New York Dordrecht Heidelberg London, 2012.

Edwards, P. M., Aikin, K. C., Dube, W. P., Fry, J. L., Gilman, J. B., de Gouw, J. A., Graus, M. G., Hanisco, T. F., Holloway, J., Huber, G., Kaiser, J., Keutsch, F. N., Lerner, B. M., Neuman, J. A., Parrish, D. D., Peischl, J., Pollack, I. B., Ravishankara, A. R., Roberts, J. M., Ryerson, T. B., Trainer, M., Veres, P. R., Wolfe, G. M., Warneke, C., and Brown, S. S.: Transition from high- to low-NOx control of night-time oxidation in the southeastern US, Nature Geoscience, 10, 490-+, 10.1038/ngeo2976, 2017.

Ehn, M., Thornton, J. A., Kleist, E., Sipila, M., Junninen, H., Pullinen, I., Springer, M., Rubach, F., Tillmann, R., Lee, B., Lopez-Hilfiker, F., Andres, S., Acir, I. H., Rissanen, M., Jokinen, T., Schobesberger, S., Kangasluoma, J., Kontkanen, J., Nieminen, T., Kurten, T., Nielsen, L. B., Jorgensen, S., Kjaergaard, H. G., Canagaratna, M., Dal Maso, M., Berndt, T., Petaja, T., Wahner, A., Kerminen, V. M., Kulmala, M., Worsnop, D. R., Wildt, J., and Mentel, T. F.: A large source of low-volatility secondary organic aerosol, Nature, 506, 476-+, 10.1038/nature13032, 2014.

Gilardoni, S., Liu, S., Takahama, S., Russell, L. M., Allan, J. D., Steinbrecher, R., Jimenez, J. L., De Carlo, P. F., Dunlea, E. J., and Baumgardner, D.: Characterization of organic ambient aerosol during MIRAGE 2006 on three platforms, Atmospheric Chemistry and Physics, 9, 5417-5432, 2009.

Guenther, Jiang, X., Heald, C. L., Sakulyanontvittaya, T., Duhl, T., Emmons, L. K., and Wang, X.: The Model of Emissions of Gases and Aerosols from Nature version 2.1 (MEGAN2.1): an extended and updated framework for modeling biogenic emissions, Geoscientific Model Development, 5, 1471-1492, 10.5194/gmd-5-1471-2012, 2012.

Guenther, A., Karl, T., Harley, P., Wiedinmyer, C., Palmer, P. I., and Geron, C.: Estimates of global terrestrial isoprene emissions using MEGAN (Model of Emissions of Gases and Aerosols from Nature), Atmospheric Chemistry and Physics, 6, 3181-3210, 2006.

Hallquist, M., Wenger, J. C., Baltensperger, U., Rudich, Y., Simpson, D., Claeys, M., Dommen, J., Donahue, N. M., George, C., Goldstein, A. H., Hamilton, J. F., Herrmann, H., Hoffmann, T., Iinuma, Y., Jang, M., Jenkin, M. E., Jimenez, J. L., Kiendler-Scharr, A., Maenhaut, W., McFiggans, G., Mentel, T. F., Monod, A., Prevot, A. S. H., Seinfeld, J. H., Surratt, J. D., Szmigielski, R., and Wildt, J.: The formation, properties and impact of secondary organic aerosol: current and emerging issues, Atmospheric Chemistry and Physics, 9, 5155-5236, 2009.

Hawkins, L. N., and Russell, L. M.: Oxidation of ketone groups in transported biomass burning aerosol from the 2008 Northern California Lightning Series fires, Atmospheric Environment, 44, 4142-4154, 10.1016/j.atmosenv.2010.07.036, 2010.

Hoyle, C. R., Boy, M., Donahue, N. M., Fry, J. L., Glasius, M., Guenther, A., Hallar, A. G., Hartz, K. H., Petters, M. D., Petaja, T., Rosenoern, T., and Sullivan, A. P.: A review of the anthropogenic influence on biogenic secondary organic aerosol, Atmospheric Chemistry and Physics, 11, 321-343, 10.5194/acp-11-321-2011, 2011.

Hu, W. W., Campuzano-Jost, P., Palm, B. B., Day, D. A., Ortega, A. M., Hayes, P. L., Krechmer, J. E., Chen, Q., Kuwata, M., Liu, Y. J., de Sa, S. S., McKinney, K., Martin, S. T., Hu, M., Budisulistiorini, S. H., Riva, M., Surratt, J. D., St Clair, J. M., Isaacman-Van Wertz, G., Yee, L. D., Goldstein, A. H., Carbone, S., Brito, J., Artaxo, P., de Gouw, J. A., Koss, A., Wisthaler, A., Mikoviny, T., Karl, T., Kaser, L., Jud, W., Hansel, A., Docherty, K. S., Alexander, M. L., Robinson, N. H., Coe, H., Allan, J. D., Canagaratna, M. R., Paulot, F., and Jimenez, J. L.: Characterization of a real-time tracer for isoprene epoxydiols-derived secondary organic aerosol (IEPOX-SOA) from aerosol mass spectrometer measurements, Atmospheric Chemistry and Physics, 15, 11807-11833, 10.5194/acp-15-11807-2015, 2015.

Hutzell, W. T., Luecken, D. J., Appel, K. W., and Carter, W. P. L.: Interpreting predictions from the SAPRC07 mechanism based on regional and continental simulations, Atmospheric Environment, 46, 417-429, 10.1016/j.atmosenv.2011.09.030, 2012.

Jimenez, J. L., Canagaratna, M. R., Drewnick, F., Allan, J. D., Alfarra, M. R., Middlebrook, A. M., Slowik, J. G., Zhang, Q., Coe, H., Jayne, J. T., and Worsnop, D. R.: Comment on "The effects of molecular weight and thermal decomposition on the sensitivity of a thermal desorption aerosol mass spectrometer", Aerosol Science and Technology, 50, I-XV, 10.1080/02786826.2016.1205728, 2016.

Kroll, J. H., Ng, N. L., Murphy, S. M., Flagan, R. C., and Seinfeld, J. H.: Secondary organic aerosol formation from isoprene photooxidation, Environmental Science & Technology, 40, 1869-1877, 10.1021/es0524301, 2006.

Kroll, J. H., and Seinfeld, J. H.: Chemistry of secondary organic aerosol: Formation and evolution of low-volatility organics in the atmosphere, Atmospheric Environment, 42, 3593-3624, 10.1016/j.atmosenv.2008.01.003, 2008.

Lane, T. E., Donahue, N. M., and Pandis, S. N.: Effect of NOx on secondary organic aerosol concentrations, Environmental Science & Technology, 42, 6022-6027, 10.1021/es703225a, 2008.

Lanz, V. A., Alfarra, M. R., Baltensperger, U., Buchmann, B., Hueglin, C., and Prevot, A. S. H.: Source apportionment of submicron organic aerosols at an urban site by factor analytical modelling of aerosol mass spectra, Atmospheric Chemistry and Physics, 7, 1503-1522, 2007.

Lee, B. H., Mohr, C., Lopez-Hilfiker, F. D., Lutz, A., Hallquist, M., Lee, L., Romer, P., Cohen, R. C., Iyer, S., Kurten, T., Hu, W. W., Day, D. A., Campuzano-Jost, P., Jimenez, J. L., Xu, L., Ng, N. L., Guo, H. Y., Weber, R. J., Wild, R. J., Brown, S. S., Koss, A., de Gouw, J., Olson, K., Goldstein, A. H., Seco, R., Kim, S., McAvey, K., Shepson, P. B., Starn, T., Baumann, K., Edgerton, E. S., Liu, J. M., Shilling, J. E., Miller, D. O., Brune, W., Schobesberger, S., D'Ambro, E. L., and Thornton, J. A.: Highly functionalized organic nitrates in the southeast United States: Contribution to secondary organic aerosol and reactive nitrogen budgets, Proceedings of the National Academy of Sciences of the United States of America, 113, 1516-1521, 10.1073/pnas.1508108113, 2016.

Lin, Y. H., Zhang, Z., Docherty, K. S., Zhang, H., Budisulistiorini, S. H., Rubitschun, C. L., Shaw, S. L., Knipping, E. M., Edgerton, E. S., Kleindienst, T. E., Gold, A., and Surratt, J. D.: Isoprene epoxydiols as precursors to Secondary Organic Aerosol formation: Acid-catalyzed reactive uptake studies with authentic

compounds, Environmental Science & Technology, 46, 250-258, 10.1021/es202554c, 2012.

Lin, Y. H., Zhang, H. F., Pye, H. O. T., Zhang, Z. F., Marth, W. J., Park, S., Arashiro, M., Cui, T. Q., Budisulistiorini, H., Sexton, K. G., Vizuete, W., Xie, Y., Luecken, D. J., Piletic, I. R., Edney, E. O., Bartolotti, L. J., Gold, A., and Surratt, J. D.: Epoxide as a precursor to secondary organic aerosol formation from isoprene photooxidation in the presence of nitrogen oxides, Proceedings of the National Academy of Sciences of the United States of America, 110, 6718-6723, 10.1073/pnas.1221150110, 2013.

Liu, J., Russell, L. M., Lee, A. K. Y., McKinney, K. A., Surratt, J. D., and Ziemann, P. J.: Observational evidence for pollution-influenced selective uptake contributing to biogenic secondary organic aerosols in the southeastern US, Geophysical Research Letters, 44, 8056-8064, 10.1002/2017gl074665, 2017.

Liu , J. M., D'Ambro, E. L., Lee, B. H., Lopez-Hilfiker, F. D., Zaveri, R. A., Rivera-Rios, J. C., Keutsch, F. N., Iyer, S., Kurten, T., Zhang, Z. F., Gold, A., Surratt, J. D., Shilling, J. E., and Thornton, J. A.: Efficient Isoprene Secondary Organic Aerosol Formation from a Non-IEPDX Pathway, Environmental Science & Technology, 50, 9872-9880, 10.1021/acs.est.6b01872, 2016.

Liu, J. M., D'Ambro, E. L., Lee, B. H., Lopez-Hilfiker, F. D., Zaveri, R. A., Rivera-Rios, J. C., Keutsch, F. N., Iyer, S., Kurten, T., Zhang, Z. F., Gold, A., Surratt, J. D., Shilling, J. E., and Thornton, J. A.: Efficient isoprene Secondary Organic Aerosol formation from a non-IEPDX pathway, Environmental Science & Technology, 50, 9872-9880, 10.1021/acs.est.6b01872, 2016.

Liu, S., Ahlm, L., Day, D. A., Russell, L. M., Zhao, Y. L., Gentner, D. R., Weber, R. J., Goldstein, A. H., Jaoui, M., Offenberg, J. H., Kleindienst, T. E., Rubitschun, C., Surratt, J. D., Sheesley, R. J., and Scheller, S.: Secondary organic aerosol formation from fossil fuel sources contribute majority of summertime organic mass at Bakersfield, Journal of Geophysical Research-Atmospheres, 117, 21, 10.1029/2012jd018170, 2012.

Liu, Y. J., Herdlinger-Blatt, I., McKinney, K. A., and Martin, S. T.: Production of methyl vinyl ketone and methacrolein via the hydroperoxyl pathway of isoprene oxidation, Atmospheric Chemistry and Physics, 13, 5715-5730, 10.5194/acp-13-5715-2013, 2013.

Lopez-Hilfiker, F. D., Mohr, C., D'Ambro, E. L., Lutz, A., Riedel, T. P., Gaston, C. J., Iyer, S., Zhang, Z., Gold, A., Surratt, J. D., Lee, B. H., Kurten, T., Hu, W. W., Jimenez, J., Hallquist, M., and Thornton, J. A.: Molecular composition and volatility of organic aerosol in the Southeastern US: implications for IEPDX derived SOA, Environmental Science & Technology, 50, 2200-2209, 10.1021/acs.est.5b04769, 2016.

Maria, S. F., Russell, L. M., Turpin, B. J., and Porcja, R. J.: FTIR measurements of functional groups and organic mass in aerosol samples over the Caribbean, Atmospheric Environment, 36, 5185-5196, 10.1016/s1352-2310(02)00654-4, 2002.

Matsui, H., Koike, M., Kondo, Y., Takami, A., Fast, J. D., Kanaya, Y., and Takigawa, M.: Volatility basis-set approach simulation of organic aerosol formation in East Asia: implications for anthropogenic-biogenic interaction and controllable amounts, Atmospheric Chemistry and Physics, 14, 9513-9535, 10.5194/acp-14-9513-2014, 2014.

McRoberts, R. E., Bechtold, W. A., Patterson, P. L., Scott, C. T., and Reams, G. A.: The enhanced forest inventory and analysis program of the USDA Forest Service: Historical perspective and announcement of statistical documentation, Journal of Forestry, 103, 304-308, 2005.

Medeiros, P. M., Conte, M. H., Weber, J. C., and Simoneit, B. R. T.: Sugars as source indicators of biogenic organic carbon in aerosols collected above the Howland Experimental Forest, Maine, Atmospheric Environment, 40, 1694-1705, 10.1016/j.atmosenv.2005.11.001, 2006.

Middlebrook, A. M., Bahreini, R., Jimenez, J. L., and Canagaratna, M. R.: Evaluation of Composition-Dependent Collection Efficiencies for the Aerodyne Aerosol Mass Spectrometer using Field Data, Aerosol Science and Technology, 46, 258-271, 10.1080/02786826.2011.620041, 2012.

Milford, J. B., Gao, D. F., Zafirakou, A., and Pierce, T. E.: Ozone precursor levels and responses to emissions reductions analysis of regional oxidant model results, Atmospheric Environment, 28, 2093-2104, 10.1016/1352-2310(94)90476-6, 1994.

Moore, R. H., and Nenes, A.: Scanning flow CCN analysis-A method for fast measurements of CCN Spectra, Aerosol Science and Technology, 43, 1192-1207, 10.1080/02786820903289780, 2009.

Murphy, B. N., Woody, M. C., Jimenez, J. L., Carlton, A. M. G., Hayes, P. L., Liu,, S., N., N. L., Russell,, L. M., S., A., X., L., Young,, J., Z., R. A., Z., Q.,, and Pye, H. O. T.: Semivolatile POA and parameterized total combustion SOA in CMAQv5.2: impacts on source strength and partitioning, Atmos. Chem. Phys. Discuss , in review, https://doi.org/10.5194/acp-2017-193, 2017.

Ng, N. L., Chhabra, P. S., Chan, A. W. H., Surratt, J. D., Kroll, J. H., Kwan, A. J., McCabe, D. C., Wennberg, P. O., Sorooshian, A., Murphy, S. M., Dalleska, N. F., Flagan, R. C., and Seinfeld, J. H.: Effect of NOx level on secondary organic aerosol (SOA) formation from the photooxidation of terpenes, Atmospheric Chemistry and Physics, 7, 5159-5174, 2007.

Ng, N. L., Kwan, A. J., Surratt, J. D., Chan, A. W. H., Chhabra, P. S., Sorooshian, A., Pye, H. O. T., Crounse, J. D., Wennberg, P. O., Flagan, R. C., and Seinfeld, J. H.: Secondary organic aerosol (SOA) formation from reaction of isoprene with nitrate radicals (NO3), Atmospheric Chemistry and Physics, 8, 4117-4140, 2008.

Ng, N. L., Herndon, S. C., Trimborn, A., Canagaratna, M. R., Croteau, P. L., Onasch, T. B., Sueper, D., Worsnop, D. R., Zhang, Q., Sun, Y. L., and Jayne, J. T.: An Aerosol Chemical Speciation Monitor (ACSM) for Routine Monitoring of the Composition and Mass Concentrations of Ambient Aerosol, Aerosol Science and Technology, 45, 780-794, 10.1080/02786826.2011.560211, 2011.

Ng, N. L., Brown, S. S., Archibald, A. T., Atlas, E., Cohen, R. C., Crowley, J. N., Day, D. A., Donahue, N. M., Fry, J. L., Fuchs, H., Griffin, R. J., Guzman, M. I., Herrmann, H., Hodzic, A., Iinuma, Y., Jimenez, J. L., Kiendler-Scharr, A., Lee, B. H., Luecken, D. J., Mao, J. Q., McLaren, R., Mutzel, A., Osthoff, H. D., Ouyang, B., Picquet-Varrault, B., Platt, U., Pye, H. O. T., Rudich, Y., Schwantes, R. H., Shiraiwa, M., Stutz, J., Thornton, J. A., Tilgner, A., Williams, B. J., and Zaveri, R. A.: Nitrate radicals and biogenic volatile organic compounds: oxidation, mechanisms, and organic aerosol, Atmospheric Chemistry and Physics, 17, 2103-2162, 10.5194/acp-17-2103-2017, 2017.

Palen, E. J., Allen, D. T., Pandis, S. N., Paulson, S. E., Seinfeld, J. H., and Flagan, R. C.: Fourier transform infrared analysis of aerosol formed in the photooxidation of isoprene and beta pinene, Atmospheric Environment Part a-General Topics, 26, 1239-1251, 10.1016/0960-1686(92)90385-x, 1992.

Praske, E., Otkjaer, R. V., Crounse, J. D., Hethcox, J. C., Stoltz, B. M., Kjaergaard, H. G., and Wennberg, P. O.: Atmospheric autoxidation is increasingly important in urban and suburban North America, Proceedings of the National Academy of Sciences of the United States of America, 115, 64-69, 10.1073/pnas.1715540115, 2018.

Presto, A. A., Hartz, K. E. H., and Donahue, N. M.: Secondary organic aerosol production from terpene ozonolysis. 2. Effect of NOx concentration, Environmental Science & Technology, 39, 7046-7054, 10.1021/es050400s, 2005.

Presto, A. A., Gordon, T. D., and Robinson, A. L.: Primary to secondary organic aerosol: evolution of organic emissions from mobile combustion sources, Atmospheric Chemistry and Physics, 14, 5015-5036, 10.5194/acp-14-5015-2014, 2014.

Pye, H. O. T., Chan, A. W. H., Barkley, M. P., and Seinfeld, J. H.: Global modeling of organic aerosol: the importance of reactive nitrogen (NOx and NO3), Atmospheric Chemistry and Physics, 10, 11261-11276, 10.5194/acp-10-11261-2010, 2010.

Pye, H. O. T., Pinder, R. W., Piletic, I. R., Xie, Y., Capps, S. L., Lin, Y. H., Surratt, J. D., Zhang, Z. F., Gold, A., Luecken, D. J., Hutzell, W. T., Jaoui, M., Offenberg, J. H., Kleindienst, T. E., Lewandowski, M., and Edney, E. O.: Epoxide pathways improve model predictions of isoprene markers and reveal key role of acidity in aerosol formation, Environmental Science & Technology, 47, 11056-11064, 10.1021/es402106h, 2013.

Pye, H. O. T., Luecken, D. J., Xu, L., Boyd, C. M., Ng, N. L., Baker, K. R., Ayres, B. R., Bash, J. O., Baumann, K., Carter, W. P. L., Edgerton, E., Fry, J. L., Hutzell, W. T., Schwede, D. B., and Shepson, P. B.: Modeling the Current and Future Roles of Particulate Organic Nitrates in the Southeastern United States, Environmental Science & Technology, 49, 14195-14203, 10.1021/acs.est.5b03738, 2015.

Pye, H. O. T., Murphy, B. N., Xu, L., Ng, N. L., Carlton, A. G., Guo, H. Y., Weber, R., Vasilakos, P., Appel, K. W., Budisulistiorini, S. H., Surratt, J. D., Nenes, A., Hu, W. W., Jimenez, J. L., Isaacman-VanWertz, G., Misztal, P. K., and Goldstein, A. H.: On the implications of aerosol liquid water and phase separation for organic aerosol mass, Atmospheric Chemistry and Physics, 17, 343-369, 10.5194/acp-17-343-2017, 2017.

Robinson, N. H., Hamilton, J. F., Allan, J. D., Langford, B., Oram, D. E., Chen, Q., Docherty, K., Farmer, D. K., Jimenez, J. L., Ward, M. W., Hewitt, C. N., Barley, M. H., Jenkin, M. E., Rickard, A. R., Martin, S. T., McFiggans, G., and Coe, H.: Evidence for a significant proportion of Secondary Organic Aerosol from isoprene above a maritime tropical forest, Atmospheric Chemistry and Physics, 11, 1039-1050, 10.5194/acp-11-1039-2011, 2011.

Rollins, A. W., Browne, E. C., Min, K. E., Pusede, S. E., Wooldridge, P. J., Gentner, D. R., Goldstein, A. H., Liu, S., Day, D. A., Russell, L. M., and Cohen, R. C.: Evidence for NOx control over nighttime SOA formation, Science, 337, 1210-1212, 10.1126/science.1221520, 2012.

Russell, L. M., Bahadur, R., Hawkins, L. N., Allan, J., Baumgardner, D., Quinn, P. K., and Bates, T. S.: Organic aerosol characterization by complementary measurements of chemical bonds and molecular fragments, Atmospheric Environment, 43, 6100-6105, 10.1016/j.atmosenv.2009.09.036, 2009.

Russell, L. M., Bahadur, R., and Ziemann, P. J.: Identifying organic aerosol sources by comparing functional group composition in chamber and atmospheric particles, Proceedings of the National Academy of Sciences of the United States of America, 108, 3516-3521, 10.1073/pnas.1006461108, 2011.

Russell, L. M.: Carbonaceous particles: Source-based characterization of their formation, composition, and structures, in: Turekian KK, editor. Treatise on Geochemistry (Second Edition), Oxford: Elsevier, p. 291-316., 2014.

Saha, P. K., Khlystov, A., Yahya, K., Zhang, Y., Xu, L., Ng, N. L., and Grieshop, A. P.: Quantifying the volatility of organic aerosol in the southeastern US, Atmospheric Chemistry and Physics, 17, 501-520, 10.5194/acp-17-501-2017, 2017.

Schwartz, R. E., Russell, L. M., Sjostedt, S. J., Vlasenko, A., Slowik, J. G., Abbatt, J. P. D., Macdonald, A. M., Li, S. M., Liggio, J., Toom-Sauntry, D., and Leaitch, W. R.: Biogenic oxidized organic functional groups in aerosol particles from a mountain forest site and their similarities to laboratory chamber products, Atmospheric Chemistry and Physics, 10, 5075-5088, 10.5194/acp-10-5075-2010, 2010.

Seinfeld, J. H., and Pandis, S. N.: Atmospheric Chemistry and Physics: From Air Pollution to Climate Change, 3rd Edition, 3rd ed., ISBN: 978-1-118-94740-1, Wiley, New York, New York, NY, 1152 pp., 2016.

Seok, B., Helmig, D., Ganzeveld, L., Williams, M. W., and Vogel, C. S.: Dynamics of nitrogen oxides and ozone above and within a mixed hardwood forest in northern Michigan, Atmospheric Chemistry and Physics, 13, 7301-7320, 10.5194/acp-13-7301-2013, 2013.

Shilling, J. E., Zaveri, R. A., Fast, J. D., Kleinman, L., Alexander, M. L., Canagaratna, M. R., Fortner, E., Hubbe, J. M., Jayne, J. T., Sedlacek, A., Setyan, A., Springston, S., Worsnop, D. R., and Zhang, Q.: Enhanced SOA formation from mixed anthropogenic and biogenic emissions during the CARES campaign, Atmospheric Chemistry and Physics, 13, 2091-2113, 10.5194/acp-13-2091-2013, 2013.

Shrivastava, M., Cappa, C. D., Fan, J. W., Goldstein, A. H., Guenther, A. B., Jimenez, J. L., Kuang, C., Laskin, A., Martin, S. T., Ng, N. L., Petaja, T., Pierce, J. R., Rasch, P. J., Roldin, P., Seinfeld, J. H., Shilling, J., Smith, J. N., Thornton, J. A., Volkamer, R., Wang, J., Worsnop, D. R., Zaveri, R. A., Zelenyuk, A., and Zhang, Q.: Recent advances in understanding secondary organic aerosol: Implications for global climate forcing, Reviews of Geophysics, 55, 509-559, 10.1002/2016rg000540, 2017.

Slowik, J. G., Brook, J., Chang, R. Y. W., Evans, G. J., Hayden, K., Jeong, C. H., Li, S. M., Liggio, J., Liu, P. S. K., McGuire, M., Mihele, C., Sjostedt, S., Vlasenko, A., and Abbatt, J. P. D.: Photochemical processing of organic aerosol at nearby continental sites: contrast between urban plumes and regional aerosol, Atmospheric Chemistry and Physics, 11, 2991-3006, 10.5194/acp-11-2991-2011, 2011.

Spracklen, D. V., Jimenez, J. L., Carslaw, K. S., Worsnop, D. R., Evans, M. J., Mann, G. W., Zhang, Q., Canagaratna, M. R., Allan, J., Coe, H., McFiggans, G., Rap, A., and Forster, P.: Aerosol mass spectrometer constraint on the global secondary organic aerosol budget, Atmospheric Chemistry and Physics, 11, 12109-12136, 10.5194/acp-11-12109-2011, 2011.

Surratt, J. D., Murphy, S. M., Kroll, J. H., Ng, a. L. N., Hildebrandt, L., Sorooshian, A., Szmigielski, R., Vermeylen, R., Maenhaut, W., Claeys, M., Flagan, R. C., and Seinfeld, J. H.: Chemical composition of secondary organic aerosol formed from the photooxidation of isoprene, Journal of Physical Chemistry A, 110, 9665-9690, 10.1021/jp061734m, 2006.

Surratt, J. D., Lewandowski, M., Offenberg, J. H., Jaoui, M., Kleindienst, T. E., Edney, E. O., and Seinfeld, J. H.: Effect of acidity on secondary organic aerosol formation from isoprene, Environmental Science & Technology, 41, 5363-5369, 10.1021/es0704176, 2007.

Surratt, J. D., Chan, A. W. H., Eddingsaas, N. C., Chan, M., Loza, C. L., Kwan, A. J., Hersey, S. P., Flagan, R. C., Wennberg, P. O., and Seinfeld, J. H.: Reactive intermediates revealed in secondary organic aerosol formation from isoprene, Proceedings of the National Academy of Sciences of the United States of America, 107, 6640-6645, 10.1073/pnas.0911114107, 2010.

Takahama , S., Schwartz, R. E., Russell, L. M., Macdonald, A. M., Sharma, S., and Leaitch, W. R.: Organic functional groups in aerosol particles from burning and non-burning forest emissions at a high-elevation mountain site, Atmospheric Chemistry and Physics, 11, 6367-6386, 10.5194/acp-11-6367-2011, 2011.

Takahama, S., Johnson, A., and Russell, L. M.: Quantification of Carboxylic and Carbonyl Functional Groups in Organic Aerosol Infrared Absorbance Spectra, Aerosol Science and Technology, 47, 310-325, 10.1080/02786826.2012.752065, 2013.

Taylor, R.: INTERPRETATION OF THE CORRELATION-COEFFICIENT - A BASIC REVIEW, Journal of Diagnostic Medical Sonography, 6, 35-39, 10.1177/875647939000600106, 1990.

Travis, K. R., Jacob, D. J., Fisher, J. A., Kim, P. S., Marais, E. A., Zhu, L., Yu, K., Miller, C. C., Yantosca, R. M., Sulprizio, M. P., Thompson, A. M., Wennberg, P. O., Crounse, J. D., St Clair, J. M., Cohen, R. C., Laughner, J. L., Dibb, J. E., Hall, S. R., Ullmann, K., Wolfe, G. M., Pollack, I. B., Peischl, J., Neuman, J. A., and Zhou, X. L.: Why do models overestimate surface ozone in the Southeast United States?, Atmospheric Chemistry and Physics, 16, 13561-13577, 10.5194/acp-16-13561-2016, 2016.

Ulbrich, I. M., Canagaratna, M. R., Zhang, Q., Worsnop, D. R., and Jimenez, J. L.: Interpretation of organic components from Positive Matrix Factorization of aerosol mass spectrometric data, Atmospheric Chemistry and Physics, 9, 2891-2918, 2009.

Usher, C. R., Michel, A. E., and Grassian, V. H.: Reactions on mineral dust, Chemical Reviews, 103, 4883-4939, 10.1021/cr020657y, 2003.

Verma, V., Shafer, M. M., Schauer, J. J., and Sioutas, C.: Contribution of transition metals in the reactive oxygen species activity of PM emissions from retrofitted heavy-duty vehicles, Atmospheric Environment, 44, 5165-5173, 10.1016/j.atmosenv.2010.08.052, 2010.

Wildt, J., Mentel, T. F., Kiendler-Scharr, A., Hoffmann, T., Andres, S., Ehn, M., Kleist, E., Musgen, P., Rohrer, F., Rudich, Y., Springer, M., Tillmann, R., and Wahner, A.: Suppression of

new particle formation from monoterpene oxidation by NOx, Atmospheric Chemistry and Physics, 14, 2789-2804, 10.5194/acp-14-2789-2014, 2014.

Xie, Y., Paulot, F., Carter, W. P. L., Nolte, C. G., Luecken, D. J., Hutzell, W. T., Wennberg, P. O., Cohen, R. C., and Pinder, R. W.: Understanding the impact of recent advances in isoprene photooxidation on simulations of regional air quality, Atmospheric Chemistry and Physics, 13, 8439-8455, 10.5194/acp-13-8439-2013, 2013.

Xu, L., Kollman, M. S., Song, C., Shilling, J. E., and Ng, N. L.: Effects of NOx on the Volatility of Secondary Organic Aerosol from Isoprene Photooxidation, Environmental Science & Technology, 48, 2253-2262, 10.1021/es404842g, 2014.

Xu, L., Guo, H. Y., Boyd, C. M., Klein, M., Bougiatioti, A., Cerully, K. M., Hite, J. R., Isaacman-VanWertz, G., Kreisberg, N. M., Knote, C., Olson, K., Koss, A., Goldstein, A. H., Hering, S. V., de Gouw, J., Baumann, K., Lee, S. H., Nenes, A., Weber, R. J., and Ng, N. L.: Effects of anthropogenic emissions on aerosol formation from isoprene and monoterpenes in the southeastern United States, Proceedings of the National Academy of Sciences of the United States of America, 112, 37-42, 10.1073/pnas.1417609112, 2015a.

Xu, L., Suresh, S., Guo, H., Weber, R. J., and Ng, N. L.: Aerosol characterization over the southeastern United States using high-resolution aerosol mass spectrometry: spatial and seasonal variation of aerosol composition and sources with a focus on organic nitrates, Atmospheric Chemistry and Physics, 15, 7307-7336, 10.5194/acp-15-7307-2015, 2015b.

Xu, L., Middlebrook, A. M., Liao, J., de Gouw, J. A., Guo, H. Y., Weber, R. J., Nenes, A., Lopez-Hilfiker, F. D., Lee, B. H., Thornton, J. A., Brock, C. A., Neuman, J. A., Nowak, J. B., Pollack, I. B., Welti, A., Graus, M., Warneke, C., and Ng, N. L.: Enhanced formation of isoprene-derived organic aerosol in sulfur-rich power plant plumes during Southeast Nexus, Journal of Geophysical Research-Atmospheres, 121, 11137-11153, 10.1002/2016jd025156, 2016.

Zhang, Q., Jimenez, J. L., Canagaratna, M. R., Ulbrich, I. M., Ng, N. L., Worsnop, D. R., and Sun, Y. L.: Understanding atmospheric organic aerosols via factor analysis of aerosol mass spectrometry: a review, Analytical and Bioanalytical Chemistry, 401, 3045-3067, 10.1007/s00216-011-5355-y, 2011.

Zhang, X., Chen, Z. M., Wang, H. L., He, S. Z., and Huang, D. M.: An important pathway for ozonolysis of alpha-pinene and beta-pinene in aqueous phase and its atmospheric implications, Atmospheric Environment, 43, 4465-4471, 10.1016/j.atmosenv.2009.06.028, 2009.

Zhang, Y. J., Tang, L. L., Sun, Y. L., Favez, O., Canonaco, F., Albinet, A., Couvidat, F., Liu, D. T., Jayne, J. T., Wang, Z., Croteau, P. L., Canagaratna, M. R., Zhou, H. C., Prevot, A. S. H., and Worsnop, D. R.: Limited formation of isoprene epoxydiols-derived secondary organic aerosol under NOx-rich environments in Eastern China, Geophysical Research Letters, 44, 2035-2043, 10.1002/2016gl072368, 2017.

Zheng, Y., Unger, N., Hodzic, A., Emmons, L., Knote, C., Tilmes, S., Lamarque, J. F., and Yu, P.: Limited effect of anthropogenic nitrogen oxides on secondary organic aerosol formation, Atmospheric Chemistry and Physics, 15, 13487-13506, 10.5194/acp-15-13487-2015, 2015.

Ziemann, P. J., and Atkinson, R.: Kinetics, products, and mechanisms of secondary organic aerosol formation, Chemical Society Reviews, 41, 6582-6605, 10.1039/c2cs35122f, 2012.

Chapter 3

High Summertime Aerosol Organic Functional Group Concentrations from Marine and Seabird Sources at Ross Island, Antarctica, during AWARE

Observations of the organic components of the natural aerosol are scarce in Antarctica, which limits our understanding of natural aerosols and their connection to seasonal and spatial patterns of cloud albedo in the region. From November 2015 to December 2016, the ARM West Antarctic Radiation Experiment (AWARE) measured submicron aerosol properties near McMurdo Station at the southern tip of Ross Island. Submicron organic mass (OM), particle number, and cloud condensation nuclei concentrations were higher in summer than other seasons. The measurements included a range of compositions and concentrations that likely reflected both local anthropogenic emissions and natural background sources. We isolated the natural organic components by separating a natural factor and a local combustion factor. The natural OM was 150 times higher in summer than in winter. The local anthropogenic emissions were not hygroscopic and had little contribution to the CCN concentrations. Natural sources that

included marine sea spray and seabird emissions contributed 56% OM in summer but only 3% in winter. The natural OM had high hydroxyl group fraction (55%), 6% alkane, and 6% amine group mass, consistent with marine organic composition. In addition, the Fourier transform infrared (FTIR) spectra showed the natural sources of organic aerosol were characterized by amide group absorption, which may be from seabird populations. Carboxylic acid group contributions were high in summer and associated with natural sources, likely forming by secondary reactions.

3.1 Introduction

West Antarctica is one of the most rapidly warming regions on Earth [*Bromwich et al.*, 2013], which has potential impacts for the melting of the Antarctic ice sheets and consequent sea level rise [*Lambeck et al.*, 2002; *Steig et al.*, 2009]. In some regions, ambient aerosols contribute substantially to the radiation balance [*Stocker et al.*, 2013], but little is known about the sign and magnitude of their contribution in Antarctica because of the lack of measurements of their abundance, composition, and sources. In fact, there are few places on Earth where measurements of aerosols and their properties are needed to constrain modeled radiation as much as in Antarctica.

Since McMurdo Station is the only site with measurements of PM (Particulate Matter), Elemental Carbon, Organic Carbon and number concentrations that is within 300 km of the Ross Ice Shelf (which covers an area of more than 500,000 km^2). Furthermore, the station is unique in that McMurdo Station is one of the two sites that have published aerosol measurements starting in 1968, with the other one being the Amundsen Scott Station at the South Pole. The site has at least 10 publications describing aerosol measurements over the past 50 years, most of which were limited to summer [*Cadle et al.*, 1968; *Giordano et al.*, 2017; *Hansen et al.*, 2001; *D Hofmann*, 1988; *Hogan*, 1975; *Kalnajs et al.*, 2013; *Khan et al.*, 2018; *Mazzera et al.*, 2001a; *Mazzera et al.*, 2001b; *Ondov et al.*, 1973a; *Warburton*, 1973]. No stations in Antarctica measured inorganic chemical composition year-round until 1978 [*Parungo et al.*, 1981], and none have measured year-round organic components. In 1966, electron micrographs of particles collected on a four-stage impactor provided some of the first aerosol measurements carried out at McMurdo Station [*Cadle et al.*, 1968]. Filter samples were collected for elemental analysis in

1970-1971 [*Ondov et al.*, 1973]. During the austral summers of 1969 and 1970, the Aitken nuclei concentration was reported to be ~1000 cm^{-3} [*Warburton*, 1973]. In another study, the number concentration was 50 to 150 cm^{-3} with continental winds and ~300 cm^{-3} with maritime winds [*Hogan*, 1975]. Balloon measurements were conducted later for stratospheric aerosols, and long distance signals from volcanic sources in tropical areas were found in the stratosphere [*Hofmann et al.*, 1986; *Solomon et al.*, 1994]. Hansen et al. [2001] measured black carbon at McMurdo in austral summer in 1995-1996. Another study [*Mazzera et al.*, 2001b] reported more detailed PM_{10} elemental composition, elemental and organic carbon, and nitrate concentrations for 1995–1996 and 1996–1997 at McMurdo. Chemical Mass Balance (CMB) receptor modeling estimated that soil dust, sea salt, combustion emissions, sulfates, methanesulfonate, and nitrates contributed 57%, 15%, 14%, 10%, 3%, and 1%, respectively, to the summertime PM_{10} mass [*Mazzera et al.*, 2001a]. Kalnajs et al. [2013] showed that ozone depletion is correlated to aerosol concentrations because halogen-containing aerosol consumed ozone. An aerosol mass spectrometer (AMS) at a site 20 km northeast from McMurdo Station during October 2014 to December 2014 and August to October 2015 [*Giordano et al.*, 2017] found sulfate accounted for more than 50% of non-refractory composition. Many measurement campaigns were limited to austral summer months because of restrictions on access [*Cadle et al.*, 1968; *Ondov et al.*, 1973a; *Warburton*, 1973] and so lack information on seasonal changes.

The few year-round aerosol concentration and composition measurements in Antarctica were collected at several sites in coastal Antarctica (all of which are more than 1500 km from McMurdo Station) [*Gras*, 1993; *Keiichiro Hara et al.*, 2004; *K. Hara et al.*, 2005; *K Hara et al.*, 2010; *Jourdain and Legrand*, 2002; *Minikin et al.*, 1998; *Read et al.*, 2008; *Wagenbach et al.*, 1998; *Rolf Weller et al.*, 2013] and at several sites on the Antarctic Peninsula (more than 3000

km from McMurdo Station) [*Asmi et al.*, 2018; *Kim et al.*, 2017; *Loureiro et al.*, 1992; *Mishra et al.*, 2004; *Savoie et al.*, 1993; *Saxena and Ruggiero*, 1990], as well as at the South Pole (more than 1000 km from McMurdo Station) [*Bodhaine*, 1983; *Bodhaine et al.*, 1986; *Hansen et al.*, 1988; *Harder et al.*, 2000; *Hogan and Barnard*, 1978; *Parungo et al.*, 1981] and at Dome C (more than 1000 km from McMurdo Station) [*Legrand et al.*, 2017a; *Legrand et al.*, 2017b; *Udisti et al.*, 2012]. At the South Pole, aerosol particle number concentration ranged from 10 to 30 cm^{-3} in winter and 100 to 300 cm^{-3} in summer [*Bodhaine*, 1983; *Hogan and Barnard*, 1978; *Parungo et al.*, 1981]. This low winter and high summer seasonal difference has been observed also at coastal Antarctic sites, but the average concentrations were typically higher with summertime concentrations ranging from 300 to 2000 cm^{-3} and wintertime concentrations from 10 to 200 cm^{-3} [*Gras*, 1993; *Kim et al.*, 2017]. Consistent with this seasonal difference in particle number concentrations, most summertime non-sea salt sulfate mass concentrations were at least 5 times higher than winter concentrations [*Asmi et al.*, 2018; *Jourdain and Legrand*, 2002; *Legrand et al.*, 2017a; *Udisti et al.*, 2012; *R. Weller and Wagenbach*, 2007], likely because of the contributions from biogenic DMS emissions from the surrounding Southern Ocean. However, most sea salt aerosols had wintertime maximum concentrations with more than two times more Na^+ mass concentrations in winter than summer [*Asmi et al.*, 2018; *Jourdain and Legrand*, 2002; *Jourdain et al.*, 2008; *Legrand et al.*, 2017a; *Legrand et al.*, 2017b; *Parungo et al.*, 1981; *Udisti et al.*, 2012; *Wagenbach et al.*, 1998; *R. Weller and Wagenbach*, 2007].

The few hygroscopicity and CCN measurements reported near West Antarctica are also recent and sparse. DeFelice et al. [1997] conducted CCN measurements at Palmer Station on the Antarctic Peninsula in January and February 1994. They collected CCN for 27 days at 0.3% and 1% SS and found CCN concentration to be between 79 and 158 cm^{-3}. Asmi et al. [2010] found

that aerosol particles over the Southern Ocean are very hygroscopic with a growth factor of 1.75 at 90 nm. At King Sejong Station on King George Island, Kim et al. [2017] found that CCN concentrations are high in summer (~200 cm^{-3}) and low in winter (~50 cm^{-3}). Biological emissions from marine sulfate sources have been proposed to explain a large fraction of CCN in the Southern Ocean region [*McCoy et al.*, 2015]. Biological sulfate aerosol accounts for 43–65% of the summer zonal mean CCN concentrations and 7–20% of the winter CCN over the oceans in the Southern Hemisphere, including the circumpolar Southern Ocean [*Korhonen et al.*, 2008]. This important role for biological sulfate in the Southern Ocean suggests that biogenic organic components may also contribute significantly to particle number and mass, but measurements of organic particles are too scarce to determine if this is the case [*McCoy et al.*, 2015].

For comparison, in marine and Arctic regions, the organic composition of particles have shown a high fraction of hydroxyl group (61% of OM for the North Atlantic and 47% of OM for the Arctic) as well as some alkane and amine groups, likely associated with sugars, carbohydrates, and amino sugars originated from biological materials in seawater [*Frossard et al.*, 2013; *Hawkins and Russell*, 2010; *Leaitch et al.*, 2017; *Modini et al.*, 2015; *L. M. Russell et al.*, 2010; *Shaw et al.*, 2010]. Organic nitrogen has also been identified as a tracer component (0.02 to 10 ng m^{-3}) in aerosol particles in various studies in Antarctic [*Barbaro et al.*, 2015; *Dall'Osto et al.*, 2017; *Schmale et al.*, 2013] and Arctic [*Dall'Osto et al.*, 2012; *Scalabrin et al.*, 2012] regions. Some of the few measurements of organic aerosol particle composition that have been made in marine and polar regions are those of amino acids, which are summarized in Table 3.1 [*Barbaro et al.*, 2015; *Kuznetsova et al.*, 2005; *Mace et al.*, 2003a; *Mace et al.*, 2003b; *Mandalakis et al.*, 2011; *Matsumoto and Uematsu*, 2005; *Scalabrin et al.*, 2012; *Shi et al.*, 2010; *Violaki et al.*, 2010; *Wedyan and Preston*, 2008]. Amino acids in remote marine and coastal regions have been

used as markers for biological activities since they are natural chemical constituents of many marine and terrestrial organisms [*Barbaro et al.*, 2015; *Cowie and Hedges*, 1992; *Milne and Zika*, 1993; *Scalabrin et al.*, 2012]. In addition, amino acids contain organic nitrogen and specifically amine groups, which are also consistent with measurements in polar regions of CHNO fragments [*Schmale et al.*, 2013] and amine groups [*Frossard et al.*, 2011; *Shaw et al.*, 2010]. Sugar, levoglucosan, phenols and anthropogenic persistent organic compounds were measured in ambient aerosols at Mario Zucchelli Station and Concordia Station [*Barbaro et al.*, 2015a; *Barbaro et al.*, 2017; *Barbaro et al.*, 2016; *Zangrando et al.*, 2016]. Carboxylic acids with low molecular weights were also measured at Mario Zucchelli Station, Concordia Station, and Dumont d'Urville [*Barbaro et al.*, 2017; *Legrand et al.*, 2012].

Table 3.1: Marine amino acid measurements.

Study	Year	Location	Season	Type	Particle Size	Amino Acid Concentration		
						Free dissolved	Combined	Total
						ng m^{-3}	ng m^{-3}	ng m^{-3}
Mace et al. 2003b	2000	Erdemli (Mediterranean coast), Turkey	Spring	Marine	TSP	33.8 (3.65–102)	–	–
Wedyan and Preston, 2008	2003	Atlantic Ocean (cruise)	Spring	Marine	TSP	1.83 (0.27–9.13)	9.13 (1.83–36.5)	–
Kuznetsova et al. 2005	2003	Ligurian Sea (NW Mediterranean Sea)	Spring	Marine	TSP	–	–	225.88
Shi et al. 2010	2006	Qingdao (Coastal China)	Spring	Marine	TSP	214	–	–
	2005	South China Sea (cruise)	Spring			44.5	–	–
	2005-2006	Yellow Sea (cruise)	Spring			131	–	–
Matsumoto et al. 2005	2000	Western Pacific Ocean (cruise)	Spring Summer	Marine	TSP	0.98 (0.14–2.81)	–	–
Mace et al. 2003a	2000	Cape Grim, Tasmania, Australia	Spring	Marine	TSP	8.74 (1.83–20.0)	–	–
Mandalakis et al. 2011	2007	Finokalia, Crete island, Greece	Summer	Marine	TSP	23.6 (0.82–88.7)	98.4 (34.8–215)	–
Violaki et al. 2010	2007	Finokalia, Crete island, Greece	Summer Autumn	Marine	PM_1	45.6 –	–	–

Table 3.1: Marine amino acid measurements. (Continued)

Scalabrin et al. 2012	2010	Svalbard Islands, Norway	Summer	Polar (Arctic)	PM_{10}	0.23 (0.02–0.52)	–	–
					$PM_{0.5}$	0.15 (0.02–0.43)	–	–
Barbaro et al. 2015	2010	Faraglione Camp, Antarctica	Summer	Polar (Antarctica)	PM_{10}	1.51	–	–
	2011				PM_1	1.55		
	2010-2011	Ross Sea (cruise)			TSP	0.48 (0.27–1.64)	–	–
	2011-2012	Dome C Station, Antarctic plateau			PM_{10}	0.11	–	–
	2012-2013	Dome C Station, Antarctic plateau				0.1		

Assuming an average amino acid molecular weight of 136.9 $g.mol^{-1}$
Assuming an average amino acid nitrogen number of 1.

The Ross Sea has a surprisingly high biological primary production rate in the summer, making it the most biologically active part of the southern polar region [*Arrigo et al.*, 2008]. Seabird emissions were linked to new particle formation [*Weber et al.*, 1998] and to particles containing CHN and CHNO fragments [*Schmale et al.*, 2013]. The CHNO fragments identified by mass spectrometry have been associated with uric acid and other nitrogen containing components that are produced from penguin guano [*Schmale et al.*, 2013]. The ammonia emissions from seabird colonies have also been shown to contribute substantially to atmospheric particle formation and cloud-albedo radiative effects in the Arctic [*Croft et al.*, 2016b]. Organic aerosol components were also associated with melt-water ponds in continental Antarctica [*Kyro et al.*, 2013]

AWARE (ARM West Antarctic Radiation Experiment) provides the most thorough yearlong aerosol and radiative property measurements yet obtained from Antarctica, and the only four-season time series of weekly FTIR measurements of organic functional groups in Antarctica. This manuscript characterizes the sources of organic aerosol across four seasons in Antarctica. Dust, sea salt, and non-sea salt sulfate mass concentrations measured by XRF are used to separate the seasonal contributions to inorganic particle components. Seasonal patterns of natural marine and coastal-sourced organic aerosol are identified from the functional groups after separation of local emissions.

3.2 Methods

The AWARE aerosol measurements were collected from 23 November 2015 to 29 December 2016 at the Cosray site on the eastern edge of McMurdo Station (77.85°S, 166.66°E), which is located on the southern tip of Ross Island in Antarctica. To quantify seasonal

differences, four seasons were defined as Summer (November through February), Fall (March through April), Winter (May through August) and Spring (September through October) (Figure 3.1). The four-month winter is characterized by irradiance of nearly zero and average temperature below -20 °C. The four-month summer had irradiance above 250 W m^{-2} and temperature higher than -10 °C. Spring and fall marked transitions between summer and winter. The station hosts more than 1000 scientists and support personnel during austral summer and consumes more than 2 million gallons of AN-8 diesel fuel (with a 0.3% sulfur content by weight) for station operations [*Mazzera et al.*, 2001a]. The aerosol inlet samples at ~10 m above ground level and has a rain guard and bug screen, 1000 L min^{-1} turbulent flow through 4.6 m of large-diameter (20 cm ID), powder-coated aluminum tubing, a 2.1 m smaller-diameter tube (4.76 cm ID) that extracts 150 L min^{-1} flow from the center of the larger-diameter tubing, and a flow distributor with five ports, each drawing 30 L min^{-1} through 25 cm of 1.59 cm (5/8") inner diameter stainless-steel tubing. The size-dependent losses were measured below 10% for particles from 10 nm to 10 μm diameter (https://www.arm.gov/publications/tech_reports/doe-sc-arm-tr-191.pdf). Other details of the measurement system can be found online in the description of the second ARM Mobile Facility (AMF2, https://www.arm.gov/capabilities/observatories/amf) and Aerosol Observing System (AOS, https://www.arm.gov/capabilities/instruments/aos).

Ambient aerosol particles were measured by CPC (Condensation Particle Counter, TSI model 3772), HTDMA (Hygroscopic Tandem Differential Mobility Analyser, Brechtel model 3002), and CCN Counter (Cloud Condensation Nuclei, DMT model CCN100) and were collected on filters for off-line FTIR and X-ray fluorescence (XRF).

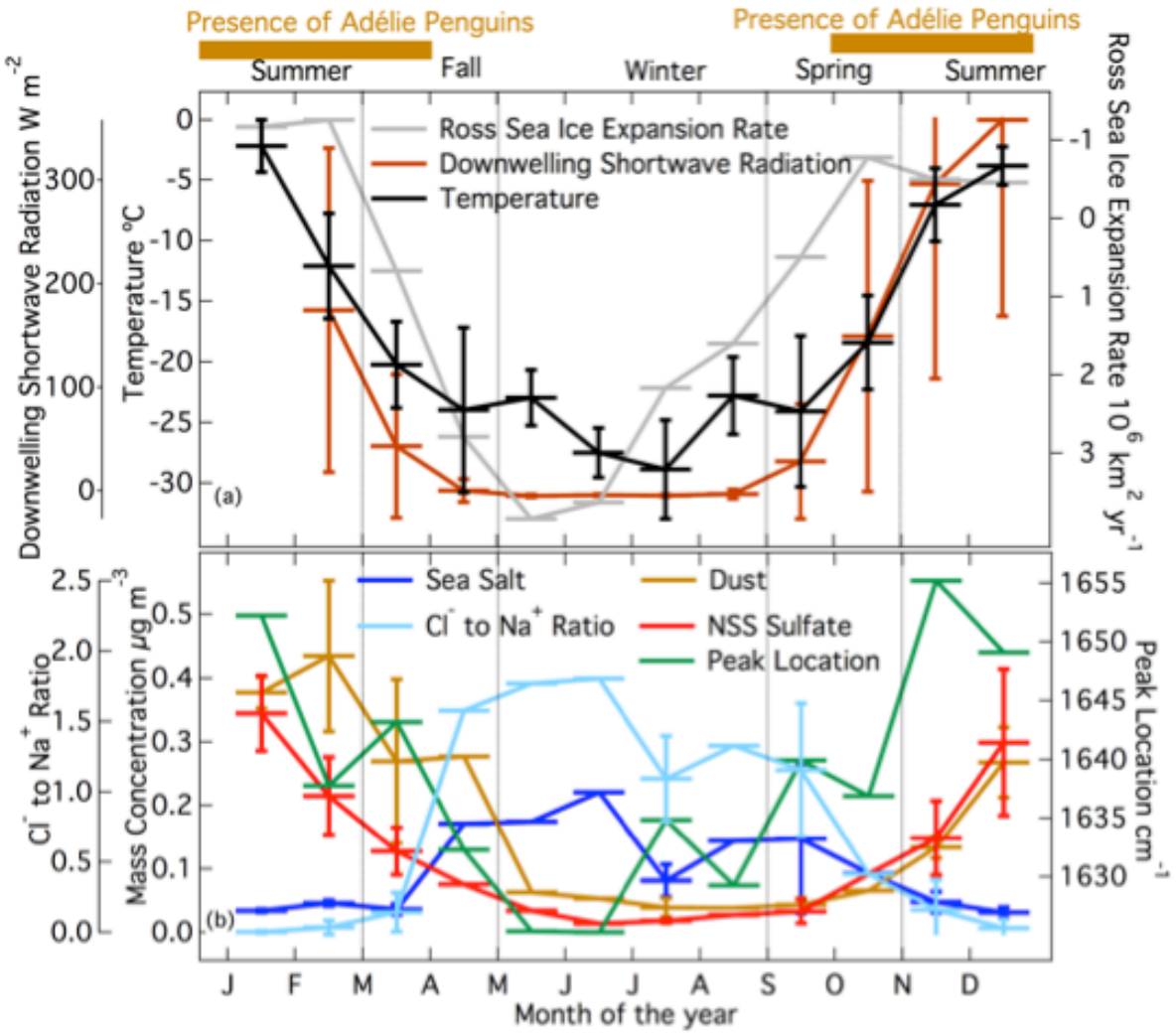

Figure 3.1: ReMonthly average of (a) Temperature, shortwave downwelling irradiance measured in this study and sea ice expansion rate of the Ross Sea [Holland, 2014]; (b) Sea salt, dust and non-sea salt sulfate concentration from XRF and FTIR peak location at 1500~1800 cm-1 wavenumber region. Standard deviations are shown on the plot as error bars.

CN (condensation nuclei from CPC) concentrations had frequent short-lived increases that typically had high concentrations (>1000 particles cm^{-3} for 1 Hz CN), which we attributed to short-term local contamination events (SLCE) (Figure 3.2). High CN concentrations (>1000 cm^{-3}) occurred 48% of the time when the wind was from the west (Figure 3.3), which is the same direction as the McMurdo Station central facilities. However, westerly winds only occurred 3% of the time, so emissions at McMurdo Station were unlikely to account for most of the emissions.

Spikes were separated using a "de-spike" algorithm based on running median filters [*Beaton and Tukey*, 1974; *Goring and Nikora*, 2002; *Tukey*, 1977; *Velleman*, 1977]. We applied a running median length of 24 hr and weighted by cosine bell running mean of 24 hr to the 1 Hz CN concentration and assigned the CN concentration above the resulting filter as SLCE. The SLCE were characterized by an average duration of less than 1 hr (0.5 min$\pm$6 min), rapid rate of concentration change (8520$\pm$36780 cm^{-3} min^{-1}), and concentrations exceeding 1000 cm^{-3}. After SLCE (spikes) were removed, the 24-hr running median concentration was interpreted to be the natural background CN, for reasons discussed in Section 3.

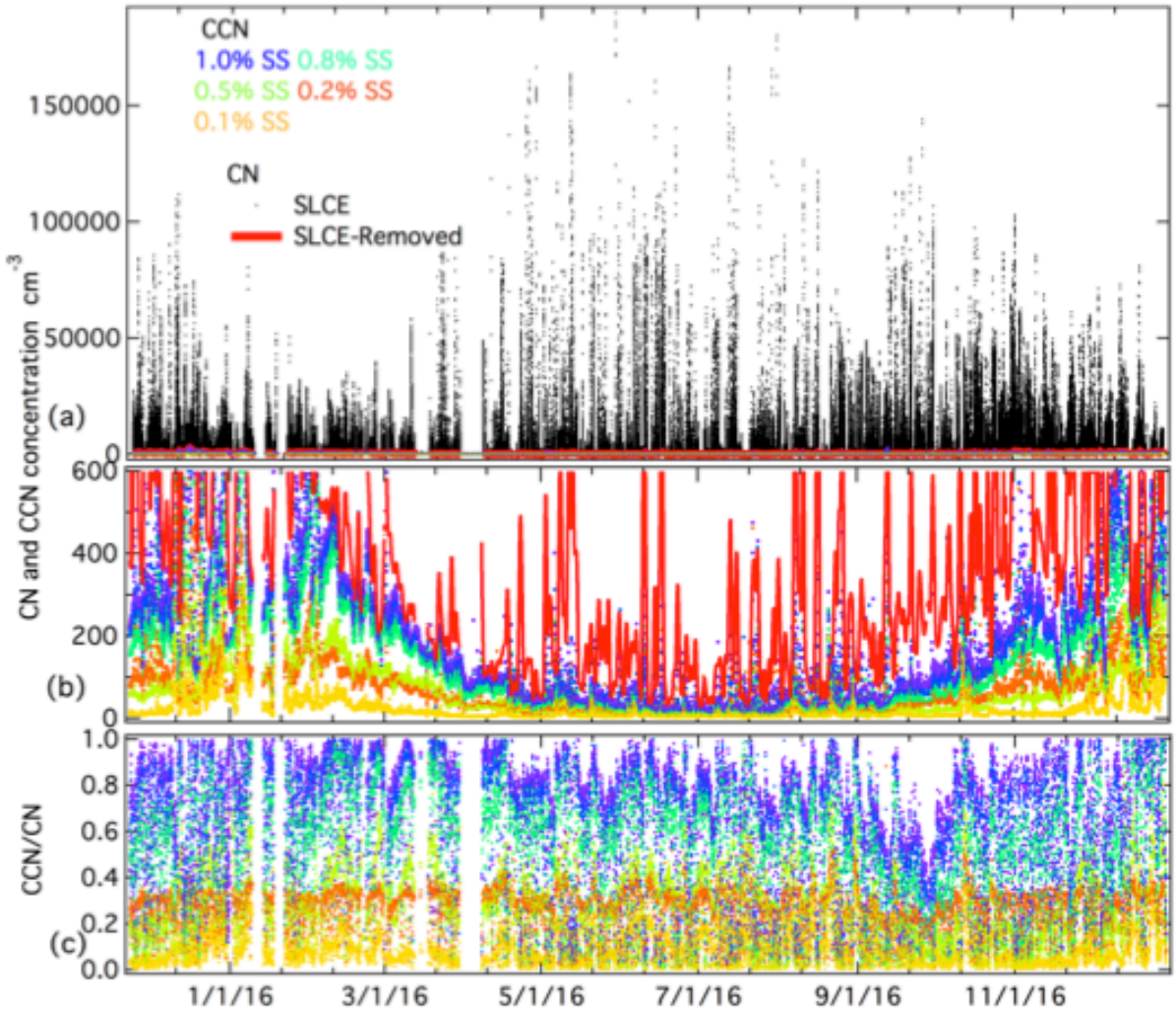

Figure 3.2: Concentrations of: (a) measured CN, (b) SLCE-removed CN and measured CCN, and (c) ratio of CCN to SLCE-removed CN.

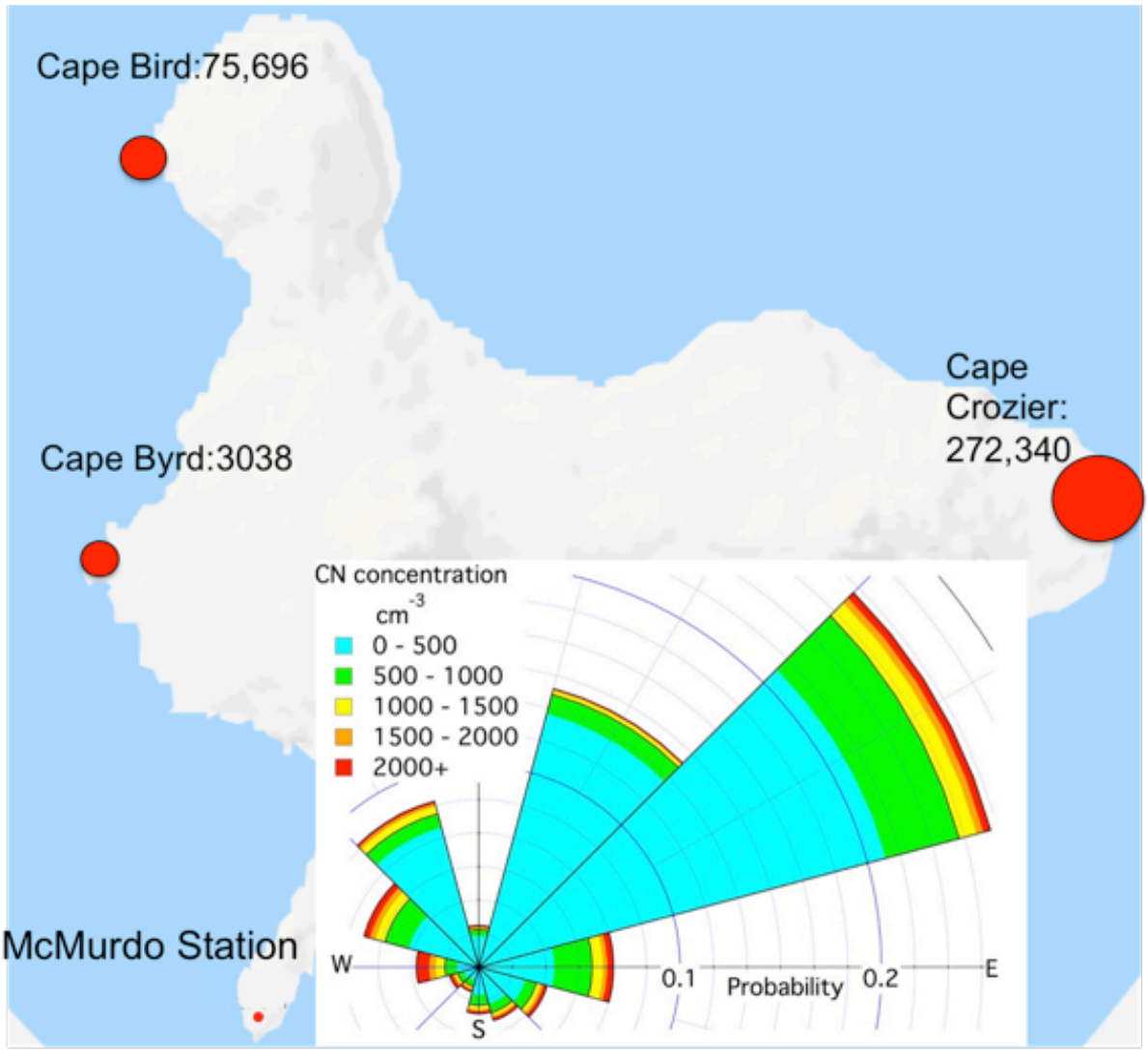

Figure 3.3: Map of Ross Island with McMurdo Station and penguin colonies (penguin numbers from Lyver et al., (2014)) marked on the map. Windrose of CN concentration at the Cosray site is shown on the map.

Submicron aerosol particle samples were collected on pre-scanned Teflon filters (Teflon, Pall Life Science Inc., 37 mm diameter, 1.0 μm pore size) behind a PM_1 sharp-cut cyclone (SCC2.229 PM_1, BGI Inc.). One sample filter and one background filter were collected each week. Samples were frozen and transported to the UCSD laboratory for FTIR spectroscopy. A

Bruker Tensor 27 FTIR spectrometer with a deuterated triglycine sulfate (DTGS) detector (Bruker, Waltham, MA) was used to scan the filters both before and after sampling. An automated algorithm was applied to quantify the mass of the organic functional groups [*L. M. Russell et al.*, 2009; *Takahama et al.*, 2013]. Four groups (alkane, amine, hydroxyl and carboxylic acid) were quantified by the area of absorption peaks and the sum of the mass of the five functional groups. Other groups (organonitrate, organosulfate and non-acid carbonyl) were fit but all samples were below detection limit. The detection limit and error for each functional group is the larger of twice the standard deviation of the absorption values associated with blank filters and the visual determination of the minimum peak size that could be distinguished from spectral noise [*Maria et al.*, 2002]. The detection limit of OM was 0.09 μg based on the sum of the detection limits of the three largest functional groups during the project (alkane, hydroxyl and amine). For the weekly air sampling volume of 80 m^3 used in this study, this loading corresponds to a concentration of 0.001 μg m^{-3}. OM is calculated as the sum of all functional groups measured above detection, based on the assumptions of Russell [2003]. Subsequent evaluations and intercomparisons [*Maria et al.*, 2002; *L. M. Russell et al.*, 2009; *Takahama et al.*, 2013]have shown that errors associated with functional groups that are not quantified because of Teflon interference and semivolatile properties are accounted for within the stated $\pm$20% uncertainty for ambient particle compositions. The ammonium mass is not quantified by FTIR of Teflon filter samples because ammonium nitrate is semi-volatile. The location of absorption by sulfate in FTIR coincides with the location of Teflon absorption. Since the absorption by the Teflon filter far exceeds that of the sulfate particles, sulfate cannot be measured on this substrate. Sulfur was measured by XRF and is expected to be largely ammonium sulfate, since organosulfate and bisulfate were below the limit of quantification. Pure (>99%) uric acid

(Sigma-Aldrich) and urea (Fisher Scientific) were dissolved in water, atomized and collected on triplicate Teflon filters to provide FTIR reference spectra for comparison of the amide group region. FTIR spectra were baselined by subtracting a combination of piecewise linear and polynomial regressions from the spectrum using an automated algorithm [*Takahama et al.*, 2013]

Positive Matrix Factorization (PMF) was applied to the baselined FTIR spectra for the PM_1 samples collected in 2016 at McMurdo Station with PMF2 V4.2 [*Paatero*, 1997; *Paatero and Tapper*, 1994]. Six-factor solution spaces (1~6) were considered. Fpeak values from -2 to 2 at 0.5 increments were considered. Seeds of 1, 10 and 100 were used at each Fpeak and factor number to examine the robustness of each solution. There was little change in solutions with rotations for all solutions. Q/Qexpected decreases as factor number increases for all solutions (Table 3.2). The two-factor solution is considered robust because the spectra are almost identical for all rotations and seeding conditions (Figure 3.4). The solution leaves an average of 23% of the OM as residual. The two factors are not correlated in time and do not have similar spectra (Table 3.2). The new factor identified from the 3-factor solutions is either degenerate or very similar (cosine similarity =0.99) to one of the first two factors. Similarly for 4 or more factor solutions two or more degenerate or duplicate factors are found. This makes the two-factor solution with Fpeak of 0 optimal for the AWARE data set. The small number of factors identified compared to other regions [*Russell et al.*, 2011]is the result of both the low aerosol concentrations and limited personnel access at AWARE, which reduced the time resolution of FTIR samples to one week each and yielded only 54 samples in one year. The low variability during the study also meant that PMF was unable to separate more than two factors.

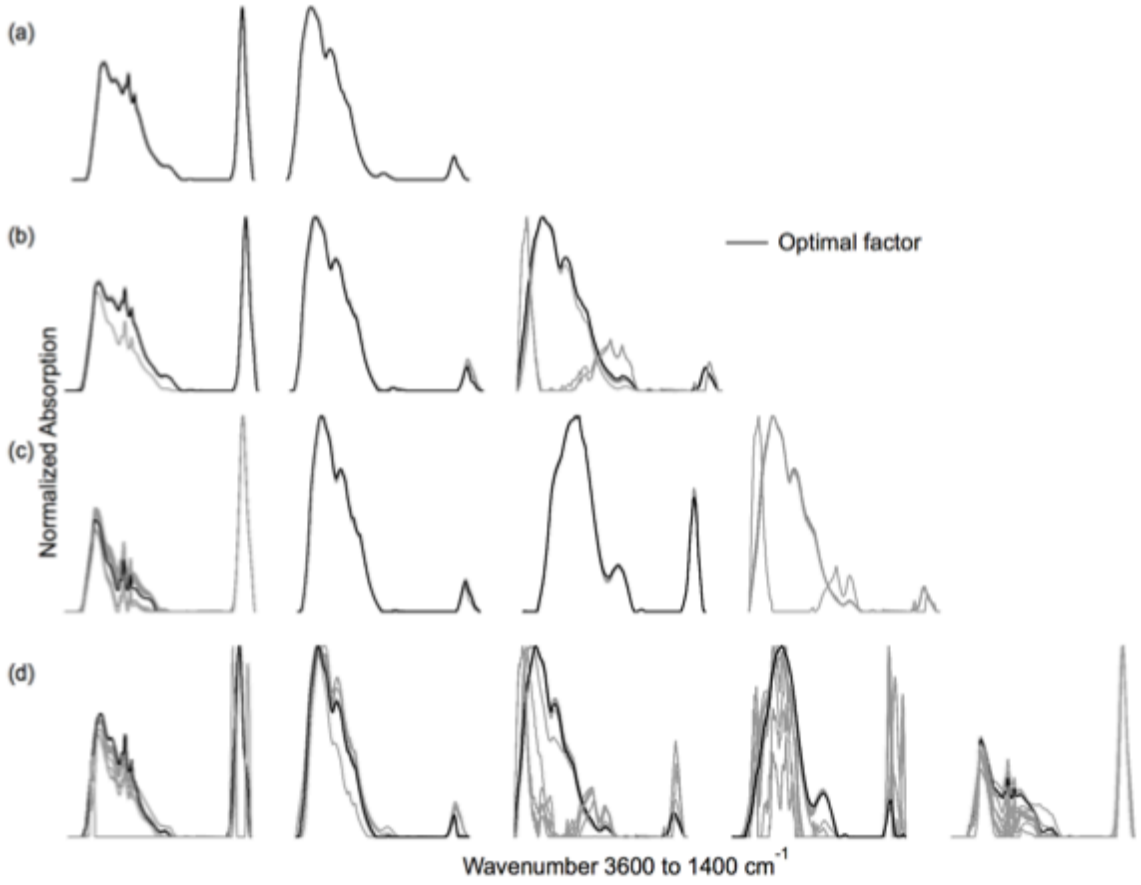

Figure 3.4: FTIR PMF factors in 2 to 5 factor and -2 to 2 fpeak spaces

Table 3.2: Parameters for FTIR PMF factor and K-means clustering evaluation.

Criteria \ Number of Factors	2	3	4	5	6
Q/Q_{exp}	7.06	6.02	4.75	3.90	3.25
Absolute residual	23.6%	21.7%	17.4%	14.2%	12.0%
Temporal correlation factor strength (r>0.8)	None	None	None	None	None
Number of similar factor spectra (Cosine similarity>0.8)	None	1 pair	1 pair	2 pairs	4 pairs
Factors with less than 10% OM	None	None	None	1	1
Number of similar cluster centroids (Cosine similarity>0.95)	None	1 pair	3 pairs	4 pairs	6 pairs

In addition, K-means clustering (Hartigan and Wong, 1979) was applied to the baselined FTIR spectra (Takahama et al., 2013). Solutions with 1 to 10 clusters were evaluated. The 2-cluster solution was chosen because solutions with 3 or more clusters included at least one pair of clusters with centroids with cosine similarity higher than 0.95 (Table 3.2), making those clusters effectively overlapping. The two clusters and two PMF factors were identified as associated with Fossil Fuel Combustion (FFC) and Marine and Seabird (M&S) sources, as described below. Factorization techniques like PMF are applied to separate each individual composition measurement into the independent factors that contribute to its composition, where

these factors may represent different sources as well as different formation processes. On the other hand, clustering algorithms are used to sort similar measurements into categories, each of which may contain a mixture of different sources and formation processes and is characterized by the centroid to which all measurements in that category are most similar. The similarity of the k-means centroids and PMF factors (cosine similarity > 0.97) indicates that both separations are robust. Since the PMF residual is the fraction of OM that could not be assigned to either factor, the ratio of the residual to the factor OM provides a measure of the uncertainty of the PMF separation – namely the fraction of OM that could be missing from the factor. The ratio of the PMF residual to the FFC OM varies from 29% in winter to 63% in summer, making this result more likely to represent all of the FFC OM in winter when FFC OM is a larger relative fraction of OM. Similarly, the PMF residual is 33% of M&S OM in summer, indicating the source separation could be missing a third of M&S OM. In contrast, the PMF residual is 9 times larger than the M&S OM in winter (Table 3.3), making the quantification of M&S OM in winter very uncertain.

Half of the filters (25) were selected for X-ray fluorescence (XRF) (Chester Labnet, OR) quantification of major elements above 23 amu. The elements Na, Mg, Al, Si, P, S, Cl, K, Ca, Ti, V, Cr, Mn, Fe, Co, Ni, Cu, Zn, Br, Rb, Sr, Zr, Ag, Pb and Ba had mass above detection limit (3 times the uncertainty) for 95% of the samples and are used here. The mass of dust was calculated from XRF metal concentrations, assuming dust consists of $MgCO_3$, Al_2O_3, SiO_2, K_2O, $CaCO_3$, TiO_2, Fe_2O_3, MnO and BaO [*Usher et al.*, 2003] after excluding mass associated with sea salt. Sea salt particle mass components were calculated from XRF-measured Na and Cl concentration [*Frossard et al.*, 2014b; *Modini et al.*, 2015].

The CPC measured particles with diameters larger than 10 nm and operated continuously, except from 29 March to 7 April 2016 when a malfunction occurred (Figure 3.2). The CCN Counter measured the particle concentration activated at supersaturations of 0.1%, 0.2%, 0.5%, 0.8%, and 1.0% during AWARE, with only short time periods of missing data (Figure 3.2). HTDMA provided humidified aerosol size distributions for five dry particle sizes at specified relative humidity (RH = 90%) for two periods during the campaign: 23 November to 20 December 2015 and 16 to 31 January 2016. Aerosol particle growth factors (GF_i) from the HTDMA measurements were calculated as the ratio of humidified particle diameter of size i to the selected dry diameter. Mean growth factors (GF) and hygroscopicity parameters (κ) [*Petters and Kreidenweis*, 2007; *Su et al.*, 2010] were calculated from Equation. 3.1 and Equation 3.2:

$$\overline{GF} = \frac{\sum_i GF_i(\frac{dN}{dlogD_p})_i}{\sum_i(\frac{dN}{dlogD_p})_i} \quad (3.1)$$

$$\kappa = \frac{(\overline{GF}^3-1)(1-a_w)}{a_w} \quad (3.2)$$

where N is the measured number concentration and a_w is water activity [*Rickards et al.*, 2013].

Meteorological variables (temperature, humidity, wind speed and wind direction) were measured with a Vaisala model WXT-520 (Helsinki, Finland). The Surface Energy Balance System (SEBS) included upwelling and downwelling solar and infrared radiometers at the measurement site at McMurdo Station from 4 February to 29 December 2016. Aerosol absorption was measured at three wavelengths (470, 522 and 660 nm) by a Particle Soot Absorption Photometer (PSAP; Radiance Research, Seattle, WA). The PSAP absorption at 660 nm was used as a proxy for black carbon (BC) because it is expected to have the least interference from brown carbon [*Olson et al.*, 2015].

3.3 CN, CCN, Hygroscopicity, and Inorganic Particle Measurements

19% of the 1-Hz CN measurements recorded during the project were identified as SLCE, and the average of the concentrations for those times contributed 55% of the project-average CN concentrations. The distribution of SLCE duration and timing (Figure 3.5) shows that SLCE events were approximately two times more frequent during local daytime than nighttime. This short duration and largely daytime timing of SLCE suggests that site maintenance and nearby road traffic are likely responsible for many of the high CN events.

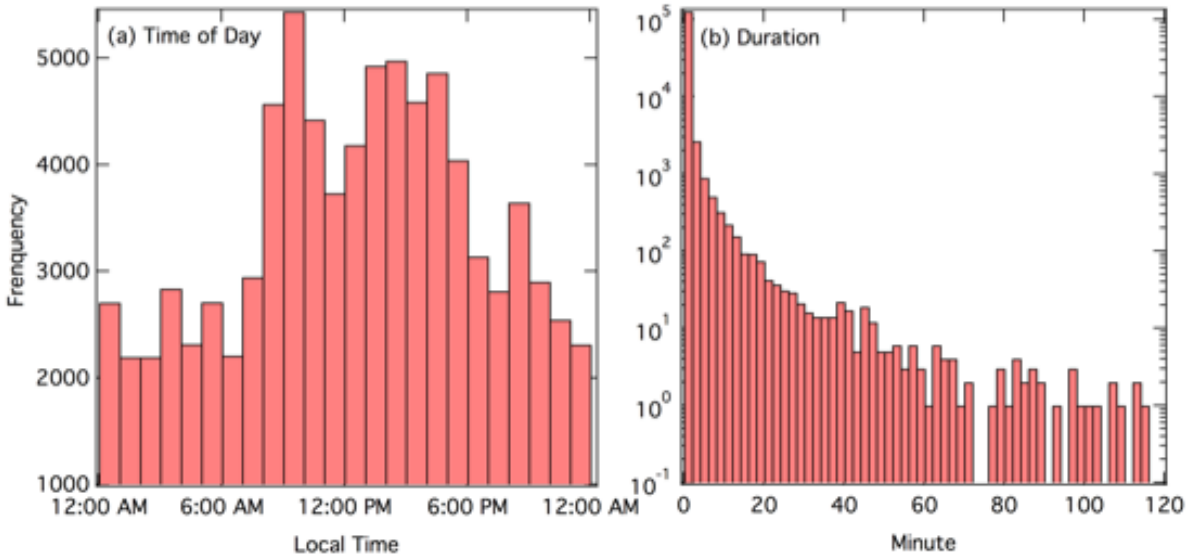

Figure 3.5: Frequency distribution of SLCE with (a) Time of day, and (b) Duration.

There are two reasons why the CN concentrations that remain after SLCE (spikes) are removed are considered representative of the natural background rather than local pollution from McMurdo Station activities: First, the SLCE CN concentration is correlated weakly to BC (r=0.48), but the background CN is correlated negatively to BC absorption (r=-0.4). Second, the two indicators of combustion-related pollution (BC absorption and the FFC factor) were

approximately two times higher in summer than winter (Table 3.3), which is similar to the two-fold increase in SLCE CN in summer compared to winter but not enough to account for the seven-fold increase in the background (SLCE-removed) CN in summer compared to winter. Consequently, this larger summertime difference in background CN is likely associated with the higher productivity of natural sources in summer. More specifically, the CN concentration associated with natural sources was very low (~60 cm^{-3}) in winter during low phytoplankton activity but as high as 2000 cm^{-3} in summer (Figure 3.2), indicating a significant increase in biogenic (sulfate or organic) CN.

Table 3.3: Mean concentrations and ratios with standard deviations during 2016 at McMurdo.

Season		Spring	Summer	Fall	Winter
CCN Number Concentration cm^{-3} (CCN/SLCE-Removed CN)	0.1 % SS	11.2±13.3 (0.07±0.06)	40.1±34.2 (0.08±0.06)	9.7±6.6 (0.06±0.05)	7.1±8.5 (0.1±0.09)
	0.2 % SS	37.9±36.4 (0.19±0.11)	131±80.2 (0.26±0.12)	48.2±29.3 (0.29±0.11)	18.6±20.5 (0.26±0.14)
	0.5 % SS	72.1±48.5 (0.37±0.20)	276.4±147.9 (0.56±0.24)	104±60.7 (0.63±0.20)	33.3±25.3 (0.49±0.26)
	0.8 % SS	99.7±73.9 (0.5±0.23)	348±203 (0.68±0.25)	124±72.3 (0.75±0.23)	42.9±39.6 (0.57±0.29)
	1 % SS	117±110 (0.55±0.24)	371±234 (0.73±0.26)	132±77.5 (0.8±0.23)	48.5±50.2 (0.6±0.30)
$CN\ cm^{-3}$	CN SLCE-Removed	161±94	400±228	141±88	65±77
	CN	376±571	740±693	241±187	237±502
Absorption mM^{-1}		0.2±0.47	0.34±0.66	0.16±0.66	0.2±0.50
Measured FTIR OM $\mu g\ m^{-3}$		0.06±0.04	0.27±0.16	0.07±0.06	0.04±0.02
PMF of FTIR OM	FFC OM $\mu g\ m^{-3}$	0.03±0.01	0.06±0.05	0.03±0.02	0.03±0.02
	M&S OM $\mu g\ m^{-3}$	0.018±0.028	0.155±0.121	0.026±0.046	0.001±0.001
	Residual/ FFC	0.40±0.72	0.63±0.84	0.36±0.49	0.28±0.52
	Residual/ M&S	1.12±097	0.33±0.46	1.03±0.63	9.22±7.74

SLCE had nearly no contribution to CCN, which is consistent with SLCE particles being extremely low hygroscopicity and freshly emitted from fuel combustion [*Wex et al.*, 2010] (Figure 3.2). The CCN measurements did not have short-term spikes even at the highest supersaturation level (1%), at which only 0.1% of the measurements were 5% higher than the background CN. The absence of the SLCE in the CCN measurements is likely the result of the local pollution being both too small and too low hygroscopicity to serve as CCN at 1% or below. The CCN concentration correlated moderately or strongly to background CN (r=0.80, 0.83, 0.87 and 0.88 for 0.2%, 0.5%, 0.8% and 1% SS, respectively). CCN and CN were 5 to 7 times higher during summer, but the ratio of CCN/CN changed less than 30% throughout the year (Table 3.3). CCN/CN was largely constant at all five supersaturations during most of 2016, but from late September to early October the ratio of CCN/CN decreased to 0.5 at 1% supersaturation (Figure 3.2). This decrease of the ratio of CCN to background (spike-removed) CN during the winter-spring transition could be caused by changes in particle size and composition. One such cause would be additional CN that are too small to contribute to CCN. Previous observations at a site 10 km from McMurdo Station showed an increase in the fraction of CN smaller than 250 nm at polar sunrise (September-October), although a specific cause was not clear (Giordano et al., 2017). The higher CCN/CN ratio in the summer (Table 3.3) is consistent with both the higher biogenic sulfate contributions during the highest productivity season (summer) and the slightly larger diameter of the accumulation mode particles observed in previous summers (Kim et al., 2017).

The growth factors and hygroscopicity parameters were both nearly constant during the two measurement periods (Figure 3.6), with values of 1.5 ± 0.3 for growth factors and 0.4 ± 0.1 for hygroscopicity parameters. These numbers were constant across the measured size range of

50 nm to 250 nm diameter and are comparable to other observations in the Antarctic region [*Asmi et al.*, 2010; *Kim et al.*, 2017; *Wex et al.*, 2010]. The particles that had too low hygroscopicity to grow measurably may be those that were emitted by local anthropogenic emissions. The moderate correlation of BC absorption to the fraction of particles that did not grow at increased relative humidity in the HTDMA (R=0.52, Figure 3.7 (a)) indicates that the BC-containing particles could be the particles that have low hygroscopicity. In addition, BC absorption correlated moderately to the non-activated CN particles (1-CCN/CN) (R=0.34 for 1% supersaturation, Figure 3.7 (b)). Since BC-containing particles, such as those freshly emitted from combustion sources, have been shown to have low hygroscopicity (Peng et al., 2017; Vu et al., 2017), these correlations are consistent with the particles that did not take up water being those that were emitted by local combustion activities.

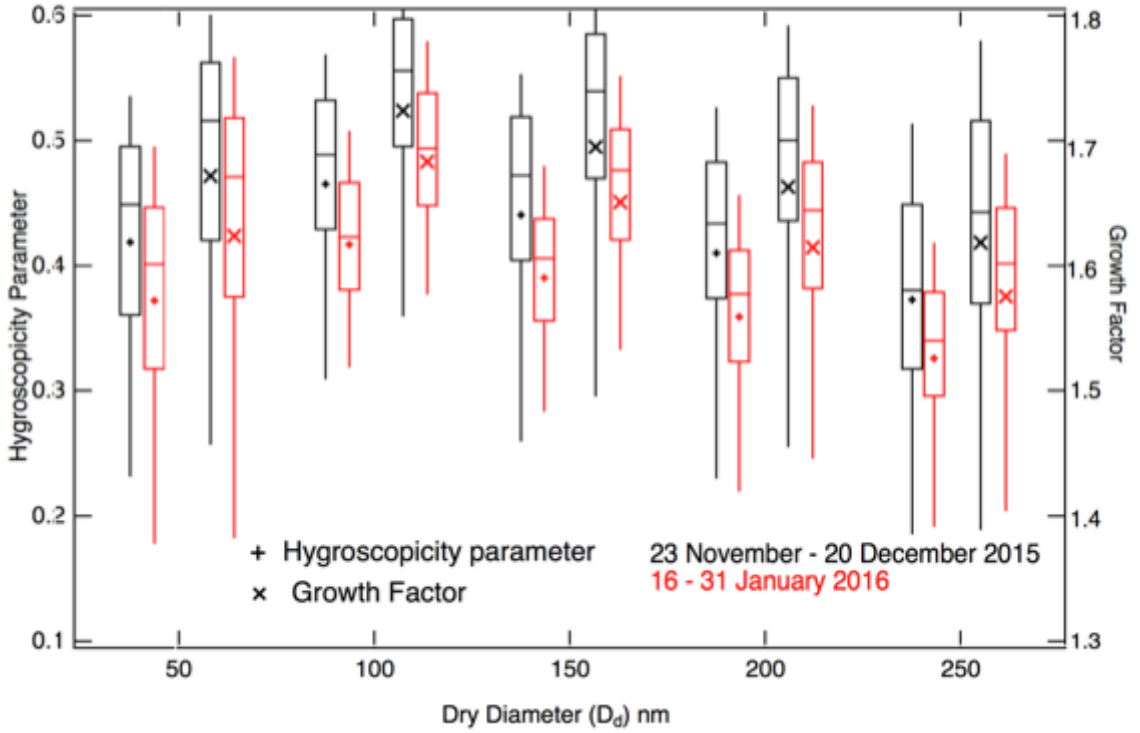

Figure 3.6: Distribution of growth factor and hygroscopcity parameter κ in the two measurement periods from HTDMA. 5th, 25th, 50th, 75th and 90th percentiles are shown by the boxes and whiskers. Means are shown by the markers.

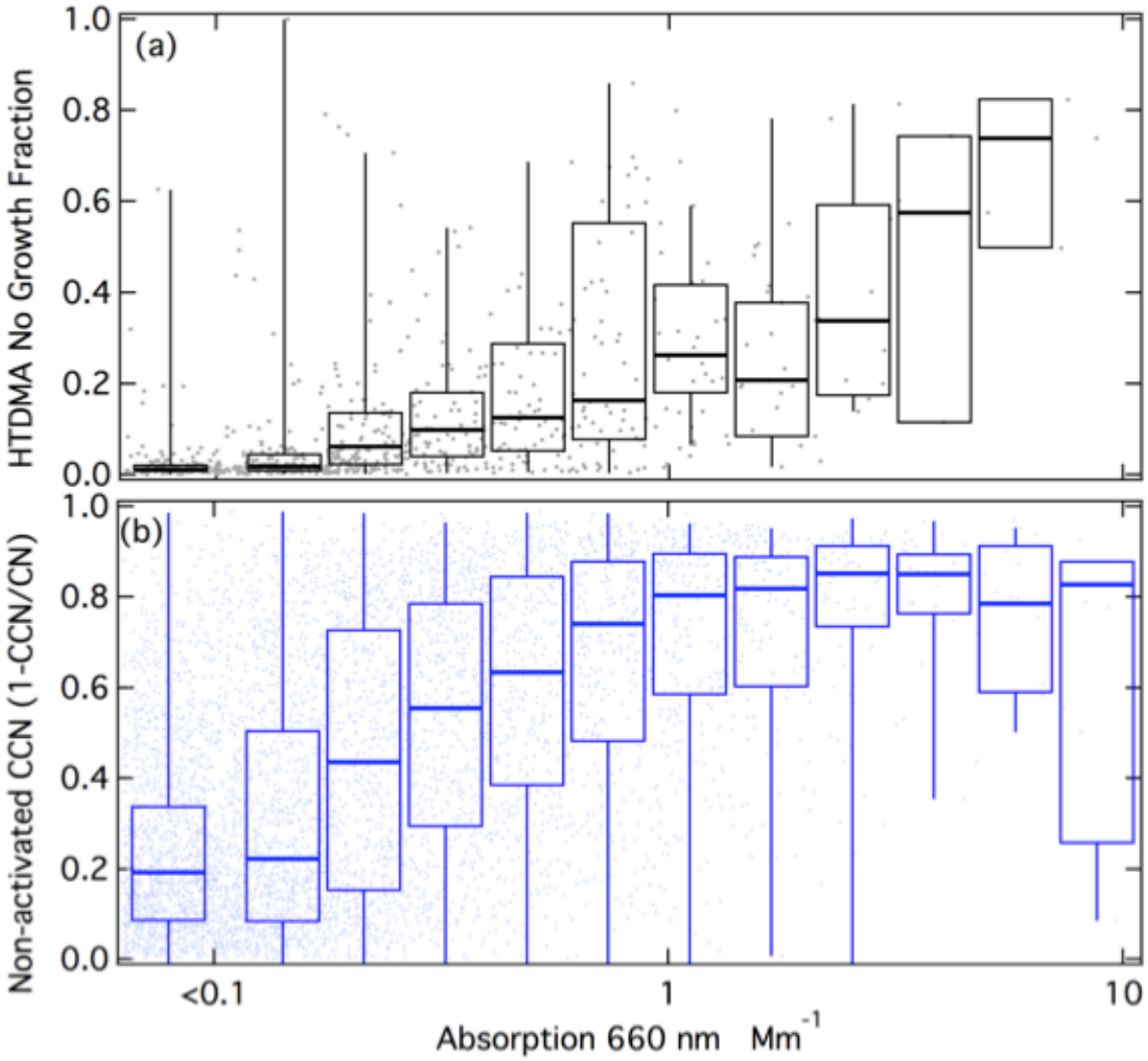

Figure 3.7: (top) Scatter and box-whisker plot of PSAP 660 nm absorption and: (a) HTDMA no growth fration (r=0.52); (b) Non-activated CCN fraction (1-CCN/SLCE-removed CN) for 1% supersatuartion (r=0.34). The boxes show the 25th, 50th and 75th percentile values; the Whiskers show the minimum and maximum values.

XRF measurements of elemental concentrations of S, P, K, Ca, Si, Mn, Al, Ag, Fe, and V were 2 to 15 times higher in summer than in winter (Figure 3.8). Submicron dust mass concentration was 7 times higher in summer, consistent with the lack of exposed soil in winter (Figure 3.1). Sea salt particle mass concentration (Figure 3.1) was 3 times higher in winter than in summer, consistent with the higher circumpolar wind speed providing more sea spray in

winter than summer [*Bintanja et al.*, 2014]. The measured Cl^-/Na^+ of 2 represents a large sodium deficiency in wintertime submicron particles (Figure 3.1). The depletion of Na^+ relative to Cl^- in winter indicates a likely contribution to the aerosol submicron mass from wind-blown frost flowers (Alvarez-Aviles et al., 2008; Thomas and Dieckmann, 2003; Stein and MacDonald, 2004; Papadimitriou et al., 2007; Giannelli et al., 2001; Belzile et al., 2002; Shaw et al., 2010). This sodium depletion is the result of Na_2SO_4 precipitating out from sea ice brine before frost flowers wick up the remaining salt solution. Blowing snow could also contribute to submicron particles [*Domine et al.*, 2004], but this source has not been associated with a substantial sodium deficiency in submicron particle composition [*Gordon and Taylor*, 2009].

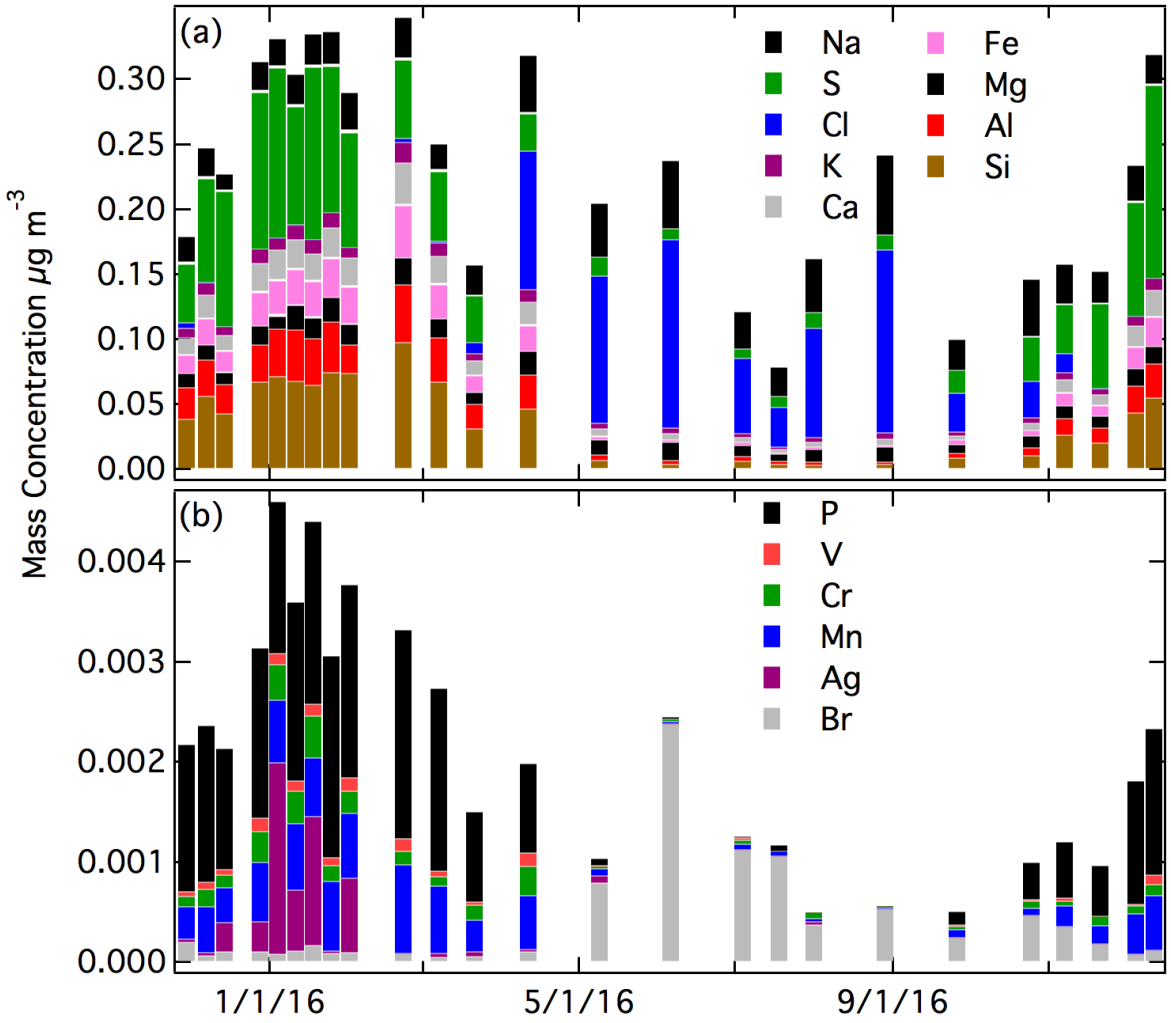

Figure 3.8: Elemental mass concentration from XRF.

If either frost flowers or blowing snow were generated near the site, we would expect a correlation of concentrations to wind speed at higher wind speeds, since both sources have been characterized as requiring wind speed thresholds of approximately 7 m s^{-1} for lofting of particles [*Schmidt*, 1981; *Shaw et al.*, 2010]. During AWARE, 1-min wind speed only exceeded this threshold by 1 m s^{-1} for 24% of the time, and the weekly average wind speed was never higher than 7 m s^{-1}. Wind speed had no correlation to CN concentration for the campaign (r=-0.32) or

for winter (r=-0.31). In addition, there was no correlation (R=-0.15) of submicron CN number with wind speed (>8m s^{-1}), as would be expected for blowing snow generated locally [*Yang et al.*, 2008]. The M&S factor concentration also showed no correlation (r=0.1) to the fraction of time with high wind speed (>8 m s^{-1}). While these relationships do not support the attribution of the wintertime salt mass to either frost flowers or blowing snow, they do not rule it out since the particles may have been lofted upwind and transported to McMurdo Station.

A recent model simulation (Huang and Jaegle, 2017) predicted that blowing snow has significantly higher contributions to submicron particle mass than frost flowers in Antarctica and the Arctic, but also showed that the region at the north edge of the Ross Ice Shelf (including Ross Island) had both higher emissions (>0.6 10^{-6} kg m^{-2} d^{-1}) and concentration (>1.5 μg m^{-3}) from frost flowers than the emissions (<0.4 10^{-6} kg m^{-2} d^{-1}) and concentration (<1.0 μg m^{-3}) from blowing snow, consistent with the finding that wintertime OM at McMurdo Station were more likely from frost flowers than blowing snow.

3.4 Organic Mass and Composition

The measured organic functional group mass concentrations are shown in Figure 3.9(c). The average OM is 0.13 μg m^{-3} for AWARE, with hydroxyl groups having the highest mass fraction (41%), followed by alkane (39%), amine (13%) and carboxylic acid (7%) groups. Similar to CN concentrations, OM was highest in summer (0.27 μg m^{-3}) and lowest in winter (0.04 μg m^{-3}). Arctic OM at Barrow and Alert showed a very different seasonal pattern with low concentrations in Arctic summer (0.03 μg m^{-3} and <0.5 μg m^{-3} in Alert and Barrow, respectively) and high concentrations in winter and spring (0.3 μg m^{-3} and 1 μg m^{-3} in Alert and Barrow, respectively) [*Frossard et al.*, 2011; *Leaitch et al.*, 2017]. Consistent with OM, CN

concentrations at these two Arctic sites, with particle size range of 80-500 nm at Alert and >100 nm at Barrow, were also low in Arctic summer (<50 cm^{-3} and 100-300 cm^{-3} at Alert and Barrow, respectively) and high in winter and spring (>100 cm^{-3} and 400-1000 cm^{-3} at Alert and Barrow, respectively) [*Croft et al.*, 2016a; *Polissar et al.*, 1999]. The springtime high concentrations in the Arctic result from long-range transport from mid latitudes after the breakup of the vortex. The lack of substantial pollution sources at southern mid-latitudes (compared to those at northern mid-latitudes) means the Antarctic does not have an equivalent haze in spring [*L.M. Russell and Shaw*, 2015; *Stohl*, 2006; *Stohl and Sodemann*, 2010]. The higher summer OM in Antarctica is likely produced by the specific local conditions of the three polar sites, namely Ross Island has higher marine and seabird activity compared to Barrow and Alert.

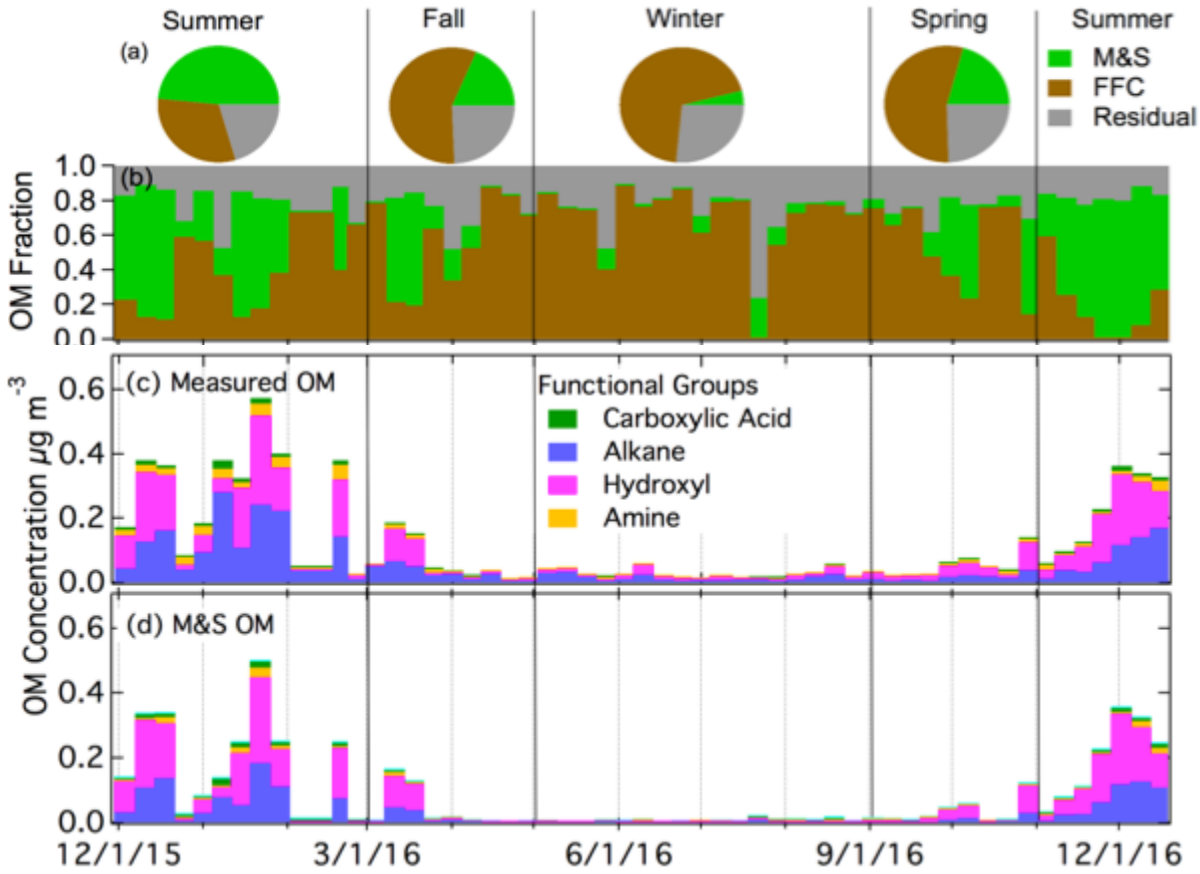

Figure 3.9: (a) Mass fraction of PMF factors in four seasons. Time series of (b) PMF factor OM fractions, (c) OM concentration with functional groups and (d) M&S OM concentration with functional groups.

The FFC cluster and factor are similar to each other (cosine similarity=0.97) and are both named because of the similarity of the spectra to factors identified as FFC previously [*Guzman-Morales et al.*, 2014; *Price et al.*, 2017; *Saliba et al.*, 2017]. The FFC Factor has two narrow peaks at 2865 and 2934 cm^{-1} that are characteristic of long-chain hydrocarbons and a cosine similiarity greater than 0.8 with factor spectra identified previously as urban combustion emissions [*Guzman-Morales et al.*, 2014] and fresh ship engine emissions [*Price et al.*, 2017]. The FFC factor has alkane and amine groups that account for 80% OM (Figure 3.10), which is consistent with urban combustion emissions and vehicle engine tests [*Guzman-Morales et al.*,

2014; *Saliba et al.*, 2017]. The FFC factor was 73% OM in winter but only 23% in summer (Figure 3.9 (a) and (b)). The FFC factor concentration is weakly or moderately correlated to Ca, P, Fe, Cu, Cr, Mn and Zn (r=0.3~0.5), which have been identified as tracers of vehicle emissions [*Cheung et al.*, 2010; *Lin et al.*, 2015].

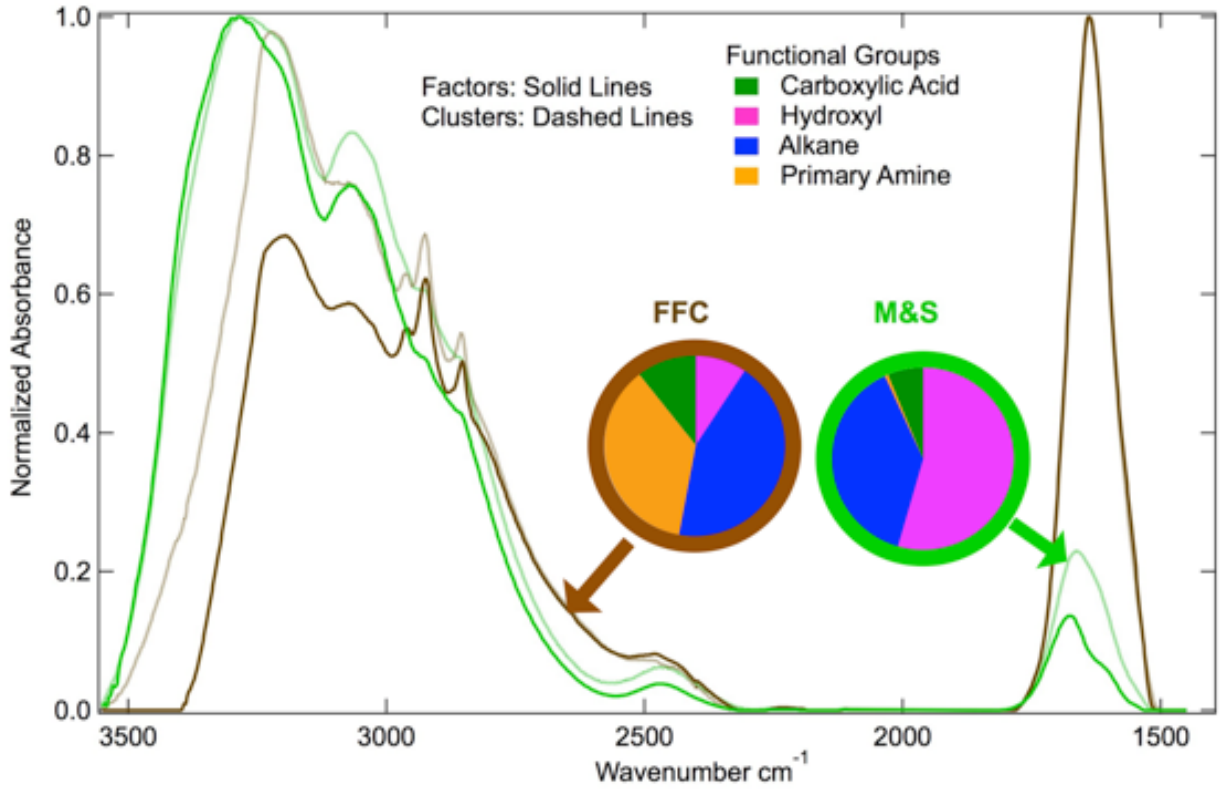

Figure 3.10: Normalized spectra from k-means clustering centroids and PMF factors. Functional group fractions of PMF factors are shown in the pie charts

The primary amine peak (1620 cm^{-1}) is present in both FFC and M&S factors at McMurdo Station (Figure 3.11), consistent with previous studies [*Guzman-Morales et al.*, 2014; *Leaitch et al.*, 2017; *Price et al.*, 2017; *Shaw et al.*, 2010]. The difference between the FFC and M&S spectra is that FFC has double sharp alkane group peaks at 3000 cm^{-1} but M&S has a broad hydroxyl group absorption at 3400 cm^{-1} (Figure 3.10). Ammonium has peaks at 3050 and 3200 cm^{-1} and contributes to both FFC and M&S spectra (Figure 3.10).

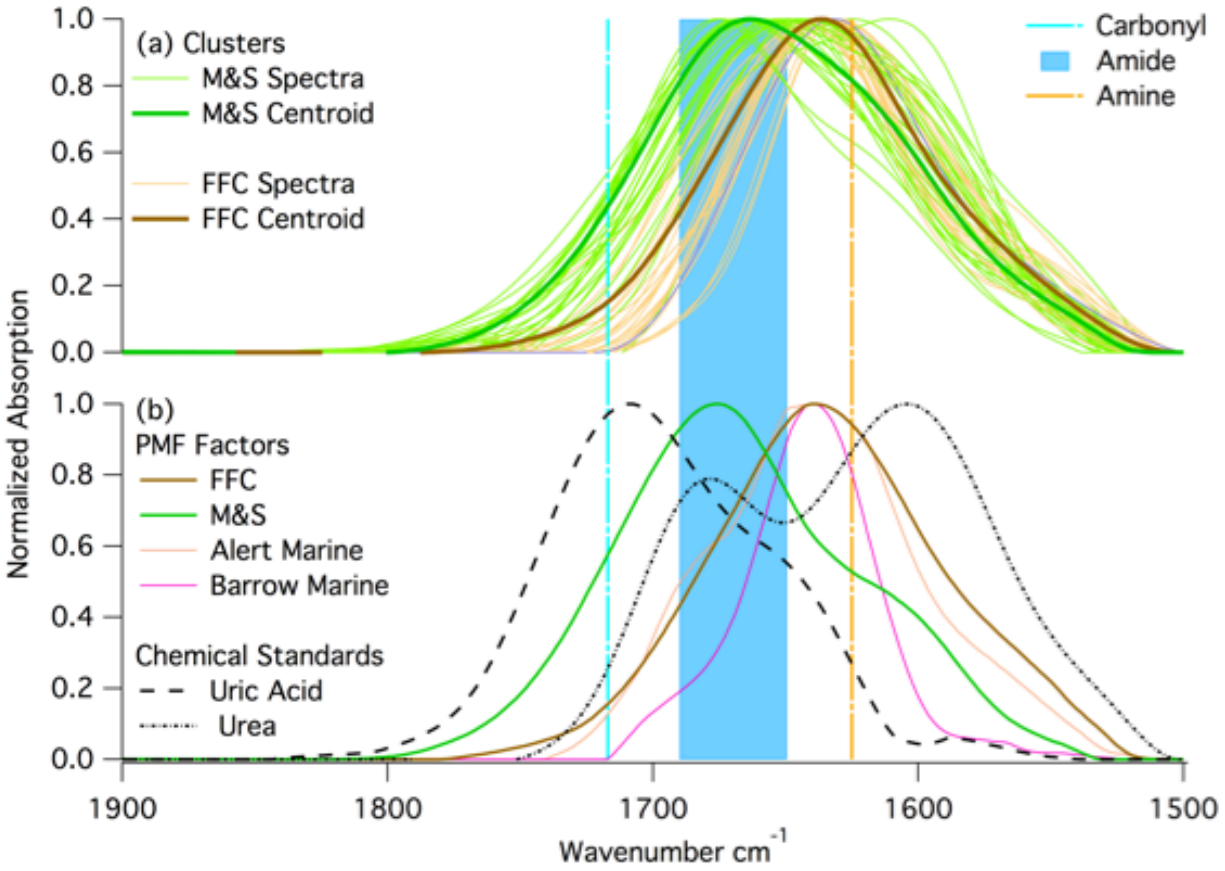

Figure 3.11: Normalized spectra at 1500 to 1800 cm-1 wavenumber region from (a) K-means clustering centroid and spectra in the clusters; (b) PMF factors from this study and two previous arctic studies, and chemical standards: urea and uric acid. Locations of primary amine and carbonyl group are marked on the figure.

The M&S Factor is identified as "marine" because of its high hydroxyl group fraction, which is similar to past marine sea spray factors (Russell et al., 2010), and as "seabird" because

of absorption from ammonium and an organic nitrogen peak that is likely associated with coastal penguin emissions. The high hydroxyl group that accounted for 55% OM in the M&S factor makes this factor overall similar to the marine factors identified in measurements at Barrow and Alert (cosine similarity=0.53-0.57) [*Leaitch et al.*, 2017; *Shaw et al.*, 2010] (Figure 3.9 and Figure 3.10). The M&S hydroxyl group fraction is lower than the Arctic marine factors that have 80% hydroxyl group [*Leaitch et al.*, 2017; *Shaw et al.*, 2010].

Barrow and Alert had higher marine OM concentrations in winter than in summer. Likely this is because these two Arctic sites did not have the large seabird contributions that contributed to the M&S factor on Ross Island during summer [*Lyver et al.*, 2014]. The smaller seabird populations near the Arctic sites also meant that Barrow and Alert OM had only very small amide contributions (Figure 3.11). The M&S factor has higher alkane (38%) and amine (8%) group mass compared to two marine factors in Arctic regions that had only 6% alkane and 6% amine group mass [*Leaitch et al.*, 2017; *Shaw et al.*, 2010]. This factor contributed a substantial fraction of organic mass in summer (58%) but very little in winter (5%) (Figure 3.9 (b)). The M&S organic mass concentration was only 0.001 μg m^{-3} during winter and was 0.15 μg m^{-3} during summer (Figure 3.9 (d)). The low winter and high summer M&S OM means that salt was not correlated to the M&S Factor organic mass, indicating the high summertime concentrations of natural OM could not be explained by primary marine aerosol contributions alone. Marine OM contributions could be high in winter relative to summer because of the higher regional wind speeds, but their absolute concentration was too low to separate and identify in this set of 54 one-week samples. Specifically, the small number of long-duration samples resulted in PMF residuals that were more than 9 times higher than the M&S factor in winter, so that the marine fraction in winter is very uncertain.

The FTIR spectra for summer samples show an absorption peak at 1680 cm^{-1} that is not present in winter (Figure 3.1). The M&S factor FTIR absorption peak (Figure 3.11) was located at a wavenumber that was both too high (>1630 cm^{-1}) to be primary amine bending and too low (<1714 cm^{-1}) to be carbonyl bending (Figure 3.11) [*Takahama et al.*, 2013]. Seabirds excrete urea that degrades to uric acid, and the amide groups found in both urea and uric acid could explain the 1680 cm^{-1} peak in the summer FTIR spectra (Figure 3.11). The ammonium peaks (Figure 3.10) associated with the M&S factor are also consistent with ammonia emissions from guano [*Legrand et al.*, 1998], which is taken up on particles as ammonium.

More than 155,000 breeding pairs reside in the ice-free areas on Ross Island [*Attwood et al.*, 2014] from October to March [*Davis et al.*, 2001]. The three penguin habitats on Ross Island are all less than 100 km from McMurdo Station (Figure 3.3) [*Lyver et al.*, 2014]. Previous studies have also attributed aerosol emissions and properties to penguin activities, including ammonia-enhanced new particle formation [*Weber et al.*, 1998]and oxalate-enriched particles and organonitrogen-containing fragments from urea breakdown products [*Legrand et al.*, 2012; *Schmale et al.*, 2013]. The finding here of amide groups would be consistent both with particle formation and with substantial organonitrogen components. Since McMurdo Station is most frequently downwind from Cape Crozier (which is located to the northeast of the sampling site), its estimated ~300,000 penguins are a likely source of this organic and ammonium contribution to particles [*Lyver et al.*, 2014].

This 1680 cm^{-1} amide peak was present in very small amounts in multi-year Arctic FTIR measurements [*Leaitch et al.*, 2017; *Shaw et al.*, 2010] (Figure 3.11), but their low concentrations did not support further investigation. The 1680 cm^{-1} peak has not been observed in open ocean marine factors [*Frossard et al.*, 2014a; *L. M. Russell et al.*, 2010], suggesting that

an open ocean marine source is not likely. An alternative explanation of the amide group is emissions from seasonal ice microbiota [*Dall'Osto et al.*, 2017]. Given the proximity and abundance of seabirds at McMurdo Station, seabirds are the more likely source than are sea ice algae or other phytoplankton during AWARE. There are four reasons that the M&S factor are likely associated with marine and seabird emissions: The 1680 cm^{-1} signal has been found at two coastal Arctic sites (in small amounts) but not on open ocean marine studies [*Frossard et al.*, 2011; *Hawkins and Russell*, 2010; *Leaitch et al.*, 2017; *Shaw et al.*, 2010]. This difference suggests that the amide group is likely associated with seabirds, since they are found in coastal marine areas but generally not in open ocean marine areas. The higher concentrations of the M&S OM factor coincided with the summer breeding period of a large penguin colony at Cape Crozier, which was upwind during most of the summer. Other possible contributions, such as from algal blooms during ice melting in spring, are not consistent with the northeasterly winds, the amide group, or the seasonality of the M&S OM. HYSPLIT back trajectories [*Draxier and Hess*, 1998] did not add useful information because the day-to-day variability exceeded the differences among weekly averages. Weekly-average wind direction was always northeasterly ($\pm$45 degrees), so there was insufficient variation to identify sources in different directions. The emissions from seabirds have significant regional implications in polar areas because of their large population and wide distribution [*Croft et al.*, 2016b; *Riddick et al.*, 2012]. Chemical transport model simulations suggest that emissions of reduced nitrogen from seabirds in the Arctic could significantly increase aerosol particle formation, and in turn cloud droplet number concentration and cloud albedo, yielding as much as -0.5 W m^{-2} radiative forcing averaged over the 14,000,000 km^2 of the Arctic Ocean [*Croft et al.*, 2016b].

The measured acid group concentration is likely to be a secondary aerosol contribution since photochemical oxidation has been shown to form highly oxidized molecules including carboxylic acids by photochemical reactions [*Alfarra et al.*, 2006; *Alves and Pio*, 2005; *Barbaro et al.*, 2017; *Charbouillot et al.*, 2012; *Claeys et al.*, 2007; *Kawamura and Gagosian*, 1987; *Sax et al.*, 2005; *Stephanou and Stratigakis*, 1993; *Xu et al.*, 2013]. Acids are also present in trace amounts in seawater [*Gagosian and Stuermer*, 1977; *Kawamura and Gagosian*, 1987], but the higher concentrations measured here are likely to only be explained by secondary processes. The carboxylic acid group mass concentration that was associated with the M&S factor was correlated moderately to downwelling shortwave irradiance (r=0.75, Figure 3.12), supporting the idea that the carboxylic acid group mass was from photochemical reactions.

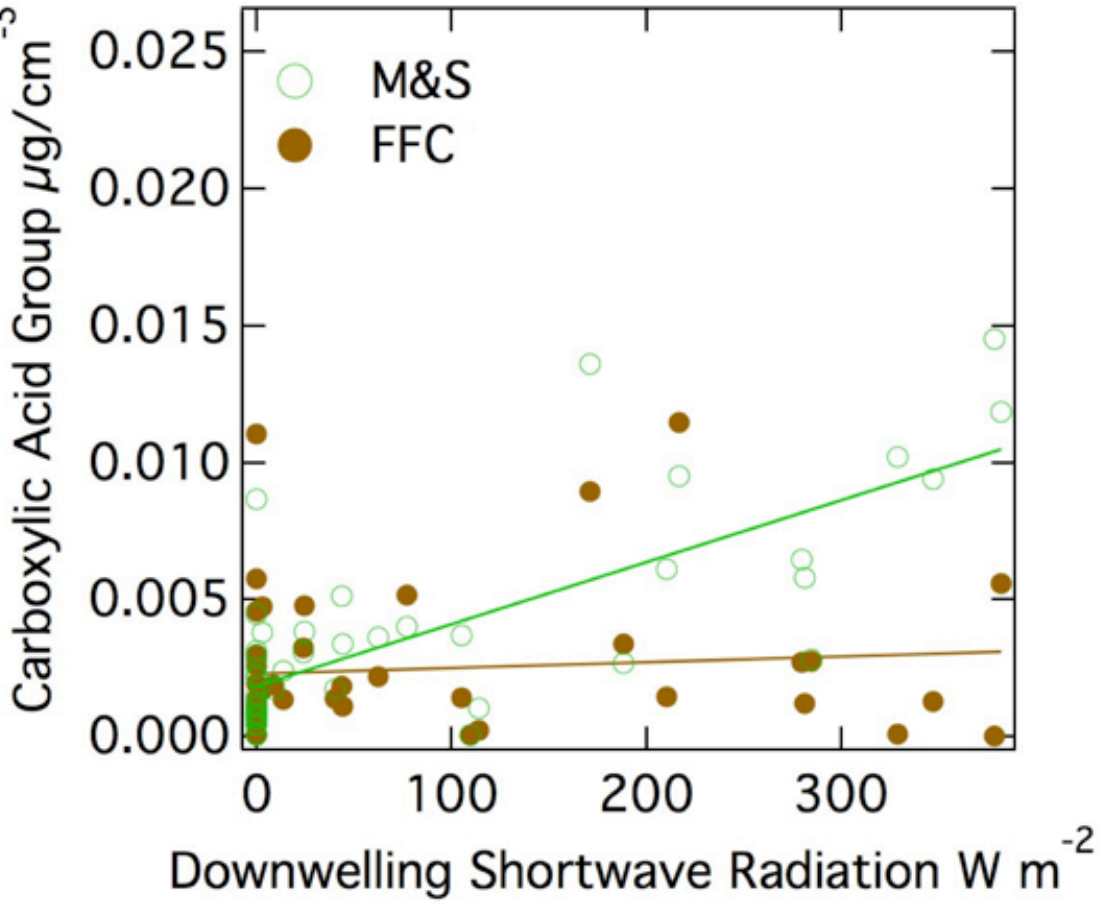

Figure 3.12: Scatter plot of (a) M&S carboxylic acid group and shortwave downwelling radiation (r=0.75) and (b) carboxylic acid group in FFC and shortwave downwelling radiation (r=0.09)

Carboxylic acid group mass fractions have also been identified as secondary photochemical products based on their correlation to solar radiation in clean, open-ocean conditions [*Frossard et al.*, 2014a]. However, since the seabird emissions were only high in summer when radiation was also generally high, the correlation to radiation does not provide evidence of photochemical contributions in this case. Interestingly, the carboxylic acid group associated with the FFC factor had no correlation (r= 0.09) to downwelling shortwave irradiance.

This difference may be because the local emissions from McMurdo Station facilities reached the Cosray site in less than 5 min (since McMurdo Station was 2 km away and wind speeds were 6 m s^{-1} on average) making them essentially "fresh" primary particles, whereas those from the large upwind penguin colony took 6 hr (since Cape Crozier was 100 km away and wind speeds were 6 m s^{-1} on average) to reach the site giving them approximately 50 times more time for photochemical reactions leading to SOA production. It is also possible that the anthropogenic gas-phase precursor emissions had lower SOA acid yields but there is little evidence to support this [*McNeill*, 2015; *Rickard et al.*, 2010; *Wyche et al.*, 2009]. The source of the vapor-phase organic precursors of the summer seabird acid groups is not known, but given their substantial contribution to mass is worthy of further investigation.

3.5 Conclusions

The first year-long organic functional group measurements in Antarctica show the seasonal trend of higher summer concentrations in most of the aerosol measurements. Short-lived contamination events (SLCE) of typically less than 1 hr (Figure 3.5) from local sources were separated from the CN time series to investigate the more regionally-representative or "background" concentrations. With SLCE removed, average CN concentrations were 65 cm^{-3} in winter but 400 cm^{-3} in summer.

The ratio of CCN to background (spike-removed) CN was largely constant for most of the measured seasons. Growth factors (1.5±0.3) and hygroscopicity parameters κ (0.4±0.1) were measured in two one-month periods during the 2015-2016 summer and are comparable to marine aerosols reported near Antarctica [*Asmi et al.*, 2010; *Kim et al.*, 2017; *Wex et al.*, 2010].

Both natural dust and biogenic as well as anthropogenic concentrations were more abundant in the summer months due to both the higher sunlight for productivity and the higher site accessibility. The mean summer OM concentration was 0.27 μg m^{-3}, which was 7 times higher than winter OM. Hydroxyl and alkane groups were found to be the most abundant and accounted for 80% of OM. Two factors were identified by PMF with an average residual of 23%: the M&S factor was associated with natural marine sea spray and coastal seabird sources, and the FFC was associated with local combustion emissions. The M&S factor mass concentration was 150 times higher in summer than winter; the FFC factor had a higher concentration than M&S in winter but the concentrations were so low that the quantification of the M&S factor in winter is very uncertain.

In addition to the primary amine peak present in past marine sea spray measurements, an FTIR absorption peak at 1680 cm^{-1} was associated with the M&S factor in summer. The likely source of this peak as well as the coincident ammonium concentrations was seabird-related emissions from penguin colonies at Cape Crozier. The carboxylic acid group mass in the M&S factor was high in summer and was likely from secondary products of photochemical reactions.

3.6 Acknowledgements

We would like to thank the ARM (Atmospheric Radiation Measurement) program for the AMF-2 AWARE campaign, which was jointly supported by National Science Foundation (NSF AWARE grant: DPP-1443549) and Department of Energy (DOE Award number: DE-SC0017981.) We also thank the AWARE personnel, Ryan C. Scott, Colin Jenkinson, Heath H. Powers, Maciej Ryczek, and Gregory Stone, for help collecting samples on site and Savannah

Lewis and Gary Cheng for assistance with sample preparation and analysis at Scripps. FTIR and XRF measurements are available at UCSD digital archives: https://doi.org/10.6075/J0WM1BKV Other data are available on the ARM Data Discovery: https://www.arm.gov/research/campaigns/amf2015aware

Chapter 3, in full, has been submitted to *Atmospheric Chemistry and Physics*. Liu, J., Dedrick, J., Russell, L.M., Senum, G.I., Uin, J., Kuang, C., Springston, S.R., Leaitch W. R., Aiken A.C. and Lubin, D, "High Summertime Aerosol Organic Functional Group Concentrations from Marine and Seabird Sources at Ross Island, Antarctica, during AWARE" The dissertation author was the primary investigator and author of this paper.

References

Alfarra, M. R., Paulsen, D., Gysel, M., Garforth, A. A., Dommen, J., Prévôt, A. S., Worsnop, D. R., Baltensperger, U., and Coe, H.: A mass spectrometric study of secondary organic aerosols formed from the photooxidation of anthropogenic and biogenic precursors in a reaction chamber, Atmospheric Chemistry and Physics, 6, 5279-5293, 2006.

Alves, C. A., and Pio, C. A.: Secondary organic compounds in atmospheric aerosols: Speciation and formation mechanisms, Journal of the Brazilian Chemical Society, 16, 1017-1029, 10.1590/s0103-50532005000600020, 2005.

Arrigo, K. R., van Dijken, G. L., and Bushinsky, S.: Primary production in the Southern Ocean, 1997-2006, Journal of Geophysical Research-Oceans, 113, 10.1029/2007jc004551, 2008.

Asmi, E., Frey, A., Virkkula, A., Ehn, M., Manninen, H. E., Timonen, H., Tolonen-Kivimaki, O., Aurela, M., Hillamo, R., and Kulmala, M.: Hygroscopicity and chemical composition of Antarctic sub-micrometre aerosol particles and observations of new particle formation, Atmospheric Chemistry and Physics, 10, 4253-4271, 10.5194/acp-10-4253-2010, 2010.

Asmi, E., Neitola, K., Teinila, K., Rodriguez, E., Virkkula, A., Backman, J., Bloss, M., Jokela, J., Lihavainen, H., De Leeuw, G., Paatero, J., Aaltonen, V., Mei, M., Gambarte, G., Copes, G.,

Albertini, M., Fogwill, G. P., Ferrara, J., Barlasina, M. E., and Sanchez, R.: Primary sources control the variability of aerosol optical properties in the Antarctic Peninsula, Tellus Series B-Chemical and Physical Meteorology, 70, 10.1080/16000889.2017.1414571, 2018.

Attwood, A. R., Washenfelder, R. A., Brock, C. A., Hu, W., Baumann, K., Campuzano-Jost, P., Day, D. A., Edgerton, E. S., Murphy, D. M., Palm, B. B., McComiskey, A., Wagner, N. L., de Sa, S. S., Ortega, A., Martin, S. T., Jimenez, J. L., and Brown, S. S.: Trends in sulfate and organic aerosol mass in the Southeast U.S.: Impact on aerosol optical depth and radiative forcing, Geophysical Research Letters, 41, 7701-7709, 10.1002/2014gl061669, 2014.

Barbaro, E., Kirchgeorg, T., Zangrando, R., Vecchiato, M., Piazza, R., Barbante, C., and Garnbaro, A.: Sugars in Antarctic aerosol, Atmospheric Environment, 118, 135-144, 10.1016/j.atmosenv.2015.07.047, 2015a.

Barbaro, E., Zangrando, R., Vecchiato, M., Piazza, R., Cairns, W. R. L., Capodaglio, G., Barbante, C., and Gambaro, A.: Free amino acids in Antarctic aerosol: potential markers for the evolution and fate of marine aerosol, Atmospheric Chemistry and Physics, 15, 5457-5469, 10.5194/acp-15-5457-2015, 2015b.

Barbaro, E., Zangrando, R., Kirchgeorg, T., Bazzano, A., Illuminati, S., Annibaldi, A., Rella, S., Truzzi, C., Grotti, M., Ceccarini, A., Malitesta, C., Scarponi, G., and Gambaro, A.: An integrated study of the chemical composition of Antarctic aerosol to investigate natural and anthropogenic sources, Environmental Chemistry, 13, 867-876, 10.1071/en16056, 2016.

Barbaro, E., Padoan, S., Kirchgeorg, T., Zangrando, R., Toscano, G., Barbante, C., and Gambaro, A.: Particle size distribution of inorganic and organic ions in coastal and inland Antarctic aerosol, Environmental Science and Pollution Research, 24, 2724-2733, 10.1007/s11356-016-8042-x, 2017.

Beaton, A. E., and Tukey, J. W.: The Fitting of Power Series, Meaning Polynomials, Illustrated on Band-Spectroscopic Data, Technometrics, 16, 147-185, 10.2307/1267936, 1974.

Bintanja, R., Severijns, C., Haarsma, R., and Hazeleger, W.: The future of Antarctica's surface winds simulated by a high-resolution global climate model: 1. Model description and validation, Journal of Geophysical Research-Atmospheres, 119, 7136-7159, 10.1002/2013jd020847, 2014.

Bodhaine, B. A.: Aerosol measurements at four background sites, Journal of Geophysical Research: Oceans, 88, 10753-10768, 1983.

Bodhaine, B. A., Deluisi, J. J., Harris, J. M., Houmere, P., and Bauman, S.: Aerosol measurements at the South Pole, Tellus B: Chemical and Physical Meteorology, 38, 223-235, 1986.

Bromwich, D. H., Nicolas, J. P., Monaghan, A. J., Lazzara, M. A., Keller, L. M., Weidner, G. A., and Wilson, A. B.: Central West Antarctica among the most rapidly warming regions on Earth, Nature Geoscience, 6, 139-145, 10.1038/ngeo1671, 2013.

Cadle, R. D., Fischer, W. H., Frank, E. R., and Lodge, J. P.: PARTICLES IN ANTARCTIC ATMOSPHERE, Journal of the Atmospheric Sciences, 25, 100-&, 10.1175/1520-0469(1968)025<0100:pitaa>2.0.co;2, 1968.

Charbouillot, T., Gorini, S., Voyard, G., Parazols, M., Brigante, M., Deguillaume, L., Delort, A. M., and Mailhot, G.: Mechanism of carboxylic acid photooxidation in atmospheric aqueous phase: Formation, fate and reactivity, Atmospheric Environment, 56, 1-8, 10.1016/j.atmosenv.2012.03.079, 2012.

Cheung, K. L., Ntziachristos, L., Tzamkiozis, T., Schauer, J. J., Samaras, Z., Moore, K. F., and Sioutas, C.: Emissions of Particulate Trace Elements, Metals and Organic Species from Gasoline, Diesel, and Biodiesel Passenger Vehicles and Their Relation to Oxidative Potential, Aerosol Science and Technology, 44, 500-513, 10.1080/02786821003758294, 2010.

Claeys, M., Szmigielski, R., Kourtchev, I., Van der Veken, P., Vermeylen, R., Maenhaut, W., Jaoui, M., Kleindienst, T. E., Lewandowski, M., and Offenberg, J. H.: Hydroxydicarboxylic acids: markers for secondary organic aerosol from the photooxidation of α-pinene, Environmental science & technology, 41, 1628-1634, 2007.

Cowie, G. L., and Hedges, J. I.: Sources and reactivities of amino acids in a coastal marine environment, Limnology and Oceanography, 37, 703-724, 10.4319/lo.1992.37.4.0703, 1992.

Croft, B., Martin, R. V., Leaitch, W. R., Tunved, P., Breider, T. J., D'Andrea, S. D., and Pierce, J. R.: Processes controlling the annual cycle of Arctic aerosol number and size distributions, Atmospheric Chemistry and Physics, 16, 3665-3682, 10.5194/acp-16-3665-2016, 2016a.

Croft, B., Wentworth, G. R., Martin, R. V., Leaitch, W. R., Murphy, J. G., Murphy, B. N., Kodros, J. K., Abbatt, J. P. D., and Pierce, J. R.: Contribution of Arctic seabird-colony ammonia to atmospheric particles and cloud-albedo radiative effect, Nature Communications, 7, 10.1038/ncomms13444, 2016b.

Dall'Osto, M., Ceburnis, D., Monahan, C., Worsnop, D. R., Bialek, J., Kulmala, M., Kurten, T., Ehn, M., Wenger, J., Sodeau, J., Healy, R., and O'Dowd, C.: Nitrogenated and aliphatic organic vapors as possible drivers for marine secondary organic aerosol growth, Journal of Geophysical Research-Atmospheres, 117, 10.1029/2012jd017522, 2012.

Dall'Osto, M., Ovadnevaite, J., Paglione, M., Beddows, D. C. S., Ceburnis, D., Cree, C., Cortes, P., Zamanillo, M., Nunes, S. O., Perez, G. L., Ortega-Retuerta, E., Emelianov, M., Vaque, D., Marrase, C., Estrada, M., Sala, M. M., Vidal, M., Fitzsimons, M. F., Beale, R., Airs, R., Rinaldi, M., Decesari, S., Facchini, M. C., Harrison, R. M., O'Dowd, C., and Simo, R.: Antarctic sea ice region as a source of biogenic organic nitrogen in aerosols, Scientific Reports, 7, 10.1038/s41598-017-06188-x, 2017.

Davis, L. S., Harcourt, R. G., and Bradshaw, C. J. A.: The winter migration of Adelie penguins breeding in the Ross Sea sector of Antarctica, Polar Biology, 24, 593-597, 10.1007/s003000100256, 2001.

Defelice, T. P., Saxena, V. K., and Yu, S. C.: On the measurements of cloud condensation nuclei at Palmer Station, Antarctica, Atmospheric Environment, 31, 4039-4044, 10.1016/s1352-2310(97)00250-1, 1997.

Domine, F., Sparapani, R., Ianniello, A., and Beine, H. J.: The origin of sea salt in snow on Arctic sea ice and in coastal regions, Atmospheric Chemistry and Physics, 4, 2259-2271, 10.5194/acp-4-2259-2004, 2004.

Draxier, R. R., and Hess, G. D.: An overview of the HYSPLIT_4 modelling system for trajectories, dispersion and deposition, Australian Meteorological Magazine, 47, 295-308, 1998.

Frossard, A. A., Shaw, P. M., Russell, L. M., Kroll, J. H., Canagaratna, M. R., Worsnop, D. R., Quinn, P. K., and Bates, T. S.: Springtime Arctic haze contributions of submicron organic particles from European and Asian combustion sources, Journal of Geophysical Research-Atmospheres, 116, 10.1029/2010jd015178, 2011.

Frossard, A. A., Russell, L. M., Keene, W. C., Kieber, D. J., Quinn, P. K., and Bates, T. S.: Regional Signatures in the Organic Composition of Marine Aerosol Particles, in: AIP Conference Proceedings, 19th International Conference on Nucleation and Atmospheric Aerosols (ICNAA), Colorado State Univ, Ctr Arts, Fort Collins, CO, 2013, WOS:000319766400136, 543-546, 2013.

Frossard, A. A., Russell, L. M., Burrows, S. M., Elliott, S. M., Bates, T. S., and Quinn, P. K.: Sources and composition of submicron organic mass in marine aerosol particles, Journal of Geophysical Research-Atmospheres, 119, 12977-13003, 10.1002/2014jd021913, 2014a.

Frossard, A. A., Russell, L. M., Massoli, P., Bates, T. S., and Quinn, P. K.: Side-by-Side Comparison of Four Techniques Explains the Apparent Differences in the Organic Composition of Generated and Ambient Marine Aerosol Particles, Aerosol Science and Technology, 48, V-X, 10.1080/02786826.2013.879979, 2014b.

Gagosian, R. B., and Stuermer, D. H.: The cycling of biogenic compounds and their diagenetically transformed products in seawater., *Marine Chemistry* 5.4-6 605-632., 1977.

Giordano, M. R., Kalnajs, L. E., Avery, A., Goetz, J. D., Davis, S. M., and DeCarlo, P. F.: A missing source of aerosols in Antarctica - beyond long-range transport, phytoplankton, and photochemistry, Atmospheric Chemistry and Physics, 17, 1-20, 10.5194/acp-17-1-2017, 2017.

Gordon, M., and Taylor, P. A.: Measurements of blowing snow, Part I: Particle shape, size distribution, velocity, and number flux at Churchill, Manitoba, Canada, Cold Regions Science and Technology, 55, 63-74, 10.1016/j.coldregions.2008.05.001, 2009.

Goring, D. G., and Nikora, V. I.: Despiking acoustic Doppler velocimeter data, Journal of Hydraulic Engineering-Asce, 128, 117-126, 10.1061/(asce)0733-9429(2002)128:1(117), 2002.

Gras, J. L.: Condensation nucleus size distribution at Mawson, Antarctica - microphysics and chemistry, Atmospheric Environment Part a-General Topics, 27, 1427-1434, 10.1016/0960-1686(93)90128-l, 1993.

Guzman-Morales, J., Frossard, A. A., Corrigan, A. L., Russell, L. M., Liu, S., Takahama, S., Taylor, J. W., Allan, J., Coe, H., Zhao, Y., and Goldstein, A. H.: Estimated contributions of primary and secondary organic aerosol from fossil fuel combustion during the CalNex and Cal-Mex campaigns, Atmospheric Environment, 88, 330-340, 10.1016/j.atmosenv.2013.08.047, 2014.

Hansen, A. D. A., Bodhaine, B. A., Dutton, E. G., and Schnell, R. C.: AEROSOL BLACK CARBON MEASUREMENTS AT THE SOUTH-POLE - INITIAL RESULTS, 1986-1987, Geophysical Research Letters, 15, 1193-1196, 10.1029/GL015i011p01193, 1988.

Hansen, A. D. A., Lowenthal, D. H., Chow, J. C., and Watson, J. G.: Black carbon aerosol at McMurdo station, Antarctica, Journal of the Air & Waste Management Association, 51, 593-600, 2001.

Hara, K., Osada, K., Kido, M., Hayashi, M., Matsunaga, K., Iwasaka, Y., Yamanouchi, T., Hashida, G., and Fukatsu, T.: Chemistry of sea-salt particles and inorganic halogen species in Antarctic regions: Compositional differences between coastal and inland stations, Journal of Geophysical Research: Atmospheres, 109, 2004.

Hara, K., Osada, K., Kido, M., Matsunaga, K., Iwasaka, Y., Hashida, G., and Yamanouchi, T.: Variations of constituents of individual sea-salt particles at Syowa station, Antarctica, Tellus Series B-Chemical and Physical Meteorology, 57, 230-246, 10.1111/j.1600-0889.2005.00142.x, 2005.

Hara, K., Osada, K., Yabuki, M., Hashida, G., Yamanouchi, T., Hayashi, M., Shiobara, M., Nishita, C., and Wada, M.: Haze episodes at Syowa Station, coastal Antarctica: Where did they come from?, Journal of Geophysical Research: Atmospheres, 115, 2010.

Harder, S., Warren, S. G., and Charlson, R. J.: Sulfate in air and snow at the South Pole: Implications for transport and deposition at sites with low snow accumulation, Journal of Geophysical Research: Atmospheres, 105, 22825-22832, 2000.

Hawkins, L. N., and Russell, L.: Polysaccharides, Proteins, and Phytoplankton Fragments: Four Chemically Distinct Types of Marine Primary Organic Aerosol Classified by Single Particle Spectromicroscopy, Advances in Meteorology, 14, 10.1155/2010/612132, 2010.

Hofmann, D.: Balloon-borne measurements of middle atmosphere aerosols and trace gases in Antarctica, Reviews of Geophysics, 26, 113-130, 1988.

Hofmann, D. J., Rosen, J. M., Harder, J. A., and Rolf, S. R.: Ozone and aerosol measurements in the springtime Antarctic Stratosphere in 1985, Geophysical Research Letters, 13, 1252-1255, 10.1029/GL013i012p01252, 1986.

Hogan, A. W.: Antarctic aerosols, Journal of Applied Meteorology, 14, 550-559, 10.1175/1520-0450(1975)014<0550:aa>2.0.co;2, 1975.

Hogan, A. W., and Barnard, S.: Seasonal and frontal variation in Antarctic aerosol concentrations, Journal of Applied Meteorology, 17, 1458-1465, 10.1175/1520-0450(1978)017<1458:safvia>2.0.co;2, 1978.

Holland, P. R.: The seasonality of Antarctic sea ice trends, Geophysical Research Letters, 41, 4230-4237, 10.1002/2014gl060172, 2014.

Jourdain, B., and Legrand, M.: Year-round records of bulk and size-segregated aerosol composition and HCl and HNO3 levels in the Dumont d'Urville (coastal Antarctica) atmosphere: Implications for sea-salt aerosol fractionation in the winter and summer, Journal of Geophysical Research-Atmospheres, 107, 10.1029/2002jd002471, 2002.

Jourdain, B., Preunkert, S., Cerri, O., Castebrunet, H., Udisti, R., and Legrand, M.: Year-round record of size-segregated aerosol composition in central Antarctica (Concordia station): Implications for the degree of fractionation of sea-salt particles, Journal of Geophysical Research-Atmospheres, 113, 10.1029/2007jd009584, 2008.

Kalnajs, L. E., Avallone, L. M., and Toohey, D. W.: Correlated measurements of ozone and particulates in the Ross Island region, Antarctica, Geophysical Research Letters, 40, 6319-6323, 10.1002/2013gl058422, 2013.

Kawamura, K., and Gagosian, R. B.: Implications of omega-oxocarboxylic acids in the remote marine atmosphere for photooxidation of unsaturated fatty acids, Nature, 325, 330-332, 10.1038/325330a0, 1987.

Khan, A. L., McMeeking, G. R., Schwarz, J. P., Xian, P., Welch, K. A., Berry Lyons, W., and McKnight, D. M.: Near-Surface Refractory Black Carbon Observations in the Atmosphere and Snow in the McMurdo Dry Valleys, Antarctica, and Potential Impacts of Foehn Winds, Journal of Geophysical Research: Atmospheres, 123, 2877-2887, 2018.

Kim, J., Yoon, Y. J., Gim, Y., Kang, H. J., Choi, J. H., Park, K. T., and Lee, B. Y.: Seasonal variations in physical characteristics of aerosol particles at the King Sejong Station, Antarctic Peninsula, Atmospheric Chemistry and Physics, 17, 10.5194/acp-17-12985-2017, 2017.

Korhonen, H., Carslaw, K. S., Spracklen, D. V., Mann, G. W., and Woodhouse, M. T.: Influence of oceanic dimethyl sulfide emissions on cloud condensation nuclei concentrations and seasonality over the remote Southern Hemisphere oceans: A global model study, Journal of Geophysical Research-Atmospheres, 113, 10.1029/2007jd009718, 2008.

Kuznetsova, M., Lee, C., and Aller, J.: Characterization of the proteinaceous matter in marine aerosols, Marine Chemistry, 96, 359-377, 10.1016/j.marchem.2005.03.007, 2005.

Kyro, E. M., Kerminen, V. M., Virkkula, A., Dal Maso, M., Parshintsev, J., Ruiz-Jimenez, J., Forsstrom, L., Manninen, H. E., Riekkola, M. L., Heinonen, P., and Kulmala, M.: Antarctic new particle formation from continental biogenic precursors, Atmospheric Chemistry and Physics, 13, 3527-3546, 10.5194/acp-13-3527-2013, 2013.

Lambeck, K., Esat, T. M., and Potter, E. K.: Links between climate and sea levels for the past three million years, Nature, 419, 199-206, 10.1038/nature01089, 2002.

Leaitch, W. R., Russell, L. M., Liu, J., Kolonjari, F., Toom, D., Huang, L., Sharma, S., Chivulescu, A., Veber, D., and Zhang, W.: Organic Functional Groups in the Submicron Aerosol at 82.5 o N from 2012 to 2014, Atmos. Chem. Phys. Discuss., https://doi.org/10.5194/acp-2017-511 2017.

Legrand, M., Ducroz, F., Wagenbach, D., Mulvaney, R., and Hall, J.: Ammonium in coastal Antarctic aerosol and snow: Role of polar ocean and penguin emissions, Journal of Geophysical Research-Atmospheres, 103, 11043-11056, 10.1029/97jd01976, 1998.

Legrand, M., Gros, V., Preunkert, S., Sarda-Esteve, R., Thierry, A. M., Pepy, G., and Jourdain, B.: A reassessment of the budget of formic and acetic acids in the boundary layer at Dumont d'Urville (coastal Antarctica): The role of penguin emissions on the budget of several oxygenated volatile organic compounds, Journal of Geophysical Research-Atmospheres, 117, 10.1029/2011jd017102, 2012.

Legrand, M., Preunkert, S., Weller, R., Zipf, L., Elsasser, C., Merchel, S., Rugel, G., and Wagenbach, D.: Year-round record of bulk and size-segregated aerosol composition in central Antarctica (Concordia site) - Part 2: Biogenic sulfur (sulfate and methanesulfonate) aerosol, Atmospheric Chemistry and Physics, 17, 14055-14073, 10.5194/acp-17-14055-2017, 2017a.

Legrand, M., Preunkert, S., Wolff, E., Weller, R., Jourdain, B., and Wagenbach, D.: Year-round records of bulk and size-segregated aerosol composition in central Antarctica (Concordia site) Part 1: Fractionation of sea-salt particles, Atmospheric Chemistry and Physics, 17, 14039-14054, 10.5194/acp-17-14039-2017, 2017b.

Lin, Y. C., Tsai, C. J., Wu, Y. C., Zhang, R., Chi, K. H., Huang, Y. T., Lin, S. H., and Hsu, S. C.: Characteristics of trace metals in traffic-derived particles in Hsuehshan Tunnel, Taiwan: size distribution, potential source, and fingerprinting metal ratio, Atmospheric Chemistry and Physics, 15, 4117-4130, 10.5194/acp-15-4117-2015, 2015.

Loureiro, A., Vasconcellos, M., and Pereira, E.: Trace element determination in aerosols from the Antarctic Peninsula by neutron activation analysis, Journal of radioanalytical and nuclear chemistry, 159, 21-28, 1992.

Lyver, P. O., Barron, M., Barton, K. J., Ainley, D. G., Pollard, A., Gordon, S., McNeill, S., Ballard, G., and Wilson, P. R.: Trends in the Breeding Population of Adelie Penguins in the Ross Sea, 1981-2012: A Coincidence of Climate and Resource Extraction Effects, Plos One, 9, 10.1371/journal.pone.0091188, 2014.

Mace, K. A., Duce, R. A., and Tindale, N. W.: Organic nitrogen in rain and aerosol at Cape Grim, Tasmania, Australia, Journal of Geophysical Research-Atmospheres, 108, 10.1029/2002jd003051, 2003a.

Mace, K. A., Kubilay, N., and Duce, R. A.: Organic nitrogen in rain and aerosol in the eastern Mediterranean atmosphere: An association with atmospheric dust, Journal of Geophysical Research-Atmospheres, 108, 10.1029/2002jd002997, 2003b.

Mandalakis, M., Apostolaki, M., Tziaras, T., Polymenakou, P., and Stephanou, E. G.: Free and combined amino acids in marine background atmospheric aerosols over the Eastern Mediterranean, Atmospheric Environment, 45, 1003-1009, 10.1016/j.atmosenv.2010.10.046, 2011.

Maria, S. F., Russell, L. M., Turpin, B. J., and Porcja, R. J.: FTIR measurements of functional groups and organic mass in aerosol samples over the Caribbean, Atmospheric Environment, 36, 5185-5196, 10.1016/s1352-2310(02)00654-4, 2002.

Matsumoto, K., and Uematsu, M.: Free amino acids in marine aerosols over the western North Pacific Ocean, Atmospheric Environment, 39, 2163-2170, 10.1016/j.atmosenv.2004.12.022, 2005.

Mazzera, D. M., Lowenthal, D. H., Chow, J. C., and Watson, J. G.: Sources of PM10 and sulfate aerosol at McMurdo station, Antarctica, Chemosphere, 45, 347-356, 10.1016/s0045-6535(00)00591-9, 2001a.

Mazzera, D. M., Lowenthal, D. H., Chow, J. C., Watson, J. G., and Grubisic, V.: PM10 measurements at McMurdo Station, Antarctica, Atmospheric Environment, 35, 1891-1902, 10.1016/s1352-2310(00)00409-x, 2001b.

McCoy, D. T., Burrows, S. M., Wood, R., Grosvenor, D. P., Elliott, S. M., Ma, P.-L., Rasch, P. J., and Hartmann, D. L.: Natural aerosols explain seasonal and spatial patterns of Southern Ocean cloud albedo, Science advances, 1, e1500157-e1500157, 10.1126/sciadv.1500157, 2015.

McNeill, V. F.: Aqueous Organic Chemistry in the Atmosphere: Sources and Chemical Processing of Organic Aerosols, Environmental Science & Technology, 49, 1237-1244, 10.1021/es5043707, 2015.

Milne, P. J., and Zika, R. G.: Amino-acid nitrogen in atmospheric aerosols - occurrence, sources and photochemical modification, Journal of Atmospheric Chemistry, 16, 361-398, 10.1007/bf01032631, 1993.

Minikin, A., Legrand, M., Hall, J., Wagenbach, D., Kleefeld, C., Wolff, E., Pasteur, E. C., and Ducroz, F.: Sulfur-containing species (sulfate and methanesulfonate) in coastal Antarctic aerosol and precipitation, Journal of Geophysical Research: Atmospheres, 103, 10975-10990, 1998.

Mishra, V. K., Kim, K.-H., Hong, S., and Lee, K.: Aerosol composition and its sources at the King Sejong Station, Antarctic peninsula, Atmospheric Environment, 38, 4069-4084, 2004.

Modini, R. L., Frossard, A. A., Ahlm, L., Russell, L. M., Corrigan, C. E., Roberts, G. C., Hawkins, L. N., Schroder, J. C., Bertram, A. K., Zhao, R., Lee, A. K. Y., Abbatt, J. P. D., Lin, J., Nenes, A., Wang, Z., Wonaschutz, A., Sorooshian, A., Noone, K. J., Jonsson, H., Seinfeld, J. H., Toom-Sauntry, D., Macdonald, A. M., and Leaitch, W. R.: Primary marine aerosol-cloud

interactions off the coast of California, Journal of Geophysical Research-Atmospheres, 120, 4282-4303, 10.1002/2014jd022963, 2015.

Olson, M. R., Garcia, M. V., Robinson, M. A., Van Rooy, P., Dietenberger, M. A., Bergin, M., and Schauer, J. J.: Investigation of black and brown carbon multiple-wavelength-dependent light absorption from biomass and fossil fuel combustion source emissions, Journal of Geophysical Research-Atmospheres, 120, 6682-6697, 10.1002/2014jd022970, 2015.

Ondov, J. M., Gladney, E. S., Zoller, W. H., Duce, R. A., and Jones, A. G.: Atmospheric particulates at South-Pole station, Antarctic Journal of the United States, 8, 182-183, 1973a.

Ondov, J. M., Gladney, E. S., Zoller, W. H., Duce, R. A., and Jones, A. G.: Atmospheric particulates at South-Pole station, Antarctic Journal of the United States, 8, 182-183, 1973b.

Paatero, P., and Tapper, U.: Positive Matrix Factorization: A Non-Negative Factor Model with Optimal Utilization of Error Estimates of Data Values, Environmetrics, 5, 111-126, 10.1002/env.3170050203, 1994.

Paatero, P.: Least squares formulation of robust non-negative factor analysis, Chemometrics and Intelligent Laboratory Systems, 37, 23-35, 10.1016/s0169-7439(96)00044-5, 1997.

Parungo, F., Bodhaine, B., and Bortniak, J.: Seasonal variation in Antarctic aerosol, Journal of Aerosol Science, 12, 491-&, 10.1016/0021-8502(81)90052-5, 1981.

Petters, M. D., and Kreidenweis, S. M.: A single parameter representation of hygroscopic growth and cloud condensation nucleus activity, Atmospheric Chemistry and Physics, 7, 1961-1971, 2007.

Polissar, A. V., Hopke, P. K., Paatero, P., Kaufmann, Y. J., Hall, D. K., Bodhaine, B. A., Dutton, E. G., and Harris, J. M.: The aerosol at Barrow, Alaska: long-term trends and source locations, Atmospheric Environment, 33, 2441-2458, 10.1016/s1352-2310(98)00423-3, 1999.

Price, D. J., Chen, C.-L., Russell, L. M., Lamjiri, M. A., Betha, R., Sanchez, K., Liu, J., Lee, A. K. Y., and Cocker, D. R.: More unsaturated, cooking-type hydrocarbon-like organic aerosol particle emissions from renewable diesel compared to ultra low sulfur diesel in at-sea operations of a research vessel, Aerosol Science and Technology, 51, 135-146, 10.1080/02786826.2016.1238033, 2017.

Read, K., Lewis, A., Bauguitte, S., Rankin, A. M., Salmon, R., Wolff, E. W., Saiz-Lopez, A., Bloss, W., Heard, D., and Lee, J.: DMS and MSA measurements in the Antarctic Boundary Layer: impact of BrO on MSA production, Atmospheric Chemistry and Physics, 8, 2985-2997, 2008.

Rickard, A. R., Wyche, K. P., Metzger, A., Monks, P. S., Ellis, A. M., Dommen, J., Baltensperger, U., Jenkin, M. E., and Pilling, M. J.: Gas phase precursors to anthropogenic secondary organic aerosol Using the Master Chemical Mechanism to probe detailed observations

of 1,3,5-trimethylbenzene photo-oxidation, Atmospheric Environment, 44, 5423-5433, 10.1016/j.atmosenv.2009.09.043, 2010.

Rickards, A. M. J., Miles, R. E. H., Davies, J. F., Marshall, F. H., and Reid, J. P.: Measurements of the Sensitivity of Aerosol Hygroscopicity and the kappa Parameter to the O/C Ratio, Journal of Physical Chemistry A, 117, 14120-14131, 10.1021/jp407991n, 2013.

Riddick, S. N., Dragosits, U., Blackall, T. D., Daunt, F., Wanless, S., and Sutton, M. A.: The global distribution of ammonia emissions from seabird colonies, Atmospheric Environment, 55, 319-327, 10.1016/j.atmosenv.2012.02.052, 2012.

Russell, L. M.: Aerosol organic-mass-to-organic-carbon ratio measurements, Environmental Science & Technology, 37, 2982-2987, 10.1021/es026123w, 2003.

Russell, L. M., Bahadur, R., Hawkins, L. N., Allan, J., Baumgardner, D., Quinn, P. K., and Bates, T. S.: Organic aerosol characterization by complementary measurements of chemical bonds and molecular fragments, Atmospheric Environment, 43, 6100-6105, 10.1016/j.atmosenv.2009.09.036, 2009.

Russell, L. M., Hawkins, L. N., Frossard, A. A., Quinn, P. K., and Bates, T. S.: Carbohydrate-like composition of submicron atmospheric particles and their production from ocean bubble bursting, Proceedings of the National Academy of Sciences of the United States of America, 107, 6652-6657, 10.1073/pnas.0908905107, 2010.

Russell, L. M., Bahadur, R., and Ziemann, P. J.: Identifying organic aerosol sources by comparing functional group composition in chamber and atmospheric particles, Proceedings of the National Academy of Sciences of the United States of America, 108, 3516-3521, 10.1073/pnas.1006461108, 2011.

Russell, L. M., and Shaw, G. E.: Arctic and Antarctic | Arctic Haze, in: Encyclopedia of Atmospheric Sciences, 2nd Edition ed., edited by: North, G., Pyle, J., and Zhang, F., Elsevier 32 Jamestown Road, London NW1 7BY, UK

225 Wyman Street, Waltham, MA 02451, USA525 B Street, Suite 1800, San Diego, CA 92101-4495, USA, 116-121, 2015.

Saliba, G., Saleh, R., Zhao, Y. L., Presto, A. A., Larnbe, A. T., Frodin, B., Sardar, S., Maldonado, H., Maddox, C., May, A. A., Drozd, G. T., Goldstein, A. H., Russell, L. M., Hagen, F., and Robinson, A. L.: Comparison of Gasoline Direct-Injection (GDI) and Port Fuel Injection (PFI) Vehicle Emissions: Emission Certification Standards, Cold-Start, Secondary Organic Aerosol Formation Potential, and Potential Climate Impacts, Environmental Science & Technology, 51, 6542-6552, 10.1021/acs.est.6b06509, 2017.

Savoie, D., Prospero, J., Larsen, R., Huang, F., Izaguirre, M., Huang, T., Snowdon, T., Custals, L., and Sanderson, C.: Nitrogen and sulfur species in Antarctic aerosols at Mawson, Palmer station, and Marsh (King George Island), Journal of Atmospheric Chemistry, 17, 95-122, 1993.

Sax, M., Zenobi, R., Baltensperger, U., and Kalberer, M.: Time resolved infrared spectroscopic analysis of aerosol formed by photo-oxidation of 1,3,5-trimethylbenzene and alpha-pinene, Aerosol Science and Technology, 39, 822-830, 10.1080/02786820500257859, 2005.

Saxena, V., and Ruggiero, F.: Aerosol measurements at Palmer Station, Antarctica, Contributions to Antarctic Research I, 1-5, 1990.

Scalabrin, E., Zangrando, R., Barbaro, E., Kehrwald, N. M., Gabrieli, J., Barbante, C., and Gambaro, A.: Amino acids in Arctic aerosols, Atmospheric Chemistry and Physics, 12, 10453-10463, 10.5194/acp-12-10453-2012, 2012.

Schmale, J., Schneider, J., Nemitz, E., Tang, Y. S., Dragosits, U., Blackall, T. D., Trathan, P. N., Phillips, G. J., Sutton, M., and Braban, C. F.: Sub-Antarctic marine aerosol: dominant contributions from biogenic sources, Atmospheric Chemistry and Physics, 13, 8669-8694, 10.5194/acp-13-8669-2013, 2013.

Schmidt, R. A.: Estimates of threshold windspeed from particle sizes in blowing snow, Cold Regions Science and Technology, 4, 187-193, 10.1016/0165-232x(81)90003-3, 1981.

Shaw, P. M., Russell, L. M., Jefferson, A., and Quinn, P. K.: Arctic organic aerosol measurements show particles from mixed combustion in spring haze and from frost flowers in winter, Geophysical Research Letters, 37, 10.1029/2010gl042831, 2010.

Shi, J. H., Gao, H. W., Qi, J. H., Zhang, J., and Yao, X. H.: Sources, compositions, and distributions of water-soluble organic nitrogen in aerosols over the China Sea, Journal of Geophysical Research-Atmospheres, 115, 10.1029/2009jd013238, 2010.

Solomon, S., Sanders, R. W., Jakoubek, R. O., Arpag, K. H., Stephens, S. L., Keys, J. G., and Garcia, R. R.: Visible and near-ultraviolet spectroscopy at McMurdo-station, Antarctica. 10. Reductions of stratospheric NO2 Due to Pinatubo aerosols, Journal of Geophysical Research-Atmospheres, 99, 3509-3516, 10.1029/93jd03088, 1994.

Steig, E. J., Schneider, D. P., Rutherford, S. D., Mann, M. E., Comiso, J. C., and Shindell, D. T.: Warming of the Antarctic ice-sheet surface since the 1957 International Geophysical Year, Nature, 457, 459-462, 10.1038/nature07669, 2009.

Stephanou, E. G., and Stratigakis, N.: Oxocarboxylic and. alpha.,. omega.-dicarboxylic acids: photooxidation products of biogenic unsaturated fatty acids present in urban aerosols, Environmental science & technology, 27, 1403-1407, 1993.

Stocker, T. F., D. Qin, G. K. Plattner, M. Tignor, S. K. Allen, J. Boschung, A. Nauels, Y. Xia, V. Bex, and Midgley, P. M.: IPCC, 2013: summary for policymakers in climate change 2013: the physical science basis, contribution of working group I to the fifth assessment report of the intergovernmental panel on climate change, in, 2013.

Stohl, A.: Characteristics of atmospheric transport into the Arctic troposphere, Journal of Geophysical Research-Atmospheres, 111, 10.1029/2005jd006888, 2006.

Stohl, A., and Sodemann, H.: Characteristics of atmospheric transport into the Antarctic troposphere, Journal of Geophysical Research-Atmospheres, 115, 10.1029/2009jd012536, 2010.

Su, H., Rose, D., Cheng, Y. F., Gunthe, S. S., Massling, A., Stock, M., Wiedensohler, A., Andreae, M. O., and Poschl, U.: Hygroscopicity distribution concept for measurement data analysis and modeling of aerosol particle mixing state with regard to hygroscopic growth and CCN activation, Atmospheric Chemistry and Physics, 10, 7489-7503, 10.5194/acp-10-7489-2010, 2010.

Takahama, S., Johnson, A., and Russell, L. M.: Quantification of carboxylic and carbonyl functional groups in organic aerosol infrared absorbance spectra, Aerosol Science and Technology, 47, 310-325, 10.1080/02786826.2012.752065, 2013.

Tukey, J. W.: Exploratory Data Analysis, 1 edition (1977) ed., Behavioral Science, 1977.

Udisti, R., Dayan, U., Becagli, S., Busetto, M., Frosini, D., Legrand, M., Lucarelli, F., Preunkert, S., Severi, M., Traversi, R., and Vitale, V.: Sea spray aerosol in central Antarctica. Present atmospheric behaviour and implications for paleoclimatic reconstructions, Atmospheric Environment, 52, 109-120, 10.1016/j.atmosenv.2011.10.018, 2012.

Usher, C. R., Michel, A. E., and Grassian, V. H.: Reactions on mineral dust, Chemical Reviews, 103, 4883-4939, 10.1021/cr020657y, 2003.

Velleman, P. F.: Robust nonlinear data smoothers - definitions and recommendations., Proceedings of the National Academy of Sciences of the United States of America, 74, 434-436, 10.1073/pnas.74.2.434, 1977.

Violaki, K., Zarbas, P., and Mihalopoulos, N.: Long-term measurements of dissolved organic nitrogen (DON) in atmospheric deposition in the Eastern Mediterranean: Fluxes, origin and biogeochemical implications, Marine Chemistry, 120, 179-186, 10.1016/j.marchem.2009.08.004, 2010.

Wagenbach, D., Ducroz, F., Mulvaney, R., Keck, L., Minikin, A., Legrand, M., Hall, J. S., and Wolff, E. W.: Sea-salt aerosol in coastal Antarctic regions, Journal of Geophysical Research-Atmospheres, 103, 10961-10974, 10.1029/97jd01804, 1998.

Warburton, J. A.: Surface measurements of Aitken nuclei at McMurdo, Siple, Byrd, and South-pole stations, Antarctic Journal of the United States, 8, 236-236, 1973.

Weber, R. J., McMurry, P. H., Mauldin, L., Tanner, D. J., Eisele, F. L., Brechtel, F. J., Kreidenweis, S. M., Kok, G. L., Schillawski, R. D., and Baumgardner, D.: A study of new particle formation and growth involving biogenic and trace gas species measured during ACE 1, Journal of Geophysical Research-Atmospheres, 103, 16385-16396, 10.1029/97jd02465, 1998.

Wedyan, M. A., and Preston, M. R.: The coupling of surface seawater organic nitrogen and the marine aerosol as inferred from enantiomer-specific amino acid analysis, Atmospheric Environment, 42, 8698-8705, 10.1016/j.atmosenv.2008.04.038, 2008.

Weller, R., and Wagenbach, D.: Year-round chemical aerosol records in continental Antarctica obtained by automatic samplings, Tellus Series B-Chemical and Physical Meteorology, 59, 755-765, 10.1111/j.1600-0889.2007.00293.x, 2007.

Weller, R., Minikin, A., Petzold, A., Wagenbach, D., and König-Langlo, G.: Characterization of long-term and seasonal variations of black carbon (BC) concentrations at Neumayer, Antarctica, Atmospheric Chemistry and Physics, 13, 1579-1590, 2013.

Wex, H., McFiggans, G., Henning, S., and Stratmann, F.: Influence of the external mixing state of atmospheric aerosol on derived CCN number concentrations, Geophysical Research Letters, 37, 10.1029/2010gl043337, 2010.

Wyche, K. P., Monks, P. S., Ellis, A. M., Cordell, R. L., Parker, A. E., Whyte, C., Metzger, A., Dommen, J., Duplissy, J., Prevot, A. S. H., Baltensperger, U., Rickard, A. R., and Wulfert, F.: Gas phase precursors to anthropogenic secondary organic aerosol: detailed observations of 1,3,5-trimethylbenzene photooxidation, Atmospheric Chemistry and Physics, 9, 635-665, 10.5194/acp-9-635-2009, 2009.

Xu, G. J., Gao, Y., Lin, Q., Li, W., and Chen, L. Q.: Characteristics of water-soluble inorganic and organic ions in aerosols over the Southern Ocean and coastal East Antarctica during austral summer, Journal of Geophysical Research-Atmospheres, 118, 13303-13318, 10.1002/2013jd019496, 2013.

Yang, X., Pyle, J. A., and Cox, R. A.: Sea salt aerosol production and bromine release: Role of snow on sea ice, Geophysical Research Letters, 35, 10.1029/2008gl034536, 2008.

Zangrando, R., Barbaro, E., Vecchiato, M., Kehrwald, N. M., Barbante, C., and Gambaro, A.: Levoglucosan and phenols in Antarctic marine, coastal and plateau aerosols, Science of the Total Environment, 544, 606-616, 10.1016/j.scitotenv.2015.11.166, 2016.

Conclusions

BSOA identified at field observations in the southeastern U.S. and Antarctica was investigated to understand the processes that contributed to their formation. The first chapter focuses on the heterogeneous reactions of sulfate on isoprene-related bSOA [*Liu et al.*, 2017]. The second chapter focused on the role of NO_x on bSOA formation using both AMS and FTIR measurements during the SOAS campaign [*Liu et al.*, Submitted.]. The third chapter identifies sources and seasonal differences in biogenic OM in Antarctica [*Liu et al.*, In discussion.]. The objective of each of these studies is to identify the aerosol processes that affect bSOA formation. The motivation for these studies is to provide constraints that can be used to improve the simulation of bSOA formation in models.

The first chapter used measurements during the 2013 Southern Oxidant and Aerosol Study. Aerosol mass spectrometer measurements of submicron mass and single-particles were taken at Look Rock, Tennessee. Their concentrations increased during multi-day stagnation events characterized by low wind, little rain, and increased daytime isoprene emissions. Organic mass (OM) sources were apportioned as 42% "vehicle-related" and 54% biogenic secondary organic aerosol (bSOA), with the latter including “sulfate-related bSOA” that correlated to sulfate ($r=0.72$) and “nitrate-related bSOA” that correlated to nitrate ($r=0.65$). Single-particle mass spectra showed three composition types that corresponded to the mass-based factors with spectra cosine similarity of 0.93 and time series correlations of $r>0.4$. The vehicle-related OM with m/z 44 was correlated to black carbon, “sulfate-related bSOA” was on particles with high

sulfate, and "nitrate-related bSOA" was on all particles. The similarity of the m/z spectra (cosine similarity=0.97) and the time series correlation (r=0.80) of the "sulfate-related bSOA" to the sulfate-containing single-particle type provide evidence for particle composition contributing to selective uptake of isoprene oxidation products onto particles that contain sulfate from power plants [*Liu et al.*, 2017].

The second chapter utilized measurements during the 2013 Southern Oxidant and Aerosol Study. Fourier Transform Infrared Spectroscopy (FTIR) and Aerosol Mass Spectrometer (AMS) measurements of submicron mass were collected at Look Rock (LRK), Tennessee, and Centreville (CTR), Alabama. Carbon monoxide and submicron sulfate and organic mass concentrations were 15-60% higher at CTR than at LRK but their time series had moderate correlations (r~0.5). However, NO_x had no correlation (r=0.08) between the two sites with nighttime-to-early-morning peaks 3~10 times higher at CTR than at LRK. Organic mass (OM) maximum concentrations occurred in the afternoon at both sites but also at night at CTR. OM sources identified by FTIR Positive Matrix Factorization (PMF) had three very similar factors at both sites: Fossil Fuel Combustion (FFC) related organic aerosols, Mixed Organic Aerosols (MOA), and Biogenic Organic Aerosols (BOA). The BOA spectrum from FTIR is similar (cosine similarity > 0.6) to that of lab-generated particle mass from the photochemical oxidation of both isoprene and monoterpenes under high NO_x conditions from chamber experiments. The BOA mass fraction was highest during the night at CTR but in the afternoon at LRK. AMS PMF resulted in two similar pairs of factors at both sites and a third nighttime NO_x-related factor (33% of OM) at CTR but a daytime nitrate-related factor (28% of OM) at LRK. NO_x was correlated with BOA, LO-OOA and Factor91 for NO_x concentrations higher than 1 ppb at both sites,

producing 0.5 to 1 μg m-3 additional biogenic OM for each 1 ppb increase of NO_x [*Liu et al.*, Submitted.].

The third chapter used observations from the ARM West Antarctic Radiation Experiment (AWARE) from November 2015 to December 2016 with measured submicron aerosol properties near McMurdo Station at the southern tip of the Ross Island. Submicron organic mass (OM), particle number, and cloud condensation nuclei concentrations were higher in summer than other seasons. The measurements included a range of compositions and concentrations that likely reflected both local anthropogenic emissions and natural background sources. We isolated the natural organic components by separating a natural factor and a local combustion factor. The natural OM was 150 times higher in summer than in winter. The local anthropogenic emissions were not hygroscopic and had little contribution to the CCN concentrations. Natural sources that included marine sea spray and seabird emissions contributed 56 % of OM in the austral summer but only 3 % in the austral winter. The natural OM had high hydroxyl group fraction (55%), 6% alkane, and 6% amine group mass, consistent with marine organic composition. In addition, the Fourier transform infrared (FTIR) spectra showed the natural sources of organic aerosol were characterized by amide group absorption, which may be from seabird populations. Carboxylic acid group contributions from natural sources were correlated to incoming solar radiation, indicating secondary pathways [*Liu et al.*, In discussion.].

The measurements presented in this dissertation contribute to a better characterization of the contribution of biogenic and anthropogenic emissions to the composition and concentration of organic aerosol particles in the southeastern U.S. and coastal Antarctica. This work provides insights on specific anthropogenic-related processes that influence bSOA formation and will help

better constrain the model simulation of bSOA in the southeastern U.S. The characterization and source apportionment of organic aerosols at coastal Antarctica can contribute to determining the overall climate influence of these very remote aerosol particles.

Future work should explore more detailed chemical mechanisms that governing the reactions that lead to bSOA formation and better quantify the influences. Additional work could expand on the measurements presented here to sites with similar and different bVOC emissions and climates. The composition of natural aerosol organic functional group presented here could be used to quantify natural sources in other regions as well as to identify the impacts of the biogenic aerosols on current and future climate. The organic and inorganic composition and the hygroscopicity of aerosol particles in costal Antarctica can be used in climate models to parameterize the contribution of natural sources to the CCN and thus help us to understand the rapidly warming climate in the region.

References

Liu, J., J. Dedrick, L. M. Russell, G. Senum, J. Uin, Kuang C., Springston S.R., and D. Lubin (In discussion.), Summertime Maximum of Organic Functional Group Concentrations and High Organic Nitrogen from Ocean Biogenic Aerosols at Coastal West Antarctica during AWARE, *Atmospheric Chemistry and Physics In discussion.*

Liu, J., L. M. Russell, A. K. Y. Lee, K. A. McKinney, J. D. Surratt, and P. J. Ziemann (2017), Observational evidence for pollution-influenced selective uptake contributing to biogenic secondary organic aerosols in the southeastern US, *Geophysical Research Letters*, *44*(15), 8056-8064, doi:10.1002/2017gl074665.

Liu, J., Russell, L.M., Ruggeri G., Takahama, S., Claflin, M.S., Ziemann P.J., Pye, H.O. 4, Murphy, B.N., Xu L., Ng N,L, McKinney, K.A., Bertram, T.H., Athanasios, N. and Surratt, J.D. (in review) Regional Similarities and NOx-related Increases in Biogenic Secondary Organic Aerosol in Summertime Southeastern U.S. *J. Geophys. Res*.